THE UNIVERSITY *of* EDINBURGH

THE UNIVERSITY *of* EDINBURGH

A study of how catabolite repression and ribosome levels determine cell growth in batch cultures of *Saccharomyces cerevisiae*

Yu Huo

Thesis submitted in fulfilment of the requirements

for the degree of Doctor of Philosophy

University of Edinburgh

June 2023

To Mom and Dad.

Declaration

I declare that this thesis has been composed solely by myself and that it has not been submitted, in whole or in part, in any previous application for a degree. Except where states otherwise by reference or acknowledgment, the work presented is entirely my own.

Yu Huo

Acknowledgements

I am very grateful to my supervisor Prof Peter Swain for his supervision and his unreserved support over the past four years. It has been a joy to work with Peter, and from him I learned what makes good science and an exceptional scientist.

I would also like to thank:

- The Darwin Trust of Edinburgh, for their financial support.
- Dr Edward Wallace, who heartily offered more help than most second supervisors and guided me through the RNAseq experiment.
- Prof David Tollervey, for his feedback as the chair of my thesis committee.
- Iseabail Fraquhar, who helped me to construct the fluorescent strains for the *GAL* and *MAL* networks and taught me molecular biology techniques.
- Dr Kevin Correia, who taught me molecular biology techniques, microfluidics experiments and gave me lots of helpful advice.
- Dr Alán Muñoz, a great friend and colleague of mine, for sharing great ideas and tools with me.
- Dr Ivan Clark, for teaching me how to run microfluidics experiments and helping me with lab tasks.
- Dr Lucia Bandiera, for teaching me how to run plate reader experiments at the beginning of my project.
- Hongpei Li, Jack Thomson, Kim Mailliet and Xiao Wang, for their valuable experimental work in collaboration with me. Hongpei, Jack and Xiao contributed to the data in Chapter 2.

- Other members and former members in the Swain lab, for feedbacks and discussion during lab meetings and in the office, for the software infrastructure, and for taking care of my yeasts during the COVID restriction.
- Weronika Danecka, for teaching me how to handle RNA and some cheerful chats in the lab.
- Dr Sam Haynes and the team of Edinburgh Clinical Research Facility, for helping me with the RNAseq experiment.
- Dr Tessa Moses, for helping me with the metabolomics experiment.
- Dr Alex McVey, for the helpful advice during my PhD application.
- My friends in Edinburgh, Beijing and Guangdong.
- Emacs developers for the amazing tools they created.

Last, I would like to thank my family for their love, support and understanding over the past four years, especially during the COVID pandemic when life was uncertain and travelling was almost impossible.

Abstract

In response to environmental changes, cells launch new programmes of gene expression. Here I address how cells with their finite proteomes regulate ribosomal levels as the environment changes in batch cultures and, given two carbon sources, how cells prioritise which to use. In the initial chapters, I describe how I measure the dynamics of both growth and ribosome levels in *S. cerevisiae* using microplate readers. I show that growth only enters a prolonged exponential phase if the initial sugar concentration is sufficiently high, otherwise the specific growth rate peaks rather than plateaus. Nevertheless, Monod's law still holds for the initial sugar concentration and the maximum specific growth rate. Using GFP-tagged ribosomes, I then measure the population's total ribosome level and demonstrate that the population's growth rate is proportional to this level in the early phases of growth. I go on to define the effective translation rate as the ratio between the population's growth rate and its ribosome level, and find that in exponential phase, the effective translation rate and the ribosomal fraction are constant over time. Further, the results of challenging cells with different stresses suggest an empirical upper limit to the effective translation rate. To understand these findings, I develop a minimal self-replicator model and analyse its behaviour both at and away from steady state. I extend this model to include carbon and nitrogen and derive mechanistically a form of Monod's law for two substrates. In the final chapters, I investigate how cells prioritise the use of non-glucose sugars, specifically galactose and palatinose, which is little studied. I show that cells exhibit diauxie in galactose-palatinose mixtures, prioritising galactose. In addition, I demonstrate that constitutively active Gal4 in a *gal80*Δ mutant causes a long delay in palatinose metabolism, and that this delay can be mostly alleviated by deleting the gene for the galactose transporter. To investigate the cause of this effect, I perform an RNAseq experiment, which identifies *MAL11*, the palatinose transporter, as the likely target of

Gal4 signalling. With this discovery, I build a simple model to understand how the Gal4 signal affects the inducibility of the *MAL* network, which predicts that the isomaltases are excessively expressed relative to *MAL11* when Gal4 is constitutively active. I therefore delete *IMA1*, which encodes one of the two isomaltases, from the *gal80*Δ mutant, and, as expected, this mutant can use palatinose with little lag. My results therefore provide a novel example of non-glucose catabolite repression in *S. cerevisiae* and how one network can affect another by changing its inducibility.

中文摘要

细胞通过表达不同的基因来应对环境的变化。在本论文中我将会探讨两个问题：其一是酿酒酵母(*S. cerevisiae*) 细胞在蛋白质组大小有限的条件之下，如何调节核糖体的水平来应对批次培养(batch culture) 中环境的变化；其二是酵母细胞在存在两种碳源的条件下，如何决定优先使用何种碳源。在前几章，我将讲述如何使用微孔板读板机(microplate reader) 同时测量生长和核糖体水平随时间的变化。我的结果表明生长只会在初始碳源浓度足够高的条件下方可进入指数生长，否则比生长速率会呈现出的是峰，而非平台。但是，若我们用最大比生长速率代替指数期生长速率，莫诺方程(Monod's law) 仍然成立。利用绿色荧光蛋白标记的核糖体蛋白，我测量了在批次培养的群体中核糖体的总水平，数据表明，在早期的生长阶段，群体的生长速率与之呈正比例关系。于是我把群体生长速率与群体核糖体总水平之比定义为有效翻译速率(effective translation rate), 并且发现在指数生长阶段，有效翻译速率和比核糖体水平皆保持不变。此外，通过对比在细胞面临不同的压力之下的有效翻译速率，我发现该速率有一个经验上限。为理解上述结果，我写了一个简略的自复制模型(self-replicator model) 并且分析了模型的在稳态和稳态以外的行为。这个模型可扩展以同时描述碳源和氮源，我通过扩展过的模型推导出了莫诺方程扩展到两个底物的形式。在后几章，我探讨了细胞在存在两种非葡萄糖碳源的情况下，是否仍优先使用其中一个。我主要研究的是细胞在半乳糖和较少研究的异麦芽酮糖下的反应。我发现细胞在半乳糖和异麦芽酮糖的混合液中呈现二次生长(diauxie)，因其优先消耗半乳糖。此外，我发现在*gal80*Δ 突变体中持续活跃的Gal4 会强烈延迟异麦芽酮糖的代谢，但进一步敲除半乳糖转运蛋白基因能令延迟有所缩短。为研究其中的机制，我进行了核糖核酸测序(RNAseq)，结果表明异麦芽酮糖转运蛋白基因*MAL11* 很可能被Gal4 的信号抑制。我于是建了一个简单的模型去解释Gal4 的信号如何影响麦芽糖代谢网络(*MAL*) 的可诱导性(inducibility)，该模型预测在Gal4 持续活跃之下异麦芽糖酶(isomaltase) 的表达相对*MAL11* 过量。因此，我在*gal80*Δ 突变体中进一步敲除了两个异麦芽糖酶基因之一

的*IMA1* 基因，与预期一致，该突变体能够正常代谢异麦芽酮糖。本成果作为酿酒酵母非葡萄糖引起的分解代谢物阻遏(catabolite repression) 的崭新实例，揭示了代谢网络可以通过改变另一个网络的可诱导性来影响另一个网络。

Lay Summary

Most microbes, like the baker's yeast in this research, are single cells. They live in changing environments — as there can be sometimes more nutrients and sometimes fewer. Small and simple they may seem, they need to respond to a change in the environment to survive and thrive — for example, before baking when yeast cells are mixed with flour, in which multiple types of sugars co-exist, the yeast cells must make transporter proteins that take the sugars into the cell. Moreover, they sometimes need to make decisions — when multiple sugars co-exist, yeast cells prefer glucose which supports fast growth over another sugar that supports slower growth. This is because each cell has limited resources to make proteins, and some enzymes can only break down a certain type of sugar, and if they make enzymes that break down glucose, they grow faster.

The first question I address in this thesis is: when two non-glucose sugars are present, will yeast prefer one over another? The answer is sometimes yes — I found that baker's yeast cells prefer galactose, a sugar abundant in dairy products, over palatinose, another that exists in honey. Each of the two sugars has its own set of enzymes, and the production of enzymes is controlled by a gene expression network that acts like a switch — when the sugar is present *inside* the cell, the corresponding network senses the sugar and switches on to produce the enzymes. The network for galactose is *GAL* and that for palatinose is *MAL* (because the same network is responsible for maltose consumption). To "focus" on galactose, cells must "ignore" palatinose by preventing the *MAL* network from switching on. But how? I found that the active *GAL* network prevents the palatinose transporter from being highly produced, and without the transporter, palatinose outside the cell cannot be taken in and sensed by the *MAL* network, and so the *MAL* network remains off. Perhaps more intriguingly, we can change the preference of yeast cells by changing the *MAL* network's structure — if we delete one gene within the network encoding an

enzyme for palatinose, the *MAL* network will overcome the repression from *GAL*.

In addition to breaking down sugars, yeast cells also need to make proteins to grow, and the ribosome is the machinery that makes proteins from amino acids. It is known that in fast-growing cells ribosomes take up more mass of the cells, because the cells need to produce protein faster to keep up with the demand of growth. The cells may need to adjust the number of ribosomes according to the demand because a cell's resources are limited — if the ribosome level is kept higher than demand, it will take up the resource of proteins for other purposes (for example, breaking down sugars). So the second question I address is: how do growth and ribosome levels change together over time? We developed a method to automatically measure the ribosome levels and cell growth simultaneously, and with this method, we found that the cells may adjust the ribosome levels on demand, so that the ribosomes work at a constant efficiency, at least when the yeast population is not too dense and the environment is favourable. Cells can even maintain this efficiency under stress by weak acids, but they cannot when exposed to drugs that interfere with the ribosomes' function.

Baker's yeast is widely used in the industrial production of valuable chemical compounds and fermentation, in which the cells are driven to perform human-desired tasks. My results reveal how yeast cells respond to a complex environment by allocating their limited resources to different tasks, and thus may help to increase industrial production.

Contents

List of Figures

List of Abbreviations

ADP adenosine diphosphate

ATP adenosine triphosphate

bp base pair

cAMP cyclic adenosine monophosphate

cAMP-PKA cAMP-protein kinase A

cAMP-CRP cAMP-cAMP receptor protein

ChIP chromatin immunoprecipitation

CHX cycloheximide

CPM counts per million reads

CRISPR clustered regularly interspaced short palindromic repeats

CV coefficient of variation

DEG differentially expressed gene

GC-MS gas chromatography-mass spectrometry

GFP green fluorescent protein

GO gene ontology

G418 geneticin

HOG hyper-osmolarity-glycerol

KEGG Kyoto Encyclopedia of Genes and Genomes

LoFlo low fluoscence SC

NADP nicotinamide adenine dinucleotide phosphate

NTC nourseothrycin

OD optical density

ODE ordinary differential equation

PAM protospacer adjacent motif

PCA principle component analysis

PCR polymerase chain reaction

PEG polyethylene glycol

PKA protein kinase A

PP1 protein phosphatase 1

RNA ribonucleic acid

RNAseq RNA sequencing

RT-qPCR quantitative reverse transcription PCR

SAGA Spt-Ada-Gcn5 acetyltransferase

SC synthetic complete

SUTs stable unannotated transcripts

TBP TATA-binding protein

TORC target of rapamycin complex

YEP yeast extract peptone

Fru fructose

Gal galactose

Glu glucose

Pal palatinose

Pyr pyruvate

Raf raffinose

Suc sucrose

Chapter 1

Introduction

"*Omnis cellula e cellula* (all cells come from cells) (Virchow 1860)." This assertion may seem obvious nowadays, but it reveals the intricacy of a cell — even the most delicate artefact in the world cannot reproduce itself *de novo*. A microbial cell must grow before completing its reproduction by dividing, and cell growth involves catabolic enzymes and anabolic enzymes (e.g. ribosomes). Cells grow in fluctuating environments where multiple substrates or signals may co-exist, but the proteome of a cell is finite, so cells must make decisions on gene expression to maximise their fitness or to prepare for future change in the environment (Perkins and Swain 2009; Bruggeman et al. 2020). In this study with *Saccharomyces cerevisiae*, a single-cell eukaryote, I will address two questions:

1. how cells regulate ribosomal levels as the environment changes in batch cultures;

2. given two non-glucose carbon sources, how cells prioritise which to use.

To build the general context of this study, in this chapter, I will first review how cells coordinate the ribosome levels with growth, especially the well studied "growth laws" in *Escherichia coli*. Then, I will review the galactose *GAL* and palatinose *MAL* networks in *S. cerevisiae*, before moving to the glucose repression of *GAL* and *MAL*, the best known case of cells prioritising one substrate over another in *S. cerevisiae*. Last, I will review how mechanistic models explain Monod's equation and how this law can be generalised to multiple limiting substrates to give context to the result from our mechanistic model in Section 3.4.

1.1 The microbial "growth laws"

To grow, microbes import nutrients from the environment, convert the nutrients into biomass precursors, and synthesise biomass to duplicate themselves. This process is highly complicated, involving a large set of genes and biochemical reactions, but simple behaviours like the "growth laws" emerge from this complexity.

1.1.1 The steady-state growth of *Escherichia coli* can be characterised by simple "growth laws"

Cell growth requires ribosomes, and Schaechter *et al* (Schaechter, MaalØe, and Kjeldgaard 1958) first discovered that the mass of ribonucleic acid (RNA) per 10^7 cells, which is proportional to the ribosomal mass fraction, linearly increases with the specific growth rate at steady-state growth in *Salmonella typhimurium* when the growth rate is controlled by the medium (Fig 1.1A). Scott *et al* (Scott et al. 2010) revisited this empirical observation in *E. coli* and formalised it by writing the ribosome level (r) as a function of specific growth rate (λ), sometimes known as the "first law":

$$r = r_0 + \frac{\lambda}{\gamma} \tag{1.1}$$

where r_0 and γ are constants over different growth conditions. r_0 is interpreted as the inactive ribosomal fraction and γ the translation rate per active ribosome. Under this interpretation, γ should change if translation is perturbed, and indeed, γ changes in translational mutants or under chloramphenicol treatment (which affects translation by reversibly binding to the ribosomes) (Scott et al. 2010). In the dataset with chloramphenicol treatment (Scott et al. 2010), focusing on how r and λ change with increasing concentrations of chloramphenicol, Scott *et al* found that r increases linearly with decreasing λ (Fig 1.1A), sometimes known as the "second law":

$$r = r_{max} - \frac{\lambda}{\kappa_n} \tag{1.2}$$

where r_{max} and κ_n are constant. The interpretation of r_{max} is the maximum ribosome level that cells can achieve, at which the growth rate approaches zero.

In addition, Scott *et al* (Scott et al. 2010) reported that the expression of unregulated proteins linearly decreases with increasing specific growth rate, and that the specific growth rate decreases linearly with increasing expression of gratuitous proteins.

1.1.2 The "growth laws" emerge from a proteome allocation constraint and flux balance at steady-state growth

How do the simple "growth laws" emerge from the complexity of cell growth? Scott *et al* (Scott et al. 2010) proposed a simple model assuming the total mass concentration of protein in a cell is constant. In this model, the size of the proteome is fixed and divided (or "coarse-grained") into three sectors — the fixed core sector Q, the ribosome sector R and the metabolic sector P. Sectors R and P change with the specific growth rate but are constrained by the fixed size of proteome — the proteome allocation constraint, and the metabolic flux through P and the translation flux through R must match at steady-state growth (Scott et al. 2010).

This simple model can explain the "growth laws" in the previous section. For the "first law", when the nutrient quality increases, the R sector expands with higher growth rate because the nutrient is readily consumed by a smaller P sector; for the "second law", when the concentration of chloramphenicol increases, the translation rate decreases and the R sector must expand to balance the flux from the P sector (Scott et al. 2010). Similarly, the unregulated protein decreases with the specific growth rate because the R sector expands, and the specific growth rate decreases with the increasing expression of gratuitous proteins because this expands the Q sector (Scott et al. 2010).

Subsequent work from the same lab added details to this model. You *et al* (You et al. 2013) found that the catabolic flux matches the anabolic flux at steady-state growth by titrating the catabolic and anabolic fluxes, and this result suggests that the P sector can be further divided into the catabolic sector C and the anabolic sector A (and the "uninduced" sector U). Given that each proteome sector except Q has a characteristic dependency on growth rate under catabolic, anabolic and translation flux limitations, Hui *et al* (Hui et

al. 2015) identified the proteins and their corresponding gene ontology (GO) terms in each sector with proteomics.

How do cells decide when to expand or shrink a proteome sector in *E. coli*? In a recent review by Scott and Hwa (Scott and Hwa 2022) (Fig 1.1B), cells detect flux mismatch by the sizes of the α-keto acid pool and the amino acid pool — when the carbon flux is larger than the anabolic flux, cells accumulate α-keto acid, which represses the C sector via the cAMP-Crp signalling system; when the anabolic flux is larger than the translation flux, cells accumulate amino acids, which represses the A sector by end-product inhibition and expands the R sector by activating ribosome biogenesis via ppGpp signalling.

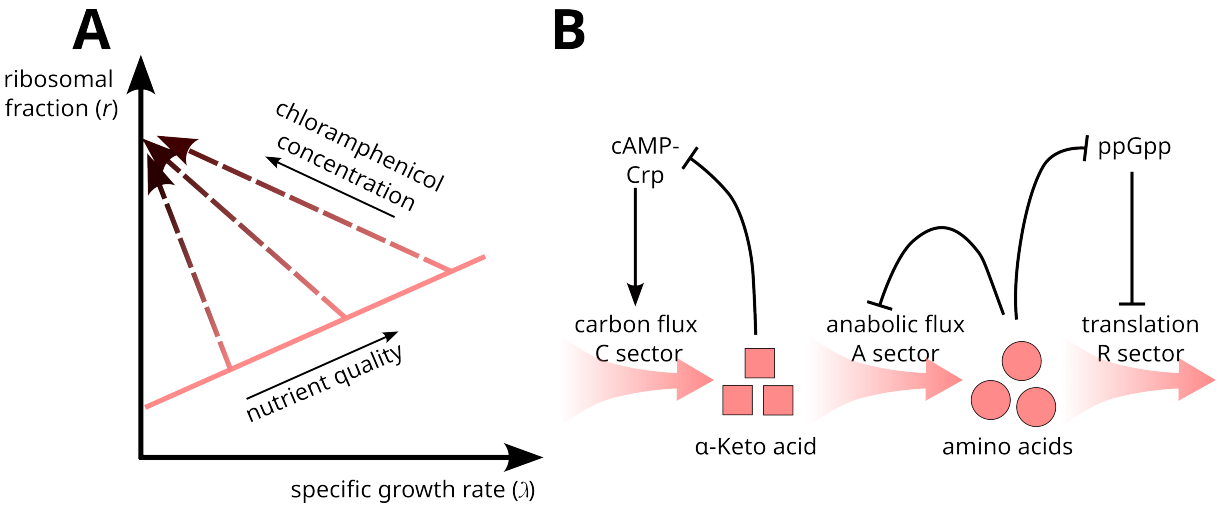

Figure 1.1: **(A)** The microbial "growth laws" and **(B)** a model proposed by (Scott and Hwa, 2022). Both panels are adapted from (Scott and Hwa, 2022).

1.1.3 The linearity of the "growth laws" can emerge from flux sensing motifs or highly efficient enzymes, but slow growth may challenge the linearity

Perhaps the most striking aspect of the "growth laws" are their linearity — if we ignore the intercept for now, the linearity means the sector size (or enzyme concentration) is proportional to the flux through it.

Scott and Hwa (Scott and Hwa 2022) showed that the proportionality between flux and enzyme concentration can be achieved using a simple flux sensing motif, in which (1) the signalling molecule S shares the same linear pathway as enzyme Z; (2) the flux as a function of $[S]$ is Michaelis-Menten; (3) regulation guarantees that $[Z] = c[S] \propto [S]$

and (4) the flux is not "too small". In the simplest case where S is the direct substrate of Z, the flux $v = \frac{k_{cat}[Z][S]}{[S]+K_s} = \frac{k_{cat}[Z]}{1+cK_s/[Z]} \approx k_{cat}[Z](1 - cK_s/[Z]) = k_{cat}([Z] - cK_s)$, and the approximate linearity requires $(K_s/[S])^2 \ll 1$. In the current model (Scott and Hwa 2022), the α-keto acid and the charged tRNAs are the substrates of the A sector and R sector, respectively.

Alternatively, Bruggeman *et al* (Bruggeman et al. 2020) proposed that this linearity may arise from the enzymes (e.g. ribosomes) have high affinities to substrates and low affinities to products, such that the flux per unit protein is maximised.

However, slow growth may challenge the linearity of the "growth laws". First, the above flux sensing motif requires the flux not to be too small. Second, in the current model (Scott and Hwa 2022), each proteome sector is divided into a basal part Φ_i^0 and the growth-dependent part $\Delta\Phi_i(\lambda)$, and the flux is assumed to be proportional to *only* the growth-dependent part: $v \propto \Delta\Phi_i$. It remains unclear what the nature of the basal part is and how the basal part contributes to growth when growth is slow and the basal part dominates the sector.

1.1.4 How general do the "growth laws" apply to microbes, and why?

Experimental data showed that the "first law" holds for multiple microbial species. Scott *et al* (Scott et al. 2010) compiled the data of *Aerobacter aerogenes*, *Candida utilis*, *Neurospora crassa* and *Euglena gracilis* and showed that the "first law" holds in those bacterial species. Metzl-Raz *et al* showed that the "first law" also holds for *S. cerevisiae* (Metzl-Raz et al. 2017).

Given that these species are adapted to different ecological niches and even include both prokaryotes and eukaryotes, the question why it is so general. If the protein concentration is the constraint that limits growth (see Section 1.1.2), Bruggeman *et al* (Bruggeman et al. 2020) argued that a small percentage of deviation from the optimal level of ribosome leads to a large fitness effect. Even for microbes in which the protein concentration is not the constraint, deviation from the optimal level could still have fitness effect, because making excessive ribosomes costs energy and amino acids. Thus, for fast-growing

microbes which compete for limited resources, the ones which gets the closest to the optimal level (and hence shows the "first law") are most likely survive, which could explain the generality of the "first law".

1.2 Diauxie of microbes

Diauxie is a phenomenon first discovered by Monod (Monod 1947) that the growth of a bacterial population on a mixture of two carbon sources experienced two exponential phases, separated by a lag. The cause of diauxie is that the cells exclusively consume one carbon source, and upon the depletion of the first one, they "adapt" to consuming the other. This was first shown by Monod by varying the concentration of the two carbon sources and measuring the increase in cell number (measured by optical density (OD)) during each exponential phase of growth — the concentrations of the first and second carbon sources respectively correlate with the increase during the first and second exponential phases (Monod 1947).

Associated with the diauxic growth is a lag phase between the two exponential phases, during which the cells adapt their metabolism to the second carbon source ("enzymatic adaptation") (Monod 1947). The length of this lag depends on the concentration of the two carbon sources and may depend on the growth history before the cells were inoculated into the mixture of carbon sources — the lag disappeared when the concentration of the first carbon source is low, and the lag can be shortened when the cells were exposed to the second carbon source prior to the growth on the mixture (Monod 1947).

1.2.1 Diauxic lag and adaptation lag

The concept of a diauxic lag is closely related to but different from the adaptation lag when cells are faced with an abrupt shift from one environment to another (e.g. from one carbon source to another). For example, a recent study by Basan *et al* (Basan et al. 2020) showed that when a shift from a glycolytic substrate to a gluconeogenic substrate occurs, the inverse of adaptation lag is proportional to the pre-shift growth rate, and the bottleneck of this adaptation is the number of gluconeogenic enzymes. This is similar to the diauxic lag in the sense that they both involve an adaptive process, yet different

because the diauxic lag involves the repression of the adaptation to the second carbon source when the cells exclusively consume the first carbon source. In fact, when exposed to one glycolytic substrate and one gluconeogenic substrate, cells co-consume both of them in the tested cases of *E. coli*, in which co-consumption leads to a higher growth rate than consuming a single carbon source (Hermsen et al. 2015), and thus, there is no diauxic lag despite the existence of the adaptation lag.

1.2.2 Known cases and rules of diauxie or sequential utilisation

Before one can move on to ask the principles behind diauxie, one must first review the known cases of diauxie and find general rules. I also include some cases where cells sequentially use two carbon sources, but there is no visible lag.

In *B. subtilis*, the substrates can be divided into two sets in which the enzyme of the substrate is either "constitutive" (set A) or "adaptive" (set B), and this division is not associated with the chemical configuration of the substrates (Monod 1947). Cells show diauxie whenever growing on a mixture of one substrate in set A and the other in set B, whereas cells growing on mixtures of sugars in set A do not show diauxie (Monod 1947).

In *E. coli*, cells prioritise glucose over lactose and other carbon sources via both global control of the cAMP-cAMP receptor protein (cAMP-CRP) system, operon-specific inducer exclusion and induction prevention (Görke and Stülke 2008). They also prioritise lactose over glycerol when the lactose import flux is high enough and otherwise co-utilise both (Okano et al. 2020). Arabinose is prioritised over xylose in a concentration-dependent manner (Koirala, Wang, and Rao 2016).

In budding yeast *S. cerevisiae*, cells prioritise glucose over galactose, maltose, sucrose, ethanol (Gancedo 1998) and substrates of the Jen1 transporter (Chambers, Issaka, and Palecek 2004) including lactate and pyruvate. They also prioritise fructose, mannose and sucrose over Jen1's substrates (Chambers, Issaka, and Palecek 2004), and acetate over ethanol (Simpson-Lavy and Kupiec 2019). A close look into the doubling time of the *gal80*Δ mutant strain growing on raffinose suggests that cells might prioritise galactose over raffinose (Ideker et al. 2001).

A rule that appears to emerge in both *E. coli* and budding yeast is that if sequential

utilisation is observed, the first carbon source to be metabolised supports growth at a higher rate, with exceptions where the first and second carbon sources supports a similar growth rate, for example, glucose and lactose in some *E. coli* strains (Okano, Hermsen, and Hwa 2021), glucose and sucrose in budding yeast, and mixtures of A substrates in *B. subtilis*. However, this rule does not hold *vice versa*, i.e. if carbon source A supports faster growth than B, there is no guarantee that cells prioritise A over B. Also, the chemical configuration of substrates is unlikely to determine the order of consumption (Monod 1947).

1.2.3 The objectives and constraints behind diauxie

Why must cells prioritise one carbon source over another? If such prioritisation is an optimal strategy selected by natural selection, an objective and a constraint should exist. An intuitive guess on the objective based on the rule in the previous section is to maximise the growth rate at steady state, and as noted in Section 1.1.2, in *E. coli*, a constraint on size of the proteome, or the concentration of the total intracellular protein can exist (Scott et al. 2010; You et al. 2013). If this pair of objective and constraint is true, it will be disadvantageous if a cell simultaneously expresses the enzymes of both carbon sources, because the enzymes that metabolises the "slow" carbon source compete with those which metabolises the "fast" one, leading to a lower growth rate. However, this does not explain the exceptions to the rules mentioned above, and further question arises that why this rule does not hold *vice versa* — is it because an additional layer of regulation costs part of the proteome, or is it simply because the observed strategy is not yet fully optimal?

One can further ask whether the constraint on proteome size is also true for budding yeast, which is a eukaryote with more intracellular compartments, and in which compartment this constraint may exist. Elsemann *et al* (Elsemman et al. 2022) systematically analysed the yeast proteome growing on glucose at different growth rates, and found that the constraint on growth could be respectively hexose transport, cytosolic protein and mitochondrial capacity at low, medium and high growth rates. The constraint on hexose transport could be caused by the constraint on the number of transporters on the membrane. In fact, instead of keeping all transporters on the surface, yeast shuffles the

hexose transporters to mitigate a rate-affinity trade-off (Montaño-Gutierrez, Correia, and Swain 2022). In addition, the uptake rate of nitrogen sources by constitutive permeases decreases in proportion to the yeast cells' surface-to-volume ratio, suggesting that a space limitation may exist on the cytoplasmic membrane (Hennaut, Hilger, and Grenson 1970).

1.2.4 Why does the diauxic lag exist, and can cells avoid it?

The diauxic lag arises because it takes time for the cells to sense the second carbon source and express the corresponding enzymes when the first runs out. Although the second carbon source exists throughout, the cells may not be able to sense it when the first carbon source runs out, as shown in the example of glucose-lactose diauxie of *E. coli* (Julou et al. 2020). This raises an interesting question about whether the population can avoid this lag by preparing earlier for the adaptation to the second carbon source.

Studies on yeast's glucose-galactose and glucose-maltose diauxie suggest that although the diauxic lag is evolvable, there exists a trade-off between maximising growth rate in glucose and minimising lag during diauxic shift (Wang et al. 2015; New et al. 2014; Perez-Samper et al. 2018; Boocock et al. 2021). Some strains may start to induce the *GAL* genes hours before the depletion of glucose and therefore show a very short diauxic lag or no diauxie at all (Wang et al. 2015). This variability in the diauxic lag can be caused by a genetic variability in either the glucose repression signalling pathway or the *GAL* network. New *et al* (New et al. 2014) showed that the mutations in *HXK2* or *STD1* obtained by experimental evolution lead to a shorter lag (in glucose-maltose diauxie). Perez-Samper *et al* (Perez-Samper et al. 2018) showed that stronger respiration in the glucose phase achieved by overexpressing *HAP4* leads to a shorter lag. Boocock *et al* (Boocock et al. 2021) found that strains with alternative alleles of *GAL* genes have higher expression of *GAL* genes in glucose and show no diauxie. However, independent of specific mechanisms, strains with a shorter diauxic lag suffer a fitness penalty in glucose (Wang et al. 2015; New et al. 2014; Boocock et al. 2021), which suggests that a trade-off exists between maximising growth rate in glucose and minimising lag during diauxic shift, and the variability of the wild strains suggests that both objectives may be important, and minimising the lag could be more important for strains that live in a less stable

environment (Wang et al. 2015) or a dairy-rich environment (Boocock et al. 2021).

1.2.5 What evolutionary history gives rise to diauxie?

The strategy of a microbe to consume multiple carbon sources is contingent on its evolutionary history. In the case of budding yeast, little of which is known — we have not identified the ecological niche of *S. cerevisiae* and Goddard and Greig even proposed that it might be a nomadic species without a niche (Goddard and Greig 2015). This is different from *E. coli*, whose niche is the intestines of warm-blooded animals and reptiles, and they are the pre-dominant aerobic bacteria, albeit outnumbered by anaerobic bacteria, and they also transit in water and sediment (Tenaillon et al. 2010), although its evolutionary history is still unclear. Therefore, although *S. cerevisiae* is similar to *E. coli* in the sense that it is also a fast-growing microbe that consumes multiple carbon sources and also shows diauxie, there is no *a priori* reason to believe that the evolutionary history and principle of diauxie is the same.

The evolutionary history that gives rise to diauxie remains unclear, but we can imagine what environments may favour diauxie and what not. First, for *E. coli* in chemostats where all carbon sources occur combined and in low amounts, the strategy is co-consumption (Okano, Hermsen, and Hwa 2021), so a chemostat-like environment may not favour diauxie. Second, assuming that the diauxie is always accompanied by the trade-off between fitness and the length of the diauxic lag (reviewed in Section 1.2.4), then an environment where all carbon sources occur briefly and irregularly may not favour diauxie.

From the known cases of diauxie and co-consumption of *E. coli*, we might speculate upon its niche. The intestine and river are known habitats of *E. coli* (Tenaillon et al. 2010), which may be similar to a chemostat (Okano, Hermsen, and Hwa 2021), and such conditions should favour co-consumption of carbon sources. Yet, *E. coli* adopts the diauxic strategy in multiple combinations of carbon sources (see Section 1.2.2). This raises questions whether *E. coli* belongs to yet undiscovered niche(s), and whether this is a strategy adopted by the ancestor of *E. coli* which lives in a different habitat.

1.2.6 Motivation of this study

Above I introduced the important questions on diauxie of microbes. The first challenge of answering those questions in yeast is that we do not yet have a systematic study on the non-glucose diauxie cases. Do other examples of diauxie, or sequential utilisation of carbon sources, exist, or is glucose special? The only direct example beyond glucose that I am aware of is reported by Simpson-Lavy and Kupiec (Simpson-Lavy and Kupiec 2019), who showed that the presence of acetate represses ethanol metabolism by repressing the alcohol dehydrogenase gene *ADH2* via Haa1 but not Snf1/Adr1, which perhaps has a simple explanation: end-product inhibition which avoids accumulation of intracellular acetate.

However, looking into the literature, some evidence does suggest that glucose is not the only preferred carbon source. The earliest evidence dates back to 1947, when Spiegelman and Dunn showed that in the absence of external nitrogen source and in the presence of both maltose and galactose, the induction of "galactozymase" leads to a decrease in the induction level of "maltozymase" (Spiegelman and Dunn 1947), suggesting that galactose might be preferred over maltose. Heredia (Heredia 1998) also proposed that the presence of galactose may affect maltose transport, but this research mainly used a *gal80*Δ mutant strain and lacked a wildtype control, making the results difficult to interpret. Data in (Ideker et al. 2001) suggested that galactose may repress the metabolism of raffinose, because the *gal80*Δ mutant, in which the *GAL* network is constitutively active, shows slow growth in 2% raffinose. Consistent with this observation, Gancedo *et al* (Gancedo, Flores, and Gancedo 2015) also found that galactose prevents the induction of the *SUC2* gene by low concentrations of glucose. Metabolism of raffinose requires one extracellular enzyme, the sucrose invertase encoded by *SUC2*, so it is possible that *SUC2*'s expression is negatively affected by *gal80*Δ. Expression of *GAL2* may contribute to the repression on *SUC2*, because the *gal80*Δ *gal2*Δ double-mutant partially restore the gene expression profile (Ideker et al. 2001). In addition to *SUC2*, galactose also represses *CYB2* (Lodi, Donnini, and Ferrero 1991), which is required for lactate metabolism.

We will show in Chapters 4 and 5 that cells prioritise galactose over palatinose in budding yeast, explore the mechanism behind it and in Chapter 6, discuss how this

example, along with other non-diauxie examples, adds to the answer to the questions mentioned above.

One question, *how* cells prioritise one carbon source over another, remains to be reviewed in Section 1.5 after the molecular contexts of the *GAL* and *MAL* networks in budding yeast are built in Sections 1.3 and 1.4.

1.3 The *GAL* network in *S. cerevisiae*

The *GAL* network is responsible for the metabolism of galactose (and melibiose in some strains). The *GAL* network is inducible, but subject to glucose repression — the *GAL* genes are only expressed when galactose is present and glucose concentration is not high. The *GAL* network has been intensively studied as an example of regulatory circuit (reviewed in (Pannala et al. 2010)), catabolite repression (See Section 1.5) and cellular memory (Stockwell, Landry, and Rifkin 2015), and widely used to induce gene overexpression in both budding yeast (Lee et al. 2015) and other model organisms (Elliott and Brand 2008; Asakawa and Kawakami 2008). However, most studies focused on the local behaviour of the activation of the *GAL* network, instead of the global physiological effects *GAL* may incur. In the following sections, I will briefly review the *GAL* network's structure and activation, before moving to reviewing its effects on cell physiology beyond galactose metabolism. I will also review the metabolism of melibiose in the last section.

1.3.1 The *GAL* network consists of one metabolic pathway and one signalling pathway

The *GAL* network encodes a metabolic pathway which converts galactose into glucose-6-phosphate, which then enters glycolysis (Fig 1.2A) (Sellick, Campbell, and Reece 2008). This pathway, known as the Leloir pathway, consists of five enzymes in budding yeast: galactokinase Gal1, galactose-1-phosphate uridyl transferase Gal7, UDP-glucose-4-epimerase Gal10 and phosphoglucomutases Pgm1/2, and Gal2 or other hexose transporters transport galactose into the cell (Sellick, Campbell, and Reece 2008).

The signalling pathway has three components, the galactose sensor Gal3, the repressor Gal80 and the transcription activator Gal4 (Fig 1.2B). Gal4 is a transcription factor

that binds to a symmetric DNA sequence (`CGGA(g/c)GAC(a/t)GTC(a/t)TCCG`) (Giniger, Varnum, and Ptashne 1985) as a dimer (Marmorstein et al. 1992). This binding site is known as UAS_{GAL} and can be found in the promoters of most *GAL* genes (*GAL1*, *GAL7*, *GAL10*, *GAL2*, *GAL3*, *GAL80* and *PGM2*) and some other genes (see Section 1.3.3). In the absence of galactose, Gal80 binds to Gal4's activation domain, so Gal4 cannot activate transcription even if it binds to the UAS_{GAL}. Upon the presence of galactose, adenosine triphosphate (ATP) and nicotinamide adenine dinucleotide phosphate (NADP) induce a change of Gal3's conformation and enable it to bind to Gal80 (Lavy et al. 2012; Li, Chen, and Liu 2010; Kumar et al. 2008). This binding releases Gal4 from repression by Gal80 and thus leads to activation of the *GAL* genes, but it remains unclear whether the Gal3-Gal80 complex remains bound to Gal4 or not (Jiang et al. 2009; Abramczyk et al. 2012). Last, it is also notable that *GAL1* and *GAL3* are homologs and replacing *GAL3*'s coding sequence with *GAL1*'s results in moderate growth defect in galactose, which suggests that Gal1 can also sense galactose (Hittinger and Carroll 2007).

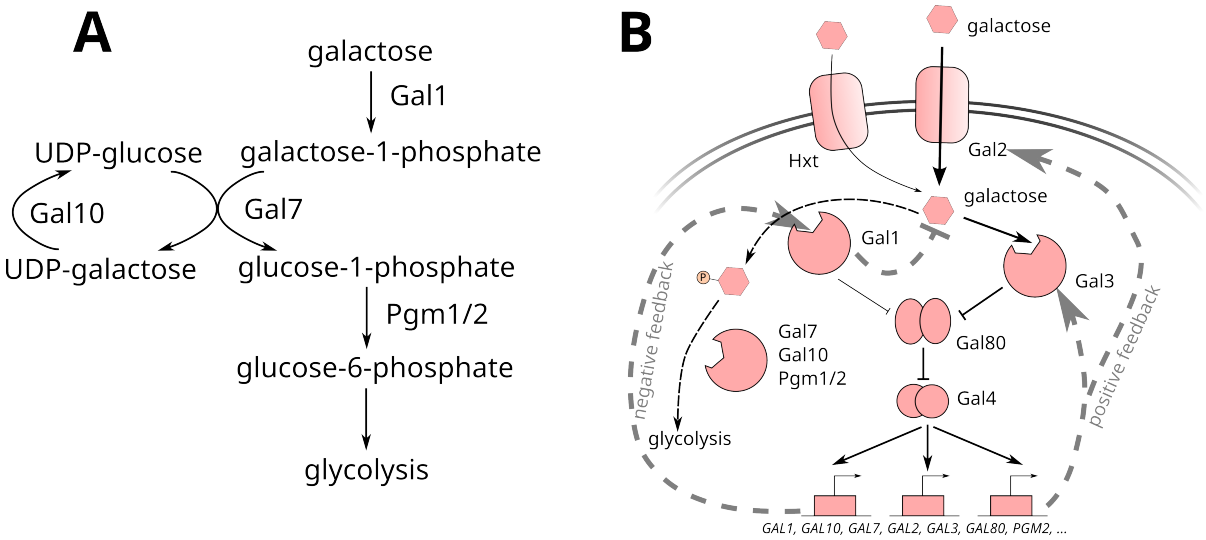

Figure 1.2: The *GAL* network of *S. cerevisiae*. **(A)** The Leloir pathway that metabolises galactose. **(B)** The regulation of *GAL* network. In (B), the black dashed lines represent the metabolic pathway, and the black solid lines represent signal transduction, and the gray dashed lines represent feedbacks.

1.3.2 The *GAL* network has multiple feedbacks and exhibits a bimodal response within a certain range of galactose concentrations

The *GAL* network has multiple feedbacks (Fig 1.2B). In the absence of galactose, one negative feedback exists — Gal4 activates the expression of *GAL80*, and Gal80 binds to Gal4 and represses its activity. When galactose is present, two positive feedbacks and one negative feedback exist (Acar et al. 2005). First, the positive feedbacks via Gal2 and Gal3 — hexose transporters and Gal2 import galactose, and intracellular galactose increases and is sensed by Gal3, and Gal3 releases Gal4 from Gal80 repression, and Gal4 activates the expression of *GAL2* and *GAL3*. Therefore the transport and sensing of intracellular galactose further increase. Second, the negative feedback — intracellular galactose increases and activates Gal4 as stated above, but Gal4 activates the expression of genes in the Leloir pathway, and intracellular galactose is metabolised and hence decreases. Additionally, as Gal1 is later found to also sense intracellular galactose like Gal3 (Hittinger and Carroll 2007), another positive feedback via Gal1 exists, which is parallel to that via Gal3.

The feedbacks within the *GAL* network generate a *steady-state* bimodal response within a range of galactose concentrations (Acar et al. 2005; Song et al. 2010; Venturelli, El-Samad, and Murray 2012). Notably, depending on whether the cells were pre-grown on raffinose (which neither induces nor represses the *GAL* network) or on galactose (which induces the *GAL* network), the range of galactose concentrations for the bimodal response is different, which is known as "persistent memory" or "hysteresis" and suggests that the *GAL* network is deterministically bistable (Acar et al. 2005; Venturelli, El-Samad, and Murray 2012). First of all, perhaps intuitively, Gal80 is required for this bistability (Biggar and Crabtree 2001; Acar et al. 2005), because Gal80 is an integral part of all feedbacks. To further understand why this bistability exists, a common method is to systematically abolish the feedback on a *GAL* gene by replacing its Gal4-responsive promoter with a P_{TET} promoter controlled by doxycycline (Acar et al. 2005; Venturelli, El-Samad, and Murray 2012) or a *CYC1* promoter (Ramsey et al. 2006). With this method, Venturelli *et al* (Venturelli, El-Samad, and Murray 2012) found that abolishing the feedback on both

GAL1 and *GAL3* leads to a graded response without bistability and ultrasensitivity to galactose concentration. This result suggests that the feedback on *GAL3* contribute to the bistability (Venturelli, El-Samad, and Murray 2012), but perhaps counter-intuitively, the feedbacks on *GAL3* and *GAL80* suppress the bimodality when the cells pre-grown in raffinose are induced with galactose and enable cells to reach the steady state faster (Ramsey et al. 2006).

1.3.3 Gal4 controls multiple genes which are not directly linked to galactose catabolism

In addition to the *GAL* genes, Gal4 also activates multiple genes which have no direct link to galactose signalling or metabolism. Magdolen *et al* (Magdolen et al. 1990) reported that *GCY1*, which encodes an oxidoreductase, is activated by Gal4. Combining chromatin immunoprecipitation (ChIP) and DNA microarray, Ren *et al* (Ren et al. 2000) systematically identified four novel Gal4 targets — uracil permease *FUR4*, oxidoreductase *GCY1*, regulator of hexose transporters *MTH1* and cyclin *PCL10*. *LAP3* (*GAL6*), which encodes a cysteine aminopeptidase, was also found to be activated by Gal4 and the *lap3*Δ mutant shows higher expression of *GAL* genes (Zheng, Xu, and Johnston 1997). *REE1* is also found to be a target of Gal4 and regulate the expression of *ENO1* (Choi et al. 2008). The Gal4 binding site can be found in all genes above, so the activation is the result of direct activation by Gal4.

1.3.4 Gal4 has physiological effects beyond activation of *GAL* genes

In the previous section, we introduced a small set of well-characterised non-*GAL* genes that are directly controlled by Gal4. In fact, the Gal4 binding sites are wide-spread in the genome — there are more than 200 putative Gal4 binding sites and at least 29 are in the promoter region of a gene (Li and Johnston 2001). Some Gal4 binding sites are within the coding sequence of a gene, and Li and Johnston (Li and Johnston 2001) found that Gal4's binding to *ACC1*'s coding sequence leads to a decrease in its expression. In addition, Gal4 can also activate the expression of a gene linked to the telomere through

telomere looping, if a binding site exists 1–2 kbase pair (bp) downstream of the gene (de Bruin et al. 2001). Therefore, Gal4 may affect multiple genes, and the change in the expression of those genes may further propagate to their downstream genes — activation of Gal4 has physiological effects beyond the local activation of the *GAL* genes.

Indeed, Gal4 indirectly affects the expression of genes without the Gal4 binding site. Overexpressing Gal4 or activating Gal4 by galactose leads to decrease in the promoter activity of promoters with Gcn4 binding sites or Hap1 and Hap2/3 binding sites (Gill and Ptashne 1988) and decrease in expression level of *GDH1* and *CYB2* (Lodi, Donnini, and Ferrero 1991), which participate in glutamate and lactate metabolism, respectively. In addition, Gill and Ptashne (Gill and Ptashne 1988) found that overexpression of Gal4 affects *HIS3*'s inducible transcription without affecting its constitutive transcription, even though *HIS3* does not have a Gal4 binding site in its promoter.

The above observations prompted hypotheses on how Gal4 may have those indirect effects — for example, Gill and Ptashne (Gill and Ptashne 1988) speculated that a TATA-binding protein (TBP) may participate in the interaction between a binding site and a transcription factor, so if Gal4 is high, it will sequester this protein and inhibit transcription regulated by other transcription factors. In fact, Gal4 activates transcription of target genes by recruiting TBP, Spt-Ada-Gcn5 acetyltransferase (SAGA), the SWI/SNF complex, the mediator and other factors to the promoter (Travan, Jelicic, and Sopta 2006). Among them, SAGA and the mediator are also required for transcriptional activation by another transcription factor Gcn4 (Fishburn, Mohibullah, and Hahn 2005), whose activity is decreased by Gal4 overexpression, as mentioned above. Although there is no direct evidence, it is possible that high Gal4 sequesters the limited pool of some intermediate factors for transcriptional activation, which are shared between transcription factors.

Above we discussed how Gal4 can directly and indirectly affect gene expression, and it is logical to expect those effects to propagate into the cells' phenotype. For example, Gal4 directly up-regulates the expression of *MTH1* (Ren et al. 2000), a regulator of the hexose transporters, so the hexose transport of the cells may change. Indeed, Ideker *et al* (Ideker et al. 2001) reported that the *gal80*Δ mutation, which leads to constitutive activation of Gal4, causes slow growth of cells on 2% raffinose, and that this growth defect can be alleviated by further deleting *GAL2*, the galactose transporter, through an

unknown mechanism. This result raises interesting questions like whether budding yeast cells prioritise galactose over raffinose and why so, yet there is no follow-up study as far as we know.

1.3.5 *MEL1* encodes a melibiase and is activated by Gal4 and possibly Mth1

In this final section, I will briefly review *MEL1*, which encodes an extracellular α-galactosidase (melibiase). Melibiose is a disaccharide consisting of one glucose and one galactose unit, and Mel1 hydrolyses melibiose into glucose and galactose (Sumner-Smith et al. 1985). The promoter of *MEL1* also has one Gal4 binding site and *MEL1*'s expression is induced in the presence of galactose or melibiose (Sumner-Smith et al. 1985). The S288c strain in this study does not have a *MEL1* gene.

The induction of *MEL1* is little studied. Torchia *et al* (Torchia et al. 1984) reported that the expression of *GAL1* and *MEL1* of the *gal80*Δ mutant is lower in galactose than in glycerol-lactate, which they referred to as "self-catabolite repression". This phenomenon could also be seen in the data of a recent preprint (Kar and Bhat 2021). In the same preprint (Kar and Bhat 2021), Kar and Bhat systematically investigated cell growth and gene expression in melibiose and found that some cells' *GAL* network are not induced when the cells were grown in 0.5% melibiose. Surprisingly, they found that the *mth1*Δ mutant has a much longer lag than the wildtype when grown in melibiose and that *mth1*Δ has low expression of *MEL1*, suggesting that Mth1 may positively regulate *MEL1* through an unknown mechanism (Kar and Bhat 2021). However, the results may provide a clue why *MTH1* is up-regulated by Gal4 (see Section 1.3.3).

1.4 The *MAL* network in *S. cerevisiae*

The *MAL* network is responsible for the metabolism of maltose and other maltose-like disaccharides and trisaccharides. Like the *GAL* network, the *MAL* network is inducible but subject to glucose repression, but unlike *GAL*, the *MAL* network is little studied. Most of the *MAL* genes are located at the sub-telomeric regions of chromosomes, a region where genes frequently duplicate and rapidly evolve (Brown, Murray, and Verstrepen

2010). As a result, different strains of *S. cerevisiae* have different copies of *MAL* genes and variable abilities to consume *MAL* substrates. In this section, I will review general knowledge on the *MAL* network, before elaborating the *MAL* network of strain S288c, which we use in this study.

1.4.1 A minimum *MAL* network consists of three components and two feedbacks

A minimum *MAL* network has a simple structure with three components — a transporter, a hydrolase and a transcription factor. When a substrate is present, the transporter imports the substrate into the cell, and the imported substrate is hydrolysed by a hydrolase into glucose and/or fructose. Meanwhile, the imported substrate is also sensed by the transcription activator, which activates the expression of *MAL* genes.

In the presence of a *MAL* substrate, this network has a positive feedback and a negative one (Fig 1.3A). First, the imported substrate causes the transcription activator to activate expression of the *MAL* transporter gene, which in turn imports more substrate and therefore forms a positive feedback. Second, the imported substrate also causes the transcription activator to activate expression of the *MAL* hydrolase gene, which results in faster removal of the imported substrate and therefore forms a negative feedback. The positive feedback in the *MAL* network makes it inducible, that is, without glucose repression, the *MAL* genes are basally expressed in the absence of *MAL* substrates but get activated soon after the substrate is present.

1.4.2 The *MAL* genes are localised in the subtelomeric regions, and some form clusters

The actual *MAL* network of *S. cerevisiae* is complex — *MAL* genes are localised in the subtelomeric regions on different chromosomes, and multiple copies of transporters, hydrolases and activators can co-exist in the genome of one strain.

Some of the *MAL* genes form clusters in the same locus and are localised onto the sub-telomreic region of a specific chromosome. Those loci are *MAL1*, *MAL2*, *MAL3*, *MAL4* and *MAL6*, on Chromsomes VII, III, II, XI and VIII, respectively (Charron et al.

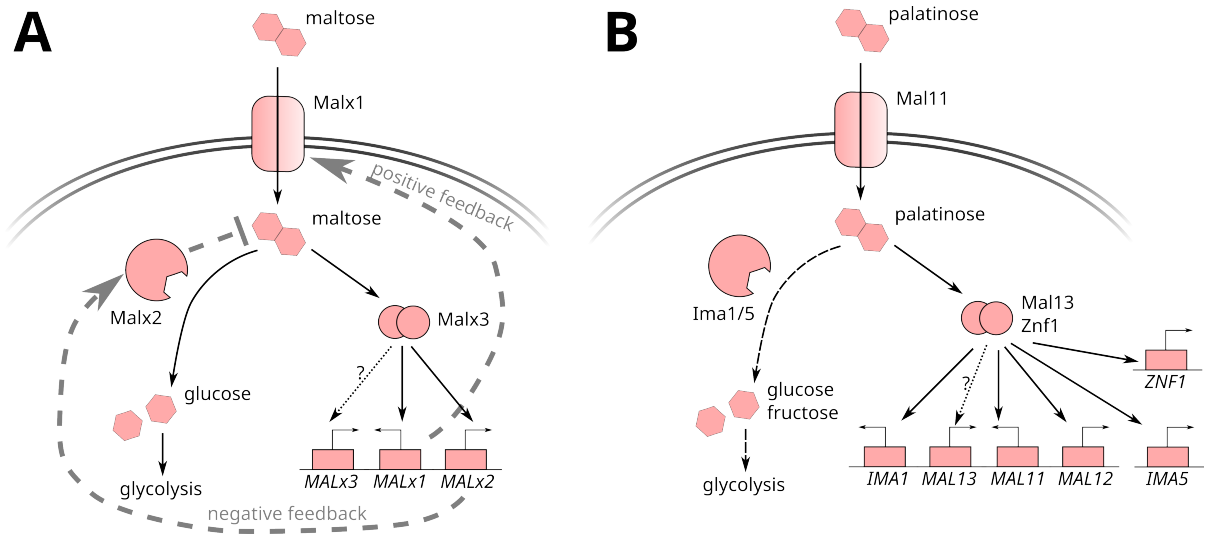

Figure 1.3: The *MAL* network of *S. cerevisiae*. **(A)** A minimal *MAL* network. **(B)** The actual *MAL* network of strain S288c. The black dashed lines represent the metabolic pathway, and the black solid lines represent signal transduction. In (A), the gray dashed lines represent feedbacks.

1989). The structure of each locus is similar (Fig 1.3A), each with a Gene 3 (activator), Gene 1 (transporter) and Gene 2 (hydrolase) in order. Gene 1 and Gene 2 share a bi-directional promoter (Levine, Tanouye, and Michels 1992). Each *MAL* gene in the clusters are named systematically in the form of *MALxy*, in which x represents the locus number and y represents the gene number. For example, *MAL12* is the Gene 2 (maltase) of the *MAL1* locus. Additionally, some clusters may have more than three genes — the *MAL6* locus in strain CB11 has another activator gene, *MAL64*, upstream of *MAL63* (Charron et al. 1989); the *MAL1* locus in the S288c strain has another hydrolase gene, *IMA1*, upstream of *MAL13* (Fig 1.3B). Meanwhile, some other *MAL* genes are not in clusters. For example, in strain S288c, genes of two transporters (*MPH2* and *MPH3*), four hydrolases (*IMA2–5*), two activators (*ZNF1* and *YPR196W*) are not in clusters.

Genes in the subtelomeric regions typically duplicate and evolve faster than other genes, which gives rise to a large functional divergence between homologs of *MAL* genes of *S. cerevisiae* (Brown, Murray, and Verstrepen 2010). (Voordeckers et al. 2012) provides an example how an ancient *MAL* hydrolase with promiscuous substrate specificity evolves into two families, the maltase family and the isomaltase family. The *MAL* activator gene can also duplicate and evolve into binding different motifs on the promoters of *MAL* genes (Pougach et al. 2014). The observations above explain why the *MAL* substrates are so diverse between homologs and between strains, and we will discuss this diversity in the

following sections.

1.4.3 The *MAL* genes metabolise various di- and trisaccharides

Table 1.1 lists the transporters and hydrolases of common *MAL* substrates. The *MAL* transporters are proton-coupled symporters, among which Mal11 (Agt1) has a broad range of substrates whereas Mal31, Mal61 and Mph2/3 are specific to 1,3- and 1,4-α-glucosides (Han et al. 1995; Day et al. 2002). The *MAL* hydrolases are divided into two families, the maltase family and the isomaltase (Ima) family — the maltases metabolise 1,3- and 1,4-α-glucosides and the isomaltases metabolise 1,6-α-glucosides (Voordeckers et al. 2012). Members of both families can also metabolise sucrose (Voordeckers et al. 2012).

1.4.4 Different strains can metabolise different substrates

Each strain only has a subset of all *MAL* genes, so each can only metabolise a subset of *MAL* substrates. Han *et al* (Han et al. 1995) systematically characterised different strains' ability to grow on various substrates. Some strains like W303 can only grow on one substrate, while other strains like CB11 can grow on at least five substrates (Han et al. 1995). In addition, Brown *et al* (Brown, Murray, and Verstrepen 2010) reported that the S288c strains can only metabolise palatinose, whereas Teste *et al* (Teste, Marie François, and Parrou 2010) showed that the CEN.PK113-7D strain can at least metabolise maltose, isomaltose and α-methylglucoside.

1.4.5 Different *MAL* activators respond to different substrates and control different *MAL* genes

MAL activators are activated by intracellular substrates, possibly through direct binding (Wang et al. 2002), and the activated *MAL* activator then binds to the promoters of *MAL* genes and activates their expression. However, given an activator, answers to two questions are largely unknown: (1) which substrates activate that activator; (2) which *MAL* genes are controlled by that activator. The answers could also be strain-dependent, so I summarise what we know so far by strains below.

In strains with the *MAL6* locus, maltose activates Mal63, which then activates the

Table 1.1: List of common *MAL* substrates. The data are compiled from (Han et al. 1995; Day et al. 2002; Teste, Marie François, and Parrou 2010; Deng et al. 2014; Voordeckers et al. 2012; Henderson et al. 2020; Stambuk and de Araujo 2001).

Substrate	**Chemical structure**	**Transporter**	**Hydrolase**
maltose	1,4-α-glucoside	Mal61, Mal11, Mal31, Mph2/3, Mal21	Mal12, Mal32
isomaltose	1,6-α-glucoside	Mal11	Ima1, Ima2, Ima5
palatinose	1,6-α-glucoside	Mal11	Ima1, Ima2, Ima5
turanose	1,3-α-glucoside	Mal61, Mal11, Mal31, Mph2/3	Mal12, Mal32
α-methylglucoside		Mal11, Mph2/3	Ima1, Ima2, Ima5, Mal12
maltotriose	1,4-α-glucoside	Mal11, Mal31, Mph2/3	Mal12, Mal32
sucrose	1,2-β-glucoside	Mal11	Mal12, Mal32, Ima1, Ima2, Ima3/4

transcription of *MAL61* and *MAL62* (Change et al. 1988). Mal64's function is unknown — it does not respond to maltose (Gibson et al. 1997).

The S288c strain can only grow on palatinose if both *MAL13* and *ZNF1* are present (Brown, Murray, and Verstrepen 2010), implying that palatinose can activate Mal13 and Znf1, which activate *MAL12*, *IMA1*, *IMA5* and *MAL11* (Pougach et al. 2014). The reason why both Mal13 and Znf1 are required is unknown, and it is possible that they form heterodimers.

The CEN.PK strains bear a mutant allele of *MAL23*, namely *MAL2-8^c*, which leads to "constitutive" expression of maltase in non-glucose conditions (Zimmermann and Eaton 1974). More recent data in (Teste, Marie François, and Parrou 2010) suggest that in the CEN.PK113-7D strain, although the basal expression of *MALx2* (maltase) is higher than that of *IMAx* by 10–100 fold, maltose can induce another 18.3-fold increase in *MALx2* level, and this induction requires *MAL2-8^c*. The same dataset showed that induction of *IMA1* and *IMA5* by isomaltose or α-methylglucoside also requires *MAL2-8^c* (Teste, Marie François, and Parrou 2010). The results above suggest that the *MALx2* maltase genes in the CEN.PK strains are not truly "constitutive", and instead, *MAL2-8^c* responds to maltose, isomaltose and α-methylglucoside and activates *MALx2*, *IMA1* and *IMA5*. Consistent with the argument on constitutivity above, Gibson *et al* (Gibson et al. 1997) also reported that the maltase activity doubled in response to maltose in a strain bearing the *MAL2-8^c* gene.

In strain RM11-1a, Brown *et al* (Brown, Murray, and Verstrepen 2010) identified two *MAL63*-like genes: *MAL63c9* and *MAL63c2*. Deleting both genes leads to no response in maltose (Brown, Murray, and Verstrepen 2010). Introducing *MAL63c9* into strain S288c enables cells to grow on multiple sugars, including maltose, turanose, maltotriose, α-methylglucoside and sucrose (Brown, Murray, and Verstrepen 2010).

The DNA binding sites of *MAL* activators are also largely unknown. Sirenko *et al* (Sirenko, Ni, and Needleman 1995) identified the Mal63 binding sequence as `(c/a)GCN9(c/a)G(c/g)`. Pougach *et al* (Pougach et al. 2014) also reported the DNA binding sites of Mal63c9 (`CGCN9CGN`) and Znf1 (`CGGN9CGG`), and by comparing the amino acid sequences between Mal63 and Znf1, they showed that the Cys12Arg substitution in Znf1 causes its binding preference for `CGG` over `CGC`.

1.4.6 Strain S288c can only consume palatinose

The wildtype strains we used in this thesis, BY4741 and FY4, are derived from S288c, so in this section, I will focus on what we know about the *MAL* network of S288c.

The S288c strain has in total 15 known *MAL* genes: 4 transporter genes (*MAL11*, *MAL31*, *MPH2* and *MPH3*), 7 hydrolase genes (*IMA1–5*, *MAL12* and *MAL32*) and 4 activator genes (*MAL13*, *MAL33*, *ZNF1* and *YPR196W*). Nonetheless, the S288c strain only grows on palatinose but not any other common *MAL* substrates. Brown *et al* (Brown, Murray, and Verstrepen 2010) showed that *MAL11*, *MAL13* and *ZNF1* are essential for cells to grow in palatinose (Fig 1.3B). Pougach *et al* (Pougach et al. 2014) showed that *MAL12*, *IMA1* and *IMA5* are induced in the presence of palatinose. We can therefore conclude that palatinose activates Mal13 and Znf1, which activate *MAL11*, *MAL12*, *IMA1* and *IMA5*. The reason why both Mal13 and Znf1 are required for palatinose metabolism is unknown, but Mal63 is known to form dimers (Sirenko, Ni, and Needleman 1995), so it is possible that Mal13 and Znf1 form heterodimers that respond to the presence of palatinose.

Why is strain S288c unable to grow on substrates other than palatinose, despite having a set of *MAL* genes that can potentially consume any substrate in Table 1.1? The simplest idea is that the existing *MAL* activators in S288c do not respond to these substrates. Indeed, S288c resumes the ability to grow in maltose, isomaltose and α-methylglucoside when another activator *MAL2-8*^{c} is introduced (Teste, Marie François, and Parrou 2010). However, the data from Brown *et al* (Brown, Murray, and Verstrepen 2010) showed that overexpressing *MAL11* enables cells to grow on turanose, sucrose and isomaltose, which suggests that some activator of S288c does respond to those sugars, but cells are unable to grow because the activator does not regulate *MAL11*, so there is no positive feedback to switch on the *MAL* network (see Section 1.4.1).

Finally, Cerulus *et al* (Cerulus et al. 2016) reported that the single-cell Ima1 level of the S288c strain grown in palatinose is highly heterogeneous, possibly as a result of the positive feedback, and that overexpressing *MAL11* suppresses this heterogeneity.

1.5 Mechanism of catabolite repression in *S. cerevisiae*

Glucose repression occurs both transcriptionally through Mig1 and post-transcriptionally through inactivation of transporters (sometimes called "glucose-induced inactivation" (Medintz et al. 1996)). In the following sections, I will briefly review the molecular mechanism of (1) the glucose signalling, (2) the molecular mechanism of transcriptional repression by Mig1, and (3) the glucose-induced inactivation of the *GAL* and *MAL* transporters.

1.5.1 Cells sense both extracellular and intracellular glucose

Cells sense intracellular substrates to activate the *GAL* and *MAL* networks, but they sense both extracellular and intracellular glucose signals (Fig 1.4A).

Extracellular glucose is sensed by two sensors on the plasma membrane, Snf3 and Rgt2, which activates casein kinases Yck1/2, which phosphorylates two repressors, Mth1 and Std1, and leads to their degradation via the SCF^{Grr1} complex (Horák 2013). The degradation of Mth1 and Std1 releases Rgt1 from repressing gene expression of some hexose transporter genes (Horák 2013). In addition, extracellular glucose is also sensed by the G-protein coupled receptor Gpr1, which activates the G-protein Gpa2, which activates the cAMP-protein kinase A (cAMP-PKA) pathway together with Ras1/2 (Broach 2012). The activated protein kinase A (PKA) hyper-phosphorylates Rgt1 and turns it into an activator that activates expression of *HXT1* (Mosley et al. 2003).

How cells sense intracellular glucose is unclear. Hexose kinases Hxk1, Hxk2 and Glk1 phosphorylate intracellular glucose into glucose-6-phosphate, and Hxk2 contributes to glucose repression (see below). The rest of glycolysis after glucose-6-phosphate does not participate in glucose repression (Rose, Albig, and Entian 1991).

1.5.2 Mig1 and Mig2 repress the transcription of *GAL* and *MAL* genes in high glucose

When glucose concentration is high, Mig1 binds to the promoter of *GAL*, *MAL* and other genes and forms a repressor complex, which leads to low expression of those genes even if galactose or maltose exists (Gancedo 1998). Snf1, Glc7/Reg1 and Hxk2 are key players that relay the glucose signal to Mig1 (Fig 1.4B).

Snf1 is part of a kinase complex similar to the mammalian AMPK complex. Active Snf1 moves nuclear Mig1 into the cytosol, preventing it from functioning as a repressor (Broach 2012). In high glucose, Snf1 is inactive; otherwise, Snf1 is active, which requires phosphorylation by Sak1, Elm1 or Tos3 kinase (Sutherland et al. 2003). However, glucose is not known to directly regulate those three kinases, so the activity of Snf1 is more likely to be regulated by protein phosphatase 1 (PP1) (Kayikci and Nielsen 2015).

PP1 consists of Glc7 and Reg1, which can dephosphorylate and hence inactivate Snf1. Glucose activates PP1, which requires activation of the cAMP-PKA pathway (Castermans et al. 2012), but adenosine diphosphate (ADP) protects Snf1 against this dephosphorylation (Mayer et al. 2011). Reg1 has a homolog, Reg2, which shares overlapping functions with Reg1 (Frederick and Tatchell 1996).

Hxk2 is a hexose kinase but it also participates in glucose signalling. Deleting *HXK2* abolishes glucose repression and leads to co-consumption of glucose and another carbon source (Raamsdonk et al. 2001). Hxk2 interacts with Mig1 to co-repress the *SUC2* gene which encodes the sucrose invertase (Vega et al. 2016). Hxk2 has a signalling function of preventing Snf1 from phosphorylation (Kayikci and Nielsen 2015).

In addition to Mig1, Mig2 also represses a large set of genes that overlaps with Mig1's target genes in high glucose (Westholm et al. 2008). The Mig1/2 repression on *GAL3*, *MAL11* and *SUC2* are partially redundant, but *GAL4* is only repressed by Mig1 (Westholm et al. 2008). Although Mig3 is a homolog of Mig2, it does not seem to control the same set of genes (Westholm et al. 2008).

1.5.3 The Mal61 transporter is phosphorylated, ubiquitylated, endocytosed and degraded when glucose signals are present

In high glucose, in addition to the transcriptional repression by Mig1, the existing maltose transporters are also degraded (Fig 1.5). Medintz *et al* (Medintz et al. 1996) reported that the Mal61 transporter is endocytosed and degraded after cells are switched into glucose, and a recent measurement shows that the half life of Mal61 is 25 ± 6 minutes (Hatanaka et al. 2009).

The signal for Mal61 proteolysis may come from Snf3/Rgt2 glucose-sensing pathway.

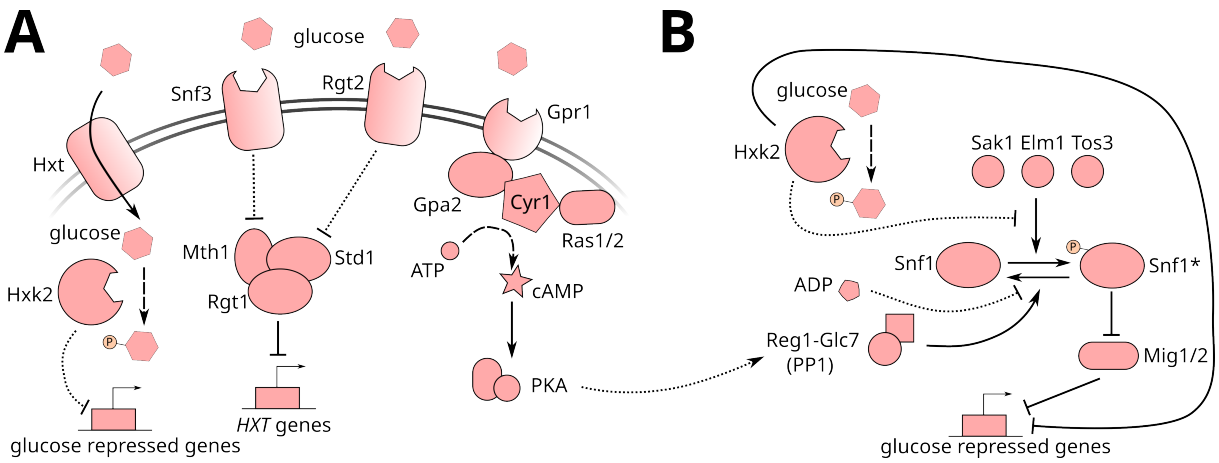

Figure 1.4: Glucose sensing and glucose repression. **(A)** Glucose sensing pathways. **(B)** Glucose repression pathways via Mig1/2. The solid lines represent direct interaction; the dashed lines represent catalytic process of small molecules; the dotted lines represent interaction that may be indirect. Hxt: hexose transporter; PKA: protein kinase A; P: phosphate.

Deleting *RGT2* blocks proteolysis of Mal61, while expressing *RGT2-1*, a dominant suppressor of the *snf3*Δ mutation, leads to constitutive proteolysis of Mal61 (Jiang, Medintz, and Michels 1997). Although deleting *GRR1* blocks both the Snf3/Rgt2 signalling and Mal61 proteolysis (Jiang, Medintz, and Michels 1997), this does not build the causality between Snf3/Rgt2 signalling and Mal61 proteolysis, because *grr1*Δ also leads to slow growth in glucose (Jiang, Medintz, and Michels 1997). In fact, the *grr1*Δ mutant grown in galactose and shows Mal61 proteolysis in even maltose (Jiang, Medintz, et al. 2000).

Additionally, signal from Hxk2/Reg1 may also contribute to Mal61 proteolysis. Deleting both *HXK1* and *HXK2* blocks Mal61 proteolysis (Jiang, Medintz, et al. 2000). Deleting *REG1*, which is part of PP1, slows down Mal61 proteolysis without changing the glucose import rate (Jiang, Tatchell, et al. 2000). Overexpressing *REG2* is the *reg1*Δ mutant partially restores Mal61 proteolysis (Jiang, Tatchell, et al. 2000).

Later, Gadura *et al* (Gadura, Robinson, and Michels 2006) reported that PP1 (Reg1-Glc7) is upstream of the casein kinases Yck1/2. Deleting *REG1*, disrupting Reg1-Glc7 interaction, deactivating Yck1/2 and disrupting the membrane-localisation of Yck1/2 by deleting *AKR1*, lead to a similar phenotype: reduced phosphorylation of Mal61, low maltose transport activity, increased maltose transport upon adding glucose and resistance to glucose-induced proteolysis (Gadura, Robinson, and Michels 2006). Notably, this finding suggests both Snf3/Rgt2 and Hxk2/Reg1 signals are required for Mal61 proteolysis:

upon addition of glucose, Snf3/Rgt2 activates Yck1/2 (Horák 2013), and this activation requires Reg1 (Gadura, Robinson, and Michels 2006), which also responds to the addition of glucose (see Section 1.5.2). Yet, this model does not explain why expressing *RGT2-1* leads to consitutive proteolysis of Mal61 (Jiang, Medintz, and Michels 1997).

The combined effect of both signals is phosphorylation of Mal61, followed by ubiquitylation and endocytosis. Mutating the phosphorylation sites in residues 29–56 prevents proteolysis (Gadura and Michels 2006). Disrupting ubiquitylation of Mal61 by deleting *RSP5*, a ubiquitin-protein lagase (E3), or *DOA4*, a ubiquitin C-terminal hydrolase (E4), also leads to slow proteolysis (Lucero and Lagunas 1997). Gadura *et al* reported that Doa4 acts downstream of Yck1/2, so phosphorylation by Yck1/2 precedes ubiquitylation (Gadura, Robinson, and Michels 2006). Mal61 is ubiquitylated in the presence of glucose, but the *end4*Δ mutation blocks its endocytosis (Hatanaka et al. 2009), suggesting that ubiquitylation precedes endocytosis.

Endocytosis may require the PEST-like region in Mal61. A PEST-like region is a region rich in proline (P), glutamate (E), aspartate (D), serine (S) and threonine (T) (Medintz et al. 2000). Deleting the PEST-like region in the N-terminal of Mal61 (residues 49–78) also leads to no ubiquitylation and longer half-life (Medintz et al. 2000). Consistently, Hatanaka *et al* (Hatanaka et al. 2009) mutated Mal61 at D46G and L50H and obtained a mutant Mal61 with a long half-life (134 minutes).

Notably, not all *MAL* transporters are subject to degradation upon addition of glucose. Mal21's half-life is 118$\pm$5 minutes upon addition of glucose, which is almost 5-fold Mal61's (25 ± 6 minutes), because Mal21 is not ubiquitylated after glucose is added (Hatanaka et al. 2009). In contrast, Mal11 is subject to degradation upon addition of glucose, with a half-life of 13.8 ± 3.8 minutes, and the E55P mutation in Mal11 leads to a long half-life (104.3 ± 7.7 minutes) (Hatanaka 2018).

1.5.4 The Gal2 transporter is ubiquitylated and degraded in the presence of glucose

Similar to Mal61, Gal2 is also endocytosed and degraded upon the addition of glucose (Horak, Regelmann, and Wolf 2002). This degradation is independent of both Gpr1-Gpa2

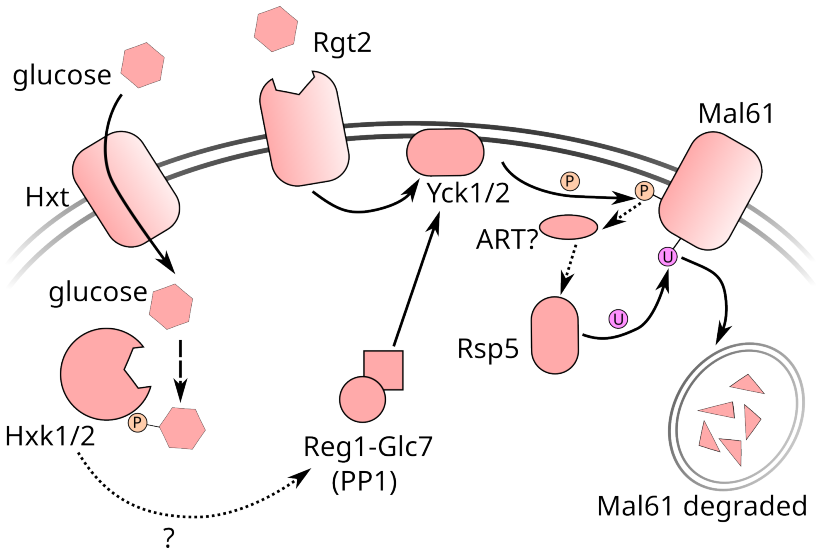

Figure 1.5: Glucose inactivation of the Mal61 transporter. The solid lines represent direct interaction; the dashed lines represent catalytic process of small molecules; the dotted lines represent interaction that may be indirect or unknown. ART: arrestin-related trafficking adaptor; U: ubiquitin; P: phosphate.

and Snf3/Rgt2 sensing systems of extracellular glucose, but depends on hexose phosphorylation by Hxk2 (in glucose, mannose or maltose) (Horak, Regelmann, and Wolf 2002). Similar to Mal61, this degradation is blocked by *grr1*Δ or *reg1*Δ mutation (Horak, Regelmann, and Wolf 2002), but deleting *GRR1* does not change the ubiquitylation pattern of Gal2 (Horak and Wolf 2005). As we mentioned in Section 1.5.3, *grr1*Δ causes slow growth in glucose (Jiang, Medintz, and Michels 1997), so it could be the slow growth (and hence slow glucose phosphorylation), rather than the lack of Grr1, that blocks Gal2 proteolysis.

1.5.5 The glucose-galactose ratio determines the fraction of *GAL*-ON population, but the glucose level determines the ON population's expression level

In Section 1.3.2, I reviewed the feedbacks and bistability of the *GAL* network without glucose repression. For glucose repression in the context of network dynamics, two questions are important — at what concentrations of glucose and galactose the *GAL* network will be repressed, and how the glucose signals alter the induction of *GAL* network.

Intuitively, one might assume that the *GAL* induction occurs if extracellular glucose drops below a threshold, but Escalante-Chong *et al* (Escalante-Chong et al. 2015) found that the *GAL* network switches ON if the ratio between galactose and glucose exceeds

a constant, and that this "ratio-sensing" phenotype is caused by the competitive binding of glucose and galactose to the hexose transporters. The data of Escalante-Chong *et al* (Escalante-Chong et al. 2015) are *steady-state* snapshots of cells grown in different combinations of glucose and galactose concentrations, and Venturelli *et al* (Venturelli et al. 2015) performed a similar experiment but they also recorded how the population reaches steady state over time. Surprisingly, in some combinations of galactose and glucose concentrations, the population diverges into two — one with early *GAL* induction and the other with late induction, and the two subpopulations merged into a single ON population at later time points (Venturelli et al. 2015). To explain this *transient* bimodality, they proposed a model in which the *GAL* network is bistable when the experiment starts, but moves into the monostable ON state when glucose concentration decreases at later time points (Venturelli et al. 2015). However, it remains unclear why extracellular galactose did not decrease at earlier time points, given that a significant subpopulation ($\sim 60\%$) is already ON (Venturelli et al. 2015).

As reviewed in Section 1.5.2, Mig1 and Mig2 respond to glucose signals and repress transcription of *GAL* genes. Does this repression change the ON fraction of the population, or the gene expression level of the ON population? It turns out that Mig1 controls the expression level of *GAL* genes without changing the ON fraction of the population (Biggar and Crabtree 2001; Ricci-Tam et al. 2021), and the transcription of *GAL4*, but not that of *GAL1*, is controlled by Mig1 (Ricci-Tam et al. 2021). Therefore, while the fraction of ON cells at steady state depends on glucose-galactose ratio (Escalante-Chong et al. 2015), the gene expression level of the ON subpopulation is controlled by glucose concentration (Ricci-Tam et al. 2021).

1.6 Monod's equation

Cell growth requires nutrients, and how fast the cells grow depends on the chemical identity of a nutrient and its concentration. Monod (Monod 1949) was the first to quantitatively characterise this dependency, known as Monod's equation. Monod's equation empirically states that given a carbon source, at *steady-state* growth, the *specific* growth rate of a bacterial population (λ) is a simple function of the extracellular nutrient con-

centration s:

$$\lambda = \lambda_K \frac{s}{K_s + s} \tag{1.3}$$

where λ_K and K_s are constants specific to the carbon source (Monod 1949). λ_K is the maximum specific growth rate when the carbon source is saturated, and K_s is the carbon source concentration when $\lambda = \lambda_K/2$. Note that this steady-state growth can be growth in chemostats or exponential growth in batch cultures.

1.6.1 Monod's equation applies to multiple microbe-substrate pairs, but how it emerges is unclear

Monod's equation applies to multiple microbes growing on glucose, including *E. coli* and *M. tuberculosis* (Monod 1949) and *S. cerevisiae* (Mrwebi 2004). Further work shows that Monod's equation applies to cells growing on other nutrients, for example, *E. coli* growing on phosphate (Shehata and Marr 1971) and *S. cerevisiae* growing on raffinose (Montaño-Gutierrez et al. 2022). Monod's equation is also assumed to hold for nitrogen sources in some modelling work (Cramer, Vlassides, and Block 2002; Coleman, Fish, and Block 2007; Henriques and Balsa-Canto 2021), and Bren *et al* (Bren et al. 2013) confirmed that for *E. coli* growing on ammonium, but older literature showed that *E. coli* growing on tryptophan (Shehata and Marr 1971) or ammonium (Lee, Ataai, and Shuler 1984) does not follow Monod's equation.

It remains unclear how Monod's equation emerges and hence how K_s, the Monod constant, should be interpreted. Liu (Liu 2007) reviewed four different approaches to derive Monod's equation, each of which derives or assumes a Monod-like transport/catabolic rate and the specific growth rate is also Monod-like because of flux balance. Alvarez-Ramirez *et al* (Alvarez-Ramirez, Meraz, and Jaime Vernon-Carter 2019) derived an approximate Monod-like growth kinetics using singular perturbation, but their model is the same as the Michaelis-Menten model with the product being auto-catalytic, so it is not surprising that a Monod-like reaction rate arises if the auto-catalytic effect is neglected in the approximation.

Recent progress in microbial growth laws and constraints (see Section 1.1) enables derivation of Monod's equation from self-replicator models. More recently, Scott *et al*

(Scott et al. 2010) derived a Monod-like dependency between specific growth rate and "nutrient quality" (instead of nutrient concentration) by assuming a fixed proteome size and flux-balance between catabolism and translation. Weiße *et al* (Weiße et al. 2015) mechanistically derived Monod's equation at steady state by assuming Michaelis-Menten kinetics of substrate transport and fixed proteome size.

1.6.2 Monod's equation is generalised to multiple nutrients in different forms

The original Monod's equation only applies to one substrate (Monod 1949), but cell growth relies on multiple substrates and their concentrations should affect the growth rate. Several mathematical forms that generalise Eq 1.3 to two substrates have been proposed:

1. the multiplicative form (Megee III et al. 1972): $\lambda = \lambda_K \frac{s_1}{K_{s_1}+s_1} \frac{s_2}{K_{s_2}+s_2}$;
2. the minimum form (Bader 1978): $\lambda = \lambda_K \times \min(\frac{s_1}{K_{s_1}+s_1}, \frac{s_2}{K_{s_2}+s_2})$;
3. the weighted form (Mankad and Bungay 1988): $\lambda = \lambda_K(\frac{K_{s_1}/s_1}{K_{s_1}/s_1+K_{s_2}/s_2} \frac{s_1}{K_{s_1}+s_1} + \frac{K_{s_2}/s_2}{K_{s_1}/s_1+K_{s_2}/s_2} \frac{s_2}{K_{s_2}+s_2})$;
4. the reciprocal form (Bertolazzi 2005): $\lambda = \lambda_K \frac{1}{1+s_1/K_{s_1}+s_2/K_{s_2}}$.

All forms have three parameters: the maximum growth rate λ_K, maximum specific growth rate when the two substrates are saturated, and two Monod constants K_{s_1} and K_{s_2}.

The multiplicative form was first assumed in (Megee III et al. 1972), and Bader (Bader 1978) later found that this form can arise from a two-substrate enzyme model if the parameters are fine tuned, and that the same model can also approximate the minimum form for another regime of parameters. However, this model (Bader 1978) only considered enzyme kinetics without taking into account that the products can be the enzymes themselves. The weighted form is empirical and different from the multiplicative form by a factor $\left(\frac{2K_1K_2}{K_1s_2+K_2s_1}+1\right) > 1$ (Mankad and Bungay 1988).

Bertolazzi (Bertolazzi 2005) first considered the mathematical properties that this generalised function $\lambda(s_1, s_2)$ should have (e.g. $\lambda(+\infty, +\infty) = \lambda_K$; $\lambda(+\infty, s_2) = \lambda_K \frac{s_2}{K_{s_2}+s_2}$)

and showed that the reciprocal form is the unique generalisation that satisfies all required properties. Bertolazzi (Bertolazzi 2005) further derived this form from a model in which exponentially growing cells grow by nutrient absorption and split at a critical mass, and the three key assumptions are 1) that nutrient absorption obeys Michaelis-Menten kinetics, 2) that the cell surface area is limited, and 3) that cells distribute the surface area to different absorption fluxes such that the ratios between fluxes are constant.

Benefiting from recent progress in microbial growth laws and constraints (see Section 1.1), we will mechanistically derive the two-substrate Monod's equation (the reciprocal form) from a self-replicator model.

1.6.3 Experimental verification of two-substrate Monod's equation is difficult

Experimental verification of two-substrate Monod's equation can be done in batch cultures (Mankad and Bungay 1988) or chemostats (Lee, Ataai, and Shuler 1984), with both substrate concentrations measured and the specific growth rate measured (in batch cultures) or controlled (in chemostats). There are multiple strategies to systematically explore the concentration combinations (s_1, s_2) and in chemostat experiments the dilution rate $D \equiv \lambda$. Lee *et al* (Lee, Ataai, and Shuler 1984) fixed the input concentrations $(s_{1,0}, s_{2,0})$ and varied the dilution rate D; Mankad and Bungay (Mankad and Bungay 1988) started with a grid of inputs $(s_{1,0}, s_{2,0})$ and measured λ, s_1 and s_2; Rutgers *et al* (Rutgers, Balk, and van Dam 1990) started with various ratios between inputs $s_{1,0}$ and $s_{2,0}$ and varied the dilution rate D. However, measuring substrate concentrations can be difficult when the concentrations are low (Lee, Ataai, and Shuler 1984), and in batch culture experiments, it could be difficult to measure the steady-state specific growth rate when the concentrations are low.

Chapter 2

Microbial Growth Laws in Batch Cultures

Disclaimer on contribution: I led this project and designed the experiments. Hongpei Li (MSc student), Jack W Thomson (BMedSci(Hons) student) and Xiao Wang (MSc student) performed the experiments under my supervision. Please refer to their dissertions for their individual contributions.

2.1 Summary

- Context: linear "growth laws" that correlates ribosomal level with growth rate emerge in *E. coli*, which can be explained by the proteome allocation constraint (Scott et al. 2010); the "first law" is also observed in *S. cerevisiae* (Metzl-Raz et al. 2017).
- Question: do similar "growth laws" also hold in *S. cerevisiae*?
- Approach: we used a strain with a GFP tagged on a ribosomal protein to monitor the dynamics of both growth and ribosome levels in microplate readers.
- Finding: in the early phases of growth, the effective translation rate is constant over time and over carbon sources, and this rate decreases under exposure to ribosome-targeting drugs or hyperosomotic stress but not under weak-acid stress.

- Outlook: our results provide a finer description of yeast growth in batch cultures, which suggests that rich information exists beyond exponential growth.

2.2 Background

Ribosomes catalyse one of the last steps of anabolism and produce proteins, which are required for cell growth and division. Meanwhile, ribosomes take up a large fraction of cellular resources, with up to 30% of the proteome (Metzl-Raz et al. 2017) and 80% of the total RNA (Warner 1999) in *S. cerevisiae*. Therefore, to maximise growth rate, cells must maintain a close-to-optimal translation rate, which allows maximal protein production per mass of ribosome (Bruggeman et al. 2020). To achieve this, cells must closely monitor the nutrient availability and control the ribosome level. In *E. coli*, cells monitor the level of α-keto acid with the cAMP-Crp system and monitor the level of amino acids with ppGpp, such that they can adjust the catabolic, anabolic and ribosomal sectors of the proteome in different environments (Scott and Hwa 2022). In budding yeast, the ribosomal biogenesis is controlled by both target of rapamycin complex (TORC) and PKA, which sense glucose and intracellular amino acids, respectively (Broach 2012).

If cells indeed maintain a constant, maximal translation rate and the total protein concentration is constant, the ribosomal fraction must increase with the specific growth rate of a cell: $r \propto \lambda$. Schaechter *et al* (Schaechter, MaalØe, and Kjeldgaard 1958) first discovered a linear relationship between the ribosomal level and the specific growth rate in *Salmonella typhimurium*. Scott *et al* (Scott et al. 2010) and Metzl-Raz *et al* (Metzl-Raz et al. 2017) confirmed this linear relationship in *E. coli* and *S. cerevisiae*, respectively. However, this linear relationship is not exactly proportional, because the ribosomal fraction r approaches a constant r_0 when the specific growth rate λ approaches 0, so it has been proposed that cells maintain a fixed amount of inactive ribosome while the active ribosomes work at a close-to-maximal elongation rate (Hui et al. 2015; Metzl-Raz et al. 2017). Scott *et al* further discovered that when the elongation rate is inhibited by chloramphenicol, a ribosome-targeting antibiotics, cells will increase the level of ribosomes (Scott et al. 2010). Elsemman *et al* found a similar response of *S. cerevisiae* exposed to cycloheximide (CHX) (Elsemman et al. 2022).

The above results were obtained for exponentially growing cells, which suggest that ribosomal levels tightly couple with growth at the exponential phase. However, cells live in dynamic environments so it is important to ask how the cells reprogram the expression of ribosomal genes among other genes in a changing environment, and how a certain strategy would benefit the cells. People have worked on how cells respond to a switch between two steady-state environment (Erickson et al. 2017; Basan et al. 2020) and how the ribosomal fraction changes over growth in a batch culture (Metzl-Raz et al. 2017), but the time resolution is limited.

Previously, researchers have used GFP-tagged ribosomal proteins (Rpl13a and Rpl26a) to monitor single-cell dynamics (Janssens and Veenhoff 2016; Guerra et al. 2022). Here, we show that we can use a strain with a green fluorescent protein (GFP) tagged ribosomal protein to monitor the dynamics of both ribosomal levels and growth in batch cultures. We can therefore estimate the dynamics of the (effective) translation rate of the population with high time resolution. Strikingly, we found that the translation rate is constant over time and over various carbon sources at the early phases of growth, which we refer to as the **linear phase**. We then analyse how the growth rate, the translation rate and the ribosomal fraction changes during and after the linear phase. We found that cells can maintain the translation rate under weak-acid stress, but not under hyperosmotic stress nor under exposure to ribosome-targeting drugs. Comparing with translation rate under stress, we suspect that under stress-free condition cells always maintain the translation rate close to an empirical upper limit at the early phases of growth. Our results in this chapter draw a detailed picture of how cell growth and ribosomal levels change with the environmental change in batch cultures and hence provide assumptions for a dynamical model of growth of budding yeast in batch cultures that I will develop in the next chapter.

2.3 Results

2.3.1 Dynamics of population growth measured by plate readers

Understanding the dynamics of population growth in batch cultures requires measuring the number of cells typically via OD at a series of time points and estimating the time

derivative of OD (or a function of OD), commonly known as "growth rate". The two most commonly used growth rates are dOD/dt and $d/dt\ \log OD$. dOD/dt represents how fast the cell number of a population increases and we will call it **population growth rate** in this chapter. $d/dt\ \log OD$, which is known as the **specific growth rate**, represents "the rate at which one unit organism is produced by one unit organism" (Berkhout et al. 2013). In this chapter, we will use λ to denote the specific growth rate:

$$\lambda \equiv \frac{d}{dt} \log OD = \frac{1}{OD} \frac{dOD}{dt} \tag{2.1}$$

where $\log OD$ represents the natural logarithm of the OD.

We measure OD in plate readers and estimate the growth rates using a Gaussian process (Swain et al. 2016). An example of growth dynamics is shown in Fig 2.1. As expected, OD increases over time, and the graph of OD as a function of time is an S-shape curve (Fig 2.1A). Accordingly, the graph of dOD/dt as a function of time has a peak, where the OD increases most rapidly (Fig 2.1B). In Fig 2.1C, the middle part of the $\log OD$ curve is almost a straight line, suggesting the specific growth rate is close to constant during that phase of growth, which is hence known as "exponential". However, estimating the specific growth rate from $\log OD$ with the Gaussian process gives finer details — for cells pre-grown in pyruvate and later inoculated into a sugar, we typically observe that λ increases, plateaus (or peaks) and decreases (Fig 2.1D), which corresponds to the acceleration phase, exponential phase and retardation phase that Monod defined (Monod 1949).

Note that we will use $\log OD$ or OD on the x-axis in the figures rather than time. This is because if we use time, the lag time is sensitive to the number of inoculated cells at the beginning of the experiment.

2.3.2 The population enters prolonged exponential growth only if the initial sugar concentration is high enough

Fig 2.2 shows the distinction between a plateauing curve of specific growth rate in a high sugar concentration, which indicates a prolonged exponential growth, and a peaking one in low sugar concentrations. We therefore conclude that population growth enters

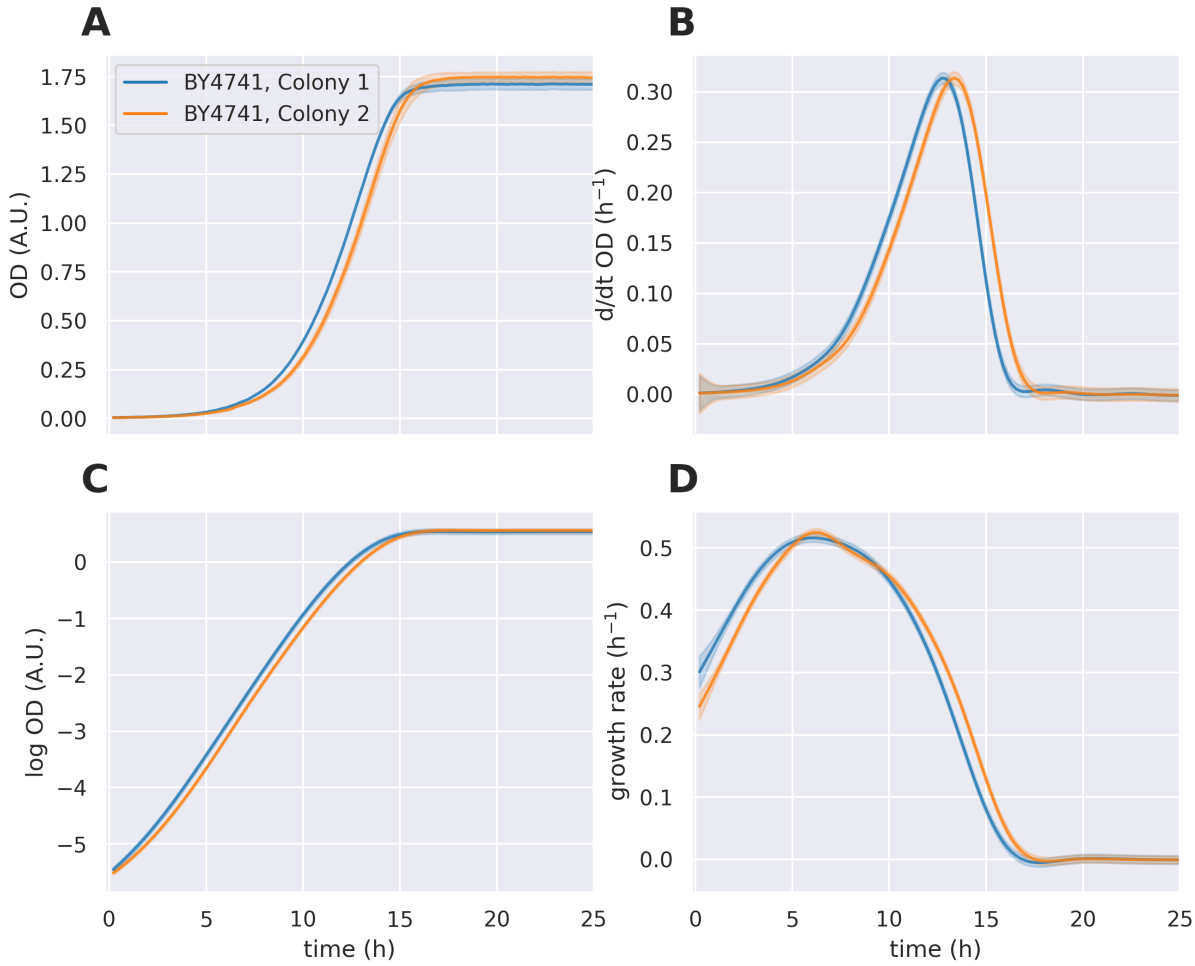

Figure 2.1: Typical growth dynamics of *S. cerevisiae* measured in a plate reader. **(A)** OD. **(B)** The time derivative of OD estimated by the Gaussian process. **(C)** The logarithm of the OD. **(D)** The specific growth rate, defined as the time derivative of $\log OD$, estimated by the Gaussian process. The cells were grown in 2% glucose. The shaded area represents the standard deviation of two technical replicates.

prolonged exponential phase only if the initial sugar concentration is high enough. We refer to the conditions in which the sugar concentration is not high enough to support prolonged exponential growth as **sugar-limiting conditions**.

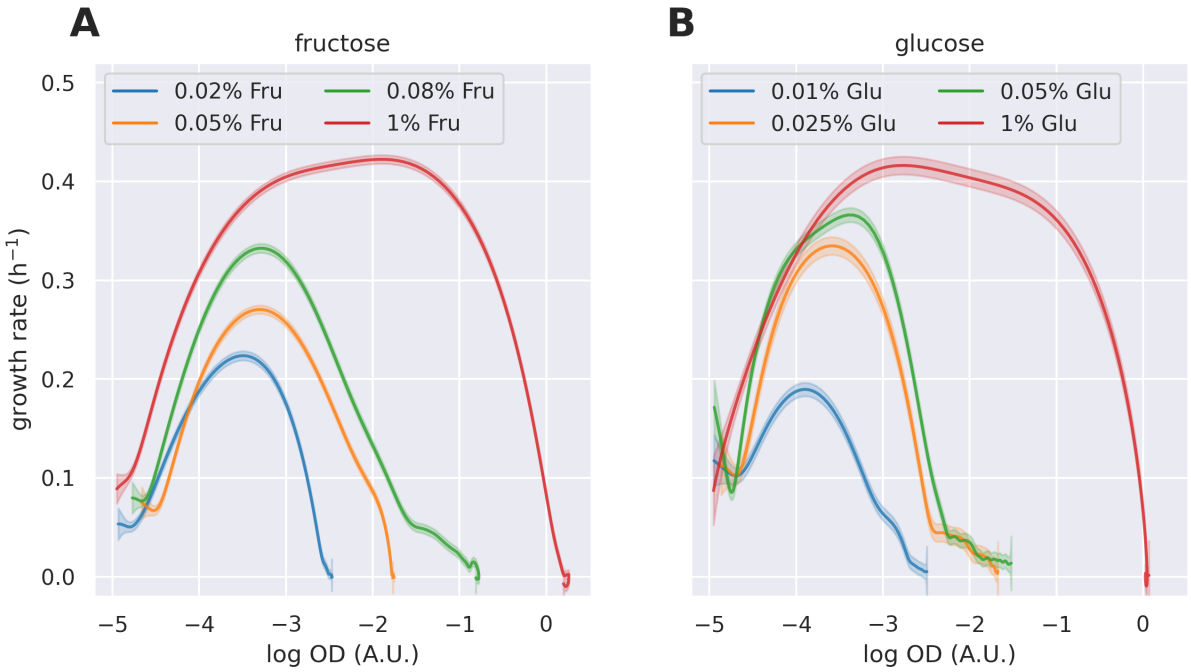

Figure 2.2: Population growth dynamics in a range of sugar concentrations. The specific growth rate as a function of $\log OD$ in **(A)** fructose and **(B)** glucose. The shaded area represents the standard deviation of two technical replicates.

2.3.3 Monod's equation holds in sugar-limiting conditions

Monod proposed an empirical relationship between the exponential growth rate and the sugar concentration (Monod 1949), written as:

$$\lambda^* = \lambda_K \frac{s}{K_s + s} \tag{2.2}$$

where λ^* is the exponential growth rate and λ_K and K_s are constant and specific to each sugar. Although growth in the sugar-limiting conditions is no longer strictly exponential, we may still ask whether Monod's equation holds for the initial sugar concentration and the maximum specific growth rate (still denoted as λ^* for convenience). We re-arranged Eq. 2.2 according to Eadie (Eadie 1942) and Hofstee's (Hofstee 1959) derivation:

$$\lambda^* = \lambda_K - K_s \frac{\lambda^*}{s} \tag{2.3}$$

As shown in Fig 2.3, Monod's equation holds for a wide range of sugars.

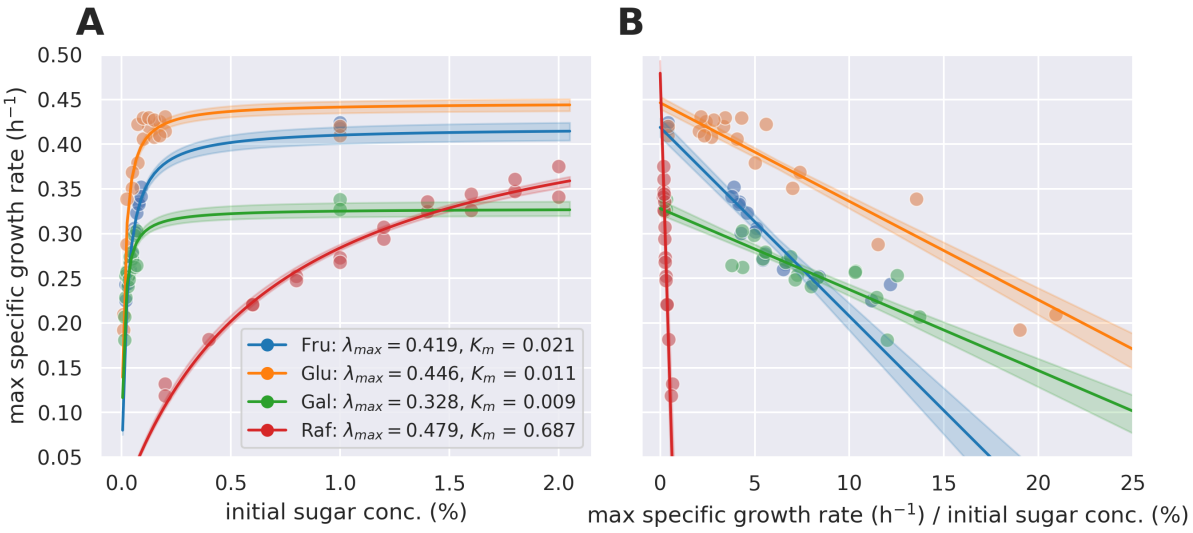

Figure 2.3: Monod's equation holds in sugar-limiting conditions. Each point represents the growth curve of one biological replicate under a certain initial sugar concentration and sugar type. The prototrophic wildtype strain (FY4) is grown in the Delft media. The parameters K_s (%) and λ_K (h^{-1}) are obtained by Bayesian parameter estimation (see Section 2.4.1). The shaded area represents the standard deviation of the predicted maximum specific growth rate propagated from the uncertainty of K_s and λ_K.

2.3.4 We dynamically measure ribosome levels with GFP to recover the "first law"

Protein production by ribosomes is essential for cell growth. If the protein production rate is proportional to growth rate, and if we denote the specific growth rate as λ (in h^{-1}), the translation rate per ribosomal fraction as γ_e (in h^{-1}) and the ribosomal fraction in the proteome as r (unitless), we have:

$$\lambda = \gamma_e r \tag{2.4}$$

At exponential growth, ribosome levels linearly increase with the specific growth rate in *S. cerevisiae*, and a constant fraction of inactive ribosome exists (denoted as r_0 below) (Metzl-Raz et al. 2017) (Fig 2.5B). Now Eq 2.4 can be written as

$$\lambda = \gamma(r - r_0) \tag{2.5}$$

or more commonly,

$$r = \gamma^{-1}\lambda + r_0 \tag{2.6}$$

where γ and r_0 are constant, and γ is interpreted as the elongation rate, which is related to the translation rate γ_e by:

$$\gamma = \frac{\gamma_e}{1 - r_0/r} \tag{2.7}$$

The linear relationship in Eq 2.6 is sometimes called the "first law".

However, the results above were obtained from a single time point of exponential growth in each condition. To comprehensively understand the dynamics of population growth, it is necessary to measure ribosome levels throughout all the growth phases. My colleague, Nahuel Manzanaro Moreno, developed a method to quantify ribosome levels in plate readers. He used an *RPL3:GFP* strain to quantify the abundance of ribosomal protein L3 in multiple carbon sources and found that the GFP level at the maximum specific growth rate positively correlates with the specific growth rate (Manzanaro Moreno 2021, 112–15), in good agreement with the mass spectrometry data in (Metzl-Raz et al. 2017).

Here, to obtain data for quantitative analysis, I worked with Jack Thomson and Xiao Wang to reproduce those experiments with three strains, *RPL3:GFP*, *RPL13B:GFP* and *RPS30A:GFP*. As proof of principle, we show that the GFP strains have similar growth to the wildtype and that our results agree with the relationship between ribosome level and doubling time shown in (Metzl-Raz et al. 2017). First, consistent with the results of Nahuel Manzanaro Moreno (Manzanaro Moreno 2021, 109–11), our results in Fig 2.4 confirmed that the maximum specific growth rate and the final OD of the fluorescent strains are similar to those of the wildtype. Second, we compared the ribosomal fraction and doubling time in (Metzl-Raz et al. 2017), with our data at OD 0.1, because the cells were harvested at 0.6 (equivalent to 0.1 in our data) in (Metzl-Raz et al. 2017). As shown in Fig 2.5, after converting the GFP levels into ribosomal fractions, the data of *RPL3:GFP* is consistent with the mass spectrometry data in (Metzl-Raz et al. 2017), but less so for the data of *RPS30A:GFP* and *RPL13B:GFP* (Fig 2.6), possibly because both *RPS30* and *RPL13* have two copies (A and B) in the genome and the two copies are differentially expressed under some conditions, but only the one tagged with GFP is

detectable.

The results suggest that the GFP level of *RPL3:GFP* provides a good estimation of total ribosome level in plate readers. We used *RPL3:GFP* henceforth and interpret the GFP level as the **population's total ribosome level**, and the GFP level per OD as the ribosome level per OD, or the **ribosomal fraction**, by the consistency seen in Fig 2.5B.

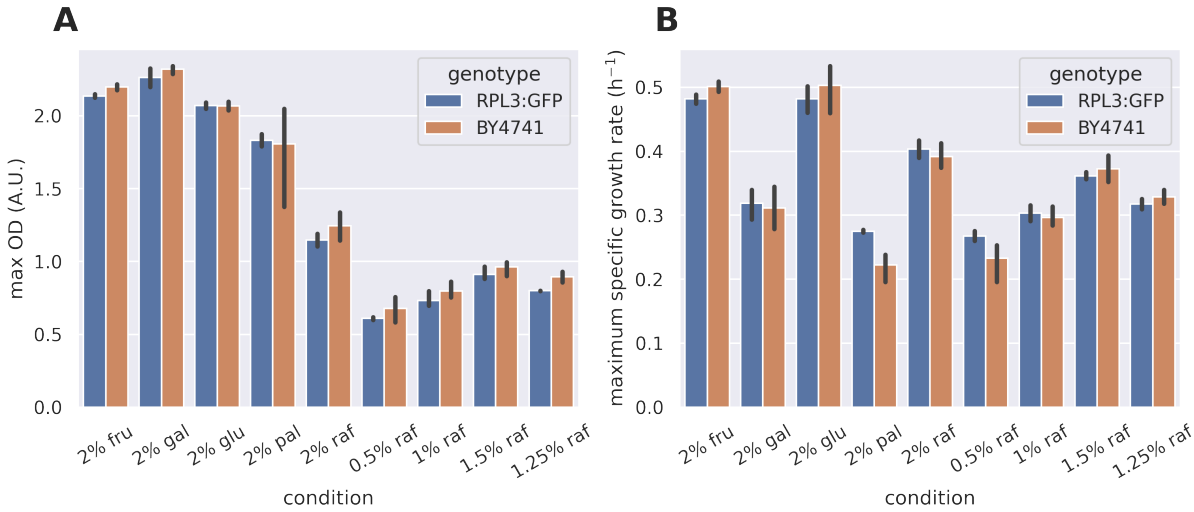

Figure 2.4: The maximum OD **(A)** and specific growth rate **(B)** of the *RPL3:GFP* strain are consistent with the wildtype (BY4741) strain across conditions. Each error bar represents a 95% confidence interval. Only 1 biological replicate was run in 0.75% raffinose, so no error bar is included.

2.3.5 In the early phases of growth, the effective translation rate is constant over time and over carbon sources

With the *RPL3:GFP* strain, we can now simutaneously measure the dynamics of both ribosomal levels and growth at the population level, which means that we can estimate the dynamics of translation rate γ_e at the population level, because if we multiply both sides of Eq 2.4 by OD, we have:

$$\frac{dOD}{dt} = \gamma_e(r \cdot OD) \propto \gamma_e \cdot GFP \tag{2.8}$$

or,

$$\gamma_e \propto \frac{dOD}{dt}/GFP \tag{2.9}$$

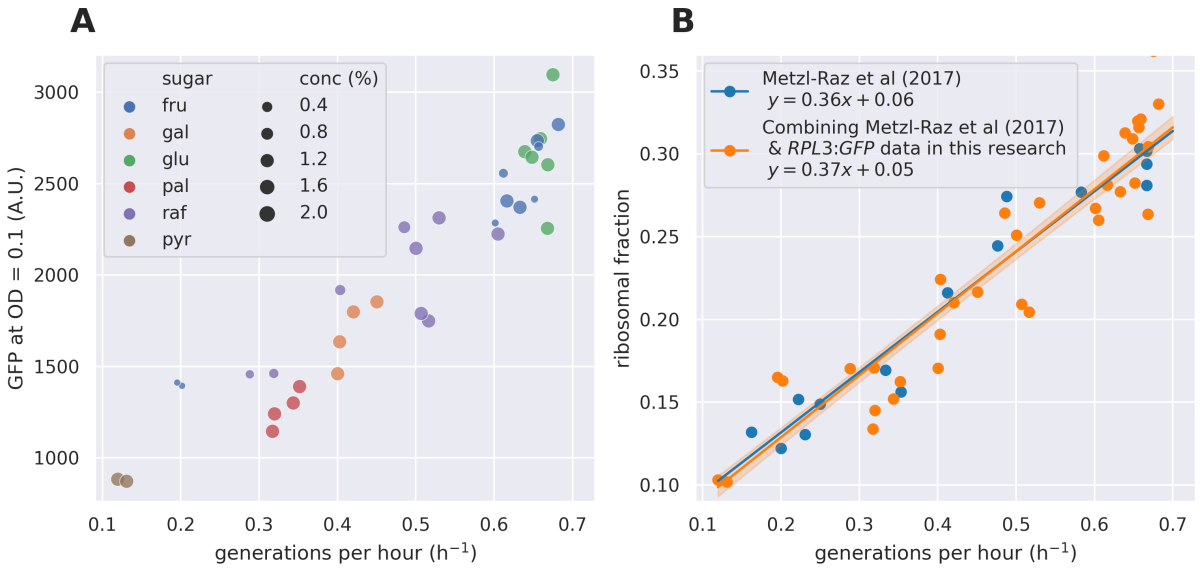

Figure 2.5: The ribosomal fractions estimated from *RPL3:GFP* are consistent with (Metzl-Raz *et al* 2017). **(A)** Each pair of GFP level and generations per hour is estimated from the growth curve of one biological replicate, at $OD = 0.1$. Generations per hour is the specific growth rate divided by $\log 2$, and we use generations per hour in this figure to be consistent with (Metzl-Raz *et al*, 2017). **(B)** The GFP level in (A) was scaled to compare with the ribosomal fraction from (Metzl-Raz *et al* 2017). We used a Bayesian approach to estimate the best scaling factor together with the slope and intercept (see Section 2.4.2), the slope and intercept are shown in the legend. The shaded area is the standard deviation of the ribosomal fraction propagated from the uncertainty of the slope and intercept.

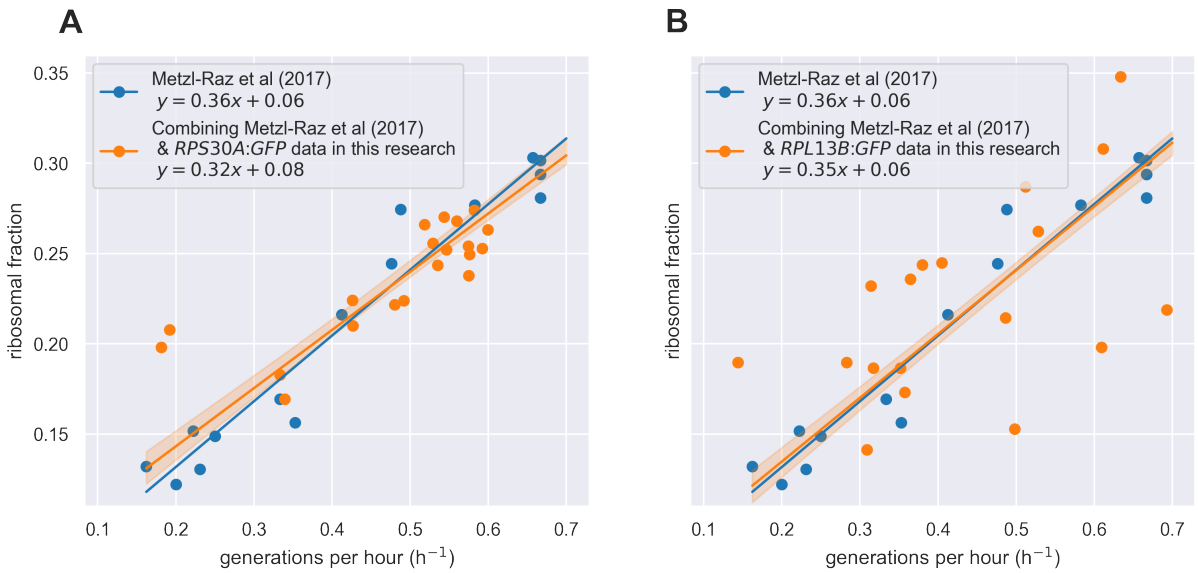

Figure 2.6: The ribosomal fractions estimated from **(A)** *RPS30A:GFP* and **(B)** *RPL13B:GFP* are less consistent with (Metzl-Raz *et al* 2017). Each pair of GFP level and generations per hour is estimated from the growth curve of one biological replicate, at $OD = 0.1$. Generations per hour is the specific growth rate divided by $\log 2$, and we use generations per hour in this figure to be consistent with (Metzl-Raz *et al*, 2017). We used a Bayesian approach to estimate the best scaling factor together with the slope and intercept (see Section 2.4.2), the slope and intercept are shown in the legend. The shaded area is the standard deviation of the ribosomal fraction propagated from the uncertainty of the slope and intercept.

However, we cannot estimate the elongation rate γ in the first law (Eq 2.5) because we cannot estimate the inactive ribosome levels. To distinguish between γ and γ_e, we refer to γ_e as the *effective* translation rate, because it is determined by both the actual elongation rate γ and the fraction of active ribosomes (Eq. 2.7).

To visualise γ_e, we plot dOD/dt against GFP in Fig 2.7A and B, which shows a striking proportionality in the early phases of growth. I developed a Bayesian approach to identify the linear regime of each curve (see Section 2.4.4) and linear regression shows that the slopes are similar across all tested conditions except the two slow growth conditions: 0.06% fructose and 2% pyruvate (Fig 2.7C). The results suggest that in the early phases of growth, the effective translation rate is constant over time and over various carbon sources. We refer to this phase of growth as the **linear phase**, because of the linear relationship between dOD/dt and GFP in this phase (Fig 2.7AB).

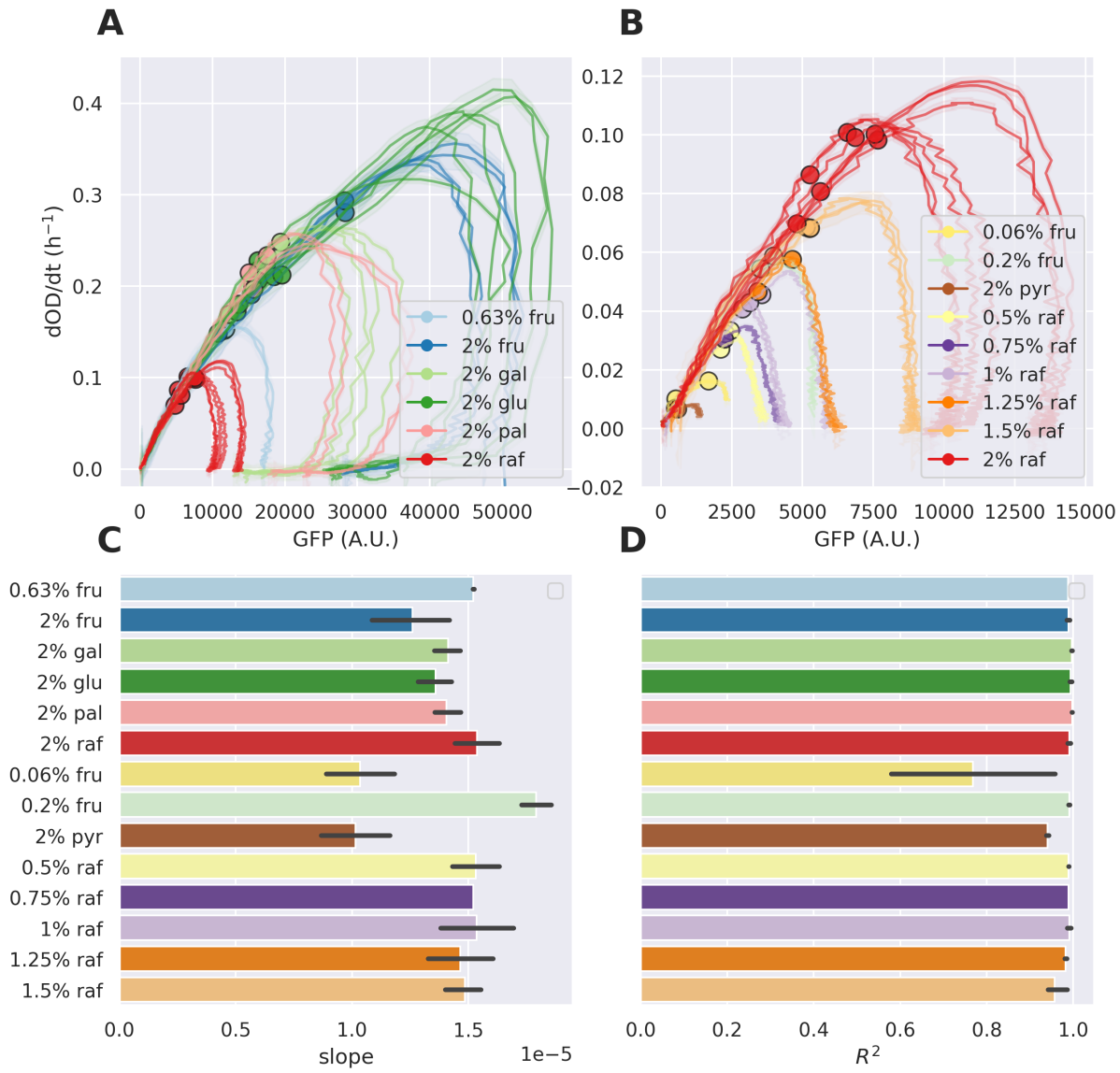

Figure 2.7: In the early phases of growth, the population growth rate is proportional to the population's total ribosome level. **(A, B)** The time derivative of the OD *versus* the GFP level of the population in different concentrations of sugars. Panel A shows the data from high concentrations of sugars and Panel B shows the data from low concentrations of sugars. For reference, 2% raffinose (in red) is included in both panels. **(C)** The slope and **(D)** the R^2 of linear regression on the linear regime in (A) and (B). The solid circles in (A) and (B) mark the end of the linear regime for each biological replicate, found with a Bayesian approach (see Section 2.4.4). Each curve in (A) and (B) represents one biological replicate, and the shaded area represents the standard deviation of two technical replicates. Each error bar in (C) and (D) represents a 95% confidence interval.

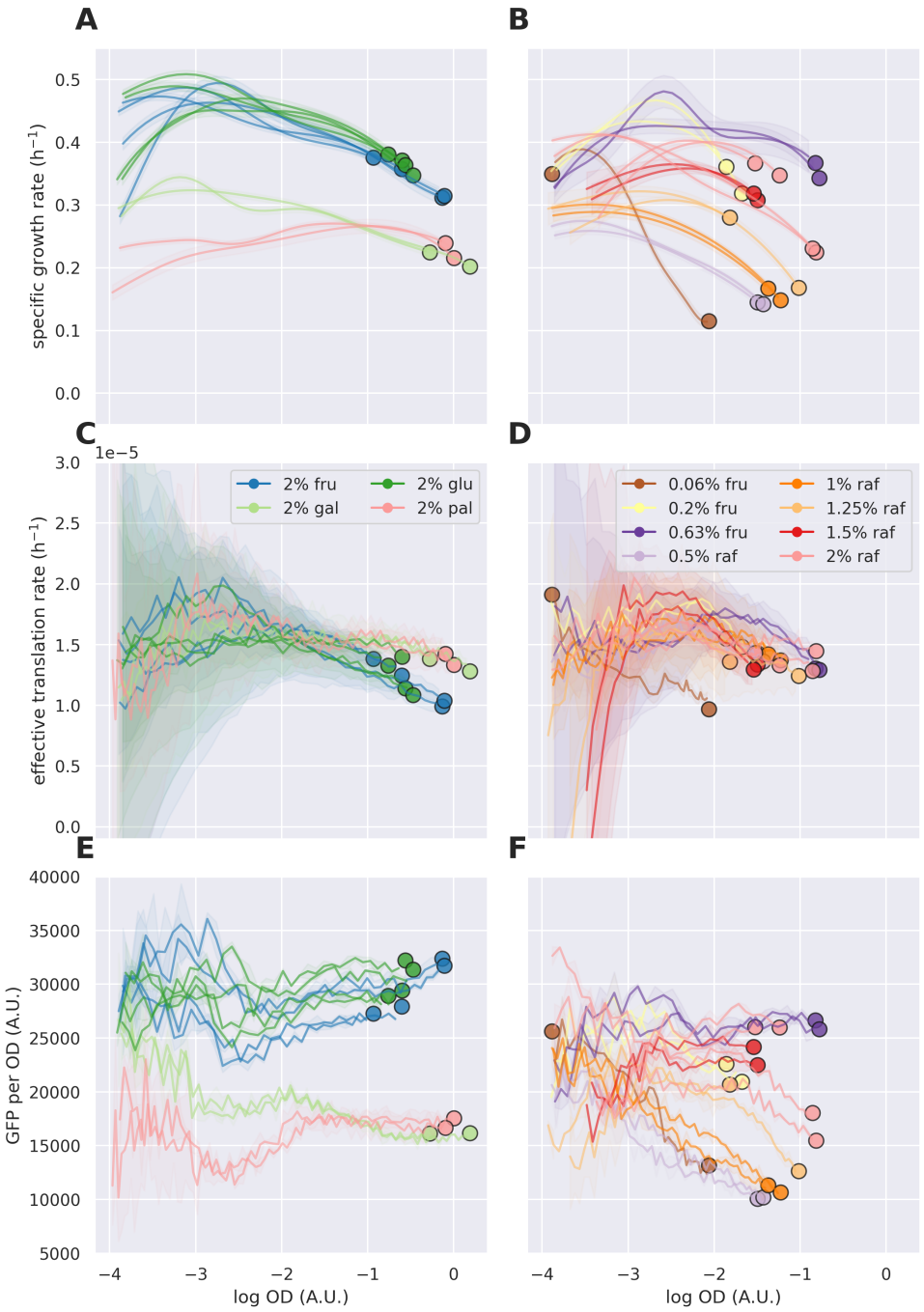

Figure 2.8: **(A, B)** The specific growth rate, **(C, D)** effective translation rate and **(E, F)** ribosomal faction during the linear phase in different carbon sources. The data are plotted against $\log OD$. The effective translation rate is defined as the ratio between the population growth rate and the population's ribosome level ($\frac{dOD}{dt}/GFP$). The ribosomal fraction is represented by GFP/OD. Each curve represents one biological replicate. The solid circles mark the end of the linear regime of dOD/dt *versus* GFP for each biological replicate. The shaded area represents the standard deviation of two technical replicates. Only data points with $OD > 0.02$ and within the linear regime are shown.

2.3.6 The linear phase extends beyond exponential growth

The specific growth rate (λ) depends on the effective translation rate (γ_e) and the ribosomal fraction (represented by GFP/OD). Dividing both sides of Eq 2.8 by OD and using the definition of $\lambda \equiv \frac{1}{OD}\frac{dOD}{dt}$ (Eq 2.1), we have:

$$\lambda \propto \gamma_e \frac{GFP}{OD} \tag{2.10}$$

By definition of the linear phase, γ_e is constant, so the specific growth rate is proportional to the ribosomal fraction in the linear phase.

At exponential growth, the specific growth rate λ is constant over conditions, so the ribosomal fraction is also constant. This is true for population growth in high sugar concentrations (Fig 2.8A, C and E), where the growth can enter a prolonged exponential growth (see Section 2.3.2).

In sugar-limiting conditions, the specific growth rate peaks rather than plateaus (see Section 2.3.2). The linear region extends after the peak, and the ribosomal fraction decreases with the specific growth rate while the effective translation rate is constant (Fig 2.8B, D and F).

2.3.7 After the linear phase, the effective translation rate always decreases but the ribosomal fraction does not in high sugar concentrations until growth stops

After the linear phase, the specific growth rate and the effective translation rate decrease as the sugar concentration further decreases (Fig 2.9A–D).

For the ribosomal fraction, we identified two distinct cases. First, in conditions that support prolonged exponential growth to a high OD (e.g. 2% glucose), the effective translation rate decreases but the ribosomal fraction does not until growth stops (Fig 2.9E). Second, in sugar-limiting conditions (in which there is no prolonged exponential growth), the ribosomal fraction decreases after the linear phase (Fig 2.9F). One potential explanation is that it takes time for cells to adjust its proteome in response to a changing environment, and in late exponential growth, the sugar concentration decreases too

quickly for cells to respond.

2.3.8 The effective translation rate decreases under exposure to ribosome-targeting drugs

Stress conditions challenge the homeostasis of cells, and cells must properly respond to the stress to reinstate their homeostasis and survive. For example, when *E. coli* is exposed to chloramphenicol, which targets its ribosome, the translation rate decreases, but the ribosomal fraction increases to "compensate" for the loss of efficiency (Scott et al. 2010), which leads to a feedforward model of regulation of ribosome fraction (Scott et al. 2014). We wondered how the effective translation rate and ribosomal fraction change under exposure to ribosome-targeting drugs. We tested three drugs: CHX, nourseothrycin (NTC) and geneticin (G418).

As expected, exposure to all three ribosome-targeting drugs leads to decrease in the specific growth rate (Figs 2.10A, 2.11A and 2.12A) and the effective translation rate (Figs 2.10CD, 2.11CD and 2.12CD). However, the cells' response depends on the drug applied: to G418, the ribosomal fraction decreases (Figs 2.10EF and 2.13D); to NTC, the ribosomal fraction does not seem to change (Fig 2.11EF); to CHX, the ribosomal fraction increases before decreasing (Figs 2.13B). The results suggest that the response of the ribosomal fraction to the decrease in the effective translation rate depend on each drug's mode of action.

2.3.9 The effective translation rate decreases under hyperosmotic stress but not weak-acid stress

Acetate is the anion of acetic acid, a weak organic acid. At low extracellular pH, it reversibly binds to a proton, diffuses across the plasma membrane and dissociates from the proton, which acidifies the cytosol and leads to growth inhibition if the cells cannot recover their internal pH by actively pumping out the protons via Pma1 (which consumes ATP) (Ullah et al. 2012). As seen in Fig 2.14A, when cells are exposed to 30 mM acetate, the specific growth rate of cells in galactose and raffinose decreases, but not in glucose (which is consistent with (Ullah et al. 2012)). However, the effective translation rate remains

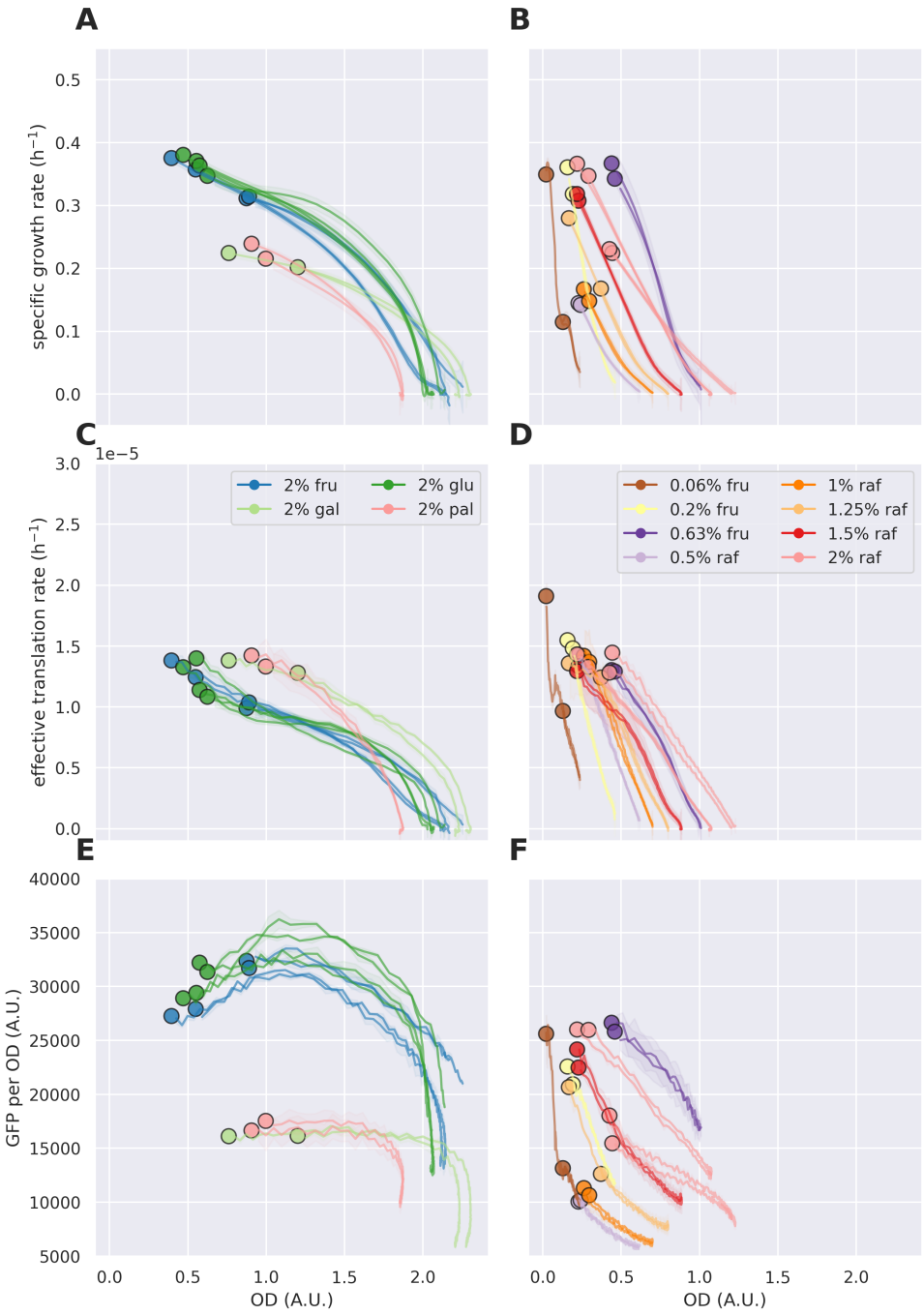

Figure 2.9: **(A, B)** The specific growth rate, **(C, D)** effective translation rate and **(E, F)** ribosomal faction after the linear phase in different carbon sources. The data are plotted against OD. The effective translation rate is defined as the ratio between the population growth rate and the population's ribosome level. The ribosomal fraction is represented by GFP/OD. Each curve represents one biological replicate. The solid circles mark the end of the linear regime of dOD/dt *versus* GFP for each biological replicate. The shaded area represents the standard deviation of two technical replicates. Only data points with $OD > 0.02$ and after the linear phase are shown.

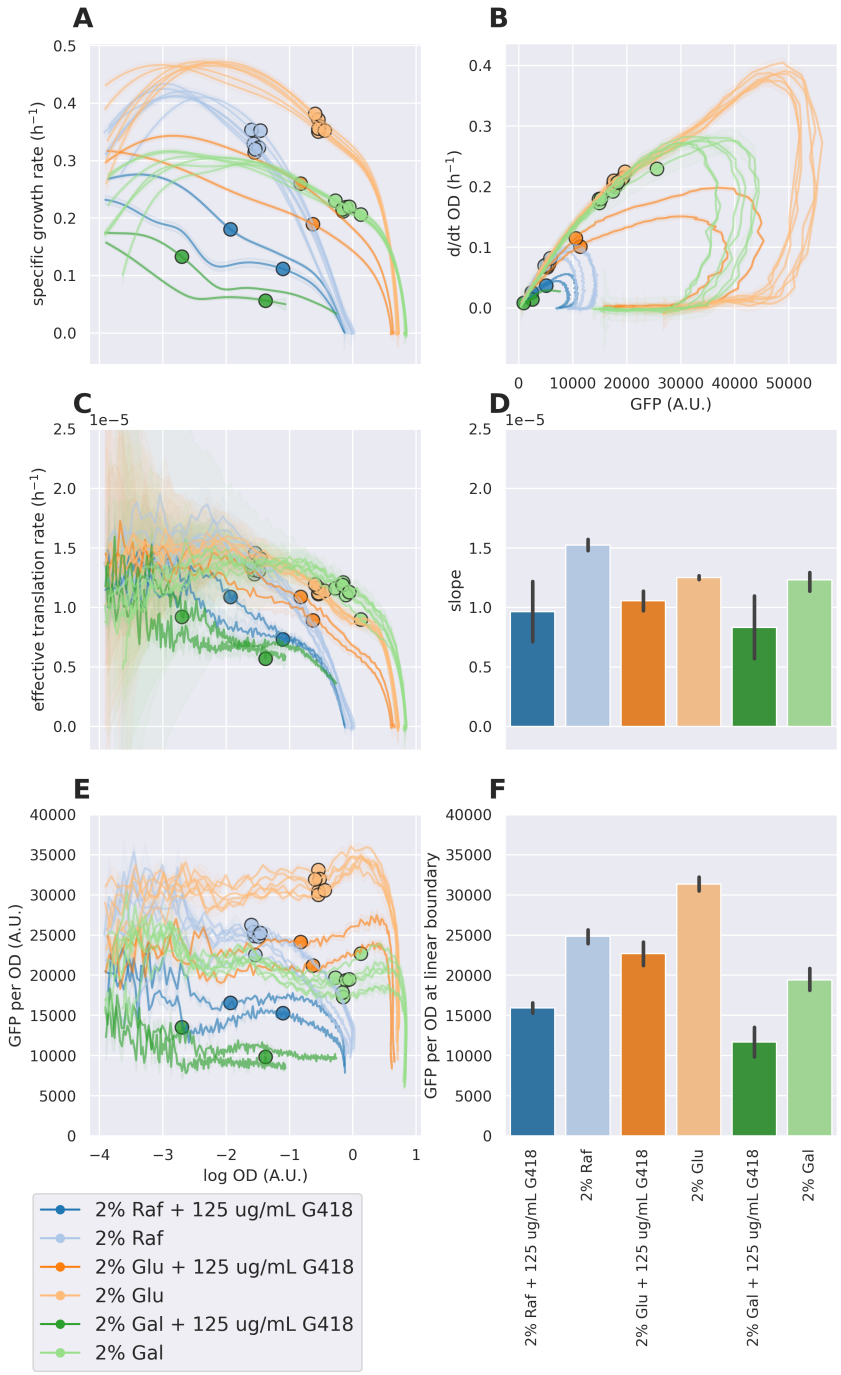

Figure 2.10: The specific growth rate, ribosomal fraction and effective translation rate of the population exposed to geneticin (G418) in different carbon sources. The **(A)** specific growth rate, **(C)** effective translation rate and **(E)** ribosomal fraction (represented by GFP per OD) of the population exposed to G418 are plotted against the logarithm of OD. **(B)** The time derivative of the OD *versus* the GFP level of the population. **(D)** The slope of linear regression on the linear regime in (B). **(F)** The ribosomal fraction (GFP/OD)) at the end of the linear regime. In all panels, the drug-free conditions are in lighter colours. In (A), (B), (C) and (E), each curve represents one biological replicate, and the shaded area represents the standard deviation of two technical replicates, and the solid circles mark the end of the linear regime (see Section 2.4.4). Each error bar in (D) and (F) represents a 95% confidence interval. Only data points with $OD > 0.02$ are shown.

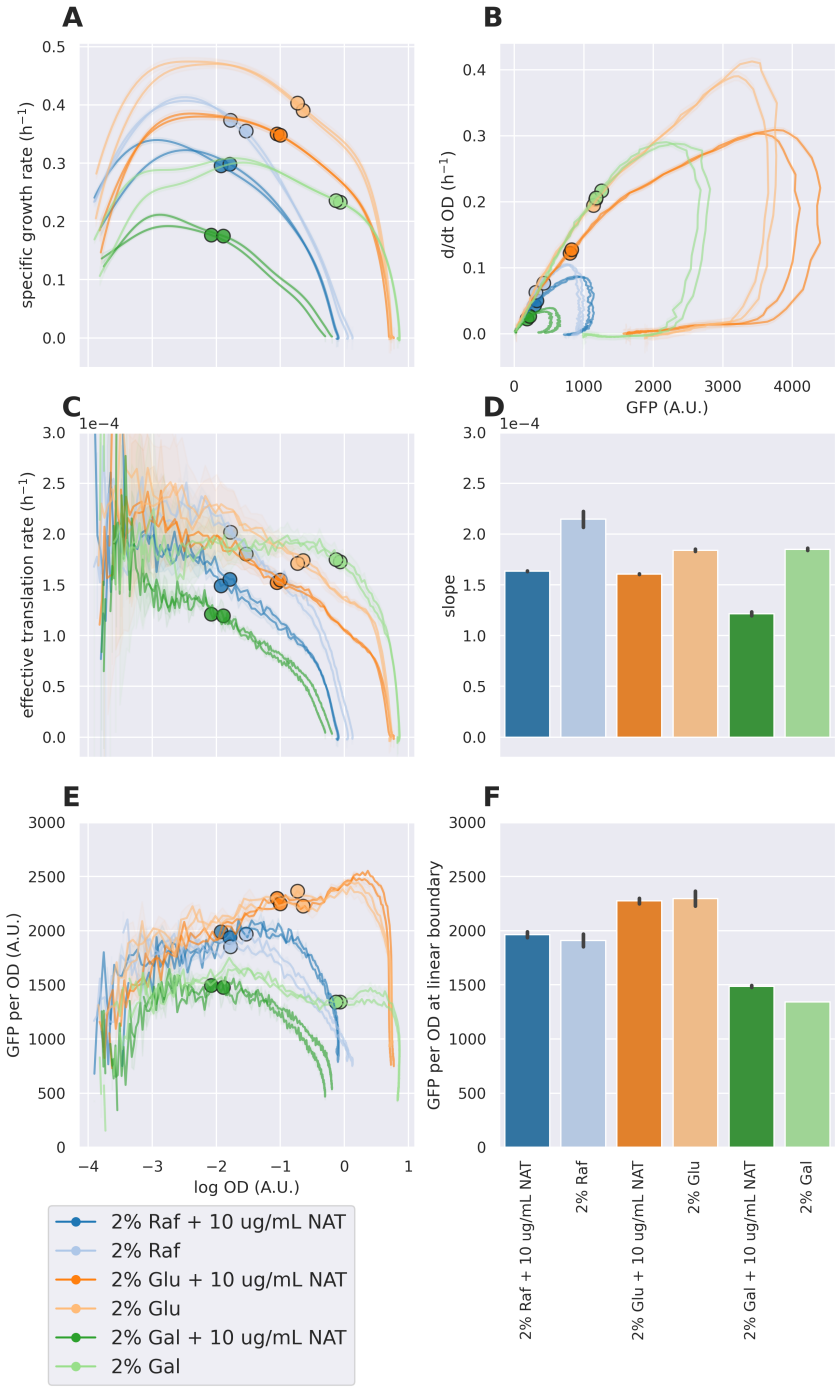

Figure 2.11: The specific growth rate, ribosomal fraction and effective translation rate of the population exposed to nourseothrycin (NTC) in different carbon sources. The **(A)** specific growth rate, **(C)** effective translation rate and **(E)** ribosomal fraction (represented by GFP per OD) of the population exposed to NTC are plotted against the logarithm of OD. **(B)** The time derivative of the OD *versus* the GFP level of the population. **(D)** The slope of linear regression on the linear regime in (B). **(F)** The ribosomal fraction (GFP/OD)) at the end of the linear regime. In all panels, the drug-free conditions are in lighter colours. In (A), (B), (C) and (E), each curve represents one biological replicate, and the shaded area represents the standard deviation of two technical replicates, and the solid circles mark the end of the linear regime (see Section 2.4.4). Each error bar in (D) and (F) represents a 95% confidence interval. Only data points with $OD > 0.02$ are shown.

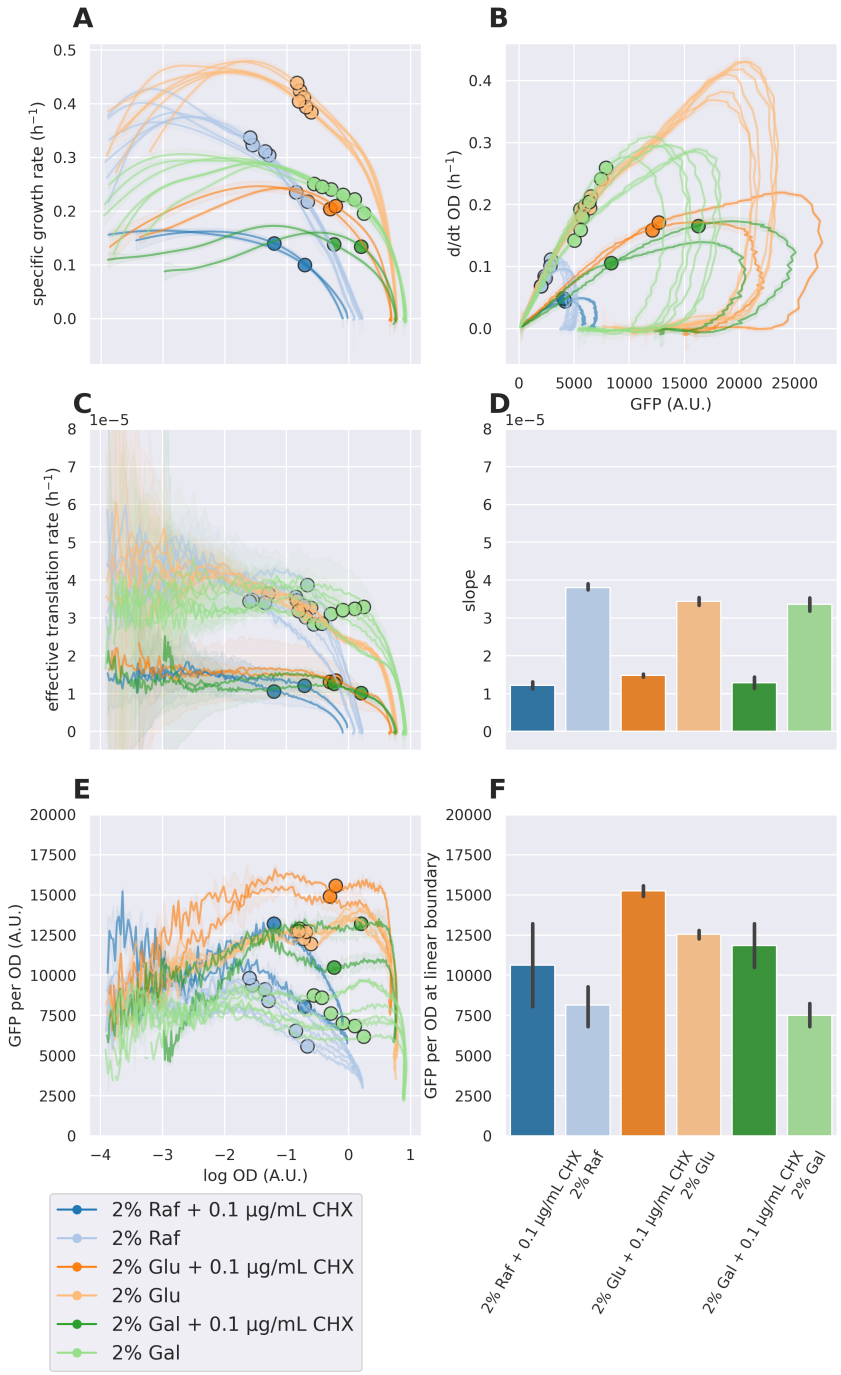

Figure 2.12: The specific growth rate, ribosomal fraction and effective translation rate of the population exposed to cycloheximide (CHX) in different carbon sources. The **(A)** specific growth rate, **(C)** effective translation rate and **(E)** ribosomal fraction (represented by GFP per OD) of the population exposed to CHX are plotted against the logarithm of OD. **(B)** The time derivative of the OD *versus* the GFP level of the population. **(D)** The slope of linear regression on the linear regime in (B). **(F)** The ribosomal fraction (GFP/OD)) at the end of the linear regime. In all panels, the drug-free conditions are in lighter colours. In (A), (B), (C) and (E), each curve represents one biological replicate, and the shaded area represents the standard deviation of two technical replicates, and the solid circles mark the end of the linear regime (see Section 2.4.4). Each error bar in (D) and (F) represents a 95% confidence interval. Only data points with $OD > 0.02$ are shown.

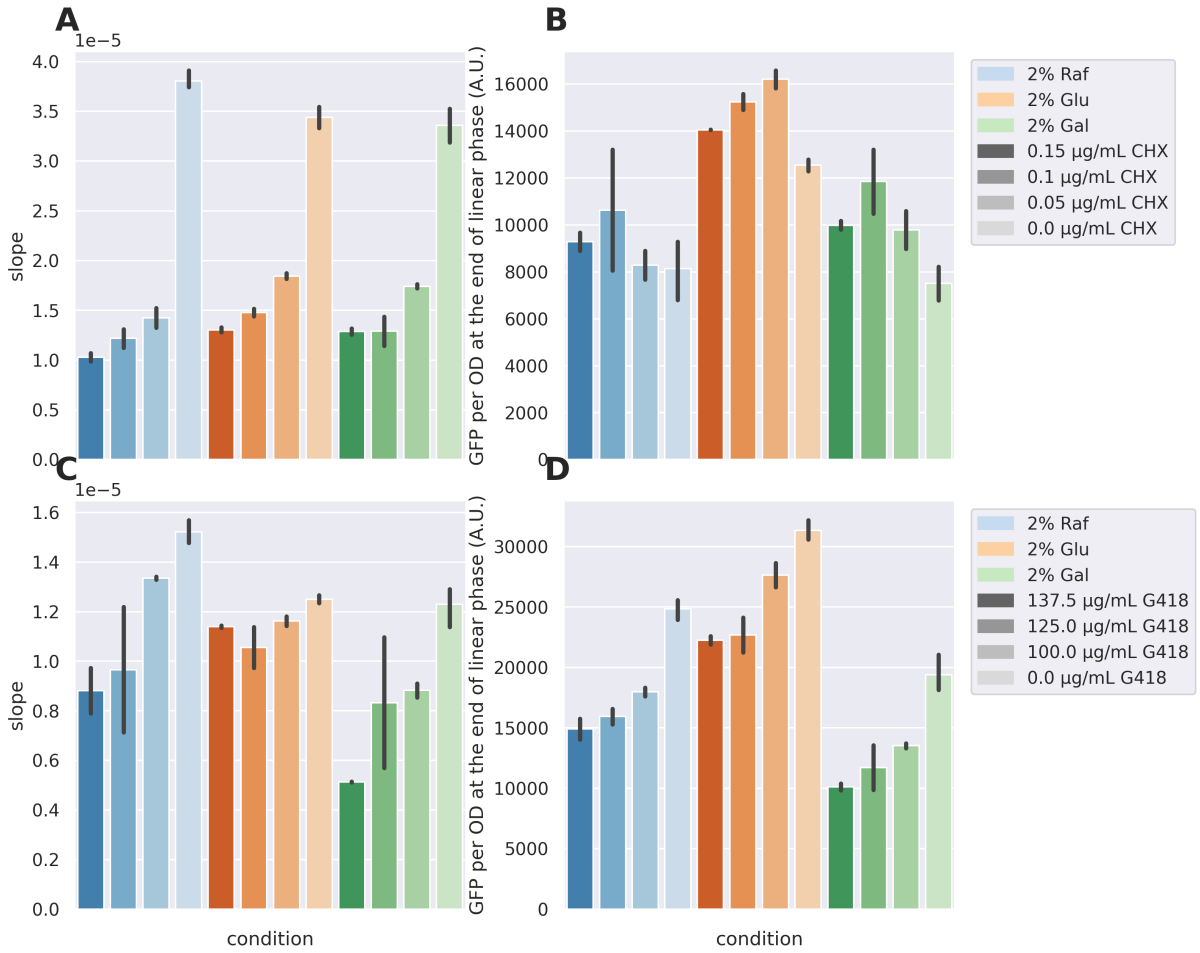

Figure 2.13: The effective translation rate and the ribosomal fraction of the population exposed to different levels of cycloheximide (CHX) or geneticin (G418). **(A)** The effective translation rate, represented by the slope of the linear phase of dOD/dt *versus* GFP and **(B)** the ribsomal fraction, represented by GFP/OD at the end of the linear phase in different levels of CHX. **(C)** The effective translation rate, represented by the slope of the linear phase of dOD/dt *versus* GFP and **(D)** the ribsomal fraction, represented by GFP/OD at the end of the linear phase in different levels of G418. The method to find the linear regime is described in Section 2.4.4. Each error bar represents a 95% confidence interval.

similar to the stress-free conditions in all carbon sources (Fig 2.14CD). Accordingly, the ribosomal fraction decreases when cells are exposed to acetate in galactose and raffinose (Fig 2.14EF).

Osmotic stress activates the cells' hyper-osmolarity-glycerol (HOG) network, which diverts glycotic flux into glycerol synthesis (Hohmann 2002), and slows down intracellular signalling, possibly caused by molecular crowding (Miermont et al. 2013). To impose a prolonged osmotic stress, we grew cells in media supplemented with 1.5 M sorbitol, in which the cells' volume decreases by about 50% (Miermont et al. 2013). When comparing conditions with and without sorbitol, we observed a decrease in the specific growth rate after the initial peak in cultures with sorbitol (Fig 2.15A), and a constantly lower effective translation rate (Fig 2.15CD). However, the ribosomal fraction of cultures with sorbitol is somewhat confusing — starting from a higher value than the stress-free conditions but decreases to and below the level of the stress-free conditions later (Fig 2.15E). We speculate that the peak of specific growth rate early in the growth curve in Fig 2.15A could be caused by the (partial) recovery of the cell volume as they adapt to the osmotic stress, which can also explain the early decrease in ribosomal fraction from a high level seen in Fig 2.15E. Nonetheless, our results suggest that under osmotic stress, both the specific growth rate and the effective translation rate are lower than the stress-free conditions.

2.4 Statistical methods

In this chapter, we used Bayesian statistics to estimate the models' unknown parameters from our data and find the linear regime of a curve.

2.4.1 Fitting the Monod's Equation

We aim to estimate the constants λ_K and K_s of Monod's equation (Eq 2.2) from our data for each sugar. To do so, we first extracted the maximum specific growth rate λ^* from each growth curve, and the initial concentration of sugar s is known. For each sugar, we have a dataset $D \equiv \{(\lambda_i^*, s_i)\}$ containing N data points. Assume (1) λ^* as a function of s follows Monod's equation (Eq 2.2), (2) the measurement error of λ_K is Gaussian with standard deviation σ, and (3) measurement of each growth curve is independent of

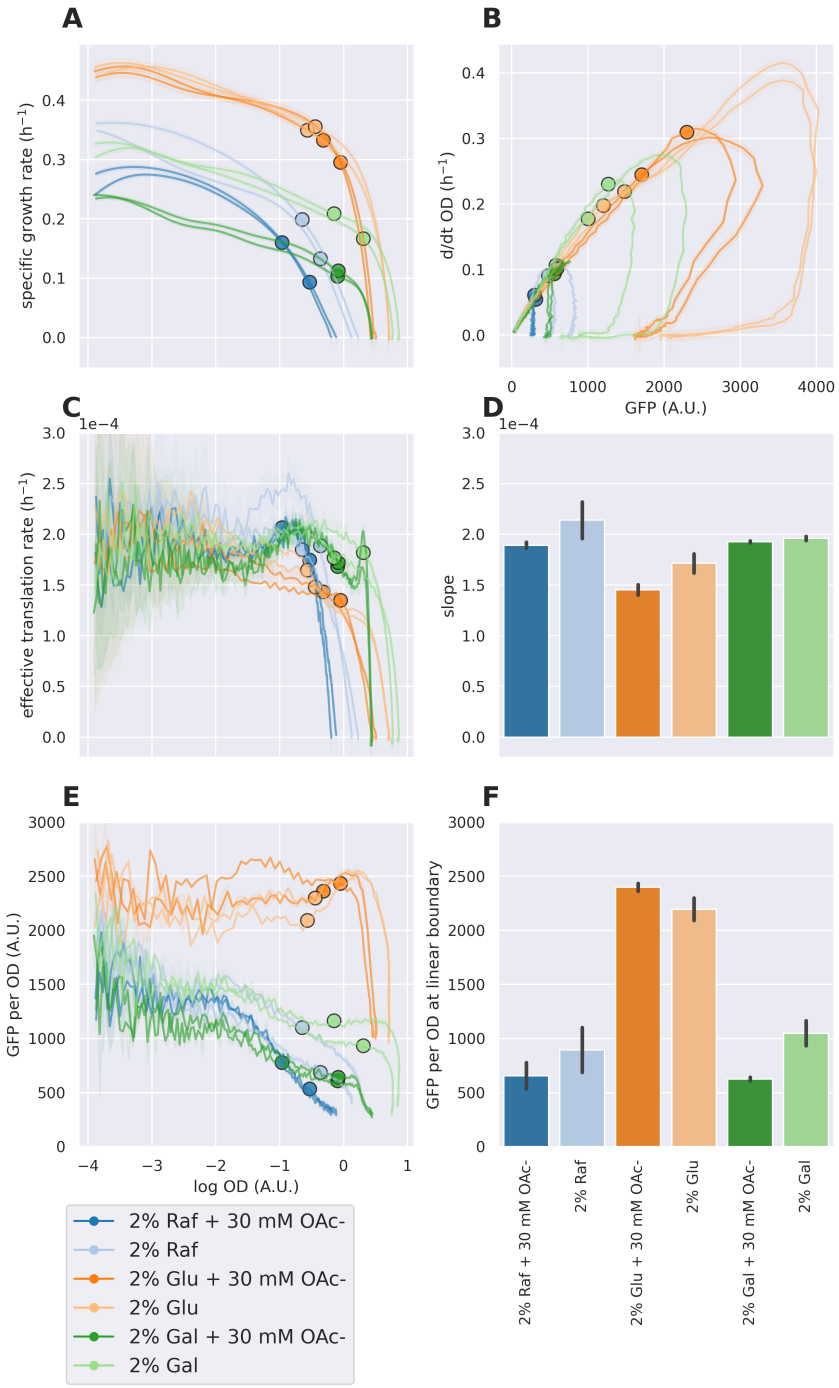

Figure 2.14: The specific growth rate, ribosomal fraction and effective translation rate of the population exposed to acetate (pH= 5) in different carbon sources. The **(A)** specific growth rate, **(C)** effective translation rate and **(E)** ribosomal fraction (represented by GFP per OD) of the population exposed to acetate are plotted against the logarithm of OD. **(B)** The time derivative of the OD *versus* the GFP level of the population. **(D)** The slope of linear regression on the linear regime in (B). **(F)** The ribosomal fraction (GFP/OD)) at the end of the linear regime. In all panels, the drug-free conditions are in lighter colours. In (A), (B), (C) and (E), each curve represents one biological replicate, and the shaded area represents the standard deviation of two technical replicates, and the solid circles mark the end of the linear regime (see Section 2.4.4). Each error bar in (D) and (F) represents a 95% confidence interval. Only data points with $OD > 0.02$ are shown.

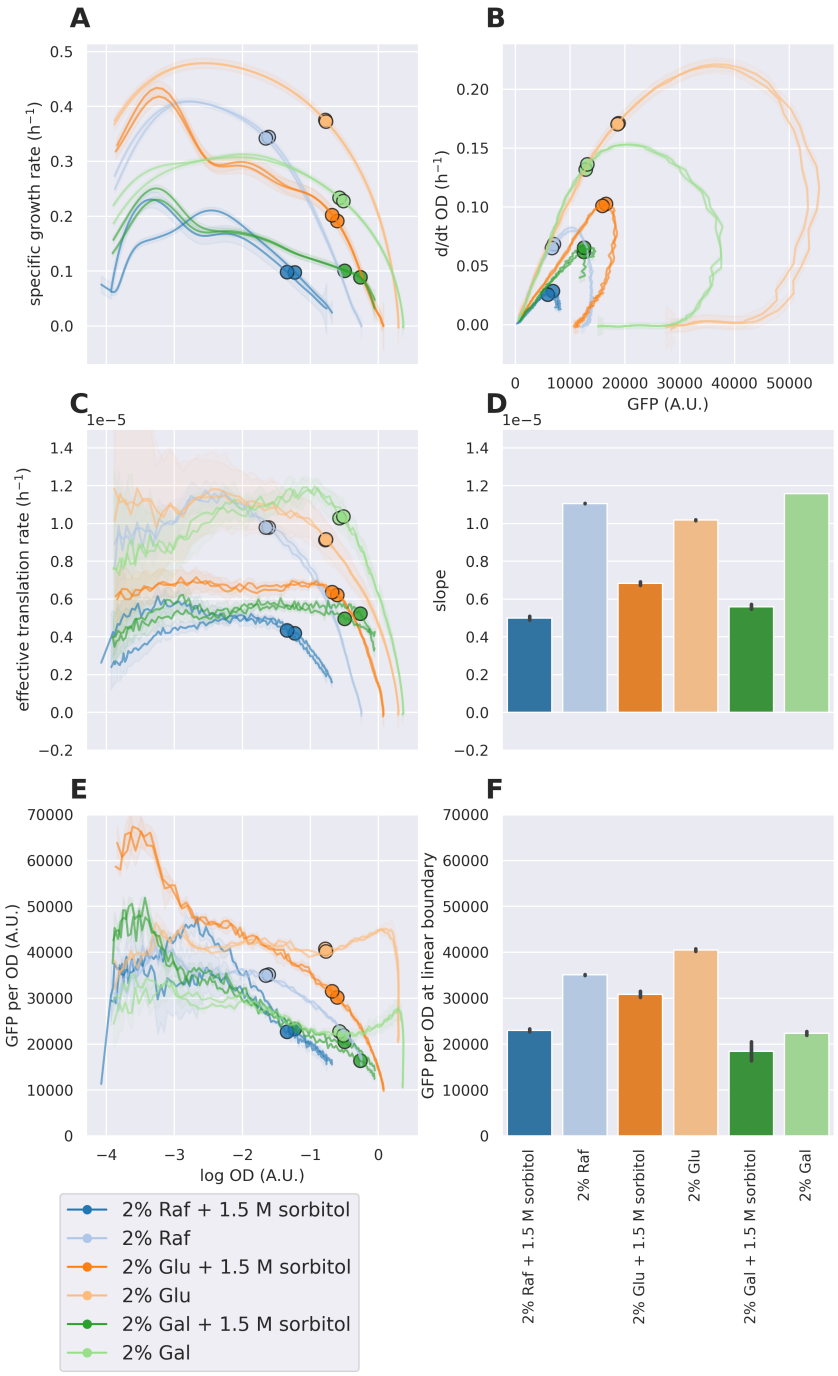

Figure 2.15: The specific growth rate, ribosomal fraction and effective translation rate of the population exposed to sorbitol in different carbon sources. The **(A)** specific growth rate, **(C)** effective translation rate and **(E)** ribosomal fraction (represented by GFP per OD) of the population exposed to sorbitol are plotted against the logarithm of OD. **(B)** The time derivative of the OD *versus* the GFP level of the population. **(D)** The slope of linear regression on the linear regime in (B). **(F)** The ribosomal fraction (GFP/OD)) at the end of the linear regime. In all panels, the drug-free conditions are in lighter colours. In (A), (B), (C) and (E), each curve represents one biological replicate, and the shaded area represents the standard deviation of two technical replicates, and the solid circles mark the end of the linear regime (see Section 2.4.4). Each error bar in (D) and (F) represents a 95% confidence interval. Only data points with $OD > 0.02$ are shown.

another. Then, we can write down the likelihood as

$$P(D|\lambda_K, K_s, \sigma) = (\sqrt{2\pi}\sigma)^{-N} \prod_{i=1}^{N} \exp\left(-\frac{(\lambda_i^* - \lambda_K \frac{s_i}{K_s+s_i})^2}{2\sigma^2}\right) \tag{2.11}$$

and we assume that the prior distribution of σ follows

$$P(\sigma) \propto \begin{cases} 1/\sigma, & \sigma > 0 \\ 0, & \sigma \leq 0 \end{cases} \tag{2.12}$$

and that the prior distribution of λ_K and K_s, $P(\lambda_K, K_s)$ is uniform, so now we can integrate the posterior over σ:

$$\begin{aligned} P(\lambda_K, K_s|D) &\propto P(D|\lambda_K, K_s) \\ &\propto \int_0^{+\infty} P(D|\lambda_K, K_s, \sigma)P(\sigma)d\sigma \\ &= \int_0^{+\infty} (\sqrt{2\pi}\sigma)^{-N} \prod_{i=1}^{N} \exp\left(-\frac{(\lambda_i^* - \lambda_K \frac{s_i}{K_s+s_i})^2}{2\sigma^2}\right) \frac{1}{\sigma}\, d\sigma \\ &\propto \left(\sum_{i=1}^{N} (\lambda_i^* - \lambda_K \frac{s_i}{K_s + s_i})^2\right)^{-\frac{N}{2}} \end{aligned} \tag{2.13}$$

The method to find (λ_K^0, K_s^0) that maximises $P(D|\lambda_K, K_s)$ is described in Section 2.4.3.

2.4.2 Estimating the scaling factor between GFP and ribosomal fraction

We aim to find the scaling factor A between GFP measurements of our data and the ribosomal fraction from (Metzl-Raz et al. 2017), assuming the two datasets can be described by the same underlying model Eq 2.5. We denote our dataset as $D_1 \equiv \{(G_i, \lambda_i)\}$ with N_1 measurements, where G is the level of GFP and λ is the specific growth rate. Similarly, we denote the dataset from (Metzl-Raz et al. 2017) as $D_2 \equiv (\{r_j, \lambda_j\})$ with N_2 measurements, where r is the ribosomal fraction. For simplicity, let γ^{-1} and r_0 in Eq 2.5 be m and c, respectively. Under the new mathematical notation, we aim to find A, m and c such that $G_i = A(m\lambda_i + c)$ and $r_j = m\lambda_j + c$.

Assume (1) D_1 and D_2 are described by the same model (i.e. m and c are shared) (2)

the measurement error of G is Gaussian with standard deviation σ_1, and that of ribosomal fraction r is also Gaussian with standard deviation σ_2, and (3) all measurements in both datasets are independent. Then, we can write down the likelihood as

$$\begin{aligned} P(D_1, D_2|A, m, c, \sigma_1, \sigma_2) = (\sqrt{2\pi}\sigma_1)^{-N_1} \prod_{i=1}^{N_1} \exp\left(-\frac{(G_i - A(m\lambda_i + c))^2}{2\sigma_1^2}\right) \times \\ (\sqrt{2\pi}\sigma_2)^{-N_2} \prod_{j=1}^{N_2} \exp\left(-\frac{(r_j - (m\lambda_j + c))^2}{2\sigma_2^2}\right) \end{aligned} \tag{2.14}$$

Assuming that the priors of both σ_1 and σ_2 follow Eq 2.12 and that the prior distribution of A, m and c, $P(A, m, c)$ is uniform, we can integrate the posterior over σ_1 and σ_2:

$$\begin{aligned} P(A, m, c|D_1, D_2) &\propto P(D_1, D_2|A, m, c) \\ &\propto \int_0^{+\infty} (\sqrt{2\pi}\sigma_1)^{-N_1} \prod_{i=1}^{N_1} \exp\left(-\frac{(G_i - A(m\lambda_i + c))^2}{2\sigma_1^2}\right) \frac{1}{\sigma_1} d\sigma_1 \times \\ &\quad \int_0^{+\infty} (\sqrt{2\pi}\sigma_2)^{-N_2} \prod_{j=1}^{N_2} \exp\left(-\frac{(r_j - (m\lambda_j + c))^2}{2\sigma_2^2}\right) \frac{1}{\sigma_2} d\sigma_2 \\ &\propto \left(\sum_{i=1}^{N_1} (G_i - A(m\lambda_i + c))^2\right)^{-\frac{N_1}{2}} \left(\sum_{j=1}^{N_2} (r_j - (m\lambda_j + c))^2\right)^{-\frac{N_2}{2}} \end{aligned} \tag{2.15}$$

The method to find (A_0, m_0, c_0) that maximises $P(D_1, D_2|A, m, c)$ is described in Section 2.4.3.

2.4.3 Finding the parameters that maximise the posterior

To find the parameters that maximise the posterior and the standard deviation of the parameters, I followed the standard method of Bayesian parameter inference (MacKay 2003).

Let the model be $y = f(x; \theta)$ where θ is the parameter set of interest, and D be data. I used `scipy` in Python to find θ_0 that minimises $-\log P(\theta|D)$ with the Broyden–Fletcher–Goldfarb–Shanno (BFGS) algorithm.

To estimate the standard deviation at θ_0, used a Python module `sympy` to find the analytical form of the Hessian matrix $-\nabla\nabla \log P(\theta|D)$ and then evaluate at $\theta = \theta_0$,

denoted as Σ^{-1}. Consider the Taylor expansion of $\log P(\theta|D)$ around θ_0:

$$\log P(\theta|D) = \log P(\theta|D)\big|_{\theta=\theta_0} - \frac{1}{2}(\theta-\theta_0)^T\Sigma^{-1}(\theta-\theta_0) + ... \tag{2.16}$$

which is a Gaussian distribution if higher order terms are negligible. To estimate the error of $y_i(x_i;\theta)$ at each $x = x_i$, I sampled from this Gaussian distribution (Eq 2.16) to get 50 samples $\{\theta_j\}_{j=1}^{50}$ and calculate $\{y_{i,j} = f(x_i;\theta_j\})_{j=1}^{50}$ as the standard deviation of this distribution.

2.4.4 Finding the linear regime between two observables

Assume that we have a set of N_{max} observations of $\{(x_j, y_j)\}_{j=1}^{N_{max}} \equiv D$, which is sorted by x_j in ascending order. We wish to find N_0 such that the linear model $y_j = mx_j + c + \epsilon_j$ holds for $j \in \{1, 2, ..., N_0\}$, where m and c are parameters and $\epsilon_j \sim \text{Normal}(0, \sigma_j^2)$ is a sample of the Gaussian noise, and we have the likelihood:

$$\begin{aligned} P(D_N|m,c,N) &= \prod_{j=1}^{N} P(y_j|x_j,\sigma_j,m,c) \\ &= \left((2\pi)^{-N/2}\prod_{j=1}^{N}\sigma_j^{-1}\right)\exp\left(-\sum_{j=1}^{N}\frac{(y_j-(mx_j+c))^2}{2\sigma_j^2}\right) \end{aligned} \tag{2.17}$$

Note that $D_N \equiv \{(x_j, y_j)\}_{j=1}^{N}$ is dependent on $N \leq N_{max}$ and a subset of D.

In the case where σ is unknown, if we assume a constant σ for all ϵ_j and its prior being $P(\sigma) = 1/\sigma$, we have:

$$\begin{aligned} P(D_N|m,c,N) &= \int_0^{+\infty}\prod_{j=1}^{N} P(y_j|x_j,\sigma,m,c)P(\sigma)d\sigma \\ &= (2\pi)^{-N/2}\int_0^{+\infty}\sigma^{-(N+1)}\exp\left(-\sum_{j=1}^{N}\frac{(y_j-(mx_j+c)^2}{2\sigma^2}\right)d\sigma \\ &= \frac{\Gamma(N/2)}{2\cdot\pi^{N/2}}\left(\sum_{j=1}^{N}(y_j-(mx_j+c)^2\right)^{-N/2} \end{aligned} \tag{2.18}$$

To compare models with different values of N, we aim to find the evidence $P(N|D)$

for each N. If we assume that priors $P(N)$ and $P(m, c)$ are constant, for each N we have:

$$\begin{aligned} P(N|D) &\propto P(D|N)P(N) \propto P(D|N) \\ &= \iint_{\mathbb{R}^2} P(D_N|m, c, N)P(m, c)dm\ dc \\ &\propto \iint_{\mathbb{R}^2} P(D_N|m, c, N)dm\ dc \end{aligned} \tag{2.19}$$

If $\{\sigma_j\}$ are known, $P(D_N|m, c, N)$ takes the form of Eq 2.17, and the integral will be analytical (Hinrichsen et al. 2017). We define $T_1 \equiv \sum_{j=1}^{N} \frac{y_j^2}{2\sigma_j^2}$, $T_2 \equiv \sum_{j=1}^{N} \frac{x_j^2}{2\sigma_j^2}$, $T_3 = \sum_{j=1}^{N} \frac{1}{2\sigma_j^2}$, $T_4 \equiv \sum_{j=1}^{N} \frac{y_j}{\sigma_j^2}$, $T_5 \equiv \sum_{j=1}^{N} \frac{x_j y_j}{\sigma_j^2}$ and $T_6 \equiv \sum_{j=1}^{N} \frac{x_j}{\sigma_j^2}$. Now the likelihood can be calculated as:

$$\begin{aligned} P(D|N) &\propto \iint_{\mathbb{R}^2} P(D_N|m, c, N)dm\ dc \\ &= \left((2\pi)^{-N/2} \prod_{j=1}^{N} \sigma_j^{-1}\right) \iint_{\mathbb{R}^2} \exp\left(-T_1 - m^2 T_2 - c^2 T_3 - cmT_6 + cT_4 + mT_5\right) dm\ dc \\ &= \left((2\pi)^{1-N/2} \prod_{j=1}^{N} \sigma_j^{-1}\right) \sqrt{\frac{1}{4T_2T_3 - T_6^2}} \exp\left(\frac{-4T_1T_2 + T_5^2 + \frac{(2T_2T_4 - T_5T_6)^2}{4T_2T_3 - T_6^2}}{4T_2}\right) \end{aligned} \tag{2.20}$$

If intercept $c = 0$,

$$\begin{aligned} P(D|N) &\propto \int_{-\infty}^{+\infty} P(D_N|m, N)dm \\ &= \left((2\pi)^{-N/2} \prod_{j=1}^{N} \sigma_j^{-1}\right) \int_{-\infty}^{+\infty} \exp\left(-T_1 - m^2 T_2 + mT_5\right) dm \\ &= \left((2\pi)^{-N/2} \prod_{j=1}^{N} \sigma_j^{-1}\right) \sqrt{\frac{\pi}{T_2}} \exp\left(-T_1 + \frac{T_5^2}{4T_2}\right) \end{aligned} \tag{2.21}$$

Otherwise, $P(D_N|m, c, N)$ takes the form of Eq 2.18, and we have:

$$\begin{aligned} P(D|N) &\propto \iint_{\mathbb{R}^2} P(D_N|m, c, N)dm\ dc \\ &\approx P(D_N|m_0, c_0, N)(\det H/2\pi)^{-1/2} \\ &= \frac{\Gamma(N/2)}{2 \cdot \pi^{N/2}} \left(\sum_{j=1}^{N} (y_j - (m_0 x_j + c_0)^2\right)^{-N/2} (\det H/2\pi)^{-1/2} \end{aligned} \tag{2.22}$$

where (m_0, c_0) maximises $\log P(D|m, c, N)$ and $H \equiv -\nabla\nabla \log P(D|m, c, N)\big|_{m=m_0, c=c_0}$.

Then, we choose the model with N_0 that maximises $P(N|D)$. The analytical form of the matrix H can be derived with `sympy.hessian` in Python, and (m_0, c_0) can be found with `scipy.optimize.minimize` in Python.

There is an alternative way to calculate $P(D|N)$ when σ is unknown:

$$\begin{aligned} P(D|N) &\propto \iint_{\mathbb{R}^2} P(D_N|m, c, N) dm\ dc \\ &= \int_0^{+\infty} \left(\iint_{\mathbb{R}^2} P(D_N|m, c, N, \sigma) dm\ dc \right) P(\sigma) d\sigma \end{aligned} \tag{2.23}$$

where the double integral is analytical (Eq 2.20 with $\{\sigma_j\}$ replaced by σ) and the integral over σ can be numerically calculated with, for example, `scipy.integrate.quad` in Python. However, this method is slower than Eq 2.22 in practice.

In practice, for each $N \in \{3, 4, ..., N_{max}\}$, I find N_0 that maximises $P(N|D)$ using Eq 2.21 (assuming intercept $c = 0$), and the linear region is $\{(x_j, y_j)\}_{j=1}^{N_0}$ (Fig 2.16). The σ_j is given by the Gaussian process that estimates dOD/dt's value from $OD(t)$ (Swain et al. 2016).

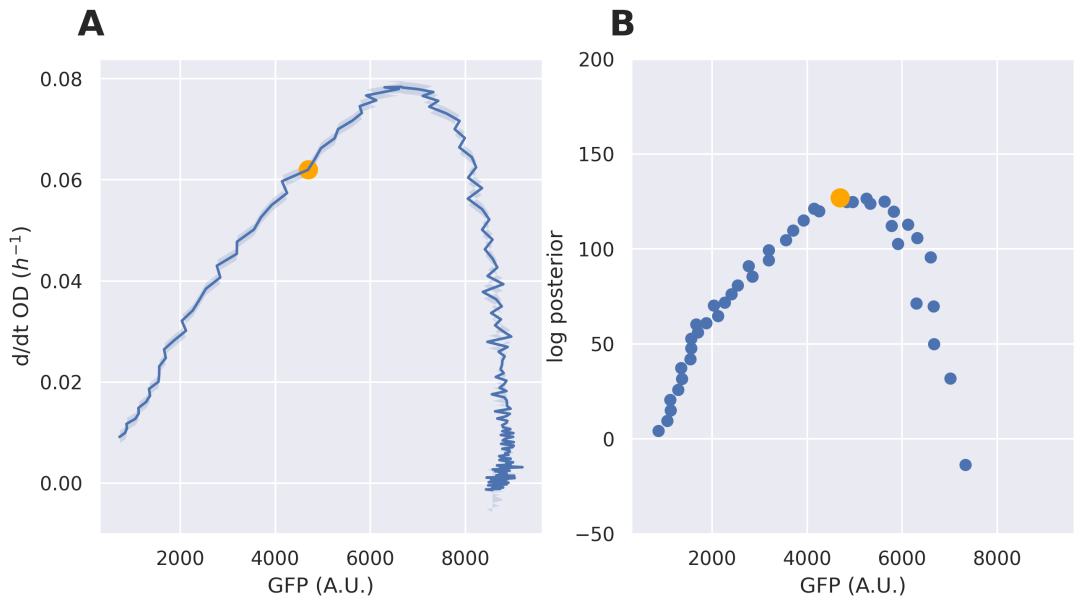

Figure 2.16: Finding the linear regime of the $d/dt\ OD$ *versus* GFP plot. **(A)** The data of one biological replicate in 1.5% raffinose. **(B)** The logarithm of the posterior given by Eq 2.20. The orange dot marks the end of the linear regime, defined by the maximum of the log posterior in (B). In (A), the shaded area represents the standard deviation of two technical replicates given by the Gaussian process to find $d/dt\ OD$.

2.5 Discussion

In this chapter, we monitored the dynamics of population growth in batch cultures. We found that the population growth enters exponential phase only if the initial sugar concentration is high enough (Fig 2.2), which challenges the traditional understanding of Monod's equation in the sense that the exponential growth rate (Monod 1949) is not well-defined when the initial sugar concentration is low. However, Monod's equation still holds if we replace the exponential growth rate with the maximum growth rate in conditions where the exponential phase is hard to identify (Fig 2.3), and in conditions that support exponential growth, the exponential growth rate corresponds to the saturation growth rate λ_K of Monod's equation (Eq 2.3).

Cells synthesise new proteins during each cell cycle before division, and ribosomes are responsible for this protein synthesis. Therefore, measuring the dynamics of ribosomes helps to understand the complex growth dynamics in batch cultures. In this chapter, we showed that we can monitor the dynamics of ribosomes using strains with GFP tagged on a ribosomal protein in *S. cerevisiae*, and the results are in good agreement with (Metzl-Raz et al. 2017) (Fig 2.5), further confirming the linear relationship between the ribosomal fraction and the specific growth rate at low OD. We introduced the effective translation rate, defined as the growth rate per ribosomal at the population level, and showed that the effective translation rate is constant over various carbon sources (Fig 2.7). We refer to this phase of growth as the linear phase. We noticed that the specific growth rate and the ribosomal fraction start to decrease during the linear phase, suggesting that the linear phase extends beyond the exponential growth (Fig 2.8). After the linear phase, the effective translation rate decreases as expected, but the ribosomal fraction does not decrease until growth stops in conditions that support prolonged exponential growth to a high OD, suggesting the cells may not have responded "in time" when the sugar concentration decreases too quickly (Fig 2.9).

With this picture in mind, we will build a minimal model in the next chapter to recapture the growth dynamics of budding yeast, aiming to clarify: (1) why the specific growth rate peaks in sugar-limiting cases (Fig 2.2) and why Monod's equation still holds for those cases (Fig 2.3); (2) what regulation on the ribosome levels is required for the

apparent linear relationship between population growth rate (dOD/dt) and the population's total ribosome level (Fig 2.7); (3) why the ribosomal fraction cannot respond "in time" when the initial sugar concentration is high (Fig 2.9).

Using this methodology, we further explored how the ribosomal fraction couples with growth under various stress conditions. Consistent with the results in *E. coli* (Scott et al. 2010), the effective translation rate decreases when cells are exposed to ribosome-targeting drugs (Figs 2.10CD, 2.11CD and 2.12CD). However, unlike the results in *E. coli* (Scott et al. 2010) the ribosomal fraction does not necessarily increase in response to a decreased translation rate (Figs 2.10EF, 2.11EF and 2.13BD), suggesting that the second growth law (Scott et al. 2010) may not be as generic as previously thought. We also showed that the effective translation rate remains unchanged during weak acid stress imposed by acetate (Fig 2.14CD) and decreases in prolonged osmotic stress (Fig 2.15CD), possibly caused by molecular crowding. Notably, the effective translation rate never exceeds the constant we observed across stress-free conditions (Fig 2.8CD), suggesting the existence of an empirical upper limit.

2.5.1 Limitation of this methodology

This methodology enables us to systematically investigate the coupling of ribosomal levels and growth. There are multiple ways to modulate growth in addition to those we adopted in this chapter, including changing the temperature, auxotrophy and overexpressing gratuitous proteins (Scott and Hwa 2022). We note that this methodology relies on the assumptions (1) that the GFP intensity is proportional to total number of ribosomes and this proportionality does not change in different conditions; (2) that the OD is a known function of the cell numbers, and therefore, caution must be taken when we interpret the data. For example, GFP brightness is a function of temperature (Patterson et al. 1997), so the proportionality may change between datasets in different temperatures. In Fig 2.15A, under hyperosmotic stress, even though we have measured the OD as a function of cell numbers separately for stress-free and hyperosmotic conditions, the OD may not be a known function of cell number at the beginning of the experiment, because the cell volume changes during adaptation to higher osmotic pressure.

Chapter 3

A self-replicator model

3.1 Summary

- Context: in Chapter 2, we measured the dynamics of growth and ribosomal levels.
- Research question: what is the simplest ordinary differential equation (ODE) model that can capture the essence of yeast growth dynamics in batch cultures?
- Approach: I built a self-replicator model assuming that the intracellular biomass density is constant.
- Finding: a three-component minimal model captures the growth and ribosome dynamics in experiments; a more complex model with two substrates generalises Monod's equation at steady state.
- Outlook: our results suggest the potential of capturing complex microbial growth dynamics with low-dimensional mathematical models.

3.2 Background

In this chapter, we aim to understand the observed dynamics of growth and ribosome in Chapter 2 within a self-replicator model.

Self-replicator models explicitly include one auto-catalytic reaction, that is, the self-replication of ribosomes. The first self-replicator model was proposed by Molenaar *et al*

(Molenaar et al. 2009). Later on, this type of model is used to address biological questions including:

1. What is the steady-state level of the cellular components in different nutrient conditions or stress conditions under the constraint of a limited proteome size (Scott et al. 2010; O'Brien et al. 2013; You et al. 2013)?

2. What is the steady-state level of cellular components that supports optimal growth, and what strategy enables cells to achieve that (Dourado and Lercher 2020; de Groot et al. 2020; Elsemman et al. 2022)?

3. How does the level of cellular components change during a nutrient upshift or downshift (i.e. from one steady-state to another) (Erickson et al. 2017; Basan et al. 2020; Yabo et al. 2022)?

Although models like (Weiße et al. 2015) can be extended to study dynamics of population growth, we would like to begin with a simpler model that is more transparent or analytical. In this chapter, we will build a framework and a self-replicator model to study the dynamics of population growth in batch cultures, where a true steady-state does not exist until all nutrients have been consumed, because the nutrient concentration is monotonically decreasing. We will compare our results with those in Chapter 2 to answer the questions in Section 2.5 and show that a minimal model can capture the essence of the growth dynamics observed in Chapter 2. We will also extend the minimal model to include one carbon and one nitrogen source, and from the extended model we will mechanistically derive a generalised form of Monod's Equation for two limiting substrates.

3.3 Mathematical framework

We model the dynamics of metabolites and proteins of cell growth by assuming that a cell consists of n species of metabolites and proteins.

3.3.1 Mass fractions z_i as state variables of a single cell

Denote mass of species i as Z_i. The mass of n species sums up to be the total biomass B in one single cell:

$$\sum_{i=1}^{n} Z_i = B \tag{3.1}$$

We further define mass fraction of species i as:

$$z_i \equiv Z_i/B \tag{3.2}$$

and from Eq 3.1 we know that mass fractions of all species in a cell must sum up to 1:

$$\sum_{i=1}^{n} z_i = 1 \tag{3.3}$$

We use mass fractions z_i as state variables in the ODEs. The mass fraction we use here is proportional to the molar concentration when the cell has a constant density. If we denote the molecular weight of chemical species i as M_i, the number of molecule in the cell as X_i, the Avogadro's constant as n_A, the cell's biomass density as ρ, and the cell's volume as V_c, we have:

$$z_i \equiv \frac{Z_i}{B} = \frac{M_i X_i}{n_A \cdot \rho V_c} \propto \frac{1}{\rho}\frac{X_i}{V_c} \tag{3.4}$$

because $\rho \equiv B/V_c$ and $Z_i = M_i X_i/n_A$. If the intracellular mass density ρ is constant, z_i is proportional to the molar concentration X_i/V_c.

3.3.2 Rate of biochemical reactions and the general form of $\dot{z}_i$

Consider first- and non-dimerising second-order elementary reactions only within the cell. The mesoscopic rate of a first-order elementary reaction is given by $R_1 = c_1 X_A$, where X_A is the number of molecule A and c_1 is constant; the mesoscopic rate of a second-order elementary reaction is given by $R_2 = c_2 X_A X_B$, where $X_A,\ X_B$ are the number of molecules A, B, respectively (Gillespie 1976).

Assume there are m biochemical reactions in a single cell, of which m_1 are first-order reactions and $m - m_1$ of which are non-dimerising second-order reactions. For each species i and each reaction j, we use $S_{i,j}$ to denote the stochiometry of species i in reaction j.

The *net* production rate of species i is

$$\frac{dX_i}{dt} = \sum_{j=1}^{m_1} S_{i,j} R_{1,j} + \sum_{k=1}^{m-m_1} S_{i,k} R_{2,k} \tag{3.5}$$

where $S_{i,j} > 0$ means that species i is a product in reaction j; $S_{i,j} = 0$ means that species i does not participate in reaction j; $S_{i,j} < 0$ means that species i is a reactant in reaction j.

Again we denote M_i as the molecular weight of species i and n_A is the Avogadro's number, and the total mass of species i is $Z_i = M_i X_i / n_A$. Differentiate Z_i over time t and use the production rate in Eq 3.5, and we have:

$$\frac{dZ_i}{dt} = \frac{M_i}{n_A}\frac{dX_i}{dt} = \frac{M_i}{n_A}\left(\sum_{j=1}^{m_1} S_{i,j} R_{1,j} + \sum_{k=1}^{m-m_1} S_{i,k} R_{2,k}\right) \tag{3.6}$$

Both R_1 and R_2 can be re-written as functions of mass fraction z_i, instead of the number of molecules X_i, because $z_i \propto X_i$ in Eq 3.4. Using Eq 3.4, the form of first-order reaction rate as a function of mass fraction z_i is

$$R_1 = c_1 X_A = c_1 \frac{n_A \cdot \rho V_c}{M_A} z_A = \tilde{c}_1 B z_A \tag{3.7}$$

where $\tilde{c}_1 \equiv c_1 n_A / M_A$ is a constant. Similarly, for a second-order reaction,

$$R_2 = c_2 X_A X_B = c_2 \frac{n_A^2 \cdot \rho^2 V_c^2}{M_A M_B} z_A z_B = \tilde{c}_2 B z_A z_B \tag{3.8}$$

where $\tilde{c}_2 \equiv c_2 V_c n_A^2 \rho / (M_A M_B)$ is also a constant, because $c_2 \propto 1/V_c$ (Gillespie 1976). We see that in both Eqs 3.7 and 3.8, the terms $\tilde{c_1} z_A$ and $\tilde{c_2} z_A z_B$ are similar to the reaction rate described by the law of mass action in terms of molar concentrations.

Now we derive the general form of ODE for each z_i. Before we start, we denote the specific growth rate of the single cell as λ, whose definition is:

$$\lambda \equiv \frac{\dot{B}}{B} \tag{3.9}$$

By the definition of z_i (Eq 3.2), we have

$$\dot{Z}_i = \dot{B} z_i + \dot{z}_i B \tag{3.10}$$

and we are interested in $\dot{z}_i$, so we rearrange Eq 3.10 into:

$$\dot{z}_i = \dot{Z}_i / B - \frac{\dot{B}}{B} z_i = \dot{Z}_i / B - \lambda z_i \tag{3.11}$$

where the second equality comes from the definition of λ (Eq 3.9).

We can calculate the $\dot{Z}_i/B$ term in Eq 3.11 from Eq 3.6:

$$\begin{aligned} \dot{Z}_i / B &= \frac{M_i}{n_A} \left(\sum_{j=1}^{m_1} S_{i,j} \frac{R_{1,j}}{B} + \sum_{k=1}^{m-m_1} S_{i,k} \frac{R_{2,k}}{B} \right) \\ &= \frac{M_i}{n_A} \left(\sum_{j=1}^{m_1} S_{i,j} \tilde{R}_{1,j} + \sum_{k=1}^{m-m_1} S_{i,k} \tilde{R}_{2,k} \right) \end{aligned} \tag{3.12}$$

where each $\tilde{R}_1$ takes the form of $\tilde{c_1} z_A$, and each $\tilde{R}_2$ takes the form of $\tilde{c_2} z_A z_B$, by Eqs 3.7 and 3.8.

So far we have only considered reactions within the cell. Substrates and ligands in the medium can bind to transporters and receptors on the surface of the cell. For a transporter T, we assume Eq 3.4 still holds. However, for the substrate S, we can no longer transform the number of molecules X_S into z_S using Eq 3.4. If we denote the volume of the *culture* as V, we can instead transform X_S into mass concentration s_S by:

$$s_S = \frac{M_S X_S}{n_A V} \tag{3.13}$$

Assume transport is a second-order elementary reaction, and similar to Eq 3.8, we have:

$$R_2 = c_2 X_S X_T = c_2 \frac{n_A^2 V}{M_T M_S} B z_T s_S \equiv \tilde{c_2}' B z_T s_S \tag{3.14}$$

where $\tilde{c_2}' \equiv \frac{c_2 V n_A^2}{M_T M_S}$ is constant, because V is constant and so is $c_2 \propto 1/V$ (Gillespie 1976). Accordingly, in Eq 3.15, this reaction will contribute a term in the form of $\tilde{R}_2' = \tilde{c}_2' z_T s_S$, which is again similar to the law of mass action, as expected.

Now we have recovered the mass action-like reaction rates for first- and second-order elementary reactions in terms of mass fractions and substrate concentrations. We substitute Eq 3.12 into Eq 3.11 and have:

$$\dot{z}_i = \frac{M_i}{n_A}\left(\sum_{j=1}^{m_1} S_{i,j}\tilde{R}_{1,j} + \sum_{k=1}^{m-m_1} S_{i,k}\tilde{R}_{2,k}\right) - \lambda z_i \tag{3.15}$$

The reaction rate of more complex reactions, for example, enzymatic reactions with Michaelis-Menten kinetics, which are derived from first- and second-order elementary reactions, is hence recovered similarly. Let $p_i \equiv \dot{Z}_i/B$. Then p_i is the sum of rates of production and consumption of species i in all reactions, and hence a function of some z_j's and some s_k's by Eq 3.12. To write it more compactly, let $\boldsymbol{z}$, $\boldsymbol{s}$ be vectors of all mass fractions and that of all mass concentrations of substrate, respectively. Then $p_i = p_i(\boldsymbol{z}, \boldsymbol{s})$. Now Eq 3.11 becomes:

$$\dot{z}_i = p_i(\boldsymbol{z}, \boldsymbol{s}) - \lambda z_i \tag{3.16}$$

which is the general form of $\dot{z}_i$ in our model.

3.3.3 Modelling single-cell growth

The state of a growing single cell is represented by the mass fraction of each species $\boldsymbol{z}$ and the mass of the cell B. The ODE of each z_i is described in Eq 3.16. For B, by Eq 3.9, we have:

$$\dot{B} = \lambda B \tag{3.17}$$

The specific growth rate λ is a function of $\boldsymbol{z}$ and $\boldsymbol{s}$. Differentiate Eq 3.3:

$$\sum_{i=1}^{n} \dot{z}_i = 0 \tag{3.18}$$

Using Eqs 3.3 and 3.16, we have:

$$0 = \sum_{i=1}^{n} \dot{z}_i = \sum_{i=1}^{n} p_i(\boldsymbol{z}, \boldsymbol{s}) - \lambda \sum_{i=1}^{n} z_i = \sum_{i=1}^{n} p_i(\boldsymbol{z}, \boldsymbol{s}) - \lambda \tag{3.19}$$

and thus,

$$\lambda = \sum_{i=1}^{n} p_i(\boldsymbol{z}, \boldsymbol{s}) \tag{3.20}$$

To summarise, we model single-cell growth by Eqs 3.16 and 3.17. If we model n biochemical species, there are in total $n + 1$ state variables including B, and Eq 3.3 imposes one constraint on the variables. Thus, this is a dynamical system of order n.

3.3.4 Modelling growth of a homogeneous, synchronous population

We extend the model from single-cell growth to growth of a homogeneous, synchronous population. Let N be the number of cells and B be the mass of each single cell. Let B_c be the critical mass of a cell, and assume a cell divides into two at $B = 2B_c$, which guarantees the cell mass to be within interval $[B_c, 2B_c)$. Then for any time interval $[t_0, t_1)$ that contains one division at time t_d (Fig 3.1), we have:

$$N(t) = \begin{cases} N_0 & t \in [t_0, t_d) \\ 2N_0 & t \in [t_d, t_1) \end{cases} \tag{3.21a}$$

$$B(t) = \begin{cases} B_1(t) & t \in [t_0, t_d) \\ B_2(t) & t \in [t_d, t_1) \end{cases} \tag{3.21b}$$

where

- $B_1(t)$ is the solution of the single-cell model (Eqs 3.16 and 3.17), with initial conditions $z_i(t_0) = z_{i,0},\ s_k(t_0) = s_{k,0}$ and $B(t_0) = B_0 \in (B_c, 2B_c)$;
- t_d is determined by $B_1(t_d) = 2B_c$;
- $B_2(t)$ is also the solution of the single-cell model, with initial conditions $z_i(t_d) = z'_{i,0},\ s_k(t_d) = s'_{k,0}$ and $B_2(t_d) = B_c$.

Below we show that the specific growth rate λ is continuous within time interval $[t_0, t_1)$ under certain assumptions. First, we assume upon division that all biochemical species

are distributed equally into the two daughter cells, such that the population remains homogeneous and synchronous after one division. Therefore, the mass fraction $\boldsymbol{z}$ should remain continuous before and after division at t_d, and mathematically, it means that the limit from the left of t_d: $\lim_{t\to t_d^-} z_i(t) = z'_{i,0}$, which guarantees that $z_i(t)$ is continuous within time interval $[t_0, t_1)$. Second, we assume that the substrate concentration $\boldsymbol{s}(t)$ is also continuous within time interval $[t_0, t_1)$. Finally, we assume $p_i(\boldsymbol{z}, \boldsymbol{s})$ is continuous, and by Eq 3.20 and by composition of continuous functions, $\lambda(\boldsymbol{z}(t), \boldsymbol{s}(t))$ is also continuous within time interval $[t_0, t_1)$, as desired.

Define population biomass $\beta \equiv NB$. Within $[t_0, t_d)$ and (t_d, t_1), we have $\dot{N} = 0$ and so:

$$\dot{\beta} = \dot{N}B + \dot{B}N = \dot{B}N = \lambda BN = \lambda\beta \tag{3.22}$$

where the second equality arises from $\dot{N} \equiv 0$ and the third arises from Eq 3.17.

Here we show that $\beta(t)$ is differentiable at $t = t_d$, and further Eq 3.22 also holds at $t = t_d$. By Eq 3.20, $\lambda_1(t_d)$ is a function of $(\boldsymbol{z}, \boldsymbol{s})$ at $t = t_d$, and $\lambda_2(t_d)$ is a function of the initial condition $\{z'_{i,0}\}$ and $\{s'_{k,0}\}$.

First, for negative Δt,

$$\begin{aligned}\lim_{\Delta t\to 0^-} \frac{\beta(t_d+\Delta t)-\beta(t_d)}{\Delta t} &= N_0 \lim_{\Delta t\to 0^-} \frac{B_1(t_d+\Delta t)-B_1(t_d)}{\Delta t} \\ &= N_0\dot{B}_1(t_d) = N_0\lambda_1(t_d)\cdot(2B_c)\end{aligned} \tag{3.23}$$

Second, for positive Δt,

$$\begin{aligned}\lim_{\Delta t\to 0^+} \frac{\beta(t_d+\Delta t)-\beta(t_d)}{\Delta t} &= 2N_0 \lim_{\Delta t\to 0^+} \frac{B_2(t_d+\Delta t)-B_2(t_d)}{\Delta t} \\ &= 2N_0\dot{B}_2(t_d) = 2N_0\lambda_2(t_d)B_c\end{aligned} \tag{3.24}$$

By continuity of $\lambda(t)$, $\lambda_1(t_d) = \lambda_2(t_d) = \lambda(t_d)$, and therefore the two one-sided limits are equal and $\beta(t)$ is differentiable at $t = t_d$:

$$\dot{\beta}(t_d) \equiv \lim_{\Delta t\to 0} \frac{\beta(t_d+\Delta t)-\beta(t_d)}{\Delta t} = 2\lambda(t_d)N_0B_c \tag{3.25}$$

$\beta(t)$ being differentiable guarantees its continuity, and so $\beta(t_d) = 2N_0B_c$. Thus,

$$\dot{\beta}(t_d) = \lambda(t_d)\beta(t_d) \tag{3.26}$$

which means Eq 3.22 holds within $[t_0, t_1)$.

For any time interval $[0, t)$ containing multiple division events, we can show that Eq 3.22 still holds following similar procedure. Furthermore, Eq 3.22 shares the same mathematical form with 3.17, which suggests the single-cell model (Eqs 3.16 and 3.17) can be applied to growth of a homogeneous, synchronous population. Therefore, we will also use B, instead of β, to denote biomass of a population.

Finally, the number of division events is $\lfloor \log_2 \frac{\beta(t)}{B_c} \rfloor$ and hence the number of cells is $N(t) = 2^{\lfloor \log_2 \frac{\beta(t)}{B_c} \rfloor}$.

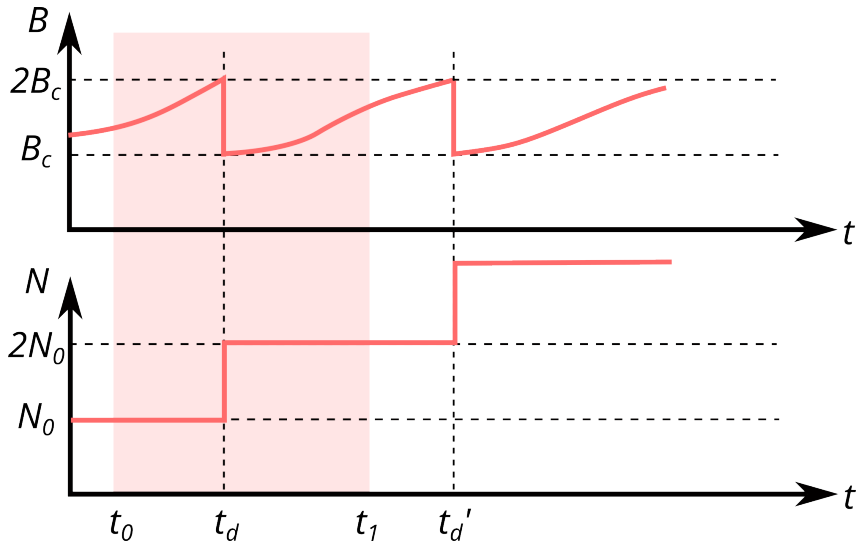

Figure 3.1: The change in biomass B and cell number N of a homogeneous synchronous population upon cell division. In Eq 3.21 we consider time interval $[t_0, t_1)$ which contains one division at time t_d. $2B_c$ is the critical biomass when a cell divides.

3.3.5 Modelling growth in batch cultures

We have shown that Eqs 3.16 and 3.17 can describe the growth of a homogeneous, synchronous population. If such growth occurs in a batch culture, the consumption of substrates by cells will affect the concentration of substrates $\boldsymbol{s}$, which in return affects the rate of substrate transport.

If we model growth in a set of substrates $\{s_k\}$ in a batch culture with a fixed volume

V, in which each substrate k contributes to a fraction of biomass $Q_k < 1$, and the yield of mass is $Y_k < 1$, then by mass conservation, we have:

$$s_k V + (B - B_0)Q_k/Y_k = s_{k,0}V \tag{3.27}$$

where $s_{k,0}$ the initial mass concentrations and B_0 is the initial biomass.

Differentiating Eq 3.27 and using Eq 3.17, we have:

$$\dot{s_k} = -\frac{Q_k \dot{B}}{Y_k V} = -\frac{\lambda B Q_k}{Y_k V} \tag{3.28}$$

with initial conditions $s_k(0) = s_{k,0}$ for each k and $B(0) = B_0$.

3.4 The minimal model

We consider a model with one carbon source (s), one biomass precursor (a), ribosome (r) and a transporter (e_T).

1. transport and metabolism: $\mathrm{s} \xrightarrow{\mathrm{e_T}} \mathrm{Y}_s\mathrm{a}$
2. Translation of transporters and ribosomes: $\mathrm{a} \xrightarrow{\mathrm{r}} f_T\,\mathrm{T} + f_r\,\mathrm{r}$, where $f_T + f_r = 1$.

where f_T and f_r describe the fraction of ribosome dedicated to production of transporters (e_T) and ribosomes (r), respectively. For simplicity, we assume the biomass is solely contributed by the carbon source ($Q_s = 1$) and the yield of mass $Y_s = 1$.

We are interested in the growth of a synchronous, homogeneous population in a batch culture. We denote the biomass of the population as B, and the volume of the culture as V, and the system is described by:

$$\dot{a} = v_T e_T - \gamma_e r - \lambda a \tag{3.29a}$$

$$\dot{r} = f_r \gamma_e r - \lambda r \tag{3.29b}$$

$$\dot{e_T} = f_T \gamma_e r - \lambda e_T \tag{3.29c}$$

$$\dot{B} = \lambda B \tag{3.29d}$$

$$\dot{s} = -\frac{\lambda B}{V} \tag{3.29e}$$

where v_T and γ_e are the substrate transport rate and effective translation rate, defined below in Eqs 3.31 and 3.32, and following Eq 3.20

$$\lambda = v_T e_T \tag{3.30}$$

The initial conditions are $a(0), r(0), e_T(0) \in (0,1)$ and $B(0), s(0) > 0$.

We assume v_T follows simple Michaelis-Menten kinetics with feedback inhibition by a:

$$v_T = v_{T,max} \frac{s}{K_s + s} \cdot \frac{1}{1 + (a/K_a)^2} \tag{3.31}$$

where K_s and K_a are constant. The feedback inhibition with $K_a \ll 1$ is necessary to keep a small, which is a reasonable assumption because the lipids and free amino acids within a cell take up only a small percentage of cell mass in budding yeast (Nissen et al. 1997). We assume that γ_e follows simple Michaelis-Menten kinetics:

$$\gamma_e = \gamma_{e,max} \frac{a}{K_r + a} \tag{3.32}$$

We further assume that f_r is a function of a, which satisfies $f_r \in [0,1]$ and $\partial f_r / \partial a > 0$.

3.4.1 The intracellular subsystem has one unique stable steady state

In this section, we focus on the **intracellular subsystem** where the biomass B is not considered and s is constant. If $B_0 \ll 1$, B and s are decoupled from the rest of the system at the early stage of growth, because $B \ll 1$ and $\dot{B} \approx 0$ by Eq 3.29d. By mass conservation (Eq 3.28), $\dot{s} = -\dot{B}/V \approx 0$, which means that the sugar concentration changes slowly compared to the intracellular state of cells. Therefore, at the fast timescale, we can focus on Eq 3.29a, b and c and view s as positive constant.

By Eq 3.3, $a + r + e_T = 1$, so we can further rewrite Eq 3.29a, b and c as:

$$\dot{a} = v_T(1 - r) - \gamma_e r - v_T(2 - r - a)a \tag{3.33a}$$

$$\dot{r} = f_r \gamma_e r - v_T(1 - r - a)r \tag{3.33b}$$

We call this 2-dimensional system the intracellular subsystem because the two variables describe the intracellular state.

If the intracellular subsystem has a steady state (a^*, r^*), then it satisfies

$$\gamma_e r = v_T(1-r) - v_T(2-r-a)a \tag{3.34a}$$

$$f_r\gamma_e = v_T(1-r) + v_T a \tag{3.34b}$$

where we omitted the $*$ sign which represents steady state. The Jacobian matrix is

$$J = \begin{pmatrix} \frac{\partial v_T}{\partial a}(1-r+a(a+r-2)) - \frac{\partial \gamma_e}{\partial a}r - v_T(2-r-2a) & -(v_T+\gamma_e) + v_T a \\ \frac{\partial (f_r\gamma_e)}{\partial a}r - \frac{\partial v_T}{\partial a}(1-r)r + r\left(v_T + \frac{\partial v_T}{\partial a}a\right) & f_r\gamma_e - v_T(1-2r) + v_T a \end{pmatrix} \tag{3.35}$$

This system has two simple fixed points if $a,\ r \in [0,1]$:

1. $a^* = 1,\ r^* = 0$. $\mathrm{Tr}(J) = f_r\gamma_e > 0$, $\mathrm{Det}(J) = f_r\gamma_e\frac{\partial v_T}{\partial a} < 0$ This is a saddle node.

2. $a^* = 0,\ r^* = 1$. $\mathrm{Tr}(J) = -\partial\gamma_e/\partial a < 0$, $\mathrm{Det}(J) = -(1-f_r)v_T(\partial\gamma_e/\partial a) < 0$. This is also a saddle node.

Here we show the existence and uniqueness of another fixed point (a^*, r^*), $a^*, r^* \in (0,1)$. Assume $a \ll 1$, $r > 0$ in Eq 3.34 and view r as a function of a, and we have from Eq 3.34b:

$$r(a) = 1 - \frac{f_r(a)\gamma_e(a)}{v_T(a)} \tag{3.36}$$

and by subtracting Eq 3.34a from b, we have:

$$r(a) = f_r(a) \tag{3.37}$$

Define function $g(a)$ by subtracting Eq 3.36 from Eq 3.37:

$$g(a) \equiv 1 - \frac{f_r(a)\gamma_e(a)}{v_T(a)} - f_r(a),\ a \in [0,1) \tag{3.38}$$

$g(a)$ is a continuous, monotonically decreasing function, given that $f_r(a)$ and $\gamma_e(a)$ monotonically increase and $v_T(a)$ monotonically decreases and $f_r(a)$, $\gamma_e(a)$ and $v_T(a)$ are all

continuous. We also know that $g(0) = 1 - f_r(0) > 0$ and $\lim_{a\to 1} g(a) = -\infty < 0$ because $\lim_{a\to 1} v_T(a) = 0$ and $\gamma_e(0) = 0$. By the intermediate value theorem, $a^* \in (0, 1)$ exists such that $g(a^*) = 0$. a^* is unique because $g(a)$ is monotonic. Accordingly, $r^* < 1$ because $a^* + r^* \leq 1$ (by Eq 3.3) and $a^* > 0$.

Here we analyse the linear stability of this fixed point. From Eqs 3.36 and 3.37, we have:

$$f_r(a^*) = r^* \tag{3.39a}$$

$$\gamma_e(a^*) f_r(a^*) = v_T(a^*)(1 - r^*) \tag{3.39b}$$

Again, assume $a \ll 1$ in the Jacobian matrix (Eq 3.35) and use Eq 3.39, and we have:

$$\mathrm{tr}(J) = \frac{\partial v_T}{\partial a}(1 - r) - \frac{\partial \gamma_e}{\partial a} r - 2\gamma_e r \tag{3.40}$$

and

$$\det(J) = \gamma_e r \left(-(1 - r)\frac{\partial v_T}{\partial a} + r\frac{\partial \gamma_e}{\partial a} + (v_T + \gamma_e)\frac{\partial f_r}{\partial a} + \gamma_e r \right) \tag{3.41}$$

where we omitted the $*$ sign for steady state again. By Eqs 3.31 and 3.32, $\partial v_T/\partial a < 0$, $\partial \gamma_e/\partial a > 0$, and we assumed $\partial f_r/\partial a > 0$, so $\det(J) > 0$, which means (a^*, r^*) is stable — either a stable node or a stable spiral. Fig 3.2 visualises the vector field around the fixed point and the nullclines approximated by Eq 3.39, which shows that the position of the fixed point can be well approximated by the intersection of Eq 3.39.

3.4.2 The intracellular subsystem recovers the growth laws at steady state

Below we show that at the stable steady state, the intracellular subsystem recovers the growth laws. We first look at **Monod's equation**, which describes an empirical relationship between the steady-state growth rate λ^* and the carbon source concentration s^* (Monod 1949). Again, the $*$ sign represents a steady-state value. Assuming $a \ll 1$, we have

$$r + e_T \approx 1 \tag{3.42}$$

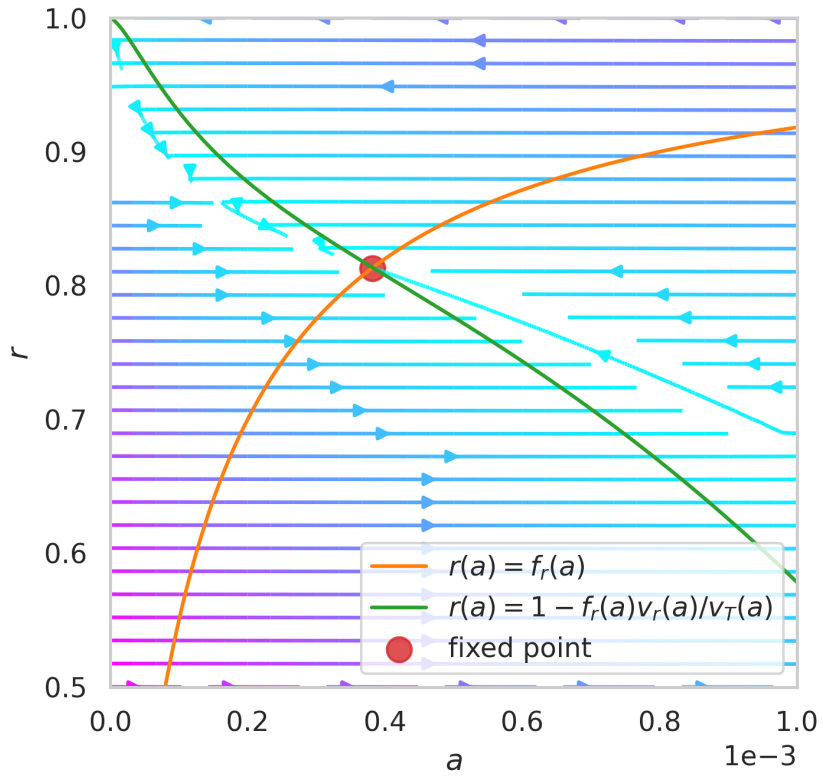

Figure 3.2: The position of the fixed point in the minimal model (Eq 3.33) can be well approximated by the intersection of Eq 3.39. The colour of the stream line represents the Euclidean norm of the vector, with bright blue and magenta indicating small and large norms, respectively. The fixed point (red dot) is found by numerical integration. The parameters are listed in Table 3.1. The initial condition is listed in Table 3.2.

Meanwhile, $a \ll 1$ and $\dot{a} = 0$ imply that

$$\gamma_e r^* \approx v_T e_T^* = \lambda \tag{3.43}$$

by 3.33a, and the second equality is from Eq 3.30. Combining Eqs 3.42 and 3.43, we have:

$$\frac{1}{\lambda^*} = \frac{1}{v_T} + \frac{1}{\gamma_e} \tag{3.44}$$

If we further assume that the end-product inhibition of the transporter is negligible at steady state, Eq 3.31 becomes:

$$v_T \approx v_{T,max} \frac{s}{K_s + s} \tag{3.45}$$

Substitute Eq 3.45 into Eq 3.44,

$$\lambda^* = \frac{v_{T,max}}{v_{T,max}/\gamma_e + 1} \cdot \frac{s}{\frac{K_s}{v_{T,max}/\gamma_e + 1} + s} \tag{3.46}$$

which recovers Monod's equation, if γ_e is constant across steady states with different s. Simulation results in Fig 3.4A (orange data points) show Monod's equation in Eadie-Hofstee form (Eadie 1942; Hofstee 1959):

$$\lambda^* = \lambda_K - s_1 \frac{\lambda^*}{s} \tag{3.47}$$

where $\lambda_K \equiv \frac{v_{T,max}}{v_{T,max}/\gamma_e + 1}$ and $s_1 \equiv \frac{K_s}{v_{T,max}/\gamma_e + 1}$.

The first growth law describes a linear relationship between the steady-state growth rate λ^* and the ribosomal level r^* (Scott et al. 2010; Metzl-Raz et al. 2017). By Eq 3.43, we immediately have

$$\lambda^* = v_T e_T^* = \gamma_e r^* \tag{3.48}$$

If γ_e is constant across steady states with different s, $\lambda^* \propto r^*$. Simulation results in Fig 3.4B (orange data points) shows the first growth law. Note that γ_e is no longer constant in conditions where r^* approaches $f_{r,min}$, a minimal ribosomal fraction to be introduced in Eq 3.62, which gives rise to the non-zero intercept in the result of linear regression in

Fig 3.4B.

When *E. coli* cells are exposed to a fixed nutrient condition and different concentrations of chloramphenicol, the steady-state ribosomal level increases linearly with the decreasing specific growth rate (Scott et al. 2010). This is sometimes called **the second growth law**. This relationship immediately follows from Eq 3.30 and 3.42 in our model:

$$\lambda = v_T(1 - r) \tag{3.49}$$

or equivalently,

$$r = 1 - \frac{\lambda}{v_T} \tag{3.50}$$

which holds whether or not the system is at steady state. Considering the steady state only, if v_T is constant across different chloramphenicol concentrations c_m, Eq 3.50 describes the linear relationship between the steady-state ribosomal level and specific growth rate, each being a function of the c_m:

$$r^*(c_m) = 1 - \frac{\lambda^*(c_m)}{v_T} \tag{3.51}$$

3.4.3 The maximum growth rate follows Monod's equation under certain assumptions

In Chapter 2, we showed that in "sugar-limiting" conditions, the growth rate peaks instead of plateaus (Fig 2.2), and this maximum growth rate as a function of initial sugar concentration also follows Monod's equation (Fig 2.3). In this section, we will derive under what condition Monod's equation will hold for this maximum growth rate.

When the growth rate λ reaches maximum, by Eq 3.30, we have:

$$\dot{\lambda} = \frac{d}{dt}(v_T e_T) = 0 \tag{3.52}$$

which is

$$v_T \dot{e_T} + \dot{v_T} e_T = 0 \tag{3.53}$$

By Eq 3.31 and assuming $a \ll K_a \ll 1$ so that $\frac{\partial v_T}{\partial a} \approx 0$, we have:

$$\dot{v_T} = \frac{\partial v_T}{\partial s}\dot{s} + \frac{\partial v_T}{\partial a}\dot{a} \approx \frac{\partial v_T}{\partial s}\dot{s} \tag{3.54}$$

in which

$$\frac{\partial v_T}{\partial s} \approx \frac{K_s v_T^2}{s^2 v_{T,max}} \tag{3.55}$$

By Eqs 3.27 and 3.29e and assuming that the initial biomass is small compared to initial mass of sugar: $B_0 \ll s_0 V$, we have:

$$\dot{s} = -\frac{\lambda B}{V} = -\lambda(s_0 - s) \tag{3.56}$$

Substituting Eqs 3.29c, 3.54, 3.55 and 3.56 into Eq 3.53, we have:

$$f_T \gamma_e r v_T - \lambda e_T v_T - \lambda \frac{(s_0 - s) e_T K_s v_T^2}{(s^2 v_{T,max})} = 0 \tag{3.57}$$

Using Eqs 3.29a and 3.30 and $v_T \approx v_{T,max}\frac{s}{K_s+s}$ (by Eq 3.31 with $a \ll K_a$), we have:

$$\lambda^2 \left(\frac{K_s s_0 + s^2}{s^2 v_{T,max}} \right) - f_T \lambda + f_T \dot{a} = 0 \tag{3.58}$$

and we solve for λ:

$$\lambda = \frac{f_T \pm \sqrt{f_T^2 - 4 f_T \dot{a} \left(\frac{K_s s_0 + s^2}{s^2 v_{T,max}} \right)}}{2 \left(\frac{K_s s_0 + s^2}{s^2 v_{T,max}} \right)} \tag{3.59}$$

and we choose the larger root because it guarantees $\lambda > 0$ for any $\dot{a}$. If we further assume: (1) $s \approx s_0$, which means that the biomass is still small when the growth rate peaks, and (2) $|\dot{a}| \ll f_T v_T/4$, which means that the biomass precursor does not fluctuate too much, and (3) $f_T(a)$ at the peak of growth rate is approximately constant over different initial sugar concentration s_0, we have:

$$\lambda \approx \frac{f_T v_{T,max} s_0}{K_s + s_0} = f_T v_T(s_0) \tag{3.60}$$

which takes the form of Monod's equation.

Note that Eq 3.60 is different from the steady-state Monod's equation (Eq 3.46). This

difference can be seen in the slope of the simulation result (Fig 3.4A), whose absolute value represents the Monod's constant. This is because the Monod constant at steady state in Eq 3.46, $\frac{K_s}{v_{T,max}/\gamma_e+1}$, is smaller than the Monod constant at the growth rate peak, K_s.

However, if we introduce the steady state constraint by setting Eq 3.29c to be zero, and using Eq 3.43, we have

$$f_T = e_T \approx 1 - r \approx 1 - \lambda/\gamma_e \tag{3.61}$$

Substituting Eq 3.61 into Eq 3.60 and solving for λ again, we get back the steady-state Monod's equation (Eq 3.46).

3.4.4 The minimal model can capture the growth and ribosomal dynamics in experiments

Now we compare the results of simulation (Figs 3.3 and 3.4) from a set of naively chosen parameters (Table 3.1) with the experimental results in Chapter 2.

In Chapter 2, we observed two families of growth curves (Fig 2.2). In conditions with low initial sugar concentrations (sugar-limiting cases), the specific growth rate peaks before decreasing; in conditions with a high sugar concentration, the growth enters a prolonged exponential growth. As shown in Fig 3.3B, this model (Eq 3.29) can reproduce this observation. By Eq 3.29e, when biomass $B \ll V$, $\dot{s} \approx 0$, and intracellular subsystem (Eq 3.33) is affected by s only via $v_T(s, a)$, so the intracellular subsystem will approach the (quasi-)steady state (Section 3.4.1). In the sugar-limiting cases, the peak of the specific growth rate can be explained by cells' approaching (but may not reaching) the steady state, soon followed by the loss of the steady state because the sugar concentration is low. In the case of prolonged exponential growth in high initial sugar concentrations, the cells approach and stay at the steady state until the sugar concentration decreases to the same magnitude of K_s.

The end of each curve in Fig 3.3D shows how ribosome level r at the end of growth depends on the initial sugar concentration $s(0)$: when s_0 is high, the ribosome level is still close to the steady state value; otherwise, the ribosome level decreases from the peak

value. This distinction was also observed in Fig 2.9.

Our simulation also captures the linear relationship between the population's growth rate (dOD/dt in Chapter 2, here dB/dt) and the total ribosome level ((GFP) in Chapter 2, here $r \cdot B$) in Fig 2.7 (Fig 3.3E). However, the model also suggests that the effective translation rate γ_e is not constant until the system reaches the quasi-steady state (Fig 3.3C), and if this model is correct, the reason why we did not observe the change in Fig 3.3E is that both $r \cdot B$ and dB/dt are small and close to the plot's origin when γ_e is not constant. Thus, further experimental verification with either a brighter fluorescent protein or a higher sensitivity of GFP measurement is required.

3.4.5 Numerical methods for the minimal model

I used the `odeint` function of the `scipy.integrate` module in Python to numerically integrate Eq 3.29 (in batch cultures) and Eq 3.33 (in constant environment). The parameters are listed in Table 3.1, which were naively chosen as a proof of principle of this model. The initial condition is listed in Table 3.2.

For the form of f_r, I assumed a simple function:

$$f_r(a) = f_{r,min} + (1 - f_{r,min}) \frac{a}{K_{fr} + a} \tag{3.62}$$

which represents a simple feed-forward motif from the accumulation of biomass precursor a to the increase in the fraction of ribosome reproducing ribosome f_r, similar to the network structure proposed by (Scott et al. 2014). $f_{r,min} > 0$ reflects the fact that the ribosome level approaches a non-zero minimum when the growth rate approaches zero.

3.5 Model with both carbon and nitrogen sources

We extend the minimal model (Eq 3.29) to include a nitrogen source. Now the model includes one carbon source (c), one nitrogen source (n), one biomass precursor (a), ribosome (r), one transporter for the carbon source ($\mathrm{e}_{T,c}$), one transporter for the nitrogen source ($\mathrm{e}_{T,n}$), and one anabolic enzyme (E) to make the precursor.

1. transporting the carbon source: $\mathrm{c} \xrightarrow{\mathrm{e_{T,c}}} \mathrm{c}_i$

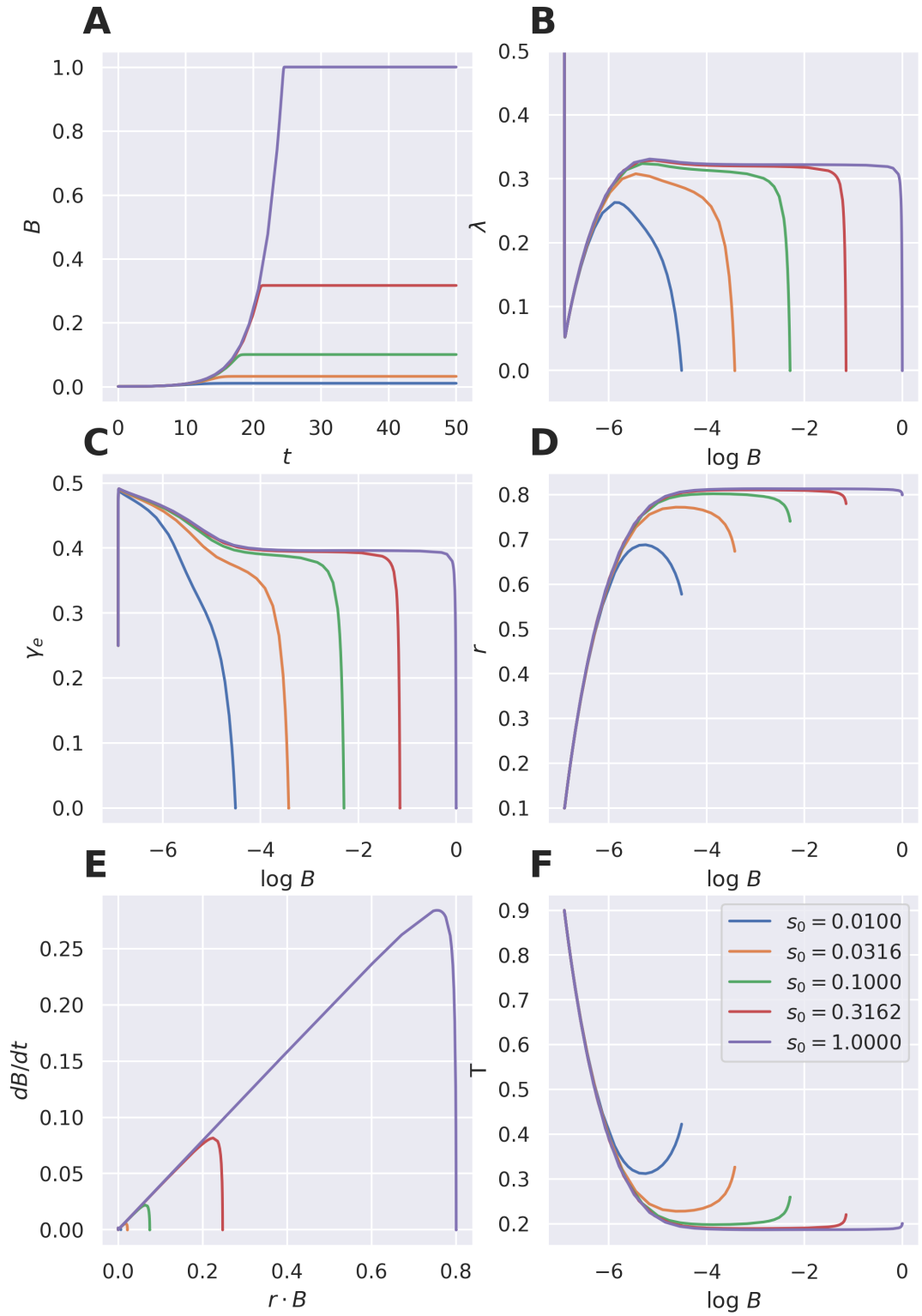

Figure 3.3: Dynamics of growth and ribosome level simulated from the minimal model (Eq 3.29). **(A)** Biomass B as a function of time t. **(B)** Specific growth rate λ *versus* $\log B$. **(C)** Effective translation rate γ_e *versus* $\log B$. **(D)** Ribosome level r *versus* $\log B$. **(E)** population growth rate dB/dt *versus* total ribosome number $r \cdot B$. **(F)** Transporter level T *versus* $\log B$. The parameters are listed in Table 3.1. The initial conditions are listed in Table 3.2.

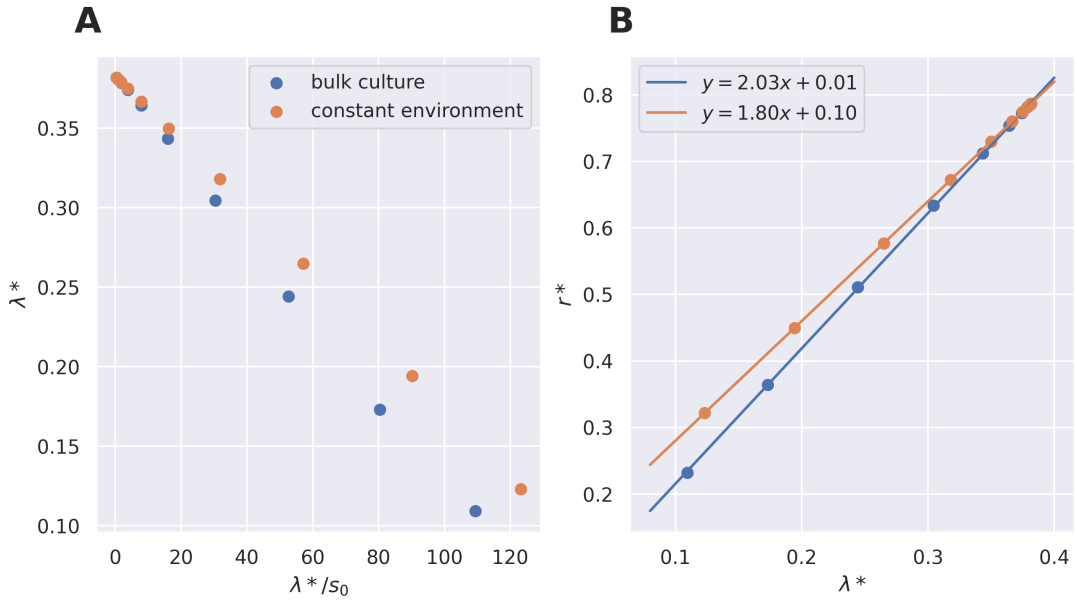

Figure 3.4: Monod's equation and the first growth law simulated from the minimal model (Eq 3.33). **(A)** Specific growth rate λ^* *versus* λ^*/s_0 and **(B)** ribosome level r^* *versus* specific growth rate λ^* in conditions with different initial sugar concentration s_0. λ^* is the maximum specific growth rate in batch cultures and the steady-state growth rate in constant environment (constant s), and r^* is the corresponding value of r when $\lambda = \lambda^*$. The equations in Panel B are results of linear regression. The parameters are listed in Table 3.1. The initial condition is listed in Table 3.2. The ten s_0 values are evenly spaced in $[10^{-3}, 1]$ on a logarithmic scale.

Table 3.1: Parameter values used in the minimal model.

parameter	value	note
V	1.0	in batch cultures only
$v_{T,max}$	2.0	
K_s	1×10^{-2}	
K_a	1×10^{-3}	
$\gamma_{e,max}$	0.5	
K_r	1×10^{-4}	
$f_{r,min}$	0.1	
K_{fr}	1×10^{-4}	
s	1.0 unless specified otherwise	in constant environment only

Table 3.2: Values of initial condition used in the minimal model.

variable	value	note
a_0	1×10^{-4}	
r_0	$f_{r,min}$	
B_0	1×10^{-4}	in batch cultures only
s_0	variable	in batch cultures only

2. transporting the nitrogen source: $\mathrm{n} \xrightarrow{\mathrm{e_{T,n}}} \mathrm{n}_i$

3. synthesis of the biomass precursor: $\mathrm{Q}_c\,\mathrm{s} + \mathrm{Q}_n\,\mathrm{n} \xrightarrow{\mathrm{E}} \mathrm{a}$

4. translation: $\mathrm{a} \xrightarrow{\mathrm{r}_a} f_{T,c}\,\mathrm{e_{T,c}} + f_r\,\mathrm{r} + f_{T,n}\,\mathrm{e_{T,n}} + f_E\,\mathrm{E}$, where $f_{T,c} + f_{T,n} + f_r + f_E = 1$.

where Q_c and Q_n describe the composition of the biomass. For simplicity, we assume the yields of mass of the carbon source and the nitrogen source are both 1: $Y_c = Y_n = 1$.

If we consider the intracellular subsystem only, it can be described by:

$$\dot{c_i} = v_{T,c}e_{T,c} - Q_c v_E E - \lambda c_i \tag{3.63a}$$

$$\dot{n_i} = v_{T,n}e_{T,n} - Q_n v_E E - \lambda n_i \tag{3.63b}$$

$$\dot{a} = v_E E - \gamma_e r - \lambda a \tag{3.63c}$$

$$\dot{r} = f_r \gamma_e r - \lambda r \tag{3.63d}$$

$$\dot{e_{T,c}} = f_{T,c}\gamma_e r - \lambda e_{T,c} \tag{3.63e}$$

$$\dot{e_{T,n}} = f_{T,n}\gamma_e r - \lambda e_{T,n} \tag{3.63f}$$

$$\dot{E} = f_E \gamma_e r - \lambda E \tag{3.63g}$$

and following Eq. 3.20, the specific growth rate is

$$\lambda = v_{T,c}e_{T,c} + v_{T,n}e_{T,n} \tag{3.64}$$

Similar to the minimal model, we assume that the transporters follows simple Michaelis-

Menten kinetics:

$$v_{T,c} = v_{T,c,max}\frac{c}{K_c + c} \tag{3.65a}$$

$$v_{T,n} = v_{T,n,max}\frac{n}{K_n + n} \tag{3.65b}$$

where $v_{T,c,max}$, $v_{T,n,max}$, K_c and K_n are constant.

3.5.1 Generalised Monod's equation with carbon and nitrogen sources

Assuming $a,\ c_i,\ n_i \ll 1$ and $\dot{a},\ \dot{c_i},\ \dot{n_i} \approx 0$, we have:

$$r + e_{T,c} + e_{T,n} + E \approx 1 \tag{3.66}$$

and

$$v_E E \approx v_{T,c} e_{T,c}/Q_c \tag{3.67a}$$

$$v_E E \approx v_{T,n} e_{T,n}/Q_n \tag{3.67b}$$

and

$$\lambda = v_{T,c} e_{T,c} + v_{T,n} e_{T,n} \approx v_E E \approx \gamma_e r \tag{3.68}$$

Combining Eqs 3.66, 3.67 and 3.68, we have:

$$\frac{1}{\lambda} = \frac{1}{\gamma_e} + \frac{1}{v_E} + \frac{Q_c}{v_{T,c} e_{T,c}} + \frac{Q_n}{v_{T,n} e_{T,n}} \tag{3.69}$$

We further substitute Eq 3.65 into Eq 3.69 and have:

$$\frac{1}{\lambda(c,n)} = \frac{1}{\lambda_{max}} + \frac{\kappa_c}{c} + \frac{\kappa_n}{n} \tag{3.70}$$

where $\lambda_{max} = 1/\left(\frac{1}{\gamma_e} + \frac{1}{v_E} + \frac{Q_c}{v_{T,c,max}} + \frac{Q_n}{v_{T,n,max}}\right)$, $\kappa_c = Q_c K_c / v_{T,c,max}$ and $\kappa_n = Q_n K_n / v_{T,n,max}$. λ_{max} is constant if γ_e and v_E are constant over c and n. Eq 3.70 can be seen as the generalised Monod's equation with carbon and nitrogen sources, in the Lineweaver-Burk form.

This form was empirically defined in Eq 2 of (Goyal and Wingreen 2007) and (Goyal et al. 2010).

Another common form of the generalised Monod's equation is in the multiplicative form (Bader 1978; Megee III et al. 1972):

$$\lambda = \lambda_{max} \frac{c}{K'_c + c} \frac{n}{K'_n + n} \tag{3.71}$$

We can approximate Eq 3.70 as Eq 3.71 by rewriting Eq 3.70 as

$$\begin{aligned} \lambda &= \frac{\lambda_{max} cn}{cn + (\kappa_c n + \kappa_n c)\lambda_{max}} \\ &= \frac{\lambda_{max} cn}{(\kappa_c \lambda_{max} + c)(\kappa_n \lambda_{max} + n) - \kappa_c \kappa_n \lambda_{max}^2} \end{aligned} \tag{3.72}$$

Ignoring the $\kappa_c \kappa_n \lambda_{max}^2$ term, Eq 3.70 takes the form of Eq 3.71, where $K'_c = \kappa_m \lambda_{max}$ and $K'_n = \kappa_n \lambda_{max}$.

3.6 Discussion

In this chapter, we formalised a mathematical framework for population growth in batch cultures. While this framework shares similarities with other self-replicator models, including the general form of the ODEs (Eq 3.16) and the mathematical equivalence between cell growth and division, we derived both from first-principle assumptions instead of accepting them as *a priori* knowledge, which helps to reveal that the dilution term in Eq 3.16 arises from a constant intracellular mass density, and that for a homogeneous, synchronous population, cell division is mathematically equivalent to cell growth (so we can neglect cell division for simplicity). Based on the mathematical framework, we built a minimal model to capture the dynamics of growth. Our analytical results guaranteed the existence and uniqueness of a stable steady state, and reproduced Monod's equation (Eq 3.46), the First Law (Eq 3.48) and the Second Law (Eq 3.51) at steady state, as expected. Moreover, beyond the steady state, we analytically showed that why Monod's equation still holds if we replace the steady-state growth rate with the maximum growth rate, as observed in Fig 2.3. Numerical integration shows that the model is able to capture the dynamics of growth and ribosome level observed in Fig 2.7 in batch cultures (Fig 3.3),

despite the simplicity of both the model and the assumed feed-forward regulation on the ribosome's expression f_r (Eq 3.62). Our results suggest the potential of capturing complex microbial growth dynamics with low-dimensional mathematical models.

In addition, we extended this model to include one carbon and one nitrogen source, which enables us to mechanistically derive the Monod's Equation with one carbon and one nitrogen source (Eq 3.70), and we showed that the multiplicative form of Monod's Equation (Eq 3.71) is an approximation, under certain conditions, of our mechanistically derived Monod's Equation.

3.6.1 Justification of the constant ρ assumption

One of the key assumption of our model is the constant intracellular mass density ρ. However, multiple reports have shown that the mass density of *S. cerevisiae* changes with cell cycle and the phase of growth (Kubitschek 1987; Bryan et al. 2010; Delgado et al. 2013). Below we estimate the coefficient of variation (CV) of ρ from experimental data to see if the constant ρ assumption holds given the measured variability.

To build the connection between ρ and the experimentally measured densities, we use a model similar to (Delgado et al. 2013), in which a cell consists of dry biomass and water. If the cell's volume V_c consists of two components, the intracellular water V_w and dry biomass V_B, we have:

$$V_c = V_w + V_B \tag{3.73}$$

Let m_w be the cell's mass of water, ρ_c the cell's buoyant density (i.e. mass density including water), and ρ_B and ρ_w the cell's *dry* biomass density and the water's density, then we also have:

$$B + m_w = \rho_c V_c \tag{3.74}$$

using $m_w = \rho_w V_w$ and Eq 3.73, then we can write:

$$B + \rho_w(V_c - V_B) = \rho_c V_c \tag{3.75}$$

Using $B = \rho_B V_B$ and dividing both sides by V_c, we have:

$$\rho_B V_B / V_c + \rho_w (1 - V_B / V_c) = \rho_c \tag{3.76}$$

and defining $v \equiv V_B / V_c$, which is the volume fraction of the dry biomass, we can re-arrange into:

$$\rho_c = \rho_c(v, \rho_B) = \rho_B v + \rho_w (1 - v) \tag{3.77}$$

where the water's density $\rho_w = 1$ g/mL is constant. Let both ρ_c and ρ_B be in units of g/mL, and substitute $\rho_w = 1$ g/mL into Eq 3.77, and we have:

$$\rho_c(v, \rho_B) = \rho_B v + (1 - v) \tag{3.78}$$

In this model, the buoyant density of the cell (ρ_c) varies as the volume fraction of the dry biomass (v) and the dry biomass density (ρ_B) vary. Both ρ_c (Bryan et al. 2010) and ρ_B (Delgado et al. 2013) are experimentally measured but v is not. We view ρ_B and v as random variables and assume that they are independent for simplicity.

In section 3.3.1, we defined $\rho \equiv B / V_c$, which gives:

$$\rho = \rho_B v \tag{3.79}$$

in this model. To estimate the CV of ρ, we are interested in its variance. We denote the expectations over the joint distribution of v and ρ_B as $\mathbb{E}(\cdot)$ and the variances as $\mathbb{V}(\cdot)$. By Eq 3.79 and the independence of ρ_B and v, the variance of ρ is given by:

$$\mathbb{V}(\rho) = \mathbb{V}(\rho_B v) = \mathbb{V}(v)[\mathbb{E}(\rho_B)^2 + \mathbb{V}(\rho_B)] + \mathbb{V}(\rho_B)\mathbb{E}(v)^2 \tag{3.80}$$

where ρ_B is measured but v is not.

To use the data on ρ_c, we take the variance of Eq 3.78:

$$\begin{aligned} \mathbb{V}(\rho_c) &= 2\mathbb{E}(v)\mathbb{E}(\rho_B v) + [\mathbb{E}(\rho_B^2 v^2) - \mathbb{E}(\rho_B v)^2] - 2\mathbb{E}(\rho_B v^2) + [\mathbb{E}(v^2) - \mathbb{E}(v)^2] \\ &= \mathbb{V}(\rho) + \mathbb{V}(v) + 2\mathbb{E}(v)\mathbb{E}(\rho_B v) - 2\mathbb{E}(\rho_B v^2) \end{aligned} \tag{3.81}$$

where the second equality is from Eq 3.79 and the fact that $\mathbb{V}(X) = \mathbb{E}(X^2) - \mathbb{E}(X)^2$ for any random variable X. By the independence between ρ_B and v, we further have $\mathbb{E}(\rho_B v) = \mathbb{E}(\rho_B)\mathbb{E}(v)$ and $\mathbb{E}(\rho_B v^2) = \mathbb{E}(\rho_B)\mathbb{E}(v^2)$. Using $\mathbb{V}(v) = \mathbb{E}(v^2) - \mathbb{E}(v)^2$ again, Eq 3.81 becomes:

$$\mathbb{V}(\rho_c) = \mathbb{V}(\rho) + [1 - 2\mathbb{E}(\rho_B)]\mathbb{V}(v) \tag{3.82}$$

Before we solve Eqs 3.80 and 3.82 for $\mathbb{V}(v)$ and $\mathbb{V}(\rho)$, we give all the measured values and infer the expectation of v. The measured values from (Bryan et al. 2010; Delgado et al. 2013) are:

$$\mathbb{E}(\rho_c) = 1.09 \quad ; \quad \mathbb{V}(\rho_c) = 0.02^2$$

$$\mathbb{E}(\rho_B) = 1.48 \quad ; \quad \mathbb{V}(\rho_B) = 0.1^2$$

where the variances of ρ_c and ρ_B are estimated from the square of the range of data. To find $\mathbb{E}(v)$, we take the expectation of Eq 3.78 and use the independence between ρ_B and v, and we have:

$$\mathbb{E}(\rho_c) = \mathbb{E}(\rho_B)\mathbb{E}(v) + 1 - \mathbb{E}(v) \tag{3.83}$$

which yields:

$$\mathbb{E}(v) = \frac{\mathbb{E}(\rho_c) - 1}{\mathbb{E}(\rho_B) - 1} = 0.19 \tag{3.84}$$

Now we solve Eqs 3.80 and 3.82 and get $\mathbb{V}(v) = 1.7 \times 10^{-4}$ and $\mathbb{V}(\rho) = 7.3 \times 10^{-4}$.

To get the CV of ρ, we first get $\mathbb{E}(\rho) = \mathbb{E}(\rho_B)\mathbb{E}(v) = 0.28$. Then, we have:

$$\mathrm{CV}(\rho) = \frac{\sqrt{\mathbb{V}(\rho)}}{\mathbb{E}(\rho)} = 0.096 \tag{3.85}$$

which is small and hence justifies the assumption that ρ is constant.

3.6.2 Is the Michaelis-Menten kinetics of transporter necessary for the validity of Monod's equation at steady state?

When deriving Monod's equation at steady state (Eq 3.46), we assumed that the transport of nutrient follows Michaelis-Menten kinetics (Eq 3.45). Is this a necessary condition for Monod's equation to hold? Below we show that it is not.

Starting from Eq 3.44, if we assume a first-order kinetics: $v_T = k_s s \propto s$, we immediately have:

$$\lambda = \frac{\gamma_e s}{\gamma_e / k_s + s} \tag{3.86}$$

which is also Monod's form if γ_e is constant at steady state, suggesting that Monod's equation could hold for substrates that do not require a transporter with Michaelis-Menten kinetics.

We can also show that if Monod's equation holds, there can only be two forms of biologically-relevant kinetics, including the Michaelis-Menten and the above first-order kinetics. From Eq 3.44, we know:

$$\lambda = \frac{\gamma_e v_T}{v_T + \gamma_e} \tag{3.87}$$

which is similar to Eq 5 of (Scott et al. 2010). If Monod's equation holds, $\lambda = \lambda_{max} \frac{s}{K_{\text{Monod}} + s}$, and substitute this into Eq 3.87, we have:

$$\lambda_{max} s(\gamma_e + v_T) = \gamma_e v_T (K_{\text{Monod}} + s) \tag{3.88}$$

which is

$$[(\lambda_{max} - \gamma_e)s - \gamma_e K_{\text{Monod}}]v_T = -\lambda_{max}\gamma_e s \tag{3.89}$$

If $\lambda_{max} = \gamma_e$,

$$v_T = \frac{\gamma_e}{K_{\text{Monod}}} s \propto s \tag{3.90}$$

which is the above simple kinetics.

If $\lambda_{max} < \gamma_e$,

$$v_T = \frac{\lambda_{max}\gamma_e s}{(\gamma_e - \lambda_{max})s + \gamma_e K_{\text{Monod}}} = \frac{\frac{\lambda_{max}\gamma_e}{\gamma_e - \lambda_{max}} s}{\frac{\gamma_e K_{\text{Monod}}}{\gamma_e - \lambda_{max}} + s} \tag{3.91}$$

which is the Michaelis-Menten form.

If $\lambda_{max} > \gamma_e$,

$$v_T = \frac{\lambda_{max}\gamma_e s}{\gamma_e K_{\text{Monod}} - (\lambda_{max} - \gamma_e)s} = \frac{\frac{\lambda_{max}\gamma_e}{\lambda_{max} - \gamma_e} s}{\frac{\gamma_e K_{\text{Monod}}}{\lambda_{max} - \gamma_e} - s} \tag{3.92}$$

which is not biologically relevant because $v_T \to +\infty$ when $s \to \frac{\gamma_e K_{\text{Monod}}}{\lambda_{max} - \gamma_e}$.

Chapter 4

The galactose-palatinose diauxie

4.1 Summary

- Context: *S. cerevisiae* consumes multiple carbon sources, and when glucose is present, cells prioritise glucose over other carbon sources.
- Question: does non-glucose catabolite repression exist in budding yeast?
- Approach: I measured the growth curves and the dynamics of GFP-tagged enzyme expression of the wildtype and mutant strains growing on a mixture of two carbon sources.
- Finding: budding yeast prioritises galactose over palatinose via an unknown signal downstream of Gal4.
- Outlook: the finding extends the carbon source hierarchy of budding yeast; however, it raises question about whether growth rate determines this hierarchy, because no clear diauxie exists when sucrose or fructose, which supports faster growth than galactose, is mixed with palatinose.

4.2 Background

Microbes respond to signals from the external environment to grow and survive stress. Signals from the external environment are dynamic and sometimes conflicting or competing. An improper response leads to a decrease in fitness. Cells use signalling networks

to properly integrate and respond to environmental signals and make decisions when the signals are conflicting or competing (Perkins and Swain 2009). How cells integrate signals and make decisions, what principles are behind a decision, and why those principles are selected, are important questions that connect physiology and evolution in the context of cellular decision-making.

A classic example of cellular decision making is catabolite repression — when cells are exposed to two carbon sources, cells prioritise the carbon source that supports faster growth over the other, despite being able to receive competing signals from both. A distinct phenotype of catabolite repression is *diauxie*, in which the cultures have two phases of exponential growth, separated by a lag (Monod 1942). Diauxie was observed in a mixture of glucose and another carbon source in bacteria (reviewed in (Monod 1947)).

More recent research finds that catabolite repression is not limited to glucose — cells also prioritise one non-glucose carbon source over another in *E. coli* (Desai and Rao 2010; Aidelberg et al. 2014; Okano et al. 2020). The phenotypes in those examples are usually more subtle than classic diauxie, but become detectable with careful measurements of gene expression or of the metabolome in addition to OD. For example, cells might sequentially use two carbon sources without an observable lag during the switch (Okano et al. 2020), or cells might partially repress the expression of metabolic genes of the inferior carbon source (Koirala, Wang, and Rao 2016). Nonetheless, the new discoveries suggest that cross-regulation between carbon metabolic networks is widespread, and more importantly, the accumulating examples of non-glucose catabolite repression reveal new principles of cell decision-making on multiple carbon sources — instead of a strict "hierarchy" at a transcriptional level determined by the chemical identity of carbon sources, cell decisions can be concentration- or flux-dependent (Koirala, Wang, and Rao 2016; Okano et al. 2020).

Similar to *E. coli*, *S. cerevisiae* is also a fast-growing microbe that consumes multiple carbon sources. Catabolite repression by glucose (i.e. glucose repression) in *S. cerevisiae* has been intensively studied, with the underlying mechanism attributed to transcriptional repression by Mig1 (reviewed in (Gancedo 1998)), and degradation of transporters of other carbon sources (Medintz et al. 1996; Paiva et al. 2009; Horak and Wolf 2005; Hatanaka et al. 2009). However, the evidence of non-glucose catabolite repression is relatively

rare. As far as we are aware, the only example is repression of ethanol metabolism by acetate, where intracellular acetate represses the expression of *ADH2*, which encodes alcohol dehydrogenase (Simpson-Lavy and Kupiec 2019). However, this example may be better understood in the context of end-product inhibition rather than cell decision-making, because the only nutrient signal in this example is the presence of acetate, which is a product of ethanol metabolism. Nonetheless, motivated by the recent findings in *E. coli*, we suspect more unknown regulation between carbon metabolic networks may also exist in *S. cerevisiae*, and with cells of budding yeast being eukaryotic, we wonder if new mechanisms and principles of cell decision-making can be revealed.

To begin the investigation of non-glucose catabolite repression in *S. cerevisiae*, we choose to study the potential cross-regulation between the *GAL* and *MAL* networks. First of all, we can directly measure the cells' commitment to both *GAL* and *MAL* networks, because they are only induced when their own substrates present, with a set of known, network-specific genes activated by a transcription factor. Perhaps more intriguingly, in the wildtype strains we use (FY4 and BY4741, both with S288c-background (Baker Brachmann et al. 1998)), cells grow much faster in galactose than in palatinose (Fig 4.1), which are the only known substrate for *GAL* and *MAL* networks in these strains. Yet, we do not know the existence of any cross-regulation between the *GAL* and *MAL* networks. If cells were to maximise growth rate, cells should somehow prioritise use of galactose instead of palatinose.

Here we show that indeed cells exhibit diauxie in galactose-palatinose mixture and they prioritise the use of galactose over palatinose. During the first phase of growth, expression of the *MAL* genes responsible for palatinose metabolism remains low. We further show that constitutively active Gal4 in the *gal80*Δ mutant causes a strong delay in palatinose metabolism in sugar mixtures that do not typically show diauxie, and that this delay can be partially alleviated by deleting *GAL2*, which encodes the galactose transporter. Whilst the exact downstream target of Gal4 is largely unknown, our evidence suggests that active Gal4 prevents the positive feedback loop of the *MAL* network from properly functioning by mechanisms post-transcriptionally. Our results provide a fresh example of non-glucose catabolite repression in *S. cerevisiae* and suggest that mechanism of catabolite repression in budding yeast can be more complex than previously thought.

4.3 Results

4.3.1 Cells growing in galactose-palatinose mixtures show diauxie

The growth rate of *S. cerevisiae* cultures varies in different carbon sources. Amongst the "best" sugars that support fast growth is glucose, whilst galactose and maltose support slower growth, and cells are expected to repress the *GAL* and *MAL* networks in the presence of glucose to prioritise the use of glucose. The wildtype strains in this study, BY4741 and FY4, are unable to consume maltose, but can consume palatinose using the *MAL* network (Brown, Murray, and Verstrepen 2010). We monitor the OD of batch cultures in plate readers and calculate the specific growth rate (Swain et al. 2016; Montaño-Gutierrez et al. 2022), and find that the specific growth rate in palatinose is much lower than galactose (Fig 4.1). We wondered whether cells prioritise galactose in galactose-palatinose mixtures, like the cases of glucose-galactose and glucose-maltose mixtures (New et al. 2014), or whether cells are able to co-consume both to grow faster as observed in some combinations of carbon sources in *E. coli* (Hermsen et al. 2015).

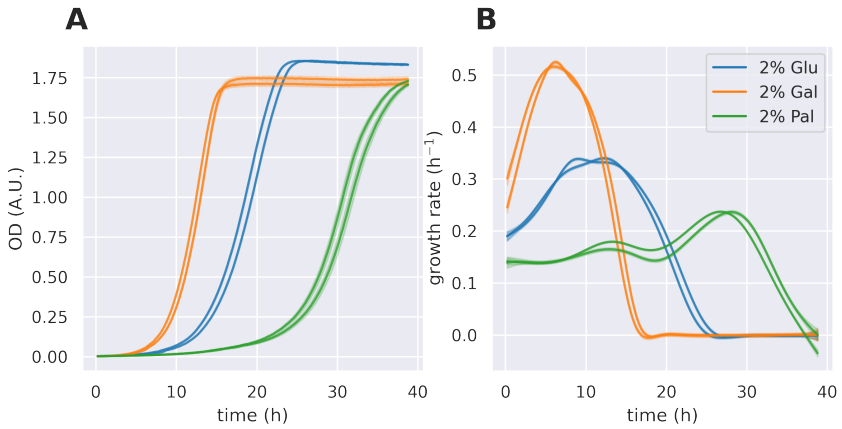

Figure 4.1: The growth dynamics of wildtype strain (BY4741) in glucose, galactose and palatinose. **(A)** OD measured in a plate reader. **(B)** The specific growth rate calculated from data in (A). Each curve represents one biological replicate. The shaded area represents the standard deviation of two technical replicates. This experiment was obtained by Xiao Wang in another project (Chapter 2) but re-analysed by me here.

"Diauxie" means "two growths", which is two exponential phases of growth separated by a lag in a batch culture (Monod 1947). Diauxie in a batch culture indicates sequential use of carbon sources (Monod 1947). We use plate readers to measure OD and to test whether cells show diauxie in galactose-palatinose mixtures.

The *MAL* network is known to be repressed by the presence of glucose (Gancedo

1998). As proof of principle, I grew cells in glucose-palatinose mixtures, which should show diauxie. Indeed, I observed diauxie in all combinations of different concentrations, as indicated by two phases of increase in the OD curve (Fig 4.2A and B) and the growth rate peaks at different timepoints and heights (Fig 4.2C and D). Then, I grew cells in galactose-palatinose mixtures, which also exhibited diauxie in all combinations (Fig 4.3), suggesting cells sequentially use galactose and palatinose.

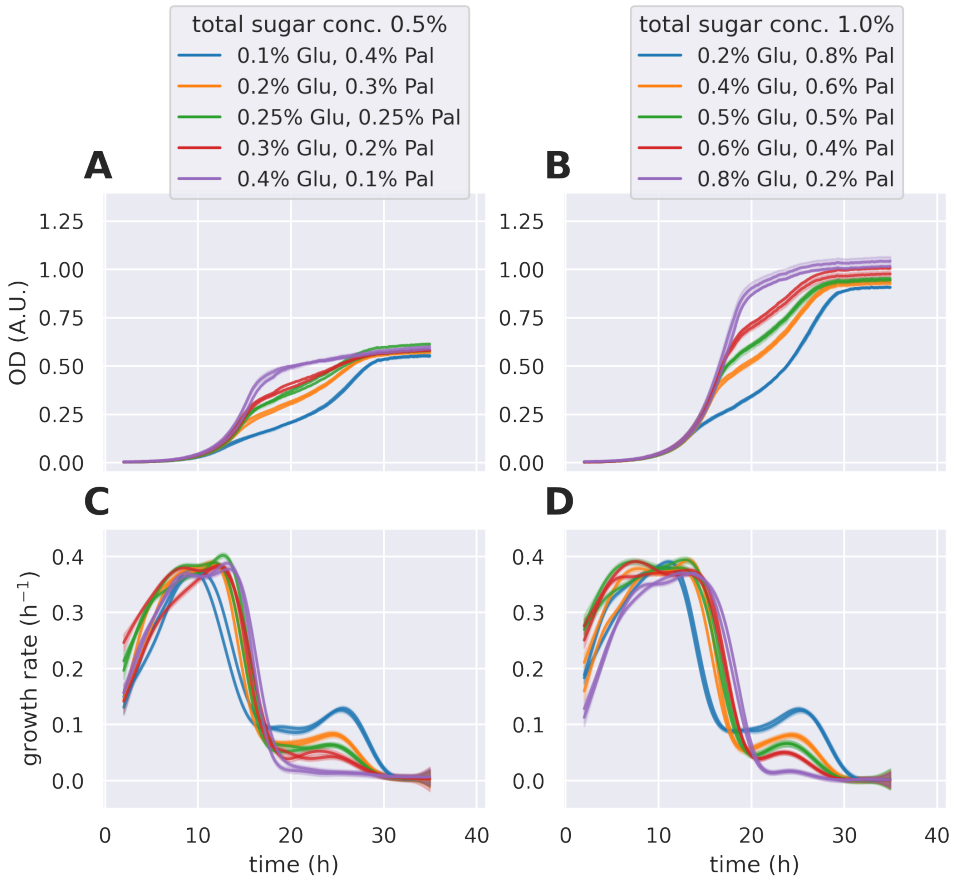

Figure 4.2: Diauxie is observed in the growth dynamics of wildtype prototrophic strain (FY4) in glucose-palatinose mixtures. **(A, B)** OD measured in a plate reader. **(C, D)** Calculated specific growth rate from data in (A) and (B). Each curve represents one biological replicate. The shaded area represents the standard deviation of two technical replicates.

4.3.2 Cells consume galactose first and then palatinose

The OD yields in the two exponential phases reveal the order of sugar consumption — the concentration of the first sugar to be consumed should positively correlate with the OD yield of the first phase of growth, and likewise for the second sugar and the OD yield of the second phase (Monod 1947).

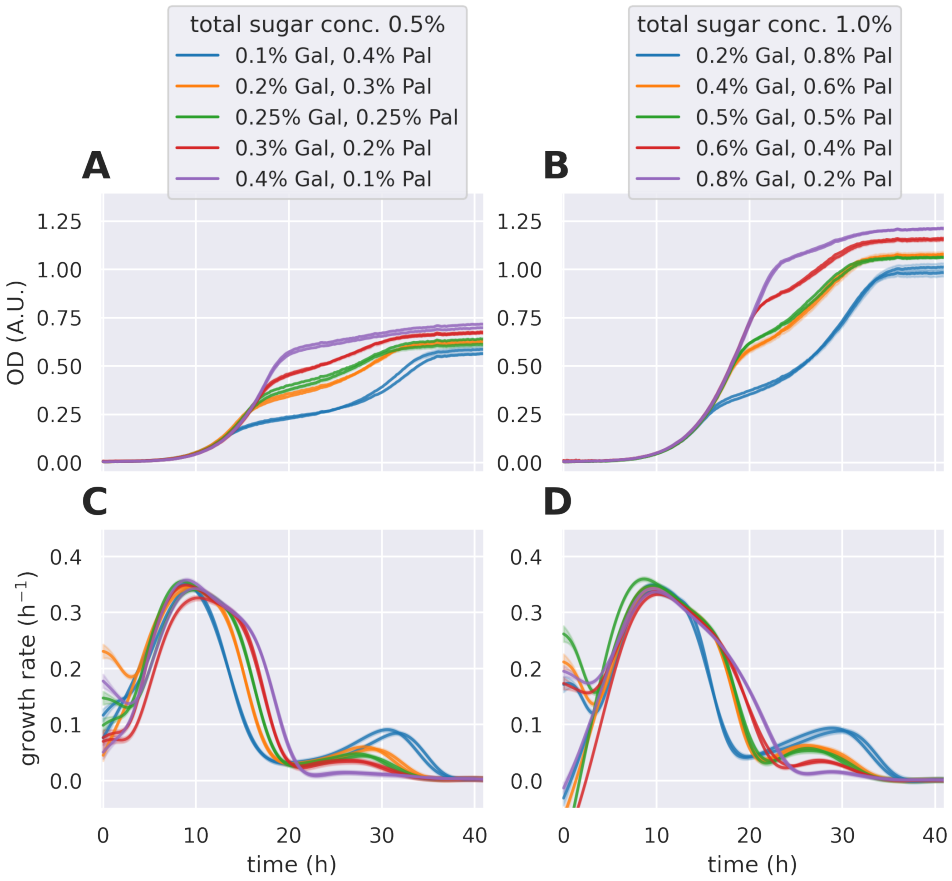

Figure 4.3: Diauxie is observed in the growth dynamics of wildtype prototrophic strain (FY4) in galactose-palatinose mixtures. **(A, B)** OD measured in a plate reader. **(C, D)** Calculated specific growth rate from data in (A) and (B). Each curve represents one biological replicate. The shaded area represents the standard deviation of two technical replicates.

To find the OD yield of both phases, I find the local minimum of the specific growth rate between the two local maxima (Fig 4.4), and its corresponding OD (OD_{switch}). Then I define the OD yield of the first phase of growth $OD_1 \equiv OD_{switch}$, and that of the second phase of growth $OD_2 \equiv OD_{final} - OD_{switch}$. As proof of principle, I first found the correlation between OD_1 and the concentration of glucose, and OD_2 with that of palatinose, in glucose-palatinose mixtures (Fig 4.5A). Similarly, in galactose-palatinose mixtures, as shown in Fig 4.5B, OD_1 and OD_2 linearly correlate with concentrations of galactose and palatinose, respectively, which suggests cells consume galactose first and then palatinose. Notably, the slopes of linear regression are consistent between Figs 4.5A and B. The positive correlation between OD_2 and palatinose also confirms that the second phase of diauxie is at least mainly caused by palatinose consumption rather than the consumption of ethanol or acetate generated in the first phase of diauxie.

To further confirm the sequential use of galactose and palatinose, I grew cells in flasks with 0.1% galactose and 0.4% palatinose and quantified the sugar concentrations in the media over time using gas chromatography-mass spectrometry (GC-MS) (Moses et al. 2014) in collaboration with Dr Tessa Moses. As shown in Fig 4.6, the concentration of galactose indeed approached 0 within 20 hours, while around 90% of the palatinose was still in the media. The concentration of palatinose slowly decreased during the lag phase after the first exponential growth and quickly decreased during the second exponential growth.

Interestingly, the duration of the lag phase after the first exponential growth (Fig 4.6) in flasks was much longer than in 96-well plates in plate readers (Fig 4.3A), and this discrepancy is reproducible. Nonetheless, the direct measurement of the sugar concentrations confirms that cells consume galactose first and then palatinose.

4.3.3 Galactose-palatinose diauxie does not depend on the preculture's history

Both *GAL* and *MAL* networks show history-dependent behaviour (Stockwell, Landry, and Rifkin 2015; Cerulus et al. 2018), and such behaviour in the *GAL* network can be explained by positive feedback within the network (Venturelli, El-Samad, and Murray

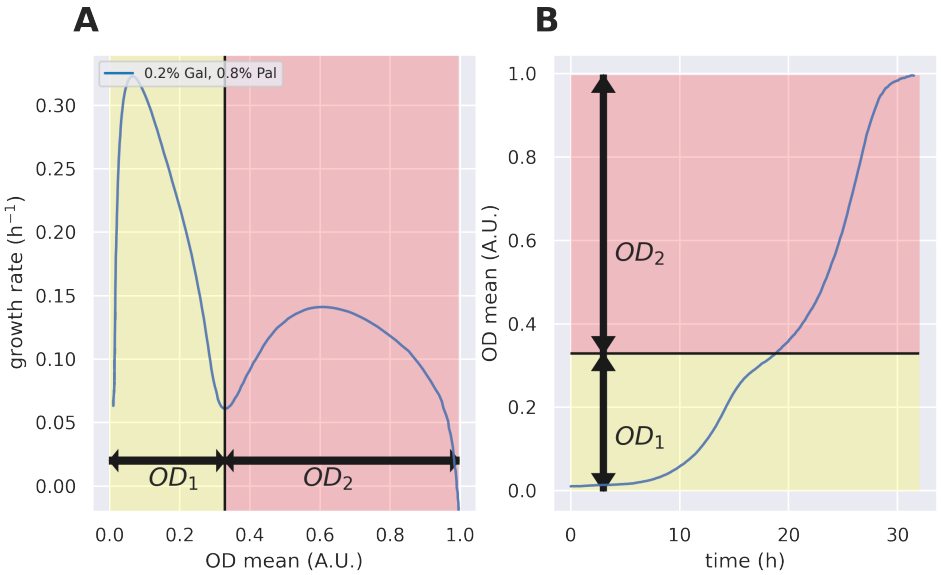

Figure 4.4: Method to quantify OD yield of each growth phase in a diauxic growth. **(A)** The local minimum of the specific growth rate is found between the two local maxima. The local minimum is assumed to be the end of growth phase 1 and the beginning of growth phase 2. Under this assumption, the OD yield of growth phase 1 (OD_1) is simply the OD at the local minimum, and the OD yield of growth phase 2 (OD_2) is the difference between the final OD and OD_1. **(B)** OD_1 and OD_2 in the OD–time plot.

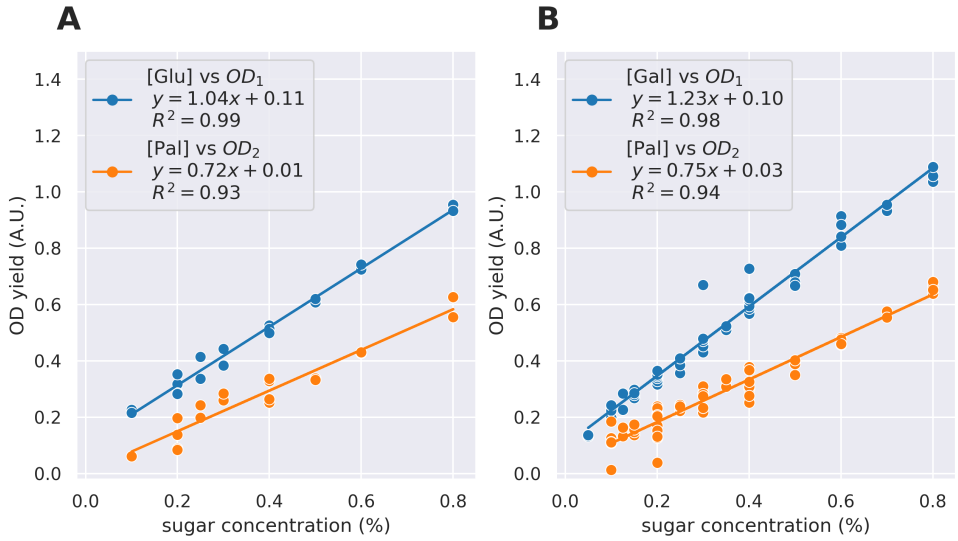

Figure 4.5: In **(A)** glucose-palatinose and **(B)** galactose-palatinose mixtures, the OD yield of growth phase 1 (OD_1) linearly correlates with glucose or galactose concentration, and OD yield of growth phase 2 (OD_2) linearly correlates with palatinose concentration. Each data point is extracted from a growth curve using method shown in Fig 4.4. The equations and R^2 values are results of linear regression.

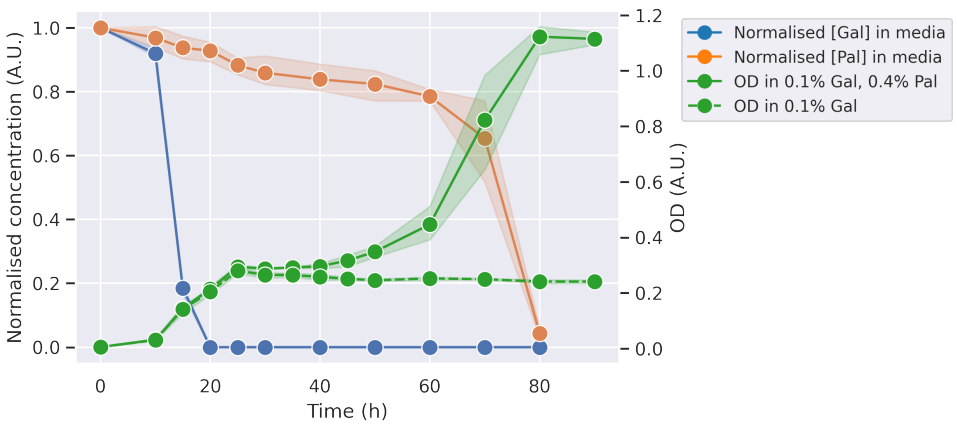

Figure 4.6: Metabolomics data confirms that wildtype (FY4) cells prioritise galactose over palatinose. Concentrations of galactose and palatinose are measured by GC-MS and are normalised to the values of the first timepoint (0 h), respectively. The OD of samples is measured in a plate reader. Each data point represents the mean of the 3 biological replicates and the shaded area represents the standard deviation. This experiment was run in collaboration with Dr Tessa Moses.

2012). Thus, I asked if galactose-palatinose diauxie depends on specific pre-culture history.

In routine experiments, I pre-cultured cells in SC with 2% sodium pyruvate (cf. Chapter 6), which should neither repress nor induce either network. To confirm the galactose-palatinose diauxie does not depend on pre-culture history in pyruvate, I pre-cultured cells in raffinose, which is another non-repressing, non-inducing carbon source of galactose (Stockwell, Landry, and Rifkin 2015). As expected, galactose-palatinose diauxie exists in cultures with raffinose history (Fig 4.7A).

Second, glucose in known to repress both *GAL* and *MAL* networks (Gancedo 1998), which might change the cells' ability to transport and sense galactose or palatinose. Does pre-culture in glucose change the diauxie behaviour? Our results show that the galactose-palatinose diauxie also exists in cultures with glucose history (Fig 4.7B).

Finally, as part of the known history-dependent behaviour in the *GAL* network, pre-exposure to galactose leads to a bigger fraction of cells with high *GAL* expression, given the same concentration of galactose (Venturelli, El-Samad, and Murray 2012; Bheda et al. 2020). I expected a similar effect in the *MAL* network and asked if pre-culturing cells in palatinose will change, if not revert, the observed diauxie. However, the diauxie is unchanged (Fig 4.7C).

In conclusion, the galactose-palatinose diauxie is not specific to a certain growth history of cells.

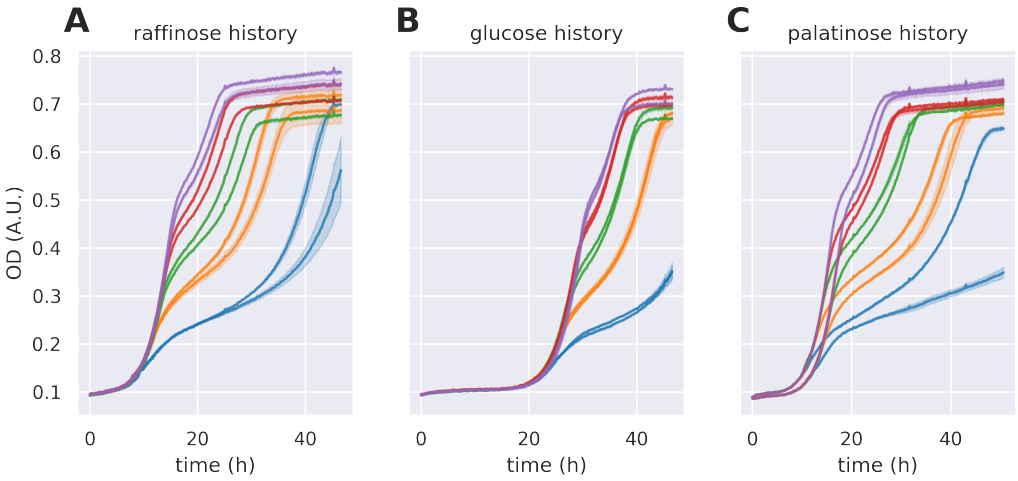

Figure 4.7: Galactose-palatinose diauxie is observed in cultures with glucose, raffinose and palatinose history. OD of wildtype prototrophic strain (FY4) cultures with **(A)** raffinose history, **(B)** glucose history and **(C)** palatinose history measured in a plate reader. Each curve represents one biological replicate. The shaded area represents the standard deviation of two technical replicates.

4.3.4 Neither separation of induction timescales nor dilution by growth explains galactose-palatinose diauxie

What is the mechanism behind the observed diauxie? As I am not aware of any cross-regulation between the *GAL* and *MAL* networks, I first tested two cross-regulation-free hypotheses to explain galactose-palatinose diauxie:

- Timer Hypothesis: separation of induction timescales (Fig 4.8A). The activation of *MAL* network is independent of but much slower than the *GAL* network, so it activates after the first exponential growth. This hypothesis is consistent with the lag phase of growth in palatinose being longer than in galactose (Fig 4.1A), but does not explain why we still observed diauxie when cells were pre-grown in palatinose (Fig 4.7).

- Dilution Hypothesis: Dilution by growth (Fig 4.8B) (Narang 2006). The activation of the *MAL* network requires import of palatinose and sensing of intracellular palatinose to trigger positive feedback (see Chapter 3). The fast growth in galactose dilutes the required transporter Mal11 and intracellular palatinose for *MAL* activation. This hypothesis is consistent with the maximum specific growth rate in galactose being higher than in palatinose (Fig 4.1B).

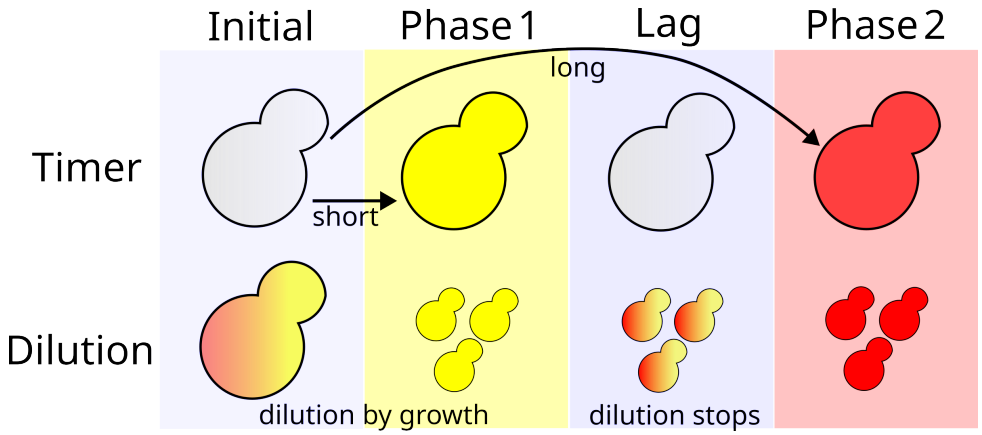

Figure 4.8: Two cross-regulation-free hypotheses on the mechanism of galactose-palatinose diauxie. Upper: Timer Hypothesis — the time required to activate the *MAL* network is longer than the time it takes to consume all galactose. Lower: Dilution Hypothesis — faster cell growth in galactose dilutes the necessary components of the *MAL* network and preventing its expression until growth stops.

The two hypotheses above are not specific to galactose and should apply to any carbon source in which the growth rate is higher and the lag is shorter, which is the case for fructose (Fig 2.3) and sucrose (data not shown), so I tested the hypotheses in sucrose-palatinose and fructose-palatinose mixtures.

As shown in Fig 4.9 and 4.10, no diauxie with a visible lag was observed in either sugar pair. Overlaying the growth curves in galactose-palatinose and fructose-palatinose mixtures reveals that the fructose-palatinose mixture is consumed faster than the galactose-palatinose mixture (Fig 4.11).

This observation is inconsistent with the Timer Hypothsis. *MAL* genes are induced in neither fructose (Fig 4.16) nor sucrose (data not shown), so the presence of fructose or sucrose should not accelerate its induction. Therefore, if the Timer Hypothesis were true, it should take at least the same amount of time for the cells to fully consume palatinose in both mixtures, but in Fig 4.11, it takes much longer to fully consume palatinose in the galactose-palatinose mixture.

Similarly, if the Dilution Hypothesis were true, the level of *MAL* genes and intracellular palatinose would be lower and a longer lag in both sucrose- and fructose-palatinose mixtures would be observed, because cells grow faster in sucrose and in fructose than in galactose (Fig 2.3). This is not true in Fig 4.11, either.

In conclusion, instead of a general mechanism that applies to multiple carbon sources, it seems more likely that a mechanism specific to galactose is behind the diauxie.

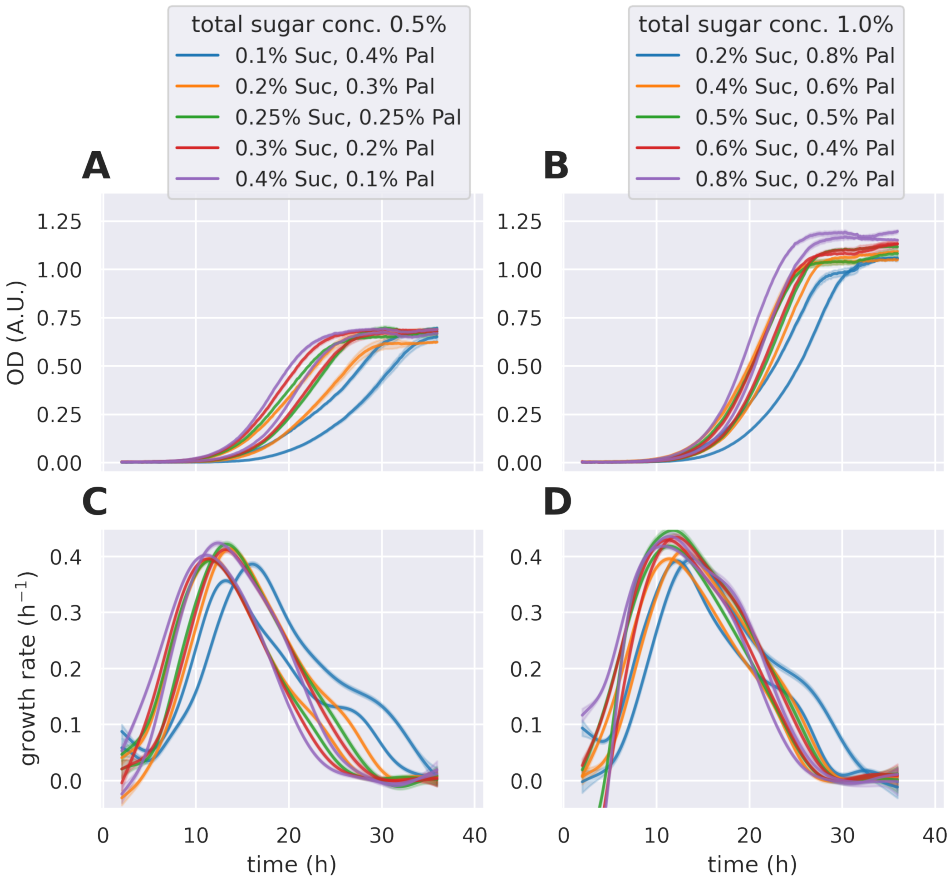

Figure 4.9: No typical diauxie is observed in the growth dynamics of wildtype prototrophic strain (FY4) in sucrose-palatinose mixtures. **(A, B)** OD measured in a plate reader. **(C, D)** Calculated specific growth rate from data in (A) and (B). Each curve represents one biological replicate. The shaded area represents the standard deviation of two technical replicates.

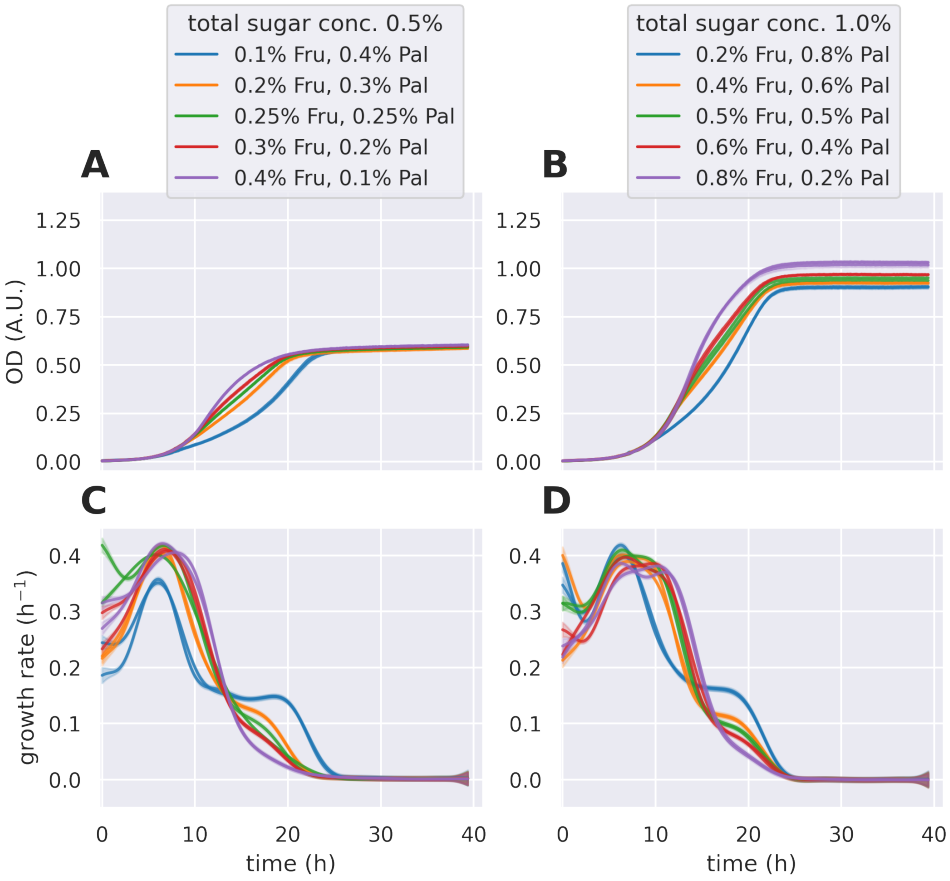

Figure 4.10: No typical diauxie is observed in the growth dynamics of wildtype prototrophic strain (FY4) in fructose-palatinose mixtures. **(A, B)** OD measured in a plate reader. **(C, D)** Calculated specific growth rate from data in (A) and (B). Each curve represents one biological replicate. The shaded area represents the standard deviation of two technical replicates.

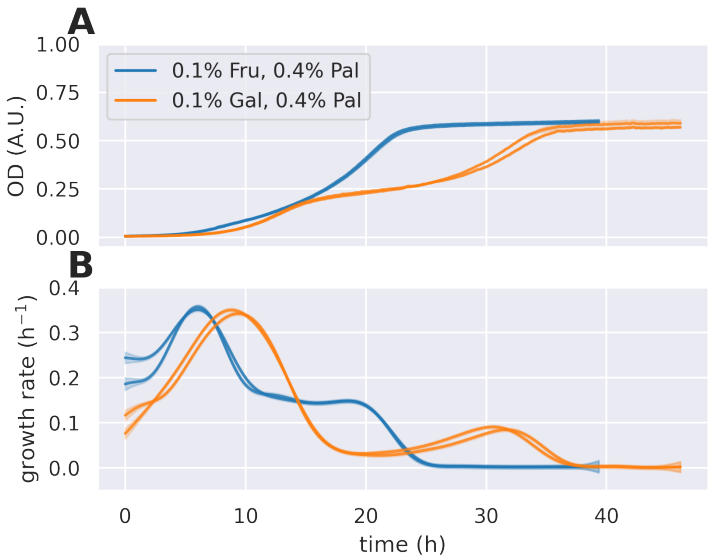

Figure 4.11: Comparison between growth dynamics in galactose-palatinose mixtures and fructose-palatinose mixtures. **(A)** OD of wildtype (FY4) cultures measured in a plate reader. **(B)** Calculated specific growth rate from data in (A). Each curve represents one biological replicate. The shaded area represents the standard deviation of two technical replicates.

4.3.5 The presence of galactose leads to low expression of *MAL* genes in palatinose

The presence of galactose may affect the consumption of palatinose in at least two ways — it either affects the induction of *MAL* genes, or blocks the hydrolysis of palatinose by isomaltases. Therefore, I investigated the expression profile of *MAL* genes in galactose-palatinose mixtures.

In galactose-palatinose mixtures, the level of isomaltases Ima1 and Ima5 is detectable, but remains low, during the first exponential growth, and only increases after the first exponential growth (Fig 4.12). In contrast, in sucrose-palatinose mixtures, the expression of Ima1 and Ima5 begins at lower OD (Fig 4.13). The results suggest that presence of galactose or activation of the *GAL* regulon negatively affects the expression of *MAL* genes in palatinose.

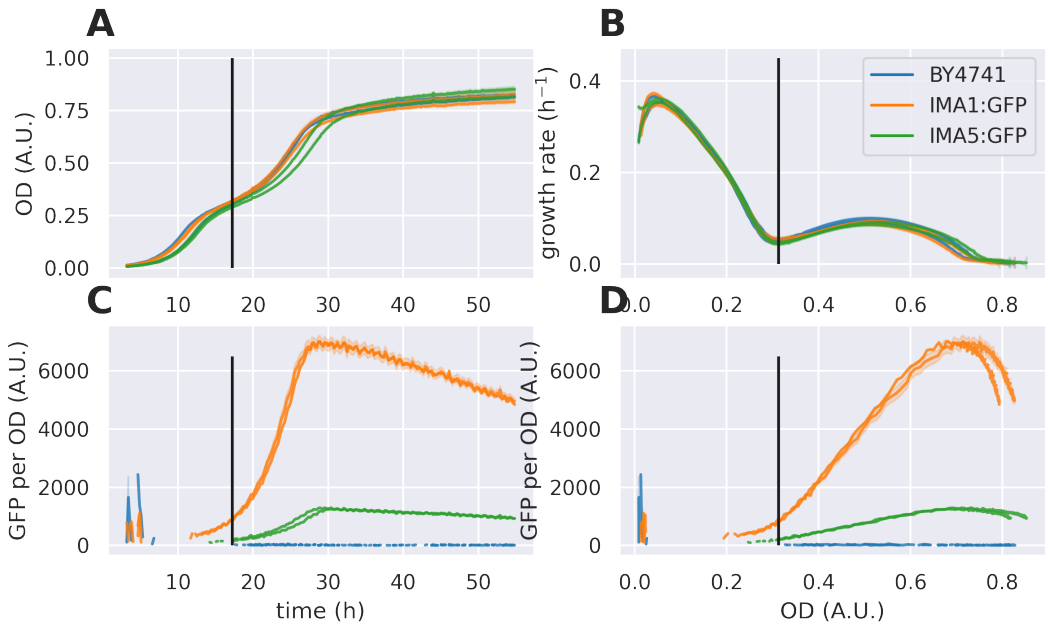

Figure 4.12: Levels of palatinases Ima1 and Ima5 remain low in galactose phase in 0.1% galactose + 0.4% palatinose. **(A)** OD measured in a plate reader. **(B)** Calculated specific growth rate as a function of OD. **(C)** GFP per unit of OD as a function of time. **(D)** GFP per unit of OD as a function of OD. Each curve represents one biological replicate. The shaded area represents the standard deviation of two technical replicates. The black bar represents the corresponding time or OD at the local minimum of specific growth rate. BY4741 is the wildtype strain and both fluorescent strains are derived from BY4741. The negative values are not displayed.

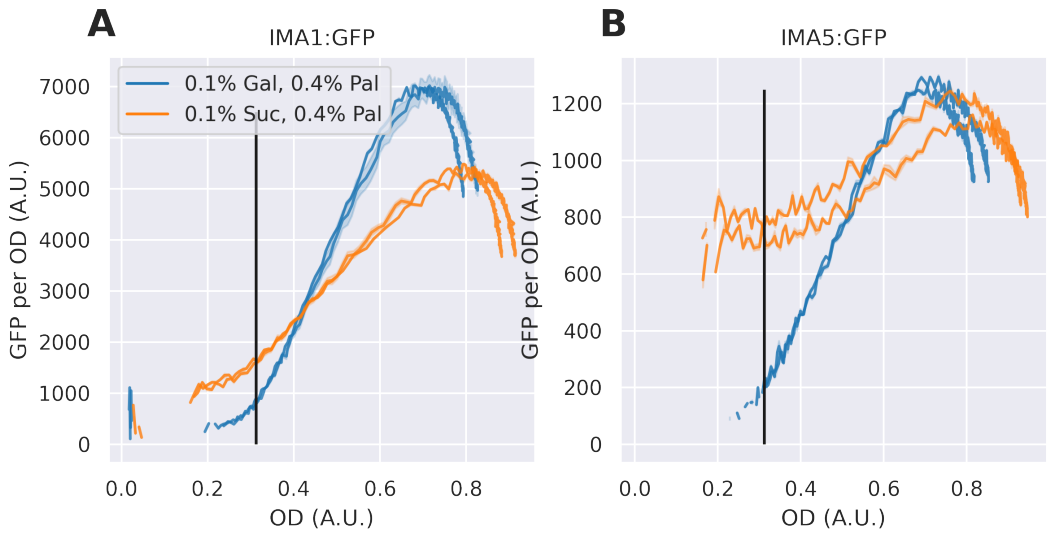

Figure 4.13: Comparison of palatinase levels between galactose-palatinose and sucrose-palatinose mixtures. **(A)** Ima1 level per unit of OD as a function of OD. **(B)** Ima5 level per unit of OD as a function of OD. Each curve represents one biological replicate. The shaded area represents the standard deviation of two technical replicates. The black bar represents the OD at the local minimum of specific growth rate in 0.1% galactose + 0.4% palatinose. The fluorescence reading is noisy when OD is low, which may be negative after being corrected for autofluorescence. Both fluorescent strains are derived from BY4741. The negative values are not displayed.

4.3.6 Deleting *GAL80* strongly delays the cells' use of palatinose in both galactose- and fructose-palatinose mixtures

The previous section shows that *MAL* genes are lowly expressed in the presence of galactose, but it remains unknown if that is a result of the presence of the galactose molecules or the activation of the *GAL* network. To distinguish between the two scenarios, I introduced a *gal80*Δ mutant. Gal80 is the repressor of the Gal4 transcription factor, and deleting *GAL80* frees Gal4 from repression and results in constitutive, high expression of *GAL* genes (Lohr, Venkov, and Zlatanova 1995), even in the absence of galactose.

As seen in Figs 4.14 and 4.19, the *gal80*Δ mutant shows a strongly delayed use of palatinose in both galactose-palatinose and fructose-palatinose mixtures, suggesting the low expression of *MAL* genes does not require the presence of galactose in this mutant.

4.3.7 Active Gal4 delays the use of palatinose

Gal80 is structurally similar to oxidoreductases (Thoden et al. 2007) and also binds to NADP (Kumar et al. 2008), and thus, it is possible that Gal80 bears an unknown

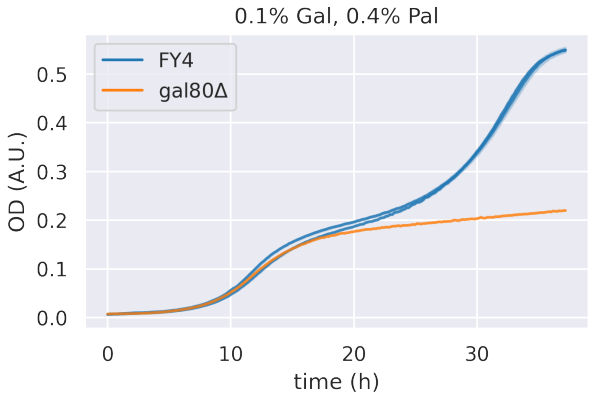

Figure 4.14: Deleting *GAL80* strongly delays growth in palatinose in galactose-palatinose mixture. OD is measured by a plate reader. Each curve represents one biological replicate. The shaded area represents the standard deviation of two technical replicates.

metabolic function related to palatinose, in addition to its role of repressing Gal4. What causes the delayed use of palatinose seen in Figs 4.14 and 4.19? Is it the active Gal4 without the Gal80 repressor, or the loss of Gal80? To distinguish the two scenarios, I introduced a *gal80*Δ *gal4*Δ double-mutant.

As shown in Fig 4.15, the *gal4*Δ *gal80*Δ double-mutant has the same phenotype as the wildtype and *gal4*Δ, which suggests that *GAL80* has no direct function in palatinose metabolism and that *GAL4* is required for the delay in using palatinose. Deleting *GAL80* leads to active Gal4, which strongly delays the cells' use of palatinose.

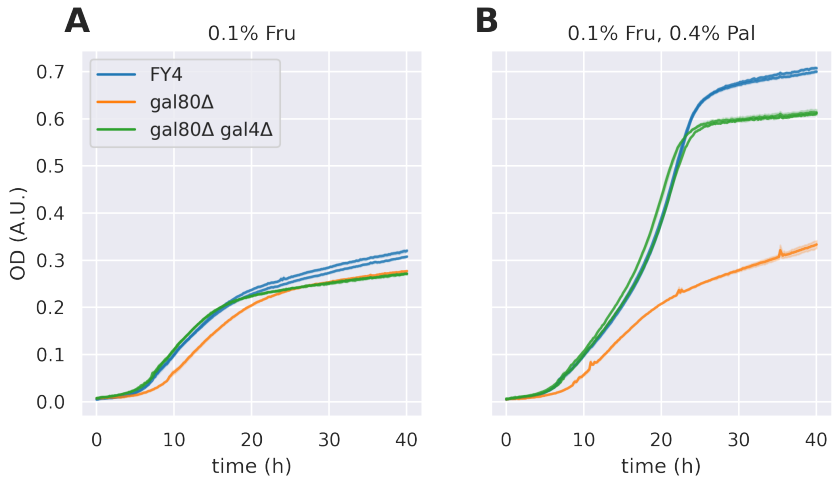

Figure 4.15: Deleting *GAL4* from the *gal80*Δ mutant recovers growth in palatinose. **(A, B)** OD measured by a plate reader. Each curve represents one biological replicate. The shaded area represents the standard deviation of two technical replicates.

4.3.8 Active Gal4 does not change the basal transcription of *MAL* genes

Active Gal4 changes the transcription profile of cells beyond the classic *GAL* genes responsible for galactose metabolism(Ideker et al. 2001; Dalal et al. 2016). Multiple genes are identified to be under direct control of Gal4 (Ren et al. 2000). The induction of the *MAL* network by palatinose requires basal expression of the transporter Mal11 and sensors Mal13 and Znf1 (see Section 1.4.1). I wondered whether active Gal4 delays palatinose metabolism by repressing basal transcription of *MAL* genes.

Cells grown in mixtures of fructose and palatinose do not show diauxie with a visible lag (Fig 4.10), and therefore, considering the network's positive feedback, the basal expression of *MAL* genes in 0.1% fructose should permit induction of *MAL* genes by palatinose, making 0.1% fructose a good reference for permissive basal *MAL* level.

To verify whether active Gal4 indeed decreases the basal *MAL* transcripts and hence delays palatinose metabolism, I quantified the relative abundance of *MAL* transcripts in 0.1% fructose and 0.1% galactose with qPCR. As seen in Fig 4.16, there is no visible difference between wildtype grown in galactose and in fructose, nor between wildtype and the *gal80*Δ mutant in fructose, which suggests that active Gal4 does not repress basal transcription of the *MAL* genes.

Further, I re-analysed the RNAseq dataset by Dalal *et al* (Dalal et al. 2016). Consistent with my qPCR results, the level of *MAL* transcripts is similar between cells grown in yeast extract peptone (YEP) and YEP-galactose (Fig 4.17).

The results suggest that the delay of palatinose metabolism in the *gal80*Δ mutant is not through repressing the basal transcription of *MAL* genes, because the basal transcription remains unchanged when Gal4 is active.

4.3.9 *GAL2* is partially responsible for the delay of palatinose metabolism

Gal4 controls the transcription of a set of genes responsible for galactose metabolism. Active Gal4 in the absence of galactose (and glucose) overexpresses those genes. Can any of the downstream *GAL* genes lead to the delay of palatinose metabolism?

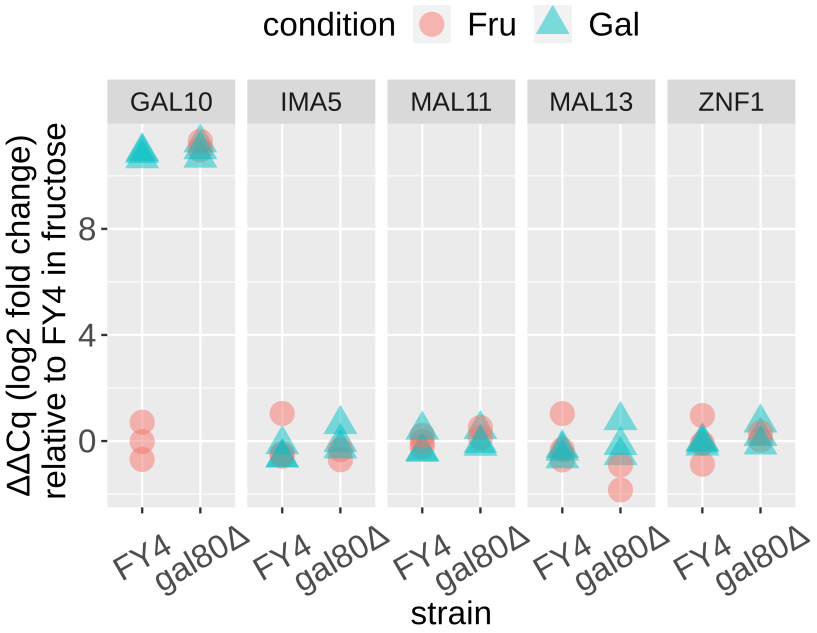

Figure 4.16: qPCR results show that basal transcript level of *MAL* genes does not change in the *gal80*Δ mutant. Each data point represents a biological replicate. The C_q value of each gene is the number of cycles required to amplify the input cDNA to a fixed threshold, using a pair of primers which targets that gene. ΔC_q of each gene in each biological replicate is the difference between the C_q of that gene and the median C_q of 3 reference genes (*ALG9*, *ACT1* and *PUS7*) in the same biological replicate. The $\Delta\Delta C_q$ of each gene in each biological replicate is the difference between the ΔC_q of that gene in that biological replicate and the median ΔC_q of that gene in fructose. The concentrations of fructose and galactose are both 0.1%. Samples are harvested at around OD 0.3.

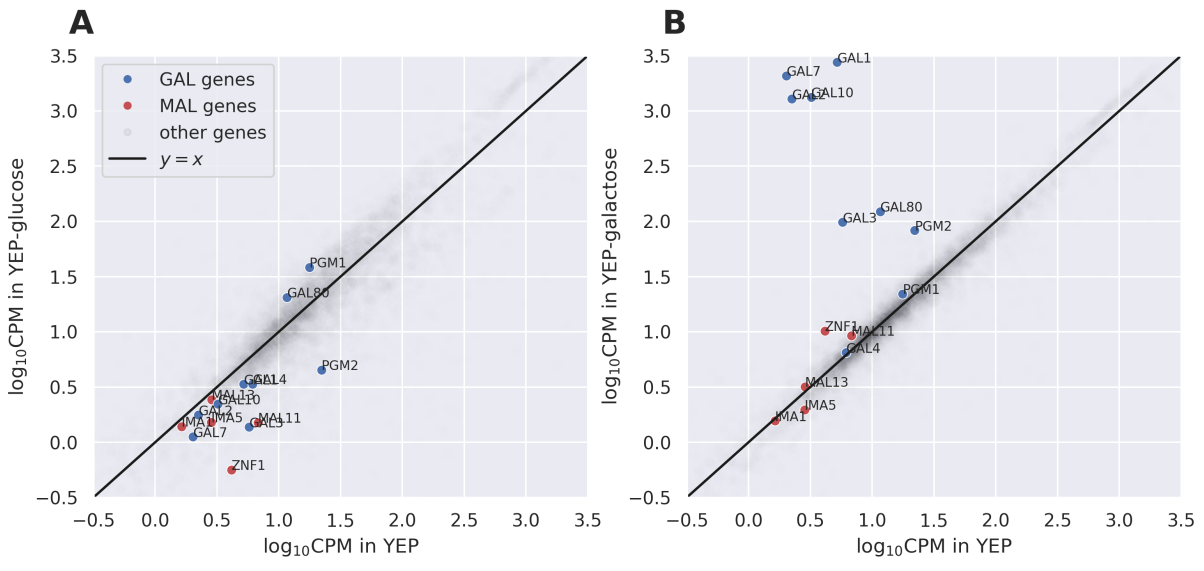

Figure 4.17: RNAseq dataset from Dalal *et al* (Dalal et al. 2016) shows that basal transcript level of MAL genes are repressed in glucose but not in galactose. The level of transcripts of each gene is represented by counts per million reads (CPM). **(A)** The CPM of each gene in YEP-glucose and in **(B)** YEP-galactose is plotted against that of each gene in YEP. The five *MAL* genes responsible for palatinose metabolism are highlighted in red, and the *GAL* genes in blue.

To investigate the potential roles of the downstream *GAL* genes in palatinose, I created a series of *GAL* deletion mutants and compared the phenotype of the mutants against the wildtype and the *gal80*Δ mutant in a plate reader. If a mutant fully recovers the ability to consume palatinose like the wildtype strain, then that deletion gene is responsible for the delay of palatinose metabolism. On the contrary, if a mutant still shows strong delay of palatinose metabolism like the *gal80*Δ mutant, the deleted gene is unlikely to be relevant.

I began with deleting the *GAL1-10-7* locus from the *gal80*Δ mutant, in which the three *GAL* genes are highly expressed and generate burden to the cells (Malakar and Venkatesh 2014), using the clustered regularly interspaced short palindromic repeats (CRISPR) technique (Shaw et al. 2019). However, similar to *gal80*Δ (Figs 4.14 and 4.15A), this mutant shows strong delay of palatinose metabolism (Fig 4.18B), which suggests none of *GAL1*, *GAL10*, or *GAL7* is the cause of delayed palatinose metabolism.

I further deleted *GAL2* and *GAL3* from the *gal80*Δ *gal1-10-7*Δ mutant (Fig 4.18C and D). Surprisingly, I found that deleting *GAL2*, which encodes the galactose permease, partially restores the ability of cells to consume palatinose (Fig 4.18C).

To confirm that the partial restoration of palatinose consumption arises solely from deletion of *GAL2*, instead of deleting *both GAL2* and *GAL1-10-7*, I created a *gal80*Δ *gal2*Δ double-mutant. Indeed, deleting *GAL2* itself is sufficient to partially restore the palatinose metabolism (Fig 4.19). This result is similar to (Ideker et al. 2001), where the *gal80*Δ mutation results in slow growth in raffinose and alters the gene expression profile, and further deletion of *GAL2* partially restores the gene expression profile. However, we do not yet know the mechanism in either case — Gal2 is not known to have a function of signal transduction.

In conclusion, within the set of classic *GAL* genes downstream of Gal4, only *GAL2*, which encodes the galactose permease, appears partially responsible for the delay of palatinose metabolism.

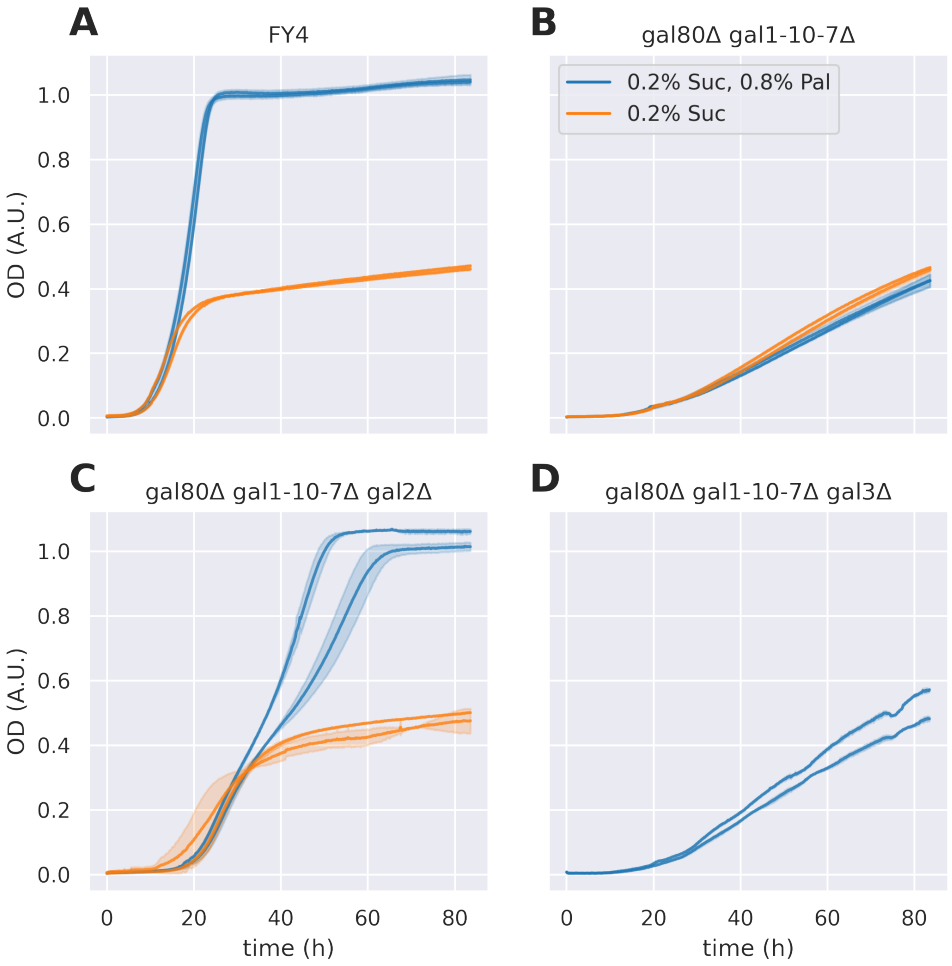

Figure 4.18: Deleting the *GAL1-10-7* locus and *GAL3* from the *gal80*Δ mutant does not shorten the delay of growth in palatinose, but deleting *GAL2* does. **(A, B, C, D)** OD measured by a plate reader. Each curve represents one biological replicate. The shaded area represents the standard deviation of two technical replicates. I should have included but did not include the 0.2% sucrose condition in the *gal80*Δ *gal1-10-7*Δ *gal3*Δ strain in the experiment.

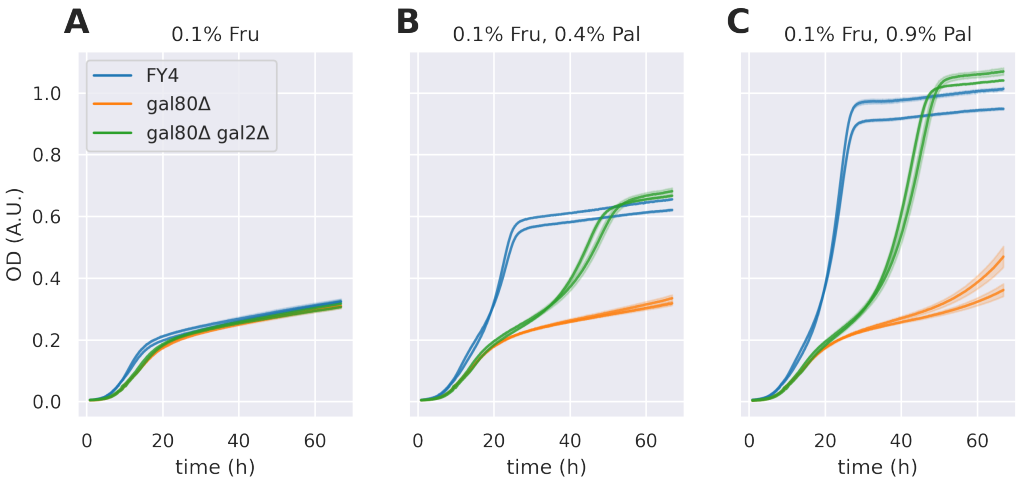

Figure 4.19: Further deleting *GAL2* from the *gal80*Δ mutant shortens the delay of growth in palatinose. **(A, B, C)** OD measured by a plate reader. Each curve represents one biological replicate. The shaded area represents the standard deviation of two technical replicates.

4.3.10 *GAL2*'s effect on delaying palatinose metabolism requires active Gal4

The results of the previous section suggest that Gal2 plays a partial role in delaying palatinose metabolism when Gal4 is active (but in the absence of galactose). To check if the effect of Gal2 requires active Gal4, I overexpressed Gal2 by integrating *pCCW12-GAL2* into the *HO* locus in the wildtype strain, using the MoClo-YTK toolkit (Lee et al. 2015). Despite high level of overexpression (Fig 4.20), Gal2 itself does not delay palatinose metabolism (Fig 4.21), suggesting the effect of *GAL2* on palatinose metabolism requires active Gal4.

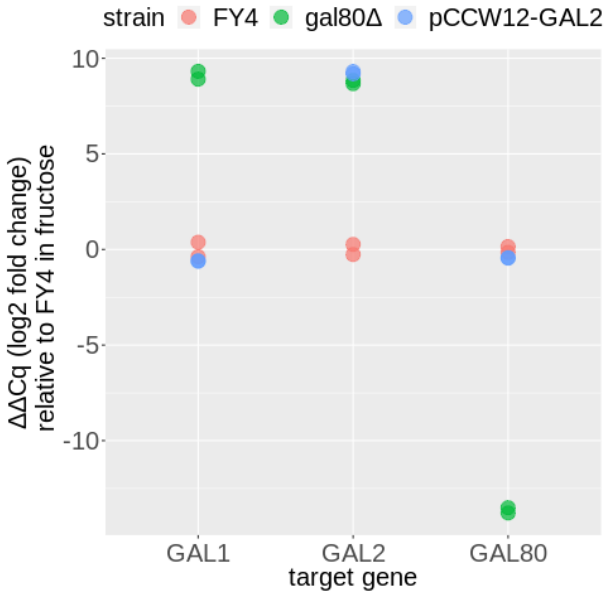

Figure 4.20: qPCR results show that the transcript level of *GAL2* driven by the *CCW12* promoter is similar to that of *GAL2* in the *gal80*Δ mutant. Each data point represents a biological replicate. The C_q value of each gene is the number of cycles required to amplify the input cDNA to a fixed threshold, using a pair of primers which targets that gene. ΔC_q of each gene in each biological replicate is the difference between the C_q of that gene and the mean C_q of 3 reference genes (*ALG9*, *ACT1* and *PUS7*) in the same biological replicate. The $\Delta\Delta C_q$ of each gene in each biological replicate is the difference between the ΔC_q of that gene in that biological replicate and the mean ΔC_q of that gene in fructose. Cells are grown in 0.1% fructose and samples are harvested at around OD 0.3.

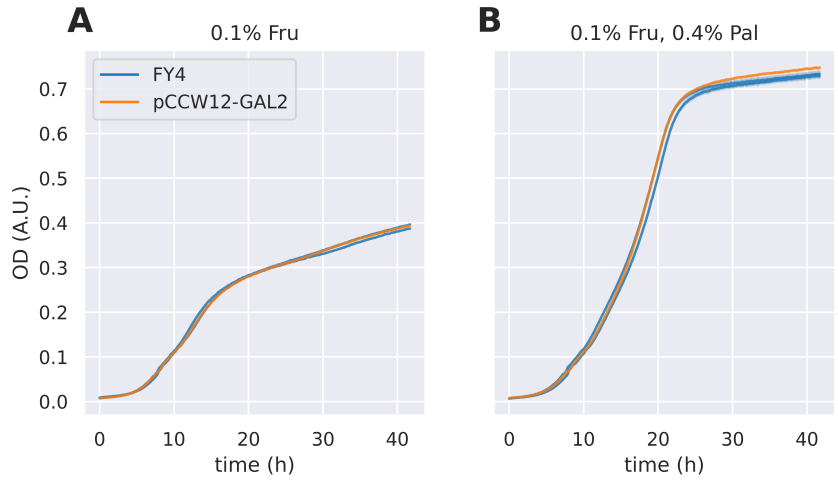

Figure 4.21: Overexpressing *GAL2* without active Gal4 does not change the growth dynamics in fructose-palatinose mixture. **(A, B)** OD of wildtype (FY4) and the *pCCW12-GAL2* strain overexpressing *GAL2* measured by a plate reader. Each curve represents one biological replicate.

4.3.11 Does the signal downstream of Gal4 act through glucose repression or inhibition components?

The *MAL* network is subject to glucose repression at the transcriptional level (Gancedo 1998), and glucose inhibition at the post-transcriptional level (through degradation of the *MAL* transporter, Mal61 or Mal21) (Gadura, Robinson, and Michels 2006). I wondered whether the *MAL*-suppressing Gal4 signal converges with the known glucose repression/inhibition signals. The single deletion mutants that were tested are listed in Table 4.1. However, all mutants except *mth1*Δ still exhibit galactose-palatinose diauxie (Fig 4.22). This suggests either that the Gal4 signal does not act through the screened glucose repression/inhibition components, or that it acts through those components, but some components are redundant. *mth1*Δ cannot metabolise palatinose (Fig 4.22C).

4.4 Discussion

The results in this chapter showed a clear example of non-glucose catabolite repression in *S. cerevisiae* — cells prioritise galactose over palatinose, which gives rise to the galactose-palatinose diauxie (Fig 4.3 and 4.6). In the presence of galactose, cells have active Gal4, which, through an unknown downstream mechanism, prevents the *MAL* genes from being highly expressed (Fig 4.12), although it does not affect the basal transcription of *MAL*

Table 4.1: Mutants that affect glucose repression or inhibition.

Genotype	Description
*mig1*Δ	Mig1 transcriptionally represses *MAL* genes (Gancedo 1998).
*mig2*Δ	Mig2 cooperates with Mig1 in glucose repression (Kaniak et al. 2004).
*rgt2*Δ	Rgt2 activates Grr1, leading to Mal61's degradation (Jiang, Medintz, and Michels 1997).
*snf3*Δ	*SNF3* is the paralog of *RGT2*.
*hxk2*Δ	*hxk2*Δ leads to co-consumption of glucose and galactose/sucrose (Raamsdonk et al. 2001).
*mth1*Δ	*MTH1*'s expression increases when Gal4 is active (Ren et al. 2000). Mth1 represses expression of hexose transporters (Flick et al. 2003) and *SUC2* (Gancedo, Flores, and Gancedo 2015).
*reg2*Δ	Reg2 cooperates with Reg1 to inactivate Mal61 (Jiang, Tatchell, et al. 2000).
*yck1*Δ	Yck1/2 kinase acts upstream of Doa4 and is required for Mal61 degradation (Gadura, Robinson, and Michels 2006).
*doa4*Δ	Doa4 is ubiquitin hydrolase. *doa4*Δ slows down the degradation of Mal61 (Lucero and Lagunas 1997).

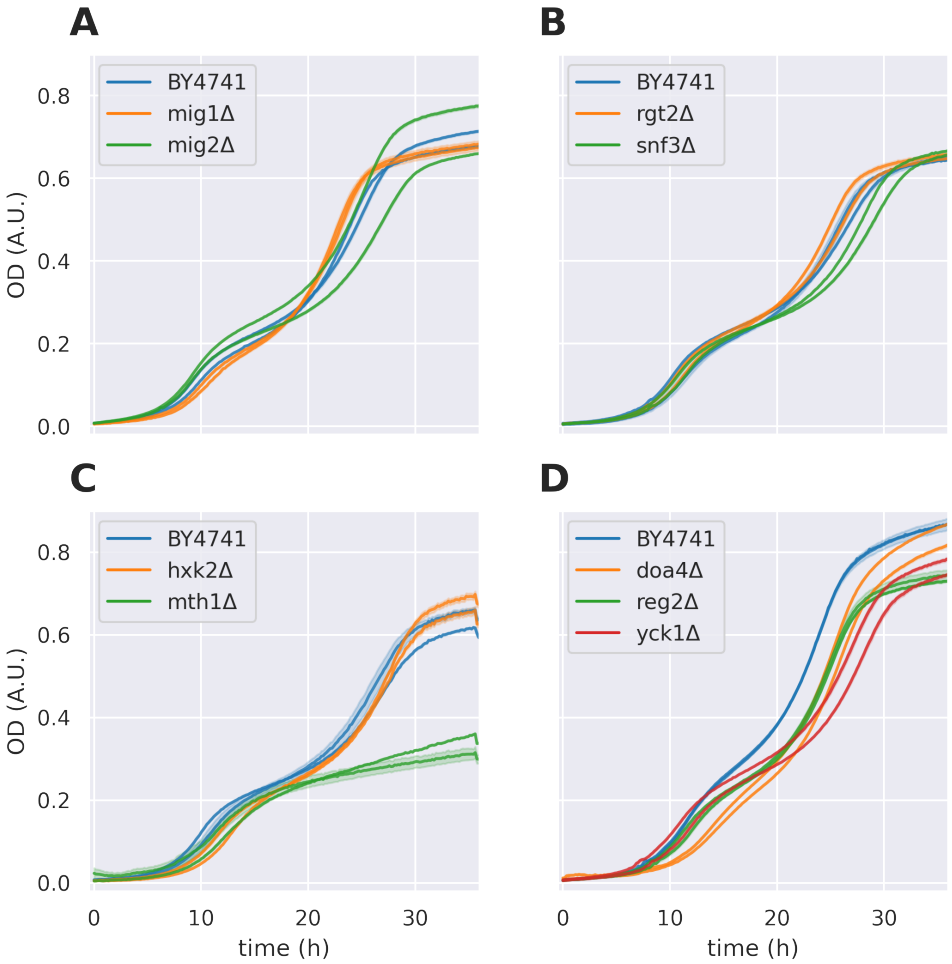

Figure 4.22: Mutants related to glucose repression/inhibition of the *MAL* network still show galactose-palatinose diauxie. **(A, B, C, D)** OD measured in a plate reader. All cultures are in 0.1% galactose + 0.4% palatinose. Each curve represents one biological replicate. The shaded area represents the standard deviation of two technical replicates.

genes (Figs 4.16 and 4.17). After galactose runs out, Gal4 is inactivated by its repressor Gal80 and cells begin to activate the *MAL* genes and consume palatinose.

In the *gal80*Δ mutant, in which Gal4 is constitutively active, consumption of palatinose is strongly delayed ((Fig 4.14). Such effect is alleviated if *GAL2*, which encodes the galactose transporter, is further deleted (Fig 4.19).

Our results added the "galactose-palatinose" hierarchy to the known "glucose-galactose" hierarchy in *S. cerevisiae*. This is consistent with the following theory of growth rate maximisation: with a limited proteome size (Scott et al. 2010), cells must increase the metabolic flux per unit of enzyme to achieve faster growth, and this predicts the existence of a "sugar hierarchy", which means cells should always prioritise a sugar that supports faster growth over another, because the amount of enzyme required to support the same metabolic flux (and hence the growth rate) would be smaller for the superior sugar (Wang et al. 2019). However, in this research, we also found that cells do not prioritise fructose or glucose over palatinose, which is inconsistent with the prediction in (Wang et al. 2019). Considering that additional regulation required from the hierarchy adds to the network's complexity (Aidelberg et al. 2014), and that a strict hierarchy slows down cells' adaptation in variable environments (Cerulus et al. 2016), further research in the regulatory mechanism in this specific example and its impact on cellular fitness in variable environments, should reveal how this strategy, together with its regulatory mechanism, was selected. In the next chapter, I will explore the molecular mechanism behind the galactose-palatinose diauxie.

Chapter 5

The interaction between *GAL* and *MAL*

5.1 Summary

- Context: budding yeast prioritises galactose over palatinose via an unknown signalling downstream of Gal4.
- Question: what is the molecular mechanism of this catabolite repression?
- Approach: we use RNA sequencing (RNAseq) to quantify the differential expression between the wildtype and the *gal80*Δ mutant in which Gal4 is constitutively activated.
- Finding: expression of *MAL11*, which encodes the palatinose transporter, is repressed, but can be overcome by strengthening the positive feedback of the *MAL* network.
- Outlook: our results provide a novel example on the mechanism of catabolite repression in budding yeast, as well as how this can be altered by the loss of one gene, which suggests evolvability of the strategy of carbon source consumption.

5.2 Background

In the previous chapter, we identified galactose-palatinose diauxie and showed that active Gal4 retards palatinose metabolism. Results in Fig 4.19 and Section 4.3.10 suggest that under Gal4 signalling, Gal2 is partially responsible for the delay of palatinose metabolism. However, the *gal80*Δ *gal2*Δ double-mutant does not fully recover the wildtype's phenotype — the wildtype shows no diauxie in fructose-palatinose mixtures but the mutant does (Fig 4.19), which suggests that other Gal4-downstream players may exist in addition to Gal2, which delays the use of palatinose. However, we are not aware of any Gal4-*MAL* signalling so far.

In addition to the *GAL* genes, Gal4 activates multiple genes which do not directly participate in galactose metabolism (Ren et al. 2000; Ostergaard et al. 2001; Choi et al. 2008), and promoters and coding sequences of more genes have Gal4 binding sites with unknown physiological effect (Li and Johnston 2001).

It is therefore possible that Gal4, which binds to DNA, directly or indirectly changes the expression of *MAL* genes, which causes the delay of palatinose metabolism. In this chapter, we investigate (1) which *MAL* gene(s) are affected by active Gal4; (2) which genes are differentially expressed in the *gal80*Δ mutant, in which Gal4 is active; (3) how *might* the change in the transcriptome propagate to the change in levels of *MAL* genes. Given the large number of genes that might be affected or directly regulated by Gal4, it would be ideal to measure the cells' transcriptome in an RNAseq experiment, whose results directly answer Questions (1) and (2). To answer Question (3), we identify a set of differentially expressed gene (DEG)s, followed by enrichment on GO terms, pathways and transcription factors. It is also possible to use ChIP to detect the genes whose promoter is directly bound by Gal4, which directly answers Question (3), but two ChIP datasets of Gal4 already exist which identified in total 12 target genes (Ren et al. 2000; Rhee and Pugh 2011) — we will use this dataset to validate our results.

The RNAseq results showed that in the wildtype strain, the isomaltases are induced earlier than the transporter *MAL11* in the presence of palatinose. *MAL11* is likely to be target of Gal4 signalling in the *gal80*Δ mutant, although it is unlikely that Gal4 directly binds to the DNA surrounding *MAL11*. Thus, in the *gal80*Δ mutant, the *MAL* network

is "locked" in a state in which the isomaltases are excessive compared to the transporter *MAL11*. To understand how active Gal4 in the *gal80*Δ mutant changes the *MAL* network's inducibility, we mathematically modelled the induction of the *MAL* network, and the model predicts that decreasing the isomaltases' expression or overexpressing *MAL11* in the *gal80*Δ mutant will alleviate the delay in palatinose metabolism. This model prediction is confirmed by the fact that cells resume ability to grow on palatinose without delay after deleting one of the two isomaltases, *IMA1*, from the *gal80*Δ mutant. In addition, by comparing the gene expression between the wildtype and the *gal80*Δ mutant, we identified a set of DEGs, using which we identified potential transcription factors that are downstream of Gal4. To elucidate the Gal4-to-*MAL* signalling, we will check if any of those transcription factors is upstream of the *MAL* network in the future.

5.3 Results

5.3.1 In the RNAseq experiment, both the wildtype and the *gal80*Δ mutant were grown in 0.1% fructose and 0.1% fructose + 0.9% palatinose

To design the RNAseq experiment, we need to choose a condition with palatinose where the *MAL* genes are induced, and a palatinose-free condition where the *MAL* genes are not induced as control. To choose the palatinose-free condition, we consider two criteria. First, *GAL4*'s expression should not be repressed in this condition, and glucose is not eligible because in glucose *GAL4* is repressed by Mig1 irrespective of the binding of Gal80 (Ricci-Tam et al. 2021). Second, active Gal4 should not change the growth rate of cells if the growth rate changes, the expression of many genes (e.g. ribosomal genes (Metzl-Raz et al. 2017)) will change, which will interfere with the identification of genes that are direct downstream of Gal4. Third, the palatinose-free condition should not repress the expression of *MAL* genes.

Eventually, we chose 0.1% fructose as the palatinose-free condition in the RNAseq experiment, because (1) 0.1% fructose does not repress the *GAL* genes, and hence the expression of Gal4 in the *gal80*Δ mutant (Fig 5.1), (2) the growth of the *gal80*Δ mutant

in 0.1% fructose is similar to the wildtype (Fig 4.19A), and (3) in fructose + palatinose mixtures, there is no typical diauxie (Fig 4.10). Accordingly, the condition with palatinose is 0.1% fructose + 0.9% palatinose.

We harvested samples at three time points (Fig 5.2). Time point 1 is the mid-log of cultures in 0.1% fructose (at OD 0.3). Time points 2 and 3 are 10 hours and 16 hours after the mid-log, respectively.

In summary, we harvested 36 samples:

- 3 biological replicates of 2 strains — wildtype and *gal80*Δ mutant,
- in 2 conditions — 0.1% fructose and 0.1% fructose + 0.9% palatinose,
- at 3 time points — mid-log, 10 hours after mid-log and 16 hours after mid-log.

I extracted those RNAs from the samples, which were then used for library preparation, before the Next-Generation Sequencing run. The reads were returned as FASTQ sequences, which were then mapped to the reference genome sequence of strain S288c and the number of reads that were mapped onto each gene's mRNA was counted. For each sample, the count of each gene was normalised by the total counts of that sample, and therefore the gene expression level has the unit counts per million reads (CPM). See Section 6.5.4 for details.

The resulting dataset is a 5697×36 count table, with genes on the rows and samples on the columns. The number of total reads that were mapped to the genes on chromosomes in each sample range between 6.02 million to 11.79 million.

5.3.2 The RNAseq dataset shows clear distinction on the expression pattern between the wildtype and *gal80*Δ mutant, and between mid-log and later time points

To ensure the quality of the RNAseq dataset, we perform principle component analysis (PCA) and cluster the samples by Pearson's correlation coefficient using DESeq2 (Love, Huber, and Anders 2014).

The PCA results show that the samples were separated by the time point at harvest on the first principle component, and by the genotype on the second principle component

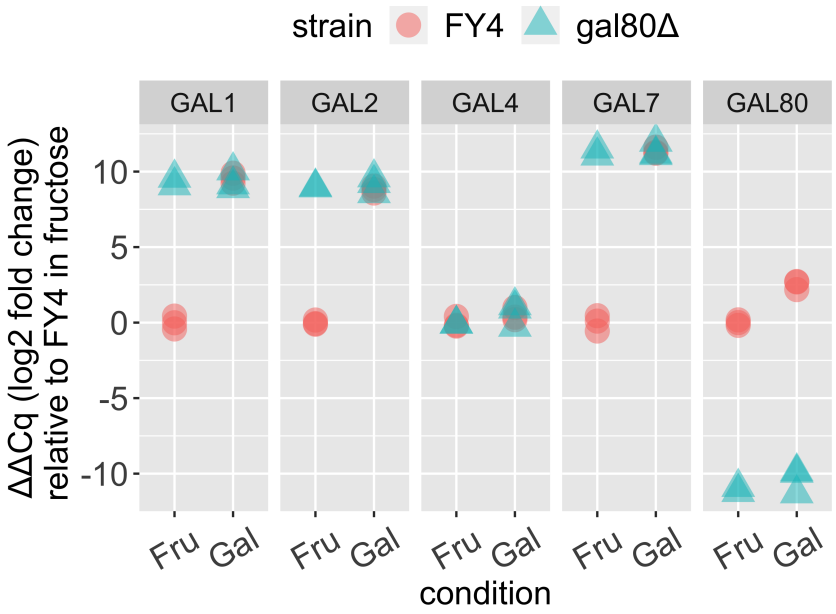

Figure 5.1: qPCR results show that the *GAL* transcript levels of the *gal80*Δ mutant in fructose is similar to that in galactose. Each data point represents a biological replicate. The C_q value of each gene is the number of cycles required to amplify the input cDNA to a fixed threshold, using a pair of primers which targets that gene. ΔC_q of each gene in each biological replicate is the difference between the C_q of that gene and the mean C_q of 3 reference genes (*ALG9*, *ACT1* and *PUS7*) in the same biological replicate. The $\Delta\Delta C_q$ of each gene in each biological replicate is the difference between the ΔC_q of that gene in that biological replicate and the mean ΔC_q of that gene in fructose. The concentrations of fructose and galactose are both 0.1%. Samples are harvested at around OD 0.3.

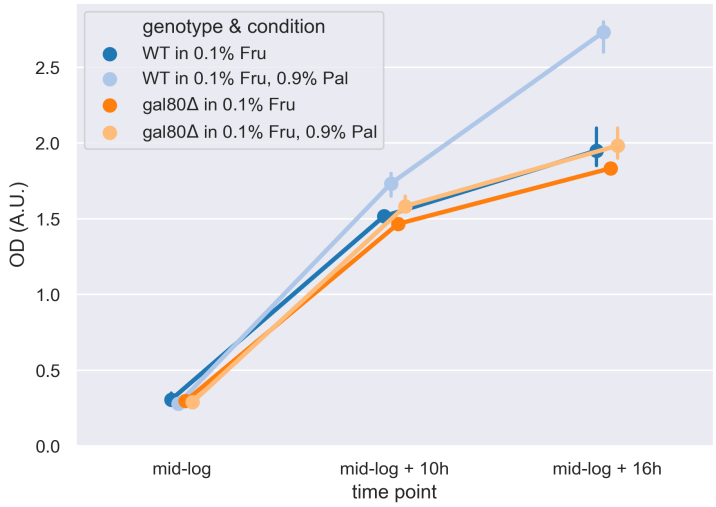

Figure 5.2: OD of samples for RNAseq when they were harvested. The error bar shows the standard deviation of three biological replicates.

(Fig 5.3). The results of hierarchical clustering also show a clear distinction between samples harvested at mid-log and those harvested at later time points, and within each first-level cluster, another clear distinction between the wildtype and *gal80*Δ genotypes (Fig 5.4). The results suggest a good data quality.

Figure 5.3: Principal component analysis (PCA) shows clear distinction in expression between the wildtype and *gal80*Δ mutant, and between the mid-log and later time points. The raw counts were transformed with variance stabilising transformation (VST) before PCA. Counts of all 5697 genes, instead of the top 500 genes with the highest row variance (the default in DESeq2), were analysed.

5.3.3 The *GAL* genes are up-regulated in the *gal80*Δ mutant, and the presence of palatinose only induces a small, well-characterised set of genes

To further check the quality of this dataset, we performed differential expression analysis with DESeq2 (Love, Huber, and Anders 2014). We compare: the gene expression profiles between (1) the wildtype and the *gal80*Δ mutant in 0.1% fructose at mid-log, and between (2) the wildtype in 0.1% fructose and the wildtype in 0.1% fructose + 0.9% palatinose at mid-log.

As is shown in Fig 5.5A, the *GAL* genes, except *GAL4*, *PGM1* and *GAL80*, are significantly up-regulated in the *gal80*Δ mutant compared to the wildtype in 0.1% fructose at mid-log. This is consistent with previous reports — *PGM1* does not have a Gal4 binding site (Boocock et al. 2021), and *GAL4*'s expression does not increase in YEP-

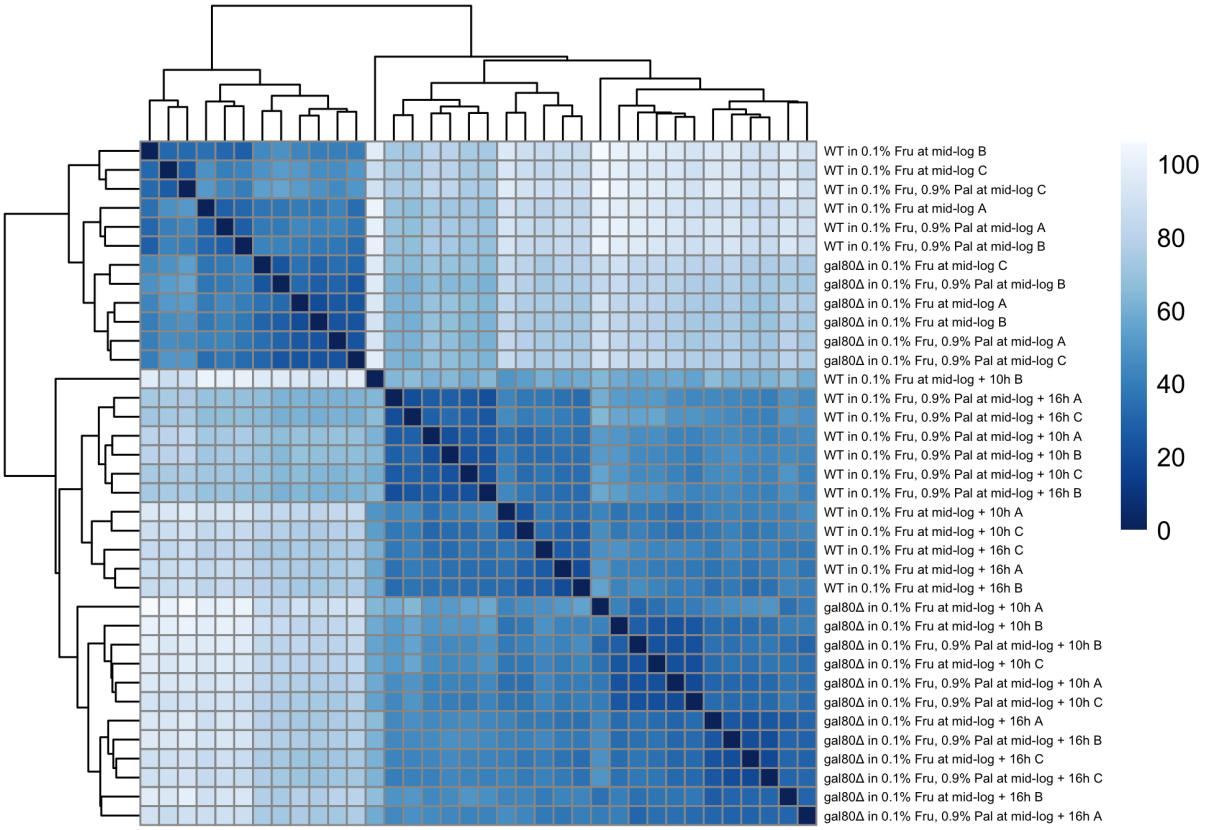

Figure 5.4: Hierarchical clustering shows a clear distinction between samples harvested at mid-log and later time points. The raw counts were transformed with variance stabilising transformation (VST) and the Euclidean distance between samples were calculated with DESeq2 before hierarchical clustering. The hierarchical clustering was performed with complete-linkage clustering. The color represents the Euclidean distance.

galactose compared to that in YEP in the dataset from (Dalal et al. 2016) (Fig 4.17). In Fig 5.5B, the set of differentially expressed genes is small and well-characterised — *MAL12*, *IMA1* and *IMA5* are part of the *MAL* network known to be induced by palatinose (Pougach et al. 2014); *YHR210C* and *YJL218W* are known to be targets of the *MAL* activator Znf1 (Pougach et al. 2014); *HXT8* and *REE1* are direct up- and down-stream genes of *IMA5*.

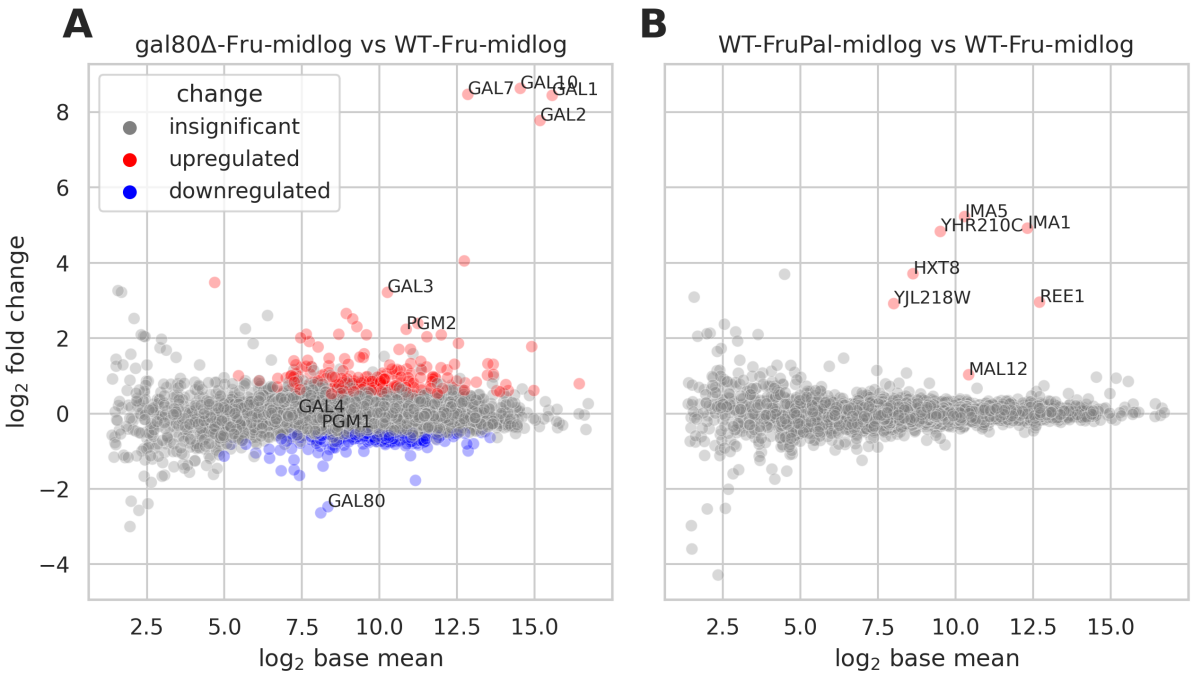

Figure 5.5: *GAL* genes are highly expressed in the *gal80*Δ mutant, and a small set of genes are induced in the wildtype when palatinose is present. Each panel plots the $\log_2$ fold change of each gene against its $\log_2$ base mean. Both values are calculated by DESeq2. The base mean is the mean of the normalised counts of all samples in the pair of conditions which we are comparing, and the counts are normalised by the sequencing depth. **(A)** We compare the transcriptome of the *gal80*Δ mutant in 0.1% fructose harvested at mid-log against that of the wildtype in the same condition and time point. **(B)** We compare the wildtype's transcriptome in 0.1% fructose + 0.9% palatinose at mid-log against that in 0.1% fructose at mid-log. The genes that are significantly up- and down-regulated are labeled red and blue, respectively. The criteria for significance are $\log_2$ foldchange > 0.5 and the adjusted p-value is smaller than 0.05.

5.3.4 In the wildtype strain, the isomaltases are induced before the transporter Mal11

We first focused on the induction dynamics of the *MAL* network in the wildtype, by comparing the transcript level between cells in 0.1% fructose and cells in 0.1% fructose +

0.9% palatinose. The genes we were interested in include the transporter gene *MAL11*, the isomaltase genes *IMA1* and *IMA5*, and the activator genes *MAL13* and *ZNF1* — they are directly involved in palatinose metabolism (Brown, Murray, and Verstrepen 2010; Voordeckers et al. 2012). Figs 5.6 and 5.7 show the CPM of all *MAL* genes of interest in both strains, both conditions and all three time points in the dataset. Below, Fig 5.8 shows part of the data in Fig 5.6.

We found that at mid-log, the expression of the two isomaltase genes, *IMA1* and *IMA5*, were already up-regulated, yet the transporter gene *MAL11* was not (Fig 5.7A-C). Instead, at the second time point, 10 hours after the mid-log, *MAL11* showed up-regulation (Fig 5.7A). *MAL13* did not show clear up-regulation at all three time points (Fig 5.7E), but *ZNF1* was up-regulated 16 hours after the mid-log (Fig 5.7F).

Interestingly, the maltase gene *MAL12*, which was thought to share a bi-directional promoter with *MAL11* (Levine, Tanouye, and Michels 1992), was also up-regulated at mid-log (Fig 5.7D), earlier than *MAL11*.

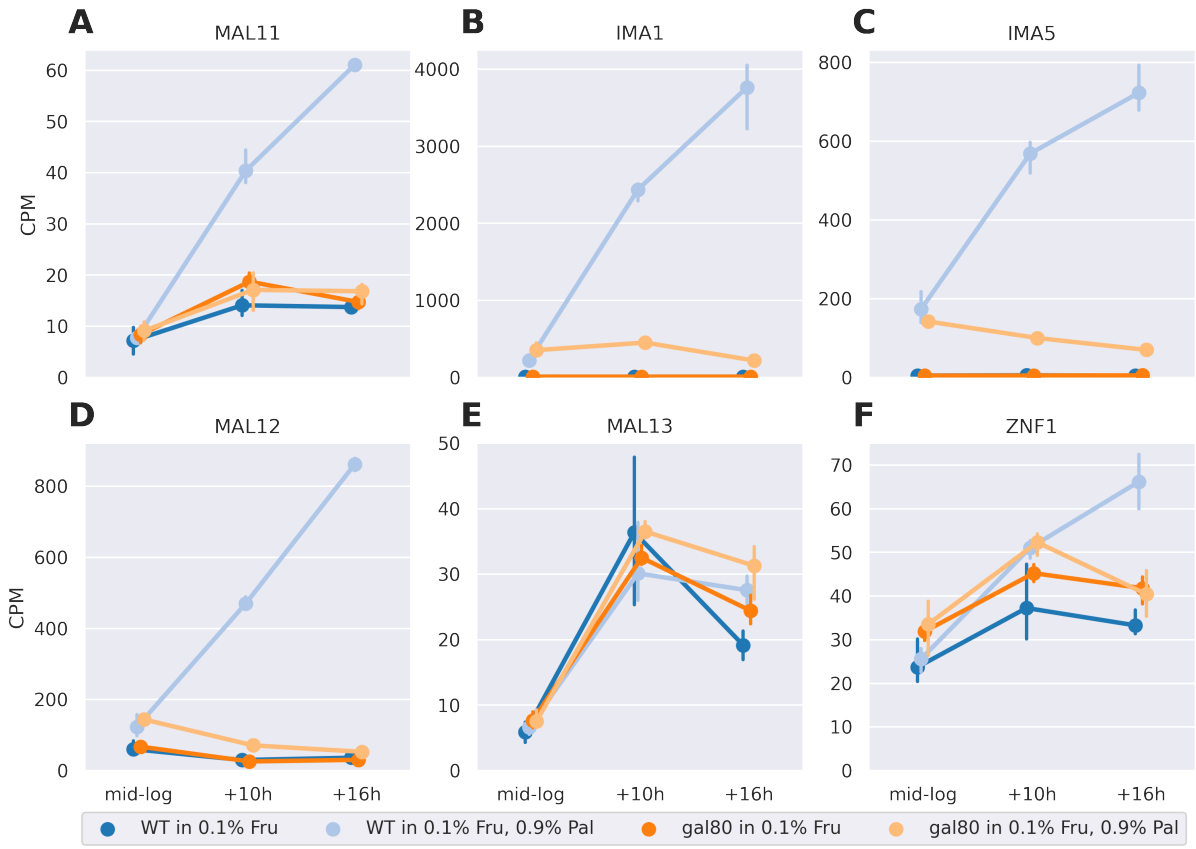

Figure 5.6: The change of *MAL* genes' transcript levels in all combinations of strains and conditions over three time points. **(A-F)** Each panel plots the counts per million reads (CPM) of each gene over three time points. The error bar represents the standard deviation of three biological replicates.

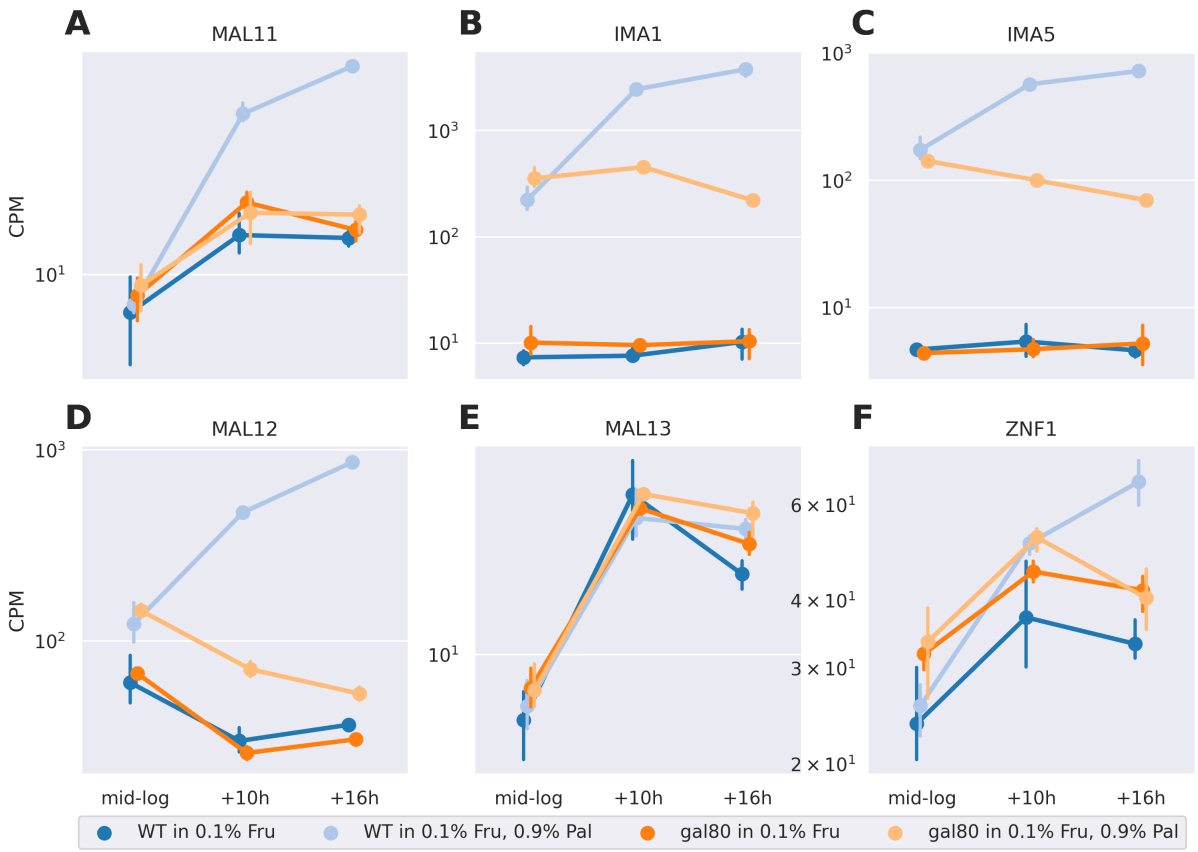

Figure 5.7: The change of *MAL* genes' transcript levels in all combinations of strains and conditions over three time points in a logarithmic scale. **(A-F)** Each panel plots the counts per million reads (CPM) of each gene over three time points. The error bar represents the standard deviation of three biological replicates.

5.3.5 Active Gal4 does not change the basal transcription of *MAL* genes, but prevents higher expression of *MAL11*

Knowing the dynamics of *MAL* induction in 0.1% fructose + 0.9% palatinose in the wildtype, we ask how the active Gal4 in the *gal80*Δ mutant changes the dynamics of induction.

First, we checked whether the basal transcription of the *MAL* network was changed in the *gal80*Δ mutant by comparing the *MAL* transcript level between the wildtype and the *gal80*Δ mutant in 0.1% fructose (without palatinose). Consistent with the results of Dalal *et al* (Dalal et al. 2016) re-analysed in Section 4.3.8, the basal transcription of the *MAL* network does not change (Fig 5.8).

At mid-log, no obvious difference between the wildtype and the *gal80*Δ mutant was observed — *IMA1*, *IMA5* and *MAL12* were induced and not for *MAL11*, *MAL13* or

ZNF1 (Fig 5.7), which suggests that the *MAL* activators Znf1 and Mal13 were still able to sense palatinose and activate the expression of *IMA1* and *IMA5* in the *gal80*Δ mutant.

However, in the later time points (10 and 16 hours after mid-log), the *MAL* network seems to be "locked" at a state similar to mid-log — cells were unable to activate higher expression of *MAL11* (Fig 5.7A) whilst the levels of *IMA1* and *IMA5* remained excessive compared to *MAL11*, although their levels decreased at later time points (Fig 5.7B and C).

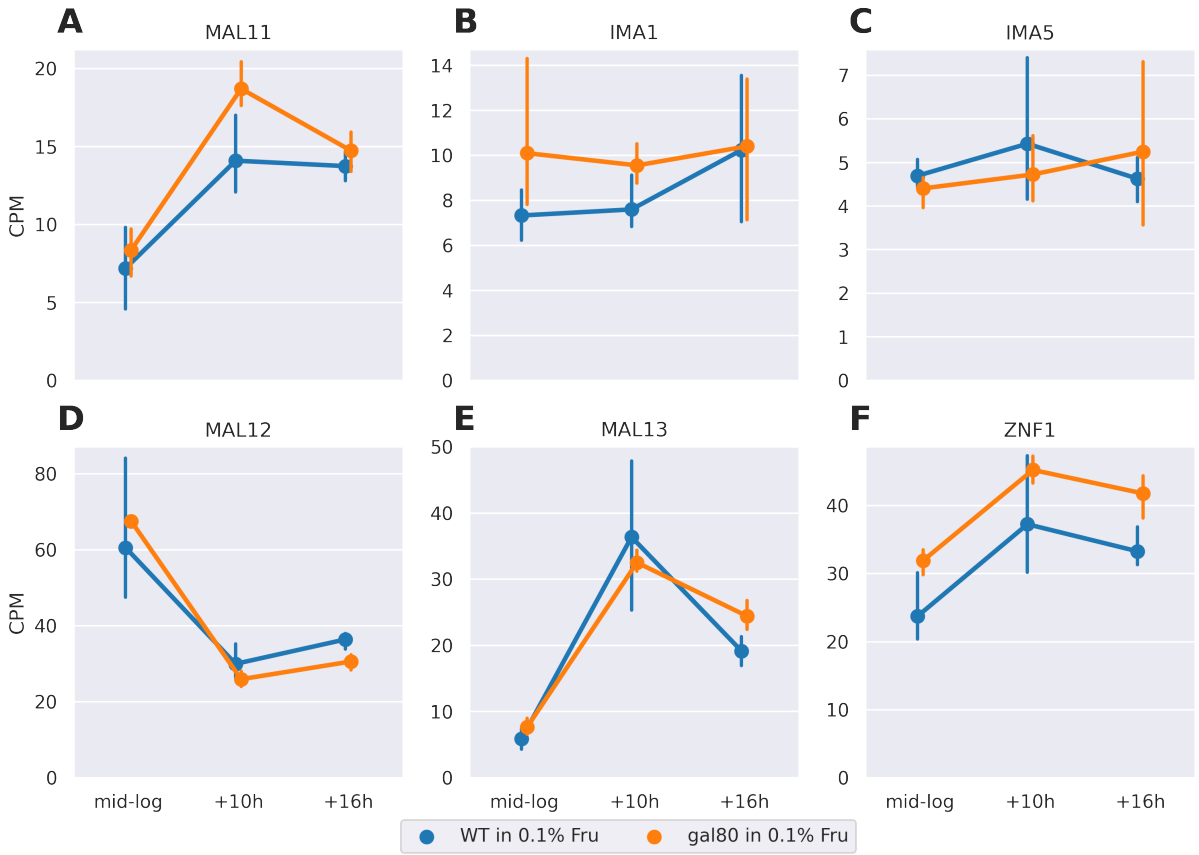

Figure 5.8: The *MAL* transcript levels in the *gal80*Δ mutant are similar to that in the wildtype. **(A-F)** Each panel plots the counts per million reads (CPM) of each gene over three time points. The error bar represents the standard deviation of three biological replicates.

5.3.6 Mathematical modeling of the *MAL* network

The *MAL* network is an inducible network, and the results in Section 5.3.4 indicate that the isomaltases are up-regulated earlier than the transporter in the presence of palatinose. Intuitively, this suggests that the isomaltases could be excessive relative to the transporter shortly after the cells are exposed to palatinose, which makes it harder to induce the *MAL*

network, because the isomaltases hydrolyse the imported palatinose, the inducer. In this section and Section 5.3.7, we will build a simple ODE model to clarify how the *MAL* network is induced by palatinose in the wildtype strain, and how the early expression of isomaltases might affect its inducibility. In Section 5.3.8, we will discuss how the active Gal4 in the *gal80*Δ may have changed its inducibility.

This model has three state variables: the concentration of intracellular palatinose p_i, transporter T and isomaltase E, and four non-negative parameters: the concentration of extracellular palatinose p_e, the degradation rate of the transporter d_T and the isomaltase d_E and the specific growth rate λ. The ODEs are:

$$\dot{p_i} = v_T(p_e)T - v_E(p_i)E - \lambda p_i \tag{5.1a}$$

$$\dot{T} = H_T(R^*) - (d_T + \lambda)T \tag{5.1b}$$

$$\dot{E} = H_E(R^*) - (d_E + \lambda)E \tag{5.1c}$$

In Eq 5.1, R^* is the active form of *MAL* activator R, and $H_T(R^*)$ and $H_E(R^*)$ are Hill-like functions of R^*:

$$H_T(R^*) = H_{T,basal} + (H_{T,max} - H_{T,basal})\frac{R^{*h_T}}{K_T^h + R^{*h_T}} \tag{5.2a}$$

$$H_E(R^*) = H_{E,basal} + (H_{E,max} - H_{E,basal})\frac{R^{*h_E}}{K_E^h + R^{*h_E}} \tag{5.2b}$$

and $H_{T,basal},\ H_{T,max},\ K_T,\ h_T,\ H_{E,basal},\ H_{E,max},\ K_E,\ h_E$ are constants. Additionally, we assume the Hill constants $h_j \geq 2$ and the basal expression levels $H_{j,basal} > 0$.

Additionally, in Eq 5.1, $v_E(p_i)$ is the rate of palatinose hydrolysis by the isomaltase, which can be approximated by simple Michaelis-Menten kinetics within the range of palatinose concentration we used (below 2% or 58 mM) (Deng et al. 2014), so $v_E(p_i)$ is:

$$v_E(p_i) = \frac{k_{cat,E}p_i}{K_{m,E} + p_i}E \tag{5.3}$$

We also assume that the palatinose import rate $v_T(p_e)$ also follows the Michaelis-Menten kinetics:

$$v_T(p_e) = \frac{k_{cat,T}p_e}{K_{m,T} + p_e}T \tag{5.4}$$

In Eqs 5.3 and 5.4, $k_{cat,E}$, $k_{cat,T}$, $K_{m,E}$ and K_{m_T} are constants.

In this model, we made the following simplification:

- there is only one isomaltase and one activator;
- the specific growth rate, λ, does not depend on p_i, T or E.

The following assumptions to further simplify the $H_T(R^*)$ and $H_E(R^*)$terms:

- the binding of palatinose to the activator follows the law of mass action and is at quasi-steady state;
- the number of palatinose molecules that are bound to the activator is much smaller than free molecules;
- the number of activators, R, is constant.

Now the production rates of the transporter and the isomaltase, H_T and H_E (Eq 5.2) are functions of intracellular palatinose p_i, because:

$$R^* \propto R \cdot p_i \propto p_i \tag{5.5}$$

To find the steady states, we set the right hand sides of Eq 5.1 to be 0, which gives:

$$v_T(p_e)T = (v_E(p_i) + \lambda)E \tag{5.6a}$$

$$T = \frac{H_T(p_i)}{d_T + \lambda} \tag{5.6b}$$

$$E = \frac{H_E(p_i)}{d_E + \lambda} \tag{5.6c}$$

By substituting Eq 5.6b and c into Eq 5.6a and moving all p_i-dependent terms onto the left hand side, we get a necessary condition for the steady state(s):

$$\frac{v_E(p_i)H_E(p_i) + \lambda(d_E + \lambda)p_i}{H_T(p_i)} = v_T(p_e)\frac{d_E + \lambda}{d_T + \lambda} \tag{5.7}$$

To visualise the solution(s) of the steady state, we define

$$y_1(p_i) = \frac{v_E(p_i)H_E(p_i) + \lambda(d_E + \lambda)p_i}{H_T(p_i)} \tag{5.8a}$$

$$y_2 = v_T(p_e)\frac{d_E + \lambda}{d_T + \lambda} \tag{5.8b}$$

For simplicity, we assume the specific growth rate $\lambda = 0$ in the analysis below. In this case, y_1 and y_2 in Eq 5.8 become:

$$y_1(p_i) \equiv \frac{v_E(p_i)H_E(p_i)}{H_T(p_i)} \tag{5.9a}$$

$$y_2 \equiv v_T(p_e)\frac{d_E}{d_T} \tag{5.9b}$$

If we plot y_1 and y_2 against p_i, the intersection(s) of y_1 and y_2 will be the steady state(s). y_2 does not depend on p_i, and therefore its graph is a horizontal line, and the graph of $y_1(p_i)$ depends on three key parameters: K_E, K_T and $K_{m,E}$ (Fig 5.9).

5.3.7 The *MAL* network of the wildtype strain shows switch-like behaviour

I infer the relative magnitude of K_E, K_T and $K_{m,E}$ from our experimental results and previously reported values. First, previous measurement showed that the intracellular concentration of maltose in a strain grown in maltose is 0.05% (1.5 mM) (Hatanaka, Mitsunaga, and Fukusaki 2018), so we assume K_T and K_E to be at the same magnitude. Moreover, the $K_{m,E}$ of Ima1 and Ima5 are 18 mM and 12 mM, respectively (Deng et al. 2014), so we assume $K_T < K_{m,E}$ and $K_E < K_{m,E}$. Second, to recover the results in Section 5.3.4, in which the isomaltases are expressed earlier than the transporter in the wildtype strain, so we assume in Eq 5.2 $K_E < K_T$.

Now we sketch the graph of y_1 as a function of p_i (Fig 5.9), assuming that $K_E < K_T < K_{m,E}$ and that the Hill coefficients $h_T,\ h_E \geq 2$. Both the numerator and denominator of y_1 increases with p_i, but when $p_i \ll K_T$, the denominator is close to constant: $H_T(p_i) \approx H_{T,basal}$. Thus, starting from $y_1(0) = 0$, y_1 increases with p_i, until p_i approaches K_T. The increase in H_T at $p_i \approx K_T$ slows down the increase or even causes a decrease in y_1.

Later, when $K_T < p_1 < K_{m,E}$, H_T approaches another constant, $H_{T,max}$, and therefore y_1 continues to increase with p_i. If the graph of y_1 monotonically increases, there will be one stable steady state. Otherwise, there can be three steady states (two stable) for a range of y_2 (Fig 5.9A).

The wildtype *MAL* system's steady state shows switch-like behaviour when we gradually increase the concentration of extracellular palatinose p_e (Fig 5.9B). The steady-state values of p_i, T, E remains small (the "OFF" state) if v_T is small, but increases abruptly (into the "ON" state) when p_e surpasses a threshold (Fig 5.9B).

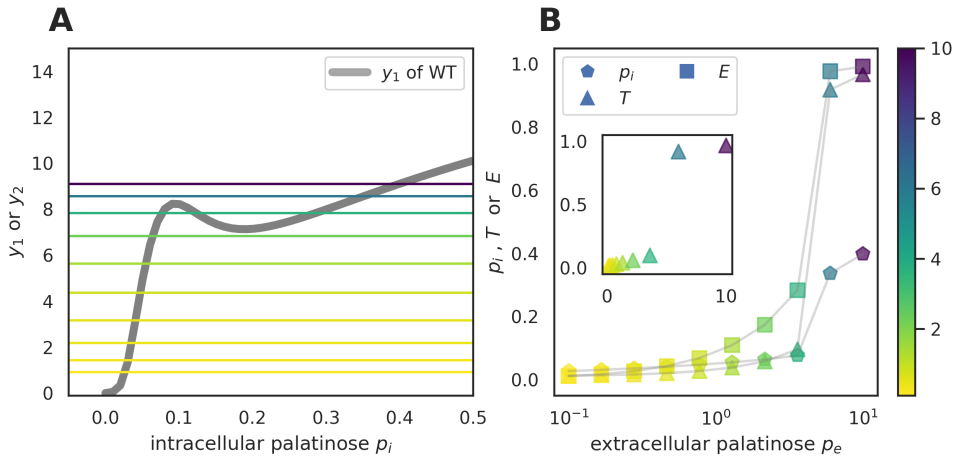

Figure 5.9: The model of *MAL* network in the wildtype strain shows switch-like behaviour. **(A)** y_1 (curve) and y_2 (horizontal line), defined in Eq 5.9, plotted against the concentration of intracellular palatinose p_i. **(B)** The steady-state values of intracellular palatinose concentration p_i, transporter level T and isomaltase level E plotted against the concentration of extracellular palatinose p_e. The inset of (B) shows the transporter level T in linear x-scale. The colors of y_2 in (A) and the steady-state values in (B) represent the value of p_e. The values of parameters and the initial condition are given in Table 5.1.

5.3.8 Active Gal4 changes the inducibility of the *MAL* network

How might the active Gal4 in the *gal80*Δ mutant have changed the steady state(s) of the *MAL* network in the wildtype? The results in Section 5.3.5 suggest the following statements:

1. the expression of *MAL11* was affected by active Gal4;
2. the cells can still sense intracellular palatinose and express the isomaltases at a level similar to the mid-log level of the wildtype strain;
3. the basal expression of the *MAL* network is not affected by *gal80*Δ.

This suggests that $H_E(p_i)$, $H_{E,basal}$ and $H_{T,basal}$ in Eq 5.1 were not changed by active Gal4, but other parameters related to the expression or the biochemical properties of Mal11 may have changed. We postulate the following two scenarios:

1. a change in the shape of y_1's graph, via an increase in K_T or a decrease in $H_{T,max}$ (e.g. caused by a repressor that competitively binds to the promoter of *MAL11*);

2. a decrease in y_2 (e.g. caused by an increase in the transporter's degradation rate d_T).

Fig 5.10 and 5.11 compare the wildtype's steady state and the *gal80*Δ's steady state in each scenario — in both scenarios, the *gal80*Δ strain requires higher extracellular palatinose p_e for the *MAL* network to induce.

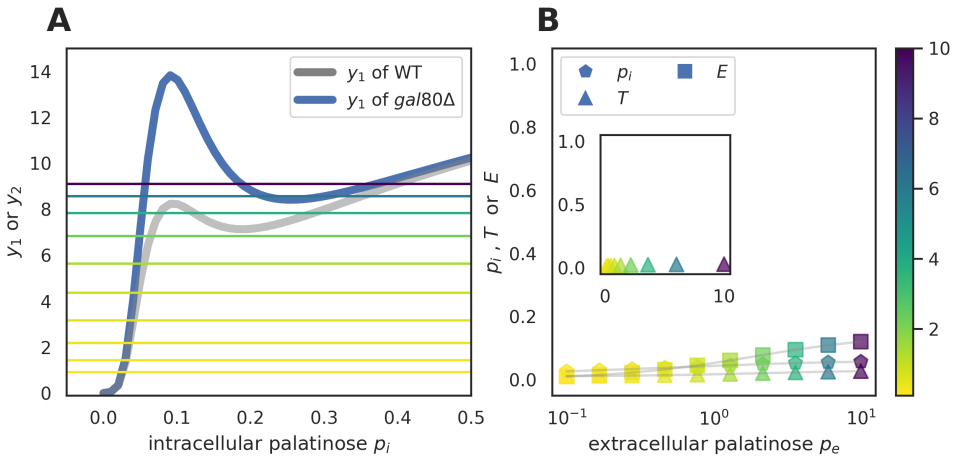

Figure 5.10: The model predicts that inducing the *MAL* network in the *gal80*Δ mutant needs higher extracellular palatinose, if active Gal4 increases K_T. **(A)** y_1 (curve) and y_2 (horizontal line), defined in Eq 5.9, plotted against the concentration of intracellular palatinose p_i. **(B)** The steady-state values of intracellular palatinose concentration p_i, transporter level T and isomaltase level E plotted against the concentration of extracellular palatinose p_e. The inset of (B) shows the transporter level T in linear x-scale. The colors of y_2 in (A) and the steady-state values in (B) represent the value of p_e. The values of parameters and the initial condition are given in Tables 5.1 and 5.2, except that in the *gal80*Δ mutant, the K_T value is increased by 20%.

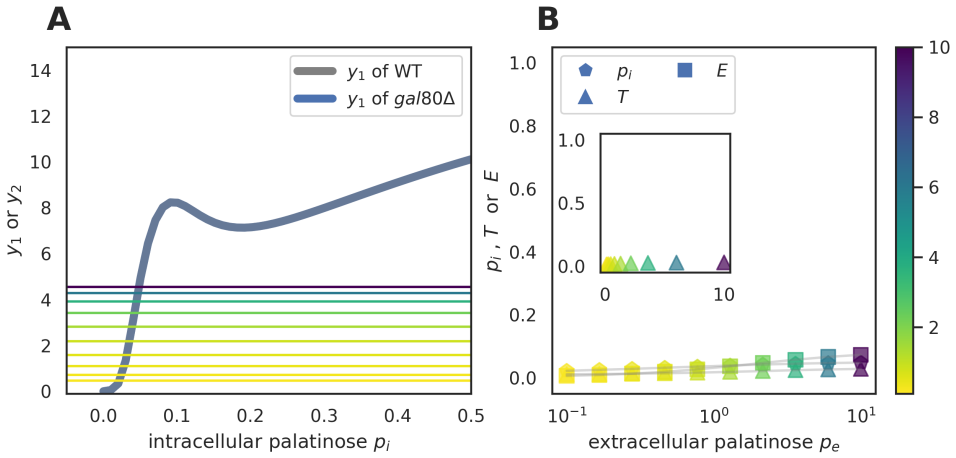

Figure 5.11: The model predicts that inducing the *MAL* network in the *gal80*Δ mutant requires higher extracellular palatinose, if active Gal4 decreases v_T. **(A)** y_1 (curve) and y_2 (horizontal line), defined in Eq 5.9, plotted against the concentration of intracellular palatinose p_i. **(B)** The steady-state values of intracellular palatinose concentration p_i, transporter level T and isomaltase level E plotted against the concentration of extracellular palatinose p_e. The inset of (B) shows the transporter level T in linear x-scale. The colors of y_2 in (A) and the steady-state values in (B) represent the value of p_e. The values of parameters and the initial condition are given in Tables 5.1 and 5.2, except that in the *gal80*Δ mutant, the $v_{T,max}$ value was halved.

5.3.9 Our model predicts that the *gal80*Δ mutant will resume ability to consume palatinose if we decrease the isomaltases' expression or overexpress *MAL11*

Intuitively, in the *gal80*Δ mutant the isomaltases seem to be excessive compared to the transporter at all three time points (Fig 5.7), if we decrease the isomaltases' level by halving the $H_{E,max}$ or constitutively overexpress *MAL11* by adding a positive, constant term $H_{T,OE}$ to $H_T(p_i)$, the *MAL* network may be inducible again. Indeed, regardless of how Gal4 changes the model parameters, the model predicts that either can decrease the threshold of p_e in the *gal80*Δ mutant back to a level similar to the wildtype (Figs 5.12 and 5.13).

5.3.10 The delay of palatinose metabolism by active Gal4 is rescued by *ima1*Δ, as predicted by the model

Based on the model prediction in the previous section, I deleted *IMA1* from the *gal80*Δ mutant to see if it can grow in palatinose without a long delay. Indeed, results in Fig

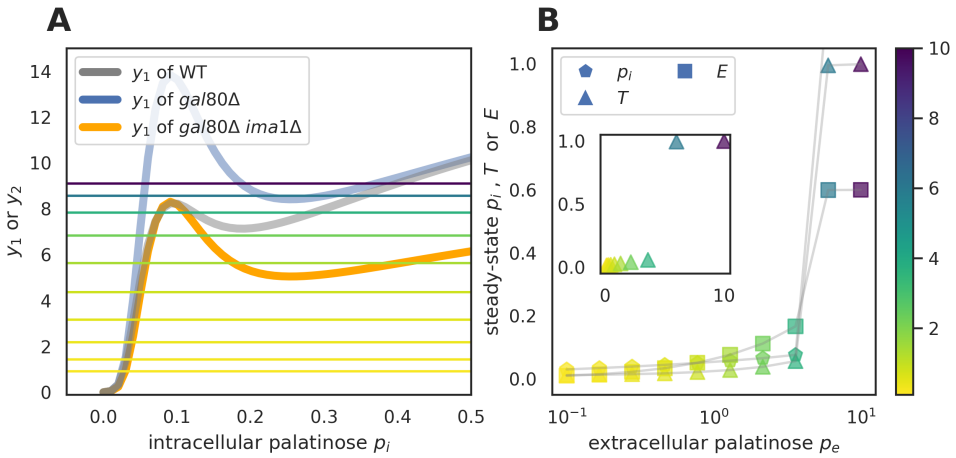

Figure 5.12: The model predicts that decreasing the isomaltases' expression in the *gal80*Δ mutant may resume cells' ability to grow on palatinose. **(A)** y_1 (curve) and y_2 (horizontal line), defined in Eq 5.9, plotted against the concentration of intracellular palatinose p_i. **(B)** the steady-state values of intracellular palatinose concentration p_i, transporter level T and isomaltase level E plotted against the concentration of extracellular palatinose p_e. The inset of (B) shows the transporter level T in linear x-scale. The colors of y_2 in (A) and the steady-state values in (B) represent the value of p_e. The values of parameters and the initial condition are given in Tables 5.1 and 5.2, except that in the *gal80*Δ mutant, the K_T value was increased by 20% and the $H_{E,max}$ value was decreased by 40%.

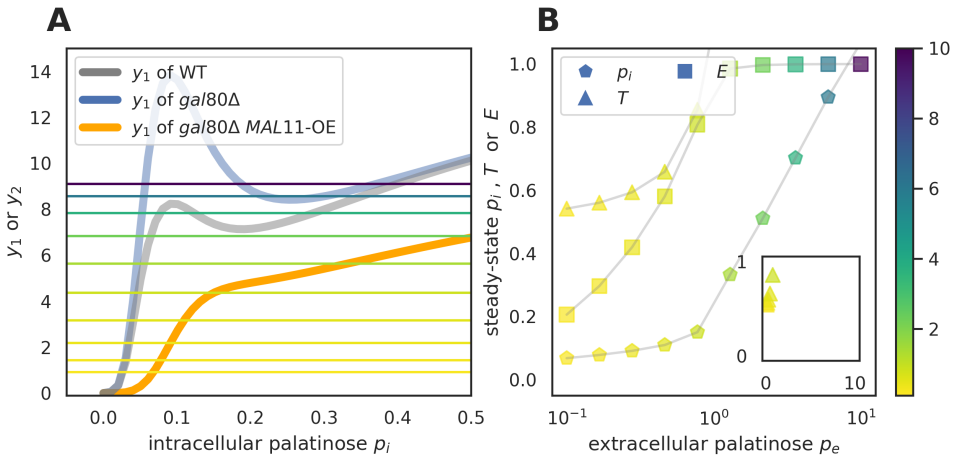

Figure 5.13: The model predicts that overexpressing *MAL11* in the *gal80*Δ mutant may resume cells' ability to grow on palatinose. **(A)** y_1 (curve) and y_2 (horizontal line), defined in Eq 5.9, plotted against the concentration of intracellular palatinose p_i. **(B)** the steady-state values of intracellular palatinose concentration p_i, transporter level T and isomaltase level E plotted against the concentration of extracellular palatinose p_e. The inset of (B) shows the transporter level T in linear x-scale. The colors of y_2 in (A) and the steady-state values in (B) represent the value of p_e. The values of parameters and the initial condition are given in Tables 5.1 and 5.2, except that in the *gal80*Δ mutant, an extra constant, $H_{T,OE} = 0.5$, was added to the definition of $H_T(p_i)$.

5.14 show that the *gal80*Δ *ima1*Δ double-mutant fully consumes galactose and palatinose without showing a visible lag. Additionally, the *ima1*Δ single-mutant has a much shorter lag between the galactose-palatinose diauxie (Fig 5.15A) and has an increased level of palatinase Ima5 before galactose runs out (Fig 5.15B).

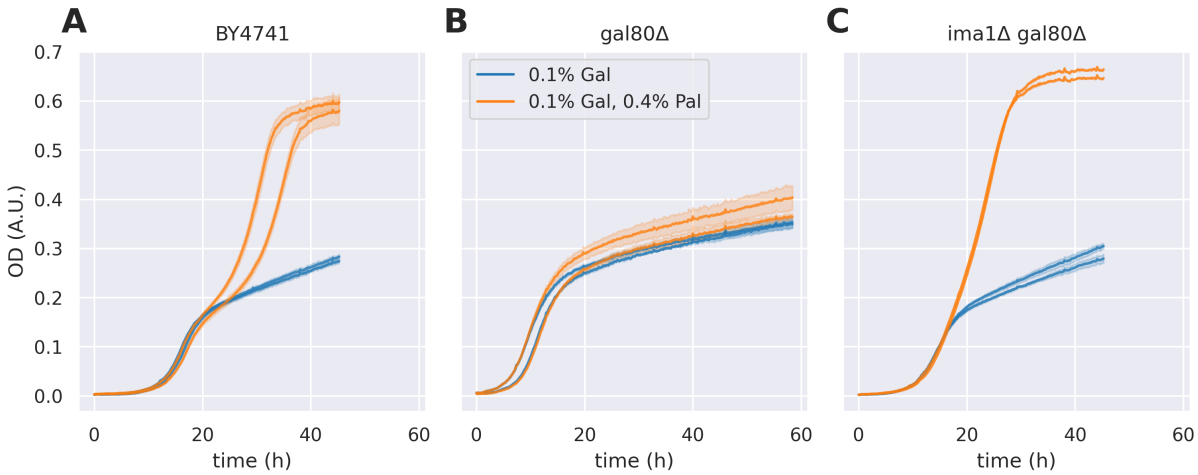

Figure 5.14: The *gal80*Δ *ima1*Δ double-mutant fully consumes galactose and palatinose without showing a visible lag. Each curve represents one biological replicate. The shaded area of each curve represents the standard deviation of two technical replicates.

5.3.11 *MAL11* is unlikely to be a direct target of Gal4 binding

At the molecular level, how does active Gal4 affect the expression of *MAL11*? Gal4 is known to bind to promoters of *GAL* genes are other genes when it is active (Travan, Jelicic, and Sopta 2006). It also binds to the coding sequence of *ACC1*, which represses *ACC1*'s expression (Li and Johnston 2001). Gal4 can also activate genes linked to the telomere by binding to an enhancer 1–2 kbp downstream of the gene (de Bruin et al. 2001), and the *MAL* locus is in the sub-telomeric region (Brown, Murray, and Verstrepen 2010). Therefore, I carried out a scan from 1 kbp upstream to 2 kbp downstream of *MAL11*'s coding sequence on the YeTFaSCo database (de Boer and Hughes 2012), and the classic Gal4 binding motif (Giniger, Varnum, and Ptashne 1985) was not found in the region surrounding *MAL11* (Fig 5.16A). However, multiple sites in this region were found to match two potential Gal4 binding motifs inferred from a high-throughput approach (Zhao, Granas, and Stormo 2009) (Fig 5.16A). To see whether these motifs are enriched around *MAL11*, I carried out another scan over the whole *MAL1* locus and found that the two motifs are unlikely to contribute to repression on *MAL11*'s expression, because

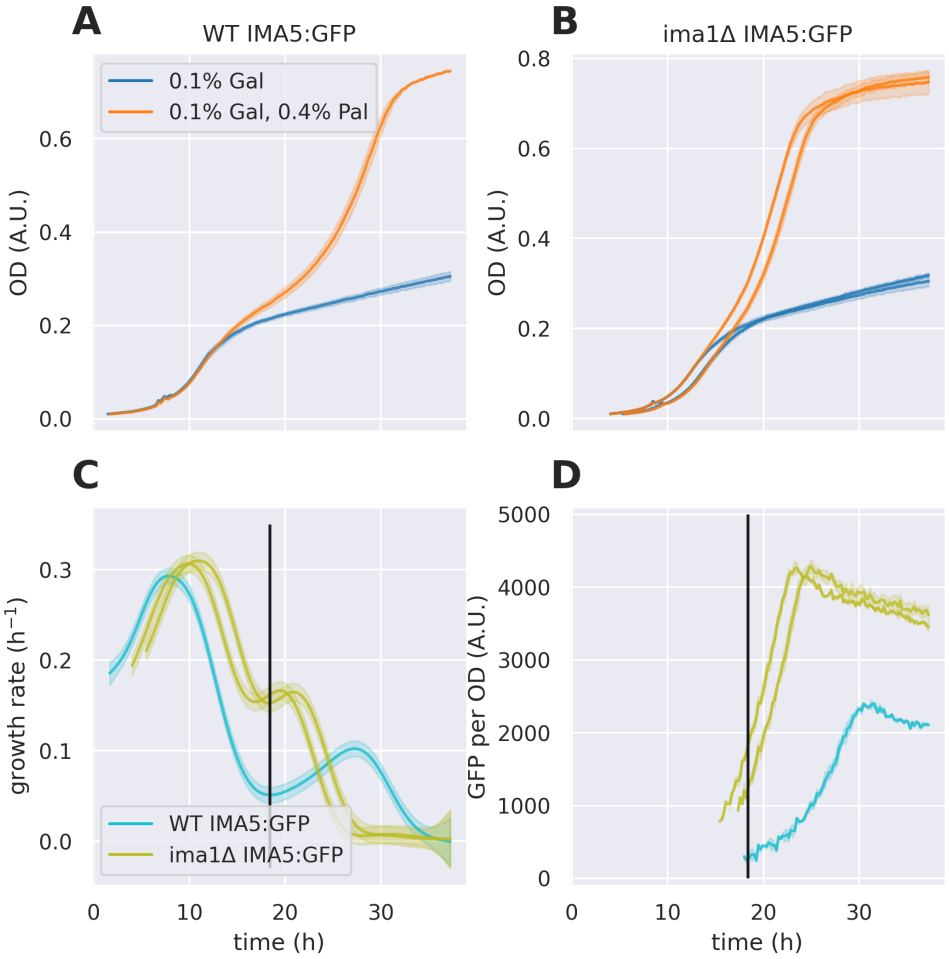

Figure 5.15: The *ima1*Δ mutant has a much shorter lag between galactose-palatinose diauxie and expresses palatinase Ima5 before galactose runs out. **(A, B)** OD measured in a plate reader. **(C)** Calculated specific growth rate as a function of time. **(D)** Ima5:GFP per OD as a function of time. Each curve represents one biological replicate. The vertical line represents the average of time points at which the two biological replicates of *IMA5:GFP* strain reaches the local minimum of the specific growth rate. The fluorescence reading is noisy when OD is low, which may be negative after being corrected for autofluorescence. The negative values are not displayed. (Note: this experiment needs to be re-run.)

they were found all over the *MAL1* locus (Fig 5.16B) but only *MAL11*'s expression was affected by active Gal4 (see Section 5.3.5). Thus, the lack of Gal4 binding sites specific to *MAL11* suggests that *MAL11* is unlikely to be a direct target of Gal4 binding.

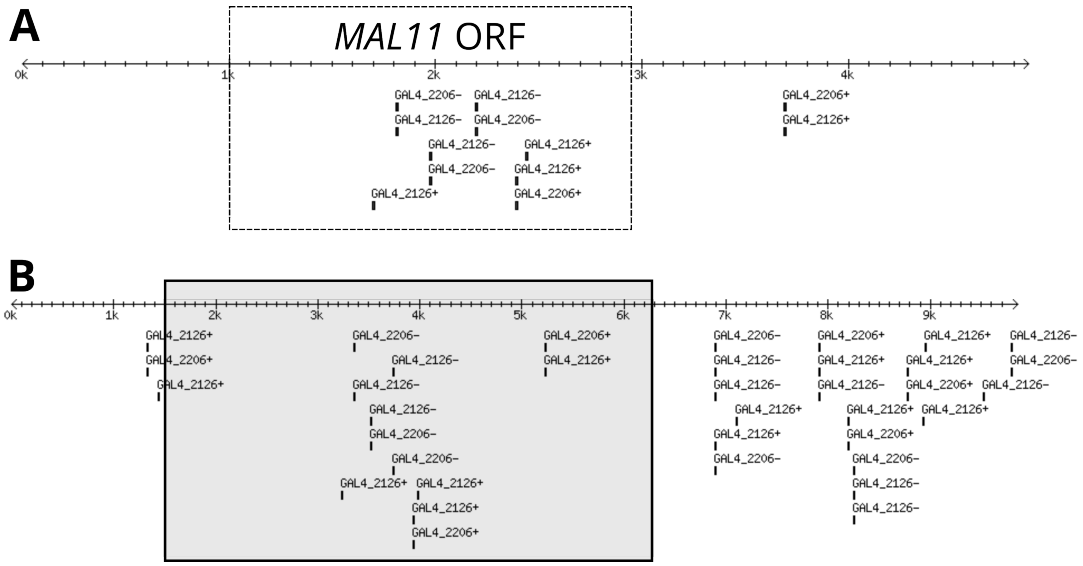

Figure 5.16: Potential Gal4 binding motifs around the *MAL1* locus from YeTFaSCo. **(A)** Gal4 binding motifs between 1 kbp upstream and 2 kbp downstream of *MAL11*'s coding sequence from YeTFaSCo. The dashed box indicates the *MAL11*'s open reading frame (ORF). **(B)** Gal4 binding motifs of the whole *MAL1* locus (from *MAL12* to *IMA1*) from YeTFaSCo. The shaded area indicates the region shown in Panel A. The scan was run using YeTFaSCo's default parameters — minimum percent of maximum score is 75% and percent A/T for background is 0.31. 2126 and 2206 are the motif IDs on the YeTFaSCo database.

5.3.12 We identified a set of DEGs which are likely downstream of Gal4

The results in this chapter so far suggest that the transcription of *MAL11* or the biochemical properties of Mal11 is likely the target of Gal4 regulation, but *MAL11* itself is unlikely to be a direct target. To find the target downstream of Gal4 and upstream of *MAL11*, we attempt to identify a set of DEGs which are likely downstream of Gal4 (instead of DEGs caused by difference in other factors, e.g. growth rate), and characterise this set of genes by performing GO and Kyoto Encyclopedia of Genes and Genomes (KEGG) (Kanehisa and Goto 2000) pathway enrichment, and then find the likely downstream transcription factor(s) by transcription factor enrichment, assuming a transcription factor exists downstream of Gal4.

Gal4's level is non-zero over all time points in both the wildtype and *gal80*Δ strains (Fig 5.17), and in 0.1% fructose, Gal4 is always inactive in the wildtype strain and always active in the *gal80*Δ strain. To identify this set of genes, we first found the DEGs between the wildtype and the *gal80*Δ mutant in 0.1% fructose at each time point respectively, and then took the intersection of the three groups of DEGs (Fig 5.18). The size of this group depends on the criterion on the significance (Fig 5.18), and we chose $|\log_2 \text{fold change}| \geq 0.5$ and adjusted p-value $p < 0.05$, which defines a group of 84 genes (Fig 5.18A). Furthermore, if this set of genes is downstream of Gal4, they will be differentially expressed over all time points, and if a gene is up- or down-regulated, it should be up- or down-regulated at all time points. Indeed, 83 out of 84 genes in this group are consistently up- or down-regulated over the three time points (Fig 5.19). Notably, all 11 genes whose promoter was shown to be bound by Gal4 in the two ChIP datasets (Ren et al. 2000; Rhee and Pugh 2011), except the deleted *GAL80* gene, are consistently up-regulated (Fig 5.19).

To characterise this group of genes, I performed GO and KEGG pathway enrichment on the YeastEnrichR platform (Chen et al. 2013; Kuleshov et al. 2016). The results of GO enrichment on biological process showed that this group of genes involves galactose catabolic process, ribosomal biogenesis, hexose transport, *etc* (Fig 5.20). Accordingly, results of KEGG pathway enrichment showed that this set of genes involves ribosome biogenesis, galactose metabolism, *etc* (Fig 5.21).

To perform transcription factor enrichment, I first split the group of genes (excluding the deleted *GAL80* and *PCR10* which changes sign of differential expression) into the "UP" subgroup and the "DOWN" subgroup. If a transcription factor X is activated by Gal4, then the genes which X activates will be in the "UP" subgroup and the genes which X represses will be in the "DOWN" subgroup. Therefore, by enriching the activators of the "UP" subgroup and the repressors of the "DOWN" subgroup on the Yeastract database (Teixeira et al. 2014) and take the union, I get a set of transcription factors which *might* be activated by Gal4 (Fig 5.22A). Likewise, by enriching the repressors of the "UP" subgroup and the activators of the "DOWN" subgroup, I get a set of transcription factors which *might* be repressed by Gal4 (Fig 5.22B). In the future, we can test whether any transcription factor in this set is regulating the *MAL* network (see Section 5.5.1).

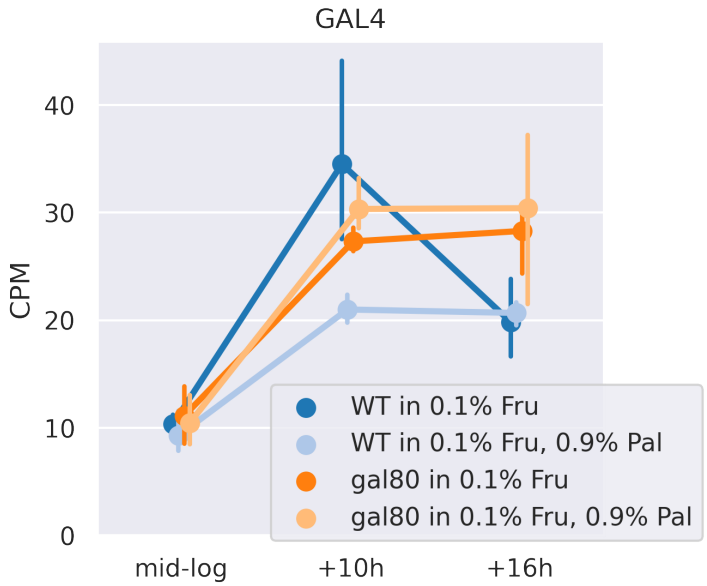

Figure 5.17: The level of *GAL4* transcripts is non-zero in both strains and in all conditions and time points. The counts per million reads (CPM) of *GAL4* represents the level of its transcripts. The error bar represents the standard deviation of three biological replicates.

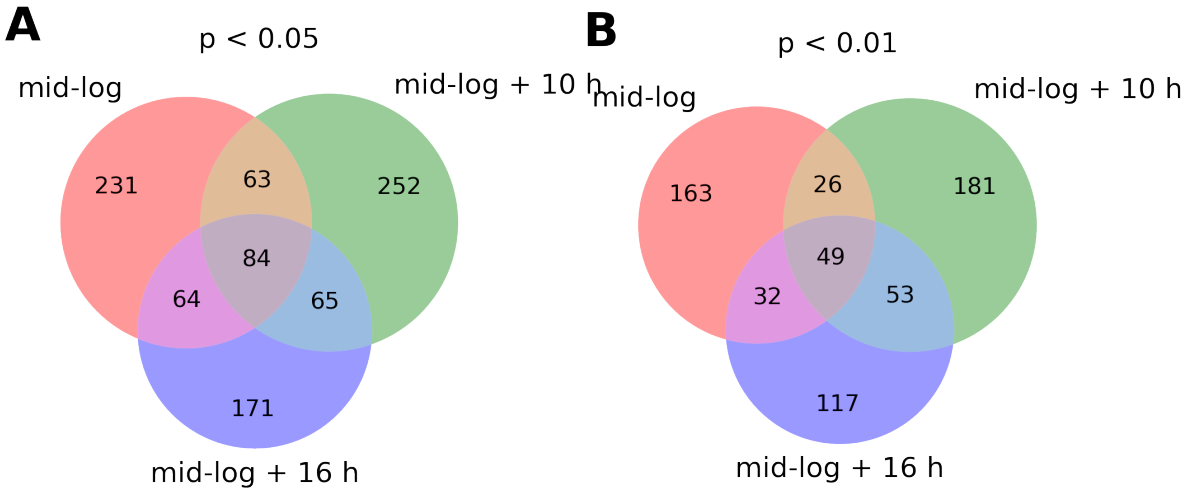

Figure 5.18: The set of differentially expressed genes (DEGs) between the wildtype and the *gal80*Δ mutant in 0.1% fructose is defined by those present over all three time points, and the size of this gene set depends on the threshold for significance. Venn diagram showing the number of genes that are differentially expressed when the threshold for significance is set at **(A)** 0.05 and **(B)** 0.01 for the adjusted p-value. Additionally, for a gene to be considered differentially expressed, its $|\log_2$ fold change$|$ is larger than 0.5. Both the adjusted p-value and the $\log_2$ fold change are calculated by DESeq2.

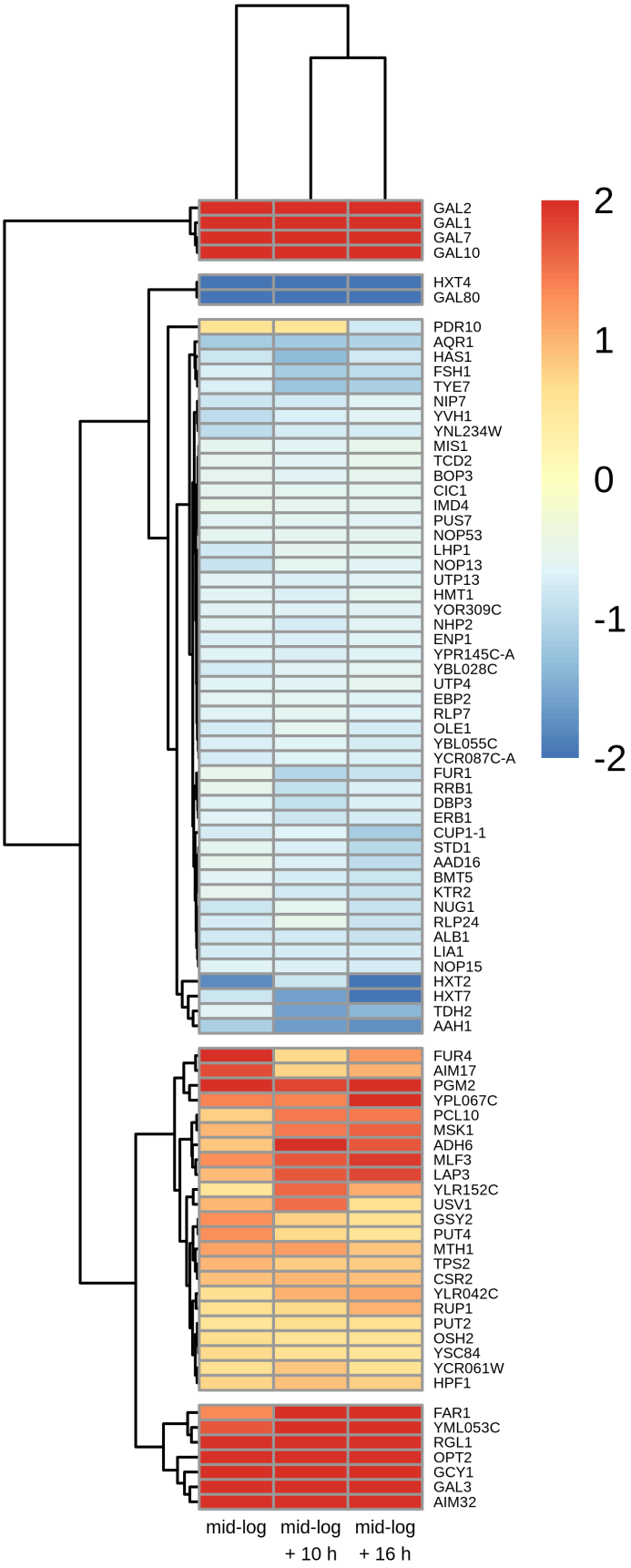

Figure 5.19: 83 out of the 84 genes which are differentially expressed at all three time points are consistently up- or down-regulated. The color shows the $\log_2$ foldchange of each gene at each time point. The hierarchical clustering is performed using complete-linkage clustering and the Euclidean distance between rows or columns.

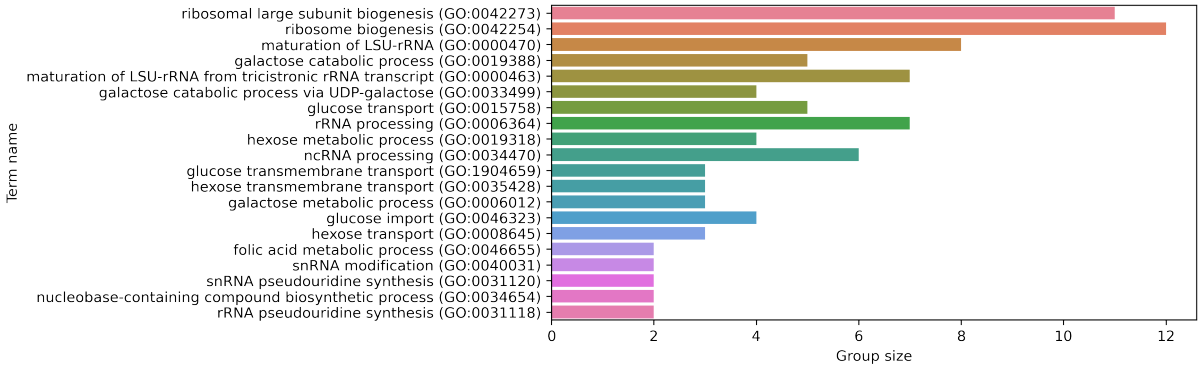

Figure 5.20: Enrichment on gene ontology (GO) biological process with the genes which are differentially expressed at all three time points. The group size of each term is the number of genes that are in both our set of DEGs and the GO term. The enrichment was performed on YeastEnrichR. Only GO terms whose group size ≥ 2 and adjusted p-value ≤ 0.01 are selected. The terms are ranked by the adjusted p-value, and only the top 20 terms are shown.

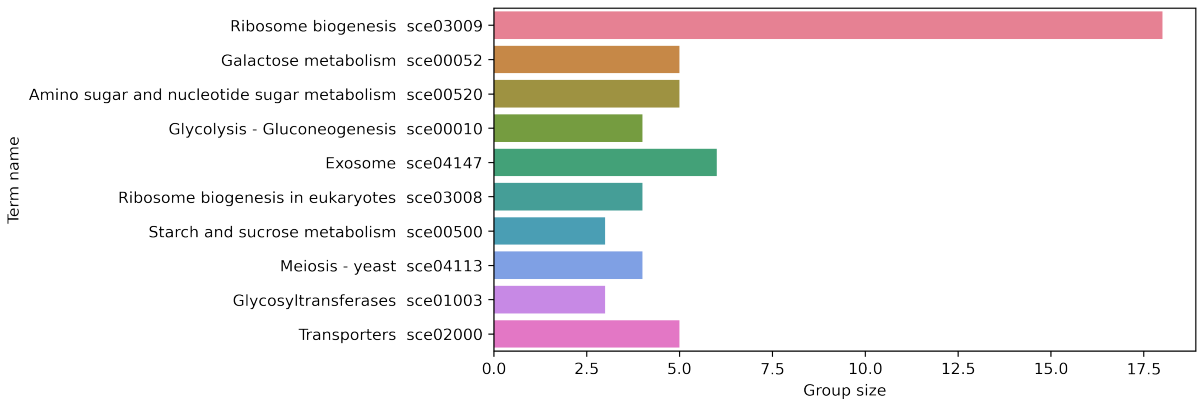

Figure 5.21: Pathway enrichment with the genes which are differentially expressed at all three time points. The terms are from the Kyoto Encyclopedia of Genes and Genomes (KEGG) database. The group size of each term is the number of genes that are in both our set of DEGs and the GO term. The enrichment was performed on YeastEnrichR. Only pathway terms whose group size ≥ 2 and adjusted p-value < 0.01 are selected. The terms are ranked by the adjusted p-value.

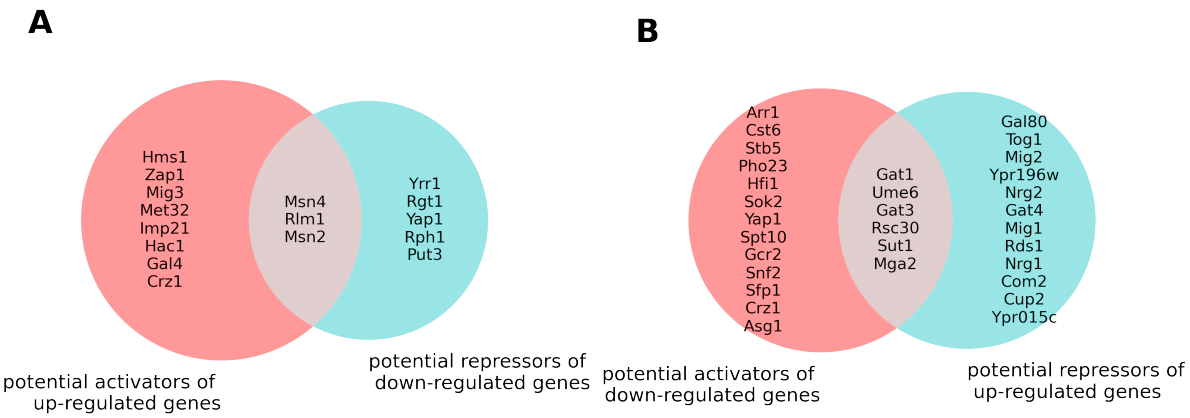

Figure 5.22: Transcription factor enrichment with the genes which are differentially expressed at all three time points. The genes are separated into the up- and down-regulated subgroups, and then enrichment of each subgroup was performed on Yeastract based on expression evidence. The transcription factors with p-value < 0.001 are selected.

5.4 Numerical methods

I used the `scipy.integrate` module in Python to numerically integrate Eq 5.1. The parameters are listed in Table 5.1, which were naively chosen as a proof of principle of this model. The initial condition is given in Table 5.2.

5.5 Discussion

To understand the downstream signalling of Gal4 responsible for the galactose-palatinose diauxie (see Chapter 4), I performed an RNAseq experiment, which leads to most results in this chapter. The results revealed that in the wildtype strain, the isomaltases *IMA1* and *IMA5* are induced before the transporter Mal11 (Fig 5.6A-C), and that active Gal4 in the *gal80*Δ does not change the basal transcription of *MAL* genes (Fig 5.8) nor the expression level of *IMA1* and *IMA5* at mid-log compared to wildtype (Fig 5.7B and C), which suggests that at mid-log, the *MAL* activators Znf1 and Mal13 can still sense palatinose and activate *IMA1* and *IMA5* in the *gal80*Δ mutant. However, the *gal80*Δ mutant cannot induce higher expression of *MAL11*, so the *MAL* network is "locked" at the state in which the isomaltases *IMA1* and *IMA5* are excessive to *MAL11* (Fig 5.6A-C).

Based on the experimental results of the wildtype, I built a minimal mathematical model of the *MAL* network. The model predicts that the *MAL* network switches from "OFF" to "ON" when we increase the extracellular concentration of palatinose (Fig 5.9).

Table 5.1: Parameter values used in the *MAL* model.

parameter	value	note
h	3.5	
p_e	1	
d_T	1	
d_E	1	
K_T	0.15	0.18 in strains with *gal80*Δ (Scenario 1)
$H_{T,max}$	1	
$H_{T,basal}$	0.01	
K_E	0.1	
$H_{E,max}$	1	0.8 in strains with *ima1*Δ
$H_{E,basal}$	0.001	
$K_{m,E}$	0.5	
$v_{E,max}$	20	
$K_{m,T}$	1	
$v_{T,max}$	10	5 in strains with *gal80*Δ (Scenario 2)
$H_{T,OE}$	0	0.5 in *MAL11* overexpression.

Table 5.2: Values of initial condition used in the minimal model.

variable	initial value
p_i	0
T	$H_{T,basal}/d_T$
E	$H_{E,basal}/d_E$

We do not know yet how active Gal4 changes the expression of *MAL11* and hence how the parameters are changed in the model, but we postulated two scenarios, both of which predict that active Gal4 in the *gal80*Δ mutant changes the extracellular palatinose required to induce the network (Figs 5.10 and 5.11). Moreover, the model predicts that if we decrease the expression level of isomaltases, the *MAL* network resume its inducibility in the *gal80*Δ mutant (Fig 5.12), which proves correct because the *gal80*Δ *ima1*Δ double-mutant indeed resume the ability to grow on palatinose (Fig 5.14).

To understand the molecular mechanism behind Gal4's signalling to *MAL11*, we first check whether the *MAL11* gene itself can be a direct target of Gal4, which turns out unlikely (Fig 5.16). I then identified a set of DEGs which are consistently up- or down-regulated compared with the wildtype at all three time points in the *gal80*Δ mutant (Fig 5.18). Surprisingly, enrichment analyses show that ribosome biogenesis is also affected in the *gal80*Δ mutant in addition to galactose metabolism (Figs 5.20 and 5.21). Using transcription factor enrichment, we identified a set of transcription factors which might be regulated by Gal4 (Fig 5.22), which enables us to design experiments in the future to test whether some of those are indeed upstream of the *MAL* network (see Section 5.5.1).

In summary, the results in this chapter provides a new example on how budding yeast cells can prioritise galactose over palatinose by changing the inducibility of the *MAL* network. We further showed that it is possible to recover the inducibility of the *MAL* network by changing the relative level between the isomaltases and the transporter within the *MAL* network. Similar to the glucose-galactose diauxie, in which the strength of catabolite repression depends on the structure of the *GAL* network (Boocock et al. 2021), our results provides another example showing that a local change in one network is sufficient to change the behaviour of catabolite repression.

5.5.1 Future work to identify the downstream signal of Gal4

The sets of activated and repressed candidates of transcription factor (Fig 5.22) will be useful for future work to identify which transcription factor leads to the Gal4-*MAL* regulation. First, we can disrupt each transcription factor X that might be activated by Gal4, by creating an *x*Δ *gal80*Δ double-mutant. This mutant has active Gal4, but the

downstream signalling by X is disrupted. If X represses the *MAL* network, this mutant will resume ability to grow on palatinose. Second, we can disrupt each transcription factor Y that might be repressed by Gal4. If Y activates the *MAL* network, the *y*Δ mutant should not be able to grow on palatinose, but can grow on other carbon sources.

5.5.2 The downstream signal of Gal4 is unlikely through the known signalling pathway of glucose repression on the *MAL* network

In Section 4.3.11, I have explored the hypothesis that the downstream signal of Gal4 acts through the same signalling pathway as glucose repression using single mutants of the glucose repression pathway, and none of those mutants will remove the lag between galactose-palatinose diauxie (Fig 4.22). Further, glucose repression changes the basal expression of *MAL* network (Fig 4.17A) but active *GAL* does not (Figs 4.17B and 5.8). Glucose leads to fast degradation of the Mal11 transporter (Hatanaka 2018), probably through endocytosis like Mal61 (Gadura, Robinson, and Michels 2006), but I did not observe a decrease in the Mal11-yECitrine signal or endocytosis in a *MAL11:yECitrine* strain (data not shown), but this is uncertain because of low signal-to-noise ratio. Therefore, with the evidence so far, the downstream signal of Gal4 is unlikely through the known signalling pathway of glucose repression on the *MAL* network.

5.5.3 Does the same downstream signal of Gal4 suppress both *MAL* and *SUC2*?

Data in (Ideker et al. 2001) suggest that *gal80*Δ supresses the metabolism of raffinose. Gancedo *et al* (Gancedo, Flores, and Gancedo 2015) also found that galactose prevents the induction of *SUC2* invertase, which is responsible for hydrolysis of sucrose and raffinose, by low concentrations of glucose. I also found that the *gal80*Δ suppresses growth on low concentrations of sucrose — the data is not shown for the *gal80*Δ single mutant, but comparing Fig 4.18A and B, we see that the *gal80*Δ *gal1-10-7*Δ mutant grows slowly on 0.2% sucrose, and further deleting *GAL2* alleviates suppression of both sucrose and palatinose metabolism (compare Fig 4.18B and C). This raises an interesting question —

does the same downstream signal of Gal4 suppress both *MAL* and *SUC2*?

SUC2's expression is coupled with glucose sensing pathways. *SUC2* transcription requires either glucose phosphorylation or G-protein coupled receptor Gpr1 (Belinchón and Gancedo 2007). The high-affinity glucose sensor Snf3 (Sucrose NonFermenting 3) is also required for growth on sucrose, and active Snf3 degrades Mth1 and hence releases Rgt1 from DNA binding as a repressor (see Section 1.5.1). Rgt1 and Mth1 represses expression of *SUC2* — deleting *RGT1* or *MTH1*, or removing the Rgt1 binding site on the *SUC2* promoter leads to an increase in Suc2 level in both non-inducing and inducing conditions (Gancedo, Flores, and Gancedo 2015).

MTH1 could mediate the *GAL*-to-*SUC2* suppression, and if so, it is unlikely to be the sole signalling pathway — the other one might be through *GAL2*. Active Gal4 increases the expression of *MTH1* (Ren et al. 2000), so the *GAL*-to-*SUC2* suppression could be mediated by *MTH1*. However, this does not explain why deleting *GAL2* from the *gal80*Δ mutant alleviates this suppression (compare Fig 4.18B and C), because *MTH1* is not known to regulate *GAL2*.

Unlike the case of *SUC2*, instead of repressing *MAL*, *MTH1* is required to metabolise palatinose (Fig. 4.22C). Therefore, it is unlikely that the increase in *MTH1* level in the *gal80*Δ mutant mediates the *GAL*-to-*MAL* suppression. Yet, the suppression on *MAL* and *SUC2* by Gal4 may share a mechanism through Gal2, given that deleting *GAL2* from the *gal80*Δ can alleviate the suppresive effect (compare Fig 4.18B and C).

5.5.4 Why does the wildtype induction of isomaltases precede that of transporter *MAL11* in palatinose?

In the wildtype strain, the isomaltases are induced before the transporter Mal11 (Section 5.3.4), which means the isomaltases are excessive relative to Mal11 at the beginning of induction, which slows down *MAL* induction. Deleting one of the two isomaltase genes that respond to palatinose induction, *IMA1*, leads to faster growth on palatinose (data not shown) and abolished the galactose-palatinose diauxic lag (Fig 5.15). Why does the induction of isomaltases precede that of the transporter?

Accumulation of maltose in the cells is known to be harmful, and so may accumulation

of palatinose be. This is because the Mal11 transporter is a proton symporter (Han et al. 1995) — unlike the reversible transport of glucose through hexose transporters (Reifenberger, Boles, and Ciriacy 1997), the transport of dissacharides like maltose and palatinose are irreversible. If the transport flux is higher than the hydrolytic flux by (iso)maltases, accumulation occurs, which can be caused by excessive transporters or high concentration of extracellular maltose. Gibney *et al* (Gibney et al. 2015) also reported that overexpressing *MAL11* in S288c-derived strains strongly inhibits growth on galactose-maltose mixtures. Postma *et al* (Postma et al. 1990) reported that maltose pulses to a maltose-limiting chemostat leads to cell death, possibly caused by an "osmotic burst". Hatanaka *et al* (Hatanaka, Mitsunaga, and Fukusaki 2018) showed that a strain with inducible maltases and overexpressed Mal21 transporter shows growth defect in high maltose concentrations, and this defect is suppressed by overexpression of maltase. They further showed that this growth defect is not caused by "osmotic burst" because placing cells in 25 – 150 mM sorbitol (which increases the extracellular osmolarity) did not suppress this growth defect (Hatanaka, Mitsunaga, and Fukusaki 2018). Instead, the protein synthesis was inhibited (Hatanaka, Mitsunaga, and Fukusaki 2018). If accumulation of palatinose is harmful, natural selection may favour mutants with faster isomaltase induction than transporter induction, at the expense of slower induction of the *MAL* network.

Chapter 6

Materials and Methods

6.1 Strains and growth media

Strains used in this research are listed in Table 6.1. The BY4741-background strains are auxotroph and the FY4-background strains are prototroph (Baker Brachmann et al. 1998). The use of prototroph strains allows growth in minimal media without amino acids, and hence excludes the possibility that cells use amino acids as an alternative carbon source in addition to the supplemented carbon source(s).

Strains were pre-cultured in synthetic complete (SC) media supplemented with 2% (w/v) sodium pyruvate for 2 days before experiments, unless specified otherwise. Cultures are then diluted 6-fold 6 hours before an experiment with fresh SC media with 2% (w/v) sodium pyruvate to ensure cells are at exponential growth when the experiment begins. During an experiment, auxotroph strains are grown in SC or low fluoscence SC (LoFlo) media supplemented with carbon source(s) and prototroph strains are grown in Delft media (Verduyn et al. 1990, 1992) supplemented with carbon source(s), unless specified otherwise.

6.2 Creating yeast strains

6.2.1 Yeast transformation and colony verification

Yeast transformation was carried out following a protocol using lithium acetate and polyethylene glycol (PEG) (Gietz and Woods 2002). The input DNA was either a

Table 6.1: Strains used in this research.

Strain ID	Genotype	Parent	Reference
SL229	BY4741 (wildtype)		(Baker Brachmann et al. 1998)
SL365	FY4 (wildtype)		(Baker Brachmann et al. 1998)
SL1145	*RPL3:GFP*		(Gunji et al. 2004)
SL1147	*PRL13B:GFP*		(Gunji et al. 2004)
SL1150	*PRS30A:GFP*		(Gunji et al. 2004)
SL1121	*IMA1:GFP*	SL229	Made by I Fraquhar
SL1425	*ima1*Δ	SL229	
SL1489	*gal80*Δ	SL365	
SL1514	*IMA5:GFP*	SL229	
SL1536	*gal80*Δ *gal1-10-7*Δ	SL1489	
SL1538	*ima1*Δ *IMA5:GFP*	SL1425	
SL1543	*gal80*Δ *gal1-10-7*Δ *gal2*Δ	SL1536	
SL1547	*ima1*Δ	SL365	
SL1549	*gal80*Δ *gal1-10-7*Δ *gal3*Δ	SL1536	
SL1553	*MAL11:yECitrine*	SL365	
SL1556	*gal80*Δ *gal2*Δ	SL1489	
SL1557	*gal4*Δ	SL365	
SL1558	*gal80*Δ *gal4*Δ	SL1489	
SL1566	*pCCW12-GAL2*	SL365	
SL1505	*hxk2*Δ		(Winzeler et al. 1999)
SL150	*mig1*Δ		(Winzeler et al. 1999)
SL151	*mig2*Δ		(Winzeler et al. 1999)
SL152	*mth1*Δ		(Winzeler et al. 1999)
SL148	*snf3*Δ		(Winzeler et al. 1999)
SL149	*rgt2*Δ		(Winzeler et al. 1999)
SL400	*yck1*Δ		(Winzeler et al. 1999)
SL1570	*doa4*Δ		(Winzeler et al. 1999)
SL1574	*reg2*Δ		(Winzeler et al. 1999)

Table 6.2: Media used in this research.

Media	Component	Purpose	Reference
XY-glucose	10 g/L Bacto yeast extract; 20 g/L Bacto Peptone; 0.1 g/L adenine; 0.2 g/L tryptophan	bring up strains from glycerol stock; outgrow after yeast transformation	
SC	1.4 g/L Edinburgh Amino Acids Mix (Formedium, EDI0100); 5 g/L $(NH_4)_2SO_4$; 1.7 g/L yeast nitrogen base without amino acids and ammonium; 50 mg/L adenine hemisulphate; 100 mg/L histidine; 100 mg/L methionine; 200 mg/L leucine; 100 mg/L tryptophan; 100 mg/L uracil	set up pre-cultures; run plate reader experiments with auxotroph strains	
LoFlo	Same as SC, except that yeast nitrogen base without amino acids is LOFLO version (Formedium)	run plate reader experiments with prototroph strains	
Delft	3 g/L KH_2PO_4; 0.5 g/L $MgSO_4{\cdot}7H_2O$; 5 g/L $(NH_4)_2SO_4$; trace metals; vitamins	run plate reader experiments with prototroph strains	(Verduyn et al. 1990, 1992)
LB	10 g/L tryptone; 10 g/L NaCl; 5 g/L yeast extract	grow *E. coli* for miniprep	
SOC	2% (w/v) tryptone; 0.5% (w/v) yeast extract; 10 mM NaCl; 2.5 mM KCl; 10 mM $MgCl_2$; 20 mM glucose	for out-growth of *E. coli* after heat-shock transformation	

polymerase chain reaction (PCR) product or a product of golden gate assembly (see Section 6.2.2) digested with the *NotI* restriction enzyme (NEB, #R0189S). 100 μL overnight culture in XY-2% glucose was inoculated into 5 mL fresh XY-2% glucose 3–5 hours before harvest. To harvest the cells, I centrifuged the cells at 3000 rpm for 5 minutes, removed the supernatant and washed the cells once with water. Then, the cells were resuspended with 100 μL water and transferred into a 360 μL solution with 240 μL 50% PEG4000, 36 μL 1 M lithium acetate, 50 μL diluted YeastMaker and 0.5–2 μg DNA. The cells were then heat-shocked in a water bath at 42 °C for 40 minutes. After the heatshock, for transformants with a nutrient selection marker (e.g. *URA3*), I centrifuged the cells at 5000 rpm for 30 seconds, removed the supernatant, resuspended the cells with 100 μL water and plate the cells onto the corresponding selection agar plate; for transformants with an antibiotic selection marker (e.g. *HPH*), I removed the supernatant as described above, resuspended the cells with 1 mL XY-2% glucose and incubated the cells at 30 °C for 1–2 hours, and then removed the media and resuspended the cells with 100 μL water and plated the cells onto the selection agar plate. For transformants with antibiotic selection markers, replica-plating onto a fresh selection agar plate was carried out one day after the plating of transformants.

The plates were incubated for two days in a 30 °C incubator, and then 3–10 single colonies were picked from each transformant for verification. For each colony, half of the colony was resuspended with 20μL water, which was added into a colony PCR reaction with *Taq* polymerase (NEB, #M0267S or Roche, #KK5005). Once the introduced mutation and all previously introduced mutations were confirmed, I amplified the region of the newly introduced mutation with Q5 (NEB, #M0491S) or Phusion polymerase (NEB, #M0530S), and the product was sent for Sanger sequencing (MRC PPU, Dundee) to further confirm the DNA sequence. After the process above, the remaining half of the colony was inoculated into XY-2% glucose and grown overnight, before being frozen at -80 °C with 25% glycerol for long-term storage.

6.2.2 Golden gate assembly

I used golden gate assembly to create custom plasmids, using the plasmids within the MoClo toolbox (Lee et al. 2015). The plasmids used in this project are listed in Table 6.3. I performed two types of assembly — *Esp3I* assembly (for creating custom Type 3 part plasmids) and *BsaI* assembly (for assembling the part plasmids into the final product). Both were performed using *Esp3I* (NEB, #R0734S) or *BsaI* (NEB, #R3733S), together with T_4 ligase buffer (Promega, #C126B) and T_7 ligase (NEB, #M0318S). The product of assembly was transformed into DH5α competent cells (NEB, #C2987H) and then plated onto selection plates. After 16–24 hours, 5–10 single colonies with the desired colour were picked and confirmed with colony PCR. The confirmed colonies were inoculated into LB media with corresponding antibiotics and shaked at 37 °C, 200 rpm. After 12–16 hours, plasmids were extracted from *E. coli* with a mini-prep kit (NEB, #T1010L). The product was then confirmed by digestion with restriction enzymes and Sanger sequencing (MRC PPU, Dundee).

Table 6.3: MoClo plasmids used in this research.

Plasmid ID	Plasmid description	Purpose
pYTK001	Part plasmid entry vector	*Esp3I* assembly
pYTK002	ConLS	Part 1 for *BsaI* assembly
pYTK010	*pCCW12*	Part 2 for *BsaI* assembly
pYTK053	*tADH1*	Part 4 for *BsaI* assembly
pYTK072	ConRE	Part 5 for *BsaI* assembly
pYTK077	KanamycinR	Part 6 for *BsaI* assembly
pYTK088	*HO* 3' homology	Part 7 for *BsaI* assembly
pYTK089	AmpR-ColE1	Part 8a for *BsaI* assembly
pYTK094	*HO* 5' homology	Part 8b for *BsaI* assembly
pYTK001-GAL2	Product of *Esp3I* assembly	Part 3 for *BsaI* assembly
HY03	Product of *BsaI* assembly	Transform *pCCW12-GAL2* into the *HO* locus

6.2.3 Gene deletion and C-terminal tagging of fluorescent proteins

Gene deletion and C-terminal tagging of fluorescent proteins require an input DNA, which contains the sequence to insert, up- and down-stream homology arms (each 40 bp). The sequence to insert is on a plasmid with a desired selection marker (and a fluorescent protein in the case of tagging). The plasmids used in this project are listed in Table 6.4. To obtain the input DNA, I performed PCR using primers with a plasmid binding site specified by the literature and a 40 bp overhang, which is the up- or down-stream homology arm. The PCR product was purified with the Zymo DNA Clean & Concentrator-5 (Zymo, #D4004) and then used as input of yeast transformation (see Section 6.2.1).

6.2.4 Multiplexing CRISPR for deleting the *GAL1-10-7* locus

The length of the *GAL1-10-7* locus is 6181 bp. If we use the standard technique in Section 6.2.3 to delete this locus, the efficiency will be low because the two 40-bp homology arms are far from each other. Thus, I used the multiplexing CRISPR technique to introduce a markerless deletion of the *GAL1-10-7* locus (Shaw et al. 2019). The design was to induce one double-strand break near each end of the *GAL1-10-7* locus with the Cas9 protein guided by the guide RNA, which triggers homology directed repair in the cells, and this repair is based on the input homologous recombination template which contains the desired edits of the genome. Therefore, three components are key to the CRISPR technique: the Cas9 cassette, the guide DNA(s) and the homologous recombination template. The Cas9 cassette, together with a *KAN* marker, was obtained by PCR from the Amp1284 plasmid. The double-stranded guide DNAs were incorporated into the Amp1278 plasmid seperately by *Esp3I* assembly (see Section 6.2.2) and then the desired region on each plasmid was obtained by PCR. The homologous recombination template consists of an upstream and a downstream homology arm, each 500 bp. To obtain the template, I used PCR to amplify the upstram and downstream homology arms separately, and then joined them using Gibson assembly. The protospacer adjacent motif (PAM) sites, which are targeted by the guide RNAs (transcribed from the guide DNAs), were removed from the template by introducing a point mutation on the PCR primers of the homologous

recombination template.

The three components were then transformed into yeast cells with the standard protocol (see Section 6.2.1). The cells were plated onto a XY-glucose plate with G418 to select the cells with the Cas9 cassette. After two days, the transformants were re-inoculated onto fresh XY-glucose plate as patches, because the homologous recombination template does not contain a selection marker. Once the patches of cells grew, I ran colony PCR and select the patch that had the strongest band for desired edit. I streaked cells from that batch of cells into single colonies on a fresh XY-glucose plate and ran colony PCR again when that plate was ready. The process, which alternates between streaking and colony PCR, continued until the band for wildtype eventually disappeared. Then, the colonies were further confirmed with Sanger sequencing (see Section 6.2.1).

Table 6.4: Plasmids used in this research.

Plasmid ID	Plasmid name	Purpose	Reference
PLSM13	pYM40	gene deletion with *HPH* marker	(Janke et al. 2004)
PLSM82	pKT128	tagging a gene with GFP, and with *HIS* marker	(Sheff and Thorn 2004)
PLSM72	pFA6a-natMX6	gene deletion with *natMX6* marker	(Hentges et al. 2005)
PLSM73	pFA6a-kanMX6	gene deletion with *kanMX6* marker	(Longtine et al. 1998)
	Amp1278	for amplifying the guide DNA that works with Amp1284	(Shaw et al. 2019)
	Amp1284	providing a Cas9 cassette for CRISPR	(Shaw et al. 2019)

6.3 Growth assay in plate readers

We used plate readers (Tecan, Infinite M200 Pro or F200) to measure the dynamics of growth and fluorescence.

6.3.1 Principle of experimental design

In theory, in a 96-well plate, one can run 96 different combinations of strains and nutrient conditions. However, considering the effect of evaporation, the empty controls and the number of replicates, I typically ran no more than 15 combinations of strains and nutrient conditions. In all my experiments,

- the wells on the edge of the plate are used for empty controls, because they usually have higher evaporation (Manzanaro Moreno 2021, 118);
- for each nutrient condition, there should be at least 2 wells of empty control with no cells;
- for each strain of interest, there should be at least 2 wells in which only the strain and the media base are added (i.e. no carbon source was added);
- for each combination of strains and conditions, there should be at least 2 biological replicates (from 2 different colonies) and at least 2 technical repliates (cells from the same colony running in different wells).

6.3.2 Running plate reader experiments

Cells were grown in SC + 2% (w/v) sodium pyruvate in a 30 °C shaking incubator at 180 rpm for about 40 hours and then diluted by 6-fold 6–8 hours before the experiment began. Before harvesting the cells, 20 μL 10x sugar stock or water was added to each well. To harvest the cells, cultures of each strain were centrifuged at 3500 rpm for 3 minutes, and then the supernatant was removed. Then, cells were washed once (for experiments with SC or LoFlo) or twice (for experiments with Delft media) using the media base to be used in that plate reader experiment. Then, the cells were resuspended with a certain volume of the media base such that the initial OD was below 0.2 as measured by the spectrophotometer. Then, 180 μL resuspended culture was added to each well, which gives a final volume of 200 μL in each well. Then, the 96-well plate was moved into the plate reader at 30 °C and shaken linearly with an amplitude of 6 mm. Measurement was automatically taken every 10 minutes.

6.3.3 Analysing plate reader data

The plate reader data are typically time series of 96 wells with OD and fluorescence readings. We used a Python package, `omniplate` (version 0.9.50) (Montaño-Gutierrez et al. 2022), to analyse the data. The typical pipeline is:

1. ignore the corrupted wells (e.g. the contaminated wells);
2. average over technical replicates and estimate the error;
3. substract the OD and fluorescence background of the media;
4. correct the non-linearity between OD and the cell number when OD is high (Lichten et al. 2014);
5. estimate the specific growth rate ($d/dt\ \log OD$) and population growth rate ($d/dt\ OD$) using the Gaussian process (Swain et al. 2016), along with other quantities (e.g. maximal OD);
6. (if fluorescence is measured) correct the auto-fluorescence from the wildtype cells (Lichten et al. 2014);
7. calculate the fluorescence reading per OD.

6.4 Measuring sugar concentrations by GC-MS

Cells of the FY4 (wildtype) strain were grown in SC+2% pyruvate in a 30 °C shaking incubator at 180 rpm for about 40 hours and then diluted by 6-fold 6 hours before the experiment. When the experiment began, the cells were washed twice with Delft media without carbon sources and then inoculated into 250 mL flasks with 25 mL Delft media supplemented with desired concentrations of galactose and palatinose. The volume of inoculated cells was calculated such that the initial OD was controlled at 0.05, and then the volume of each culture was topped up to 26 mL. The cultures were then incubated in a 30 °C shaking incubator at 180 rpm.

To harvest the cells, I sampled 1 mL of each culture into a 15 mL Falcon tube placed on ice and then immediately put the flasks back into the shaking incubator to minimise

the impact of sampling. From each 1 mL sample, I transferred 2×200 μL samples into 2 wells of a 96-well microplate for OD measurement in a Tecan plate reader (Tecan, Infinite M200 Pro). The remaining volume in the samples were centrifuged at 4000 rpm for 15 minutes at 4 °C, and then 50 μL of the supernatant was transferred into a GC vial. The GC vial was stored at -20 °C before being sent to Dr Tessa Moses in the Edinomics facility. The samples were harvested at 0, 10, 15, 20, 25, 30, 40, 50, 60, 70 and 80 hour. The final OD was measured at 90 hour. Parallel to sample harvesting, OD of cultures in 0.1% galactose, as a negative control, was also measured with the same plate reader.

6.5 RNA measurements

6.5.1 Harvesting cells

For each sample, I harvested x mL of cells, such that the value of $OD \cdot x$ is around 4, by centrifuging the cells at 3500 rpm for 3 minutes at 4 °C. The supernatant was then removed and the cell pellets were stored in -80 °C if RNA extraction did not immediately follow.

6.5.2 Extracting RNA

I adapted a column-based protocol in (Auxillos, Bayne, and Wallace 2021) to extract RNA. The cell pellets were thawed on ice and then resuspended with 400 μL RNA binding buffer. The mixtures were then transferred to 2 mL screw cap tubes with zirconia beads inside, and then cell lysis was performed on PreCellys Evolution homogeniser (Bertin Instruments) — the samples were shaken at 6000 rpm for 10 seconds for 3 cycles, with a 10-second pause between each cycle, before being placed on ice for 1 minute. The shaking-ice bath process was repeated for *another* 5 times. Then, the lysates were centrifuged for 90 seconds, and each supernatant was transferred to a Zymo Spin IIICG column (Zymo, #C1006) and centrifuged. Then, the flow through was mixed with 400 μL 100% ethanol, transferred to a Zymo Spin IIC column (Zymo, #C1011), and centrifuged at $12000 \times g$ for 1 minute. The RNA was on the column, so the flow through was discarded. Then, 400 μL DNA/RNA prep buffer (Zymo, #D7010-2), 600 μL DNA/RNA wash buffer (Zymo,

#D7010-3) and 400 μL DNA/RNA wash buffer were sequentially added and centrifuged through the column. All flow through in these steps was discarded. The column was centrifuged again before 30 μL nuclease free water (Ambion, #AM9937) was added to the column to elute the RNA from the column. All steps of centrifugation were carried out at 12000 $\times$ g for 1 minute, unless otherwise specified.

The RNA concentrations were measured with a spectrophotometer (DeNovix, #DS-11). The quality of the RNA samples was confirmed on a Fragment Analyzer (Advanced Analytical Technologies, Inc.) with the Standard Sensitivity RNA Analysis Kit (Agilent, #DNF-471).

6.5.3 Quantifying transcripts by RT-qPCR

Before the quantitative reverse transcription PCR (RT-qPCR) experiment, primer pairs that target the genes of interest were designed using the PrimerQuest tool (Integrated DNA Technologies), with optimal T_m at 62 °C, optimal GC percentage at 50%, optimal primer size at 22 bp and optimal amplicon length at 100 bp. Primer pairs for three reference genes (*PUS7*, *ALG9* and *ACT1*) were gifts from Edward Wallace's Lab (Barrass et al. 2015). All primers were validated by running an RT-qPCR experiment with the primer pairs and a serial dilution of input cDNA (1x, 5x, 25x and 125x) — a primer pair is validated if the melting temperature of the product (see below) is unique and consistent across different dilution factors and the C_q value (see below) decreases linearly with the logarithm of the dilution factor.

An RT-qPCR experiment consists of 3 steps: DNase treatment, reverse transcription and quantitative PCR. First, the extracted RNA samples (1–3 μg each) were treated with DNaseI (ThermoFisher, #EN0525) at the presence of RNase inhibitor (ThermoFisher, SuperAseIn) at 37 °C for 1 hour, and then the DNaseI was deactivated with DNase inactivation reagent (Invitrogen, #AM1907) at room temperature for 5 minutes, before the DNase inactivation reagent was spun down. Second, I added the random primer mix (NEB, #S1330S) to each sample, split the sample into two, each 5 μL for the +RT and -RT reactions, and denature the RNA at 70 °C for 5 minutes, before moving the samples onto ice. Then, into each +RT reaction, 0.75 μL 10 mM dNTP mix, 0.25 μL RNase inhibitor,

0.5 μL Superscript IV Reverse Transcriptase (Invitrogen, #18090010), 2 μL first strand synthesis buffer and 1.5 μL nuclease-free water were added. For the -RT reactions, the same reagents were added except that the transcriptase was replaced with nuclease-free water. Then, the samples were incubated at 25 °C for 5 minutes and then 55 °C for 1 hour, the product (cDNA) was then diluted by about 20-fold with nuclease-free water. Third, the quantitative PCR was run with a 384-well microplate, and each well contains 1.6 μL 2x Brilliant III Ultra-Fast SYBR Green QPCR Master mix (Agilent, #600886), 0.4 μL primer pair mix (4 μM each) and 2 μL cDNA. The microplate was then moved into a LightCycler 480 machine (Roche), with *Taq* activation at 95 °C for 3 minutes, 40 cycles of amplification (95 °C for 5 seconds and 60 °C for 10 seconds with green fluorescence reading) and melt curve measurement (ramping up from 65 °C to 95 °C at 0.29 °C/s).

Data of an RT-qPCR experiment are time series of fluorescence from each well. I used the manufacturer's software (Roche LightCycler 480 SW 1.5) to extract the C_q values of each curve, i.e., the number of cycles required to amplify the input cDNA to a fixed threshold. Then I used an R package, `tidyqpcr` (version 0.5.0), to analyse the C_q data. The pipeline is:

1. averaging over technical replicates: get the mean C_q for each gene in each biological replicate;

2. calculating ΔC_q for each gene in each biological replicate: subtract the mean C_q for each gene in each biological replicate by the mean of the mean C_q of all three reference genes;

3. calculating $\Delta\Delta C_q$ for each gene in each biological replicate: subtract the ΔC_q value of that gene in each biological replicate by the mean ΔC_q of all biological replicates of that gene in the control group.

6.5.4 RNAseq experiment

Cells of the FY4 (wildtype) and *gal80*Δ strains were grown in SC+2% pyruvate in a 30 °C shaking incubator at 180 rpm for about 40 hours and then diluted by 6-fold 6 hours before the experiment began. The cultures were diluted 6-fold 6 hours before the experiment. When the experiment began, the cells were washed twice with Delft media without carbon

sources and then inoculated into 250 mL flasks with 25 mL Delft media supplemented with desired concentrations of fructose and palatinose. The volume of inoculated cells was calculated such that the initial OD was controlled at 0.005, and then the volume of each culture was topped up to 26 mL. The cultures were then incubated in a 30 °C shaking incubator at 180 rpm.

Samples were harvested at 3 time points: mid-log (at OD 0.3), 10 hours after mid-log and 16 hours after mid-log, using the method described in Section 6.5.1. I extracted the RNA with the method described in Section 6.5.2. Then, the samples were sent to Edinburgh Clinical Research Facility, where the samples were processed on quality control, library preparation and sequencing.

According to the report from the facility, sample quality control was performed on the Fragment Analyser Automated Capillary Electrophoresis System (Agilent Technologies Inc, #5300) with the Standard Sensitivity RNA Analysis Kit (#DNF-471-0500) for quality, and on the Qubit 2.0 Fluorometer (Thermo Fisher Scientific Inc, #Q32866) with the Qubit RNA broad range assay kit (#10210) for quantification. The Qubit dsDNA HS assay kit (#Q32854) was used to quantify DNA contamination.

Libraries were generated from 400 ng of each total RNA sample with the QuantSeq 3' mRNA Library Prep Kit REV for Illumina (Lexogen Inc, #016) according to the manufacturer's protocol. The libraries were then quantified by fluorometry with the Qubit dsDNA High Sensitivity assay, followed by assessment of quality and fragment size with the Agilent Fragment Analyser with the SS NGS Fragment 1–6000 bp kit (#DNF-473-33).

A 2×50 bp paired-end sequencing was performed on the NextSeq 2000 platform (Illumina Inc, #20038897) using NextSeq 1000/2000 P2 Reagents (100 cycles) v3 (#20046811), which produced 46.49 Gbp data. The data produced by the NextSeq 1000/2000 Control Software (Version 1.4.1.39716) was then automatically uploaded to BaseSpace (Illumina), where the data were converted into FASTQ files.

RNAseq alignment and quality control were carried out using the same pipeline as (Haynes et al. 2022), written in Nextflow (Di Tommaso et al. 2017). The code of the pipeline is available online in a Git repository (`https://github.com/DimmestP/nextflow_paired_reads_pipeline`), and the softwares' versions in my run are listed in 6.5. The genome annotation file was adapted from:

`longest_full-ORF_ypd_plus_other_fixed_UTR_length_transcripts.gff`

in `./data/shared_data/raw_annotation/reference_genome_annotation/` of the same Git repository (commit `3a4c6e1`).

I modified the annotations of some *MAL* genes (*MAL32*, *IMA1*, *MAL11* and *MAL12*) and some genes that are next to a *MAL* gene (*VTH1*, *HXT8*, *VTH2* and *ALR2*) according to their actual 3' end from the reads in this experiment. I also added the annotation of *ZNF1(YFL052W)*, which was missing from the original file. The output of this pipeline is a 5697×36 table with raw counts, which was subsequently used for differential expression analysis with DESeq2 (version 1.34.0) (Love, Huber, and Anders 2014).

Table 6.5: Softwares used in the RNAseq pipeline.

Name	Version	Reference
FASTQC	0.11.9	
Cutadapt	1.18	(Martin 2011)
HISAT2	2.1.0	(Kim et al. 2019)
SAMtools	1.11	(Li et al. 2009)
BEDTools	2.30.0	(Quinlan and Hall 2010)
Subread	2.0.0	(Liao, Smyth, and Shi 2014)
MultiQC	1.13	(Ewels et al. 2016)

Chapter 7

Discussion

In this chapter, I will discuss the experimental results we obtained in Chapters 2, 3, 4 and 5, and then the main experimental method I used to measure growth in this study — the plate reader.

7.1 Chapter 2: measuring the ribosome and growth dynamics in batch cultures of budding yeast

In Chapter 2, to investigate how cells regulate ribosomal levels as the environment changes in batch cultures, we measured the dynamics of both population growth and ribosomal levels. For the growth dynamics, we found that cells will only enter the historically defined "strict" exponential growth when the sugar concentration is high enough. This raises the question about whether it is conceptually correct to ask if Monod's equation (Monod 1949) can be applied to the growth of *S. cerevisiae* as measured in plate readers (Mrwebi 2004; Montaño-Gutierrez et al. 2022), because the exponential growth rate is not well-defined in lower sugar concentrations. However, we also found that by replacing the exponential growth rate with the maximum growth rate, Monod's equation does hold (Fig 2.3), which complicates the long-standing question on how Monod's equation emerges (Liu 2007), because now the growth rate is defined to be maximum rather than exponential.

Because protein is the largest sector of the biomass of *S. cerevisiae* (45%–60%) (Nissen et al. 1997) and the ribosome catalyses the last steps of protein production, the dynamics of ribosome levels could provide insight into the growth dynamics. We then further ask

how the ribosome levels match the growth rate in batch cultures in various carbon sources and stress conditions. Previous research has shown in bacteria (Scott et al. 2010) and *S. cerevisiae* (Metzl-Raz et al. 2017) that at exponential growth, the ribosome levels increase linearly with the growth rate. Yet, the previous methods of determining the ribosomal levels have limited time resolution because it is either laborious or expensive to process the samples. Based on previous work by Nahuel Manzanaro Moreno (Manzanaro Moreno 2021), we verified a method that uses a GFP-tagged ribosomal protein (*RPL3:GFP*), which enables the dynamic measurement of the ribosome levels.

We validated our method by comparing the snapshot data of each time series at a certain OD with the proteomics data from previous research, in which the cells are harvested at the same OD (Metzl-Raz et al. 2017). The results showed good consistency (Fig 2.5B). However, a limitation of this methodology is that the OD and GFP readings are noisy when the cell number is small, and the noise will propagate when we consider quantities like the GFP level per OD, which represents the ribosomal fraction. To circumvent this issue, instead of focusing on the ribosomal fraction and the specific growth rate (Scott et al. 2010; Metzl-Raz et al. 2017), we focused on the population's total ribosome level and the population's growth rate, and we showed that the two quantities obey a simple linear relationship at the early stage of growth (Fig 2.7). The slope of the line, i.e. the constant ratio of the population's growth rate and the population's total ribosome level, has a simple biophysical interpretation — the *effective* translation rate of a unit mass of ribosome. We used the word "effective" because this is not the translation rate of a unit mass of *active* ribosome — we cannot distinguish between the active and inactive ribosome from the GFP signal, which is another limitation of our methodology. In addition, we found that the effective translation rate is constant not only over time at the early stage of growth, but also over various carbon sources that support different specific growth rates (Fig 2.7). As expected, this rate decreases when cells are exposed to ribosome-targeting drugs (Figs 2.10CD, 2.11CD and 2.12CD), which is consistent with the general understanding that ribosomal-targeting drugs decreases the translation rate (Scott et al. 2010; Greulich et al. 2015).

We used this methodology to estimate how the translation rate is affected under various stress conditions. First, under energy stress imposed by acetic acid, which depletes the

cells' proton motive force (Ullah et al. 2012), the effective translation rate remains similar to stress-free conditions (Fig 2.14), albeit there is a decrease in the ribosomal fraction and hence the specific growth rate. This result suggests that yeast cells may have diverted this ribosomal fraction of the proteome to metabolism, which helps to maintain the energy required for growth and the effective translation rate. Second, under hyperosomotic stress, the effective translation rate is lower than the stress-free condition, but as discussed in Section 2.5.1, we must interpret this result with care.

Taken together, we verified our method to measure dynamics of ribosome levels by comparing the results with the published dataset (Metzl-Raz et al. 2017), and we showed that this methodology can be used to measure the effective translation rate, which decreases as expected when cells are exposed to ribosome-targeting drugs. Our results suggest that ribosome dynamics can reveal rich information that accompanies the growth dynamics, which opens up the possibility of investigating the ribosomal dynamics and translation efficiency in other less investigated situations, for example, upon genetic perturbation.

Previous research has established the central role of ribosome, as part of the total proteome, to understand how fast the cells can grow, from both experimental and theoretical perspectives (Scott et al. 2010; Molenaar et al. 2009). Researchers have seen how *E. coli*'s ribosomal fraction, growth rate and translation rate at steady state can be successfully explained in a single, top-down model (Scott and Hwa 2022; Chure and Cremer 2023). They have also seen success, under the same framework, to explain the growth dynamics beyond steady state, especially when cells move from one steady-state growth to another (Erickson et al. 2017; Basan et al. 2020), from which we see the potential of this top-down approach beyond steady state. However, so far it is expensive and laborious to measure the dynamics of ribosome and other cellular components of interest and key parameters like the translation rate beyond steady state. Our development of the GFP reporter in yeast shows the potential of measuring ribosomal fraction and in the meantime estimating the translation rate using fluorescence, and this idea in principle could work in other microbes. Hopefully, this will help democratise research in this field, such that comprehensive examination of the generality of the "growth laws" will be possible and more simple principles shared by microbes (Bruggeman et al. 2020) discovered.

7.2 Chapter 3: the growth model

In Chapter 3, we aim to understand the observed dynamics of growth and ribosome within a self-replicator model. We began with a mathematical framework and then a minimal growth model.

The framework models cell growth using the mass fraction of biochemical species (and the total biomass if the growth of a population is considered) as state variables. Mathematically the framework is similar to those using molar concentration as state variables (Weiße et al. 2015; de Groot et al. 2020), but the use of mass fraction, similar to a recently published model (Chure and Cremer 2023), makes it more convenient to fit mass fraction data (e.g. (Metzl-Raz et al. 2017)) to a top-down model within this framework. We derived the general form of the ODEs (Eq 3.16) and generally how the growth rate is determined by fluxes (Eq 3.20), assuming the intracellular density of biomass is constant. Here we see that the dilution term comes from the assumption of constant biomass density, which is implicit in previous models (Scott et al. 2010; Weiße et al. 2015). However, it is worth noting that if the constant density is relaxed, this term may not be well-defined — for example, (Dourado and Lercher 2020) does not seem to have a clear definition of the dilution term, but treat its existence as an ansatz.

Then I built a minimal growth model within this framework, in which the intracellular subsystem is analytically shown to have a single stable steady state, which corresponds to steady-state growth if the environment remains constant. This model, built in a similar spirit as (Chure and Cremer 2023), aims to minimise the number of equations and parameters while still being able to capture the experimentally observed data, which, if successful, should help to shed light on the how cells grow despite their physiological complexity. Technically, a smaller set of parameters will also make it easier to fit experimental data to the model and to gauge the uncertainty of the model (Kirk, Babtie, and Stumpf 2015) compared to, for example, (Weiße et al. 2015; Hu et al. 2020). The existence of a stable steady state is essential, because it captures exponential growth in a stable environment — and proving this is non-trivial, as is discussed in another simple model (Chure and Cremer 2023). In our model, the existence and stability of this steady state is guaranteed by product inhibition (Eq 3.31), whereas in (Chure and Cremer 2023) the

stability is achieved by not neglecting the dilution term. Our model, despite its simplicity, is able to semi-quantitatively capture the growth and ribosomal dynamics in experiments, and to answer questions from the experimental data in Chapter 2 (Section 2.5), for example, why the specific growth rate peaks in sugar-limiting cases and why Monod's equation still holds when we replace the steady-state growth rate with the growth rate at the peak.

In this model, we analysed under what condition Monod's equation is valid in the cases of growth-rate peaks, steady-state growth rate and steady-state growth rate with two substrates. In all three cases, I derived the Monod's equation assuming Michaelis-Menten kinetics of the transporter(s), so the Monod's equation can be explained in terms of the Michaelis-Menten kinetics of the transporter, similar to (Liu 2007; Weiße et al. 2015). However, as is discussed in Section 3.6.2, this is not the only possible explanation — Monod's equation can be explained by either Michaelis-Menten kinetics or the first-order kinetics (but no other transport kinetics). Therefore, Monod's equation may be valid for substrates like ethanol, which enters the cell by diffusion.

In contrast to our "top-down" approach, with the availability of large-scale "omics" data, there are genome-scale "bottom-up" models, which provide predictions that guide further experimental analysis (Karr et al. 2012). However, validation and reporting the uncertainty of this type of complex model remains challenging, and we may not be able to distinguish between different genome-scale models given that they provide equally good fits of data (Kirk, Babtie, and Stumpf 2015). Perhaps, there is no panacea for modelling a complex system like a cell, and just like theoretical physics and chemistry, approximation is necessary to avoid getting lost in the complexity. Depending on the biological process of interest, plugging a local, mechanistic model into a "top-down" model (Boo, Ellis, and Stan 2019) may provide both mechanistic insight and good-enough predictions.

7.3 Chapters 4 and 5: a novel example of non-glucose catabolite repression in budding yeast

In Chapter 4, we investigated how cells prioritise which carbon source to use when given two non-glucose carbon sources. We found that *S. cerevisiae* shows diauxie when grown

in glucose- and galactose-palatinose mixtures (Figs 4.2 and 4.3), but does not when grown in fructose- or sucrose-palatinose mixtures (Figs 4.10 and 4.9). This is the first example of diauxie between non-glucose carbon sources in *S. cerevisiae* as far as I am aware. We confirmed that in galactose-palatinose mixtures, cells sequentially consume galactose and palatinose (Section 4.3.2), but because of the cost, we have not confirmed whether cells co-consume sucrose/fructose and palatinose or use them sequentially without a visible lag. However, measurement of the isomaltases' fluorescence suggests that palatinose is more likely to be co-consumed (Fig 4.13). Nevertheless, our results suggest that the catabolite repression of galactose on palatinose metabolism is stronger than that of sucrose/fructose on palatinose metabolism.

Because palatinose supports the lowest growth rate of the above-mentioned sugars, our findings are consistent with the known rule that if diauxie is observed, the first carbon source to be metabolised supports growth at a higher rate (Okano, Hermsen, and Hwa 2021) and the fact that this rule does not hold *vice versa* — although fructose/sucrose supports a higher growth rate, there is no diauxie. In addition, our findings suggest that the strength of catabolite repression is not necessarily stronger when growth is faster, because cells grow faster on fructose (Fig 2.3) or sucrose (data not shown) than on galactose, but diauxie was only observed in galactose-palatinose mixtures. Therefore, in *S. cerevisiae*, growth rate informs us which carbon source is to be prioritised when diauxie occurs, but growth rate does not determine whether diauxie occurs or not.

We also showed in the same chapter that the delay of palatinose metabolism does not require galactose itself, instead it is a result of *GAL* signal transduction — active Gal4 is sufficient for this delay (Fig 4.15). However, it remains unclear why deleting *GAL2*, the galactose transporter gene, alleviates the delay (Fig 4.19). Notably, this is consistent with a previous report that the *gal80*Δ, the mutant with constitutively active Gal4, changes the gene expression pattern on raffinose and leads to slow growth, and further deleting *GAL2* alleviates the change in pattern (Ideker et al. 2001). The Gal2 transporter, like other hexose transporters, has no known signal transduction function, and overexpressing *GAL2* has no effect on palatinose metabolism (Fig 4.21). It is therefore possible that it is the loss of the gene on the chromosome, rather than the loss of the transporter, that alleviates this delay. For example, the deletion of the *GAL2* gene may affect multiple

stable unannotated transcripts (SUTs) that are present near the *GAL2* gene and the one (*SUT692*) overlapping with the *GAL2* gene which bears unknown functions (Parker et al. 2017).

In Chapter 5, we investigated the mechanism of galactose-palatinose diauxie. We showed that key to the galactose-palatinose diauxie is the repression on *MAL11*. This mechanism seems to ensure flexibility of switching carbon source consumption strategies, as we showed that the diauxie — not only the lag, but probably also the sequential utilisation — can be abolished by deleting one of the two isomaltase genes, *IMA1*. This is in contrast to the glucose-galactose diauxie, which efficient expression of the *GAL* genes is not sufficient to abolish and may involve global processes like the switch from fermentation to respiration (Perez-Samper et al. 2018). The change in strategy by losing one gene is highly realistic because the *MAL* genes are located in the rapid-changing sub-telomeric region of budding yeast, where gene loss and duplication are common (Brown, Murray, and Verstrepen 2010). The change in strategy is perhaps also a necessity — *S. cerevisiae* has no identified niche yet and is perhaps a nomad (Goddard and Greig 2015), which means they might need to frequently adapt to new environments and change strategy accordingly.

Notably, what mediates the signal from Gal4 to *MAL11* remains unknown. We hoped to identify the signal by comparing the gene expression pattern of the wildtype and the *gal80*Δ mutant, and we designed the RNAseq experiment to mitigate global effects such as the growth rate and the potential catabolite repression by fructose. However, in addition to local changes within the *GAL* network and the known non-*GAL* targets (Section 1.3.3), the *gal80*Δ mutant has a set of 84 differentially expressed genes (Fig 5.19), including a group of down-regulated genes controlling ribosome biogenesis (Fig 5.20). Our results suggest that active Gal4's physiological effect may be larger than expected, which also makes it difficult to identify its downstream signal(s), although previous ChIP datasets suggest that the number of genes that are direct downstream of Gal4 is small (Ren et al. 2000; Rhee and Pugh 2011).

There are also limitations in this research. First, for the growth dynamics in fructose- and sucrose-palatinose mixtures, we did not directly confirm whether it is diauxie with an invisible lag, or co-consumption, although fluorescence and RNAseq data suggests

that co-consumption is likely the case (Figs 4.13 and 5.6). Second, we assumed that the metabolic products of the preferred sugar's consumption, including ethanol, acetate and glycerol (Ostergaard et al. 2000), do not affect the consumption of palatinose. The metabolic enzymes of these products may compete with the *MAL* enzymes as observed in *E. coli* (Hermsen et al. 2015), although this should not alter our major findings. To further exclude the effect of ethanol and acetate, we could repeat the experiments with the *icl1*Δ mutant, which cannot consume C_2 compounds (Fernández, Moreno, and Rodicio 1992).

There are still open questions on the diauxie of budding yeast to be answered in the future. Why do cells prioritise glucose and galactose (but not fructose and sucrose) over palatinose? What is the objective and what are the constraint(s) that makes co-consumption an inferior strategy? Assuming that the objective of prioritising one carbon source is to maximise the growth rate, which constraint(s) are limiting growth when enzymes of both glucose/galactose and palatinose are expressed? Is it the cytosolic proteome allocation constraint like in *E. coli* (Scott et al. 2010), or some other compartments in *S. cerevisiae* (Elsemman et al. 2022)? A better understanding of these questions are not only important for the search for principles of microbial physiology (Bruggeman et al. 2020), but also important in the fermentation industry (Randez-Gil and Sanz 1994) and metabolic engineering (Ostergaard et al. 2000).

If we go beyond diauxie and think about how cells distinguish between different nutrients, the facts that (1) *S. cerevisiae* shows diauxie in glucose-palatinose mixtures but does not in fructose-palatinose mixtures and that (2) both sugars support growth at similar rate (Fig 2.3) raise further questions on how cells distinguish between glucose and fructose and display different strategies of sugar consumption. As reviewed in Section 1.5.1, cells sense extracellular glucose via Snf3, Rgt2 and Gpr1. Gpr1 is known to activate PKA which activates downstream signaling of catabolite repression (Castermans et al. 2012). However, the Gpr1 signal is unlikely to cause glucose-palatinose diauxie, because sucrose also binds to Gpr1 and with a higher affinity than glucose and triggers downstream signaling (Lemaire et al. 2004), but we did not observe sucrose-palatinose diauxie (Fig 4.9). Glucose binding to Rgt2 leads to the degradation of a maltose transporter Mal61 (Jiang, Medintz, and Michels 1997) (Section 1.5.3), and thus cells might distinguish between glu-

cose and fructose via Rgt2. However, Rgt2 only senses high concentrations of glucose (Karhumaa, Wu, and Kielland-Brandt 2010), which makes it hard to explain the diauxie observed even at 0.1% glucose (Fig 4.2). Intracellular signaling via hexose kinases and ADP levels should be shared between glucose and fructose, and the cytosolic pH is similar between them too (Dechant et al. 2014), so the intracellular signals above are unlikely to play a distinguishing role.

7.4 Measuring growth: plate reader, growth on agar and beyond?

We extensively used plate readers in this study — the plate readers enable a medium-throughput, simple experimental set-up to measurement dynamics of population growth and gene expression in liquid cultures, although they come with several limitations. As seen in our results and others (Marešová and Sychrová 2007; Aidelberg et al. 2014), plate readers are a common and useful method in physiological studies of microbes, especially for a small-to-medium scale screening over conditions and mutants.

The advantages of plate readers are a higher throughput than flasks and a straight-forward experimental set-up. A plate reader, run with a 96-well microplate, can automatically monitor the OD and fluorescence of up to 96 parallel growth experiments of batch cultures every ten minutes for 1–3 days. The experimental set-up is straight-forward with a multi-channel pipette, so the time required for each experiment is short (2–3 hours). Thus, the plate reader method is suited for growth experiments with multiple different conditions and strains, for example, different combinations of carbon sources in Chapter 4.

Plate readers also have limitations — one must be aware of these limitations when interpreting the data.

1. They only provide information of the population mean level, so information like bimodality of a population is lost.

2. Oxygen may be limiting when the cell number is large, because the oxygen exchange is limited by the microplate's lid, which prevents contamination and evaporation of

liquid and could be the reason why we did not observe a "diauxic shift" from glucose to ethanol when we monitored growth on 2% glucose (Fig 4.1).

3. Related to the second point, the fluorescence measurement of fluorescent proteins may not be reliable when oxygen is limiting, because maturation of most fluorescent proteins requires oxygen (Tsien 1998; Chapagain, Regmi, and Castillo 2011) — we have observed biologically inexplicable dynamics using mCherry and yECitrine proteins (data not shown).

4. Cell sedimentation to the bottom of the wells after a long run time (usually after 24 hours) can affect the accuracy of OD measurements.

5. Both the OD and fluorescence signals can be noisy when the cell number is low.

6. The growth time series is sensitive to the initial cell number — a smaller initial cell number corresponds to a longer "lag" (e.g. Fig 4.9), which is not necessarily a biological growth lag but an apparent lag when the OD is increasing but still too low to be measured.

An experimental alternative is to grow cells on agar plates and monitor the size of the colonies, which enables high-throughput experiments for phenotyping and screening on agar plates with robots (Barton et al. 2018; Kamrad et al. 2020), and it is also possible to measure fluorescence (Kainth et al. 2009). This setting does not have Limitations 2, 3 and 4 of the plate reader method, and Limitation 6 could also be overcome if the robot is programmed to streak single-cell colonies (although this is not the setting in (Barton et al. 2018; Kamrad et al. 2020)). That said, growth on agar plates is not the same as growth in batch cultures, because the nutrient availability is not uniform over cells within the same colony (Wimpenny 1979), which may reveal the physiology of microbes from a different perspective.

We now have multiple ways in the laboratory to culture and monitor cell growth, including microfluidics, chemostats, batch cultures, fed-batch cultures and robotics assay on agar plates, and each provides a unique environment to interrogate the physiology of the microbes, and some of them, e.g. microfluidics, can mimic a highly dynamic environment. However, we do not have a clear idea what the environment is like for microbes (e.g.

budding yeast (Goddard and Greig 2015)) in the wild, and hence how some behaviour (e.g. diauxie) is selected. While we still need a comprehensive understanding of microbial growth in different laboratory settings, ultimately, to connect microbial physiology with evolution, we may need to understand the dynamics of the natural habitats of microbes and reproduce it in the laboratory setting.

Bibliography

Abramczyk, Dariusz, Stacey Holden, Christopher J. Page, and Richard J. Reece. 2012. "Interplay of a Ligand Sensor and an Enzyme in Controlling Expression of the Saccharomyces Cerevisiae GAL Genes." *Eukaryotic Cell* 11 (3): 334–42. https://doi.org/10.1128/EC.05294-11.

Acar, Murat, Attila Becskel, Alexander Van Oudenaarden, Attila Becskei, and Alexander Van Oudenaarden. 2005. "Enhancement of Cellular Memory by Reducing Stochastic Transitions." *Nature* 435 (7039): 220–23. https://doi.org/10.1038/nature03524.

Aidelberg, Guy, Benjamin D. Towbin, Daphna Rothschild, Erez Dekel, Anat Bren, and Uri Alon. 2014. "Hierarchy of Non-Glucose Sugars in Escherichia Coli." *Bmc Systems Biology* 8: 133. https://doi.org/10.1186/s12918-014-0133-z.

Alvarez-Ramirez, Jose, M. Meraz, and E. Jaime Vernon-Carter. 2019. "A Theoretical Derivation of the Monod Equation with a Kinetics Sense." *Biochemical Engineering Journal* 150 (October): 107305. https://doi.org/10.1016/j.bej.2019.107305.

Asakawa, Kazuhide, and Koichi Kawakami. 2008. "Targeted Gene Expression by the Gal4-UAS System in Zebrafish." *Development, Growth & Differentiation* 50 (6): 391–99. https://doi.org/10.1111/j.1440-169X.2008.01044.x.

Auxillos, Jamie, Rosey Bayne, and Edward Wallace. 2021. "RNA Extraction with Spin Columns from Yeast Cells Grown on 12-Column Deep Well Plates." *Protocols.Io*. dx.doi.org/10.17504/protocols.io.beetjben.

Bader, F. G. 1978. "Analysis of Double-Substrate Limited Growth." *Biotechnology and Bioengineering* 20 (2): 183–202. https://doi.org/10.1002/bit.260200203.

Baker Brachmann, Carrie, Adrian Davies, Gregory J. Cost, Emerita Caputo, Joachim Li, Philip Hieter, and Jef D. Boeke. 1998. "Designer Deletion Strains Derived from Saccharomyces Cerevisiae S288C: A Useful Set of Strains and Plasmids for PCR-mediated

Gene Disruption and Other Applications." *Yeast* 14 (2): 115–32. https://doi.org/10.1002/(SICI)1097-0061(19980130)14:2<115::AID-YEA204>3.0.CO;2-2.

Barrass, J. David, Jane E. A. Reid, Yuanhua Huang, Ralph D. Hector, Guido Sanguinetti, Jean D. Beggs, and Sander Granneman. 2015. "Transcriptome-Wide RNA Processing Kinetics Revealed Using Extremely Short 4tU Labeling." *Genome Biology* 16 (1): 282. https://doi.org/10.1186/s13059-015-0848-1.

Barton, David B H, Danae Georghiou, Neelam Dave, Majed Alghamdi, Thomas A Walsh, Edward J Louis, and Steven S Foster. 2018. "PHENOS: A High-Throughput and Flexible Tool for Microorganism Growth Phenotyping on Solid Media." *Bmc Microbiology* 18 (1): 9. https://doi.org/10.1186/s12866-017-1143-y.

Basan, Markus, Tomoya Honda, Dimitris Christodoulou, Manuel Hörl, Yu Fang Chang, Emanuele Leoncini, Avik Mukherjee, et al. 2020. "A Universal Trade-off between Growth and Lag in Fluctuating Environments." *Nature* 584 (7821): 470–74. https://doi.org/10.1038/s41586-020-2505-4.

Belinchón, Mónica M., and Juana M. Gancedo. 2007. "Different Signalling Pathways Mediate Glucose Induction of SUC2, HXT1 and Pyruvate Decarboxylase in Yeast." *Fems Yeast Research* 7 (1): 40–47. https://doi.org/10.1111/j.1567-1364.2006.00136.x.

Berkhout, Jan, Evert Bosdriesz, Emrah Nikerel, Douwe Molenaar, Dick de Ridder, Bas Teusink, and Frank J. Bruggeman. 2013. "How Biochemical Constraints of Cellular Growth Shape Evolutionary Adaptations in Metabolism." *Genetics* 194 (2): 505–12. https://doi.org/10.1534/genetics.113.150631.

Bertolazzi, E. 2005. "A Combination Formula of Michaelis-Menten-Monod Type." *Computers and Mathematics with Applications* 50 (1-2): 201–15. https://doi.org/10.1016/j.camwa.2004.10.045.

Bheda, Poonam, Diana Aguilar-Gómez, Nils B. Becker, Johannes Becker, Emmanouil Stavrou, Igor Kukhtevich, Thomas Höfer, et al. 2020. "Single-Cell Tracing Dissects Regulation of Maintenance and Inheritance of Transcriptional Reinduction Memory." *Molecular Cell* 78 (5): 915–25.e7. https://doi.org/10.1016/j.molcel.2020.04.016.

Biggar, Stephen R., and Gerald R. Crabtree. 2001. "Cell Signaling Can Direct Either

Binary or Graded Transcriptional Responses." *The Embo Journal* 20 (12): 3167–76. https://doi.org/10.1093/emboj/20.12.3167.

Boer, Carl G. de, and Timothy R. Hughes. 2012. "YeTFaSCo: A Database of Evaluated Yeast Transcription Factor Sequence Specificities." *Nucleic Acids Research* 40 (D1): D169–79. https://doi.org/10.1093/nar/gkr993.

Boo, Alice, Tom Ellis, and Guy-Bart Stan. 2019. "Host-Aware Synthetic Biology." *Current Opinion in Systems Biology*, Synthetic biology, 14 (April): 66–72. https://doi.org/10.1016/j.coisb.2019.03.001.

Boocock, James, Meru J. Sadhu, Arun Durvasula, Joshua S. Bloom, and Leonid Kruglyak. 2021. "Ancient Balancing Selection Maintains Incompatible Versions of the Galactose Pathway in Yeast." *Science* 371 (6527): 415–19. https://doi.org/10.1126/science.aba0542.

Bren, Anat, Yuval Hart, Erez Dekel, Daniel Koster, and Uri Alon. 2013. "The Last Generation of Bacterial Growth in Limiting Nutrient." *Bmc Systems Biology* 7. https://doi.org/10.1186/1752-0509-7-27.

Broach, James R. 2012. "Nutritional Control of Growth and Development in Yeast." *Genetics* 192 (1): 73–105. https://doi.org/10.1534/genetics.111.135731.

Brown, Chris A., Andrew W. Murray, and Kevin J. Verstrepen. 2010. "Rapid Expansion and Functional Divergence of Subtelomeric Gene Families in Yeasts." *Current Biology* 20 (10): 895–903. https://doi.org/10.1016/j.cub.2010.04.027.

Bruggeman, Frank J., Robert Planqué, Douwe Molenaar, and Bas Teusink. 2020. "Searching for Principles of Microbial Physiology." *Fems Microbiology Reviews* 44 (6): 821–44. https://doi.org/10.1093/femsre/fuaa034.

Bruin, Derik de, Zafar Zaman, Rachel A. Liberatore, and Mark Ptashne. 2001. "Telomere Looping Permits Gene Activation by a Downstream UAS in Yeast." *Nature* 409 (6816): 109–13. https://doi.org/10.1038/35051119.

Bryan, Andrea K., Alexi Goranov, Angelika Amon, and Scott R. Manalis. 2010. "Measurement of Mass, Density, and Volume during the Cell Cycle of Yeast." *Proceedings of the National Academy of Sciences* 107 (3): 999–1004. https://doi.org/10.1073/pnas.0901851107.

Castermans, Dries, Ils Somers, Johan Kriel, Wendy Louwet, Stefaan Wera, Matthias

Versele, Veerle Janssens, and Johan M Thevelein. 2012. "Glucose-Induced Posttranslational Activation of Protein Phosphatases PP2A and PP1 in Yeast." *Cell Research* 22 (6): 1058–77. https://doi.org/10.1038/cr.2012.20.

Cerulus, Bram, Abbas Jariani, Gemma Perez-Samper, Lieselotte Vermeersch, Julian Pietsch, Matthew M Crane, Aaron M New, et al. 2018. "Transition between Fermentation and Respiration Determines History-Dependent Behavior in Fluctuating Carbon Sources." *Elife* 7. https://doi.org/10.7554/eLife.39234.

Cerulus, Bram, Aaron M. New, Ksenia Pougach, and Kevin J. Verstrepen. 2016. "Noise and Epigenetic Inheritance of Single-Cell Division Times Influence Population Fitness." *Current Biology* 26 (9): 1138–47. https://doi.org/10.1016/j.cub.2016.03.010.

Chambers, Prima, Aminatu Issaka, and Sean P. Palecek. 2004. "Saccharomyces Cerevisiae JEN1 Promoter Activity Is Inversely Related to Concentration of Repressing Sugar." *Applied and Environmental Microbiology* 70 (1): 8–17. https://doi.org/10.1128/AEM.70.1.8-17.2004.

Change, Young Sook, Robert A. Dubin, Edward Perkins, Doug Forrest, Corinne A. Michels, and Richard B. Needleman. 1988. "MAL63 Codes for a Positive Regulator of Maltose Fermentation in Saccharomyces Cerevisiae." *Current Genetics* 14 (3): 201–9. https://doi.org/10.1007/BF00376740.

Chapagain, Prem P., Chola K. Regmi, and William Castillo. 2011. "Fluorescent Protein Barrel Fluctuations and Oxygen Diffusion Pathways in mCherry." *The Journal of Chemical Physics* 135 (23): 235101. https://doi.org/10.1063/1.3660197.

Charron, M. J., E. Read, S. R. Haut, and C. A. Michels. 1989. "Molecular Evolution of the Telomere-Associated MAL Loci of Saccharomyces." *Genetics* 122 (2): 307–16. https://doi.org/10.1093/genetics/122.2.307.

Chen, Edward Y., Christopher M. Tan, Yan Kou, Qiaonan Duan, Zichen Wang, Gabriela Vaz Meirelles, Neil R. Clark, and Avi Ma'ayan. 2013. "Enrichr: Interactive and Collaborative HTML5 Gene List Enrichment Analysis Tool." *Bmc Bioinformatics* 14 (April): 128. https://doi.org/10.1186/1471-2105-14-128.

Choi, Il-Dong, Mi-Young Jeong, Moon-Sik Ham, Ha-Chin Sung, and Cheol-Won Yun. 2008. "Novel Ree1 Regulates the Expression of ENO1 via the Snf1 Complex Pathway

in Saccharomyces Cerevisiae." *Biochemical and Biophysical Research Communications* 377 (2): 395–99. https://doi.org/10.1016/j.bbrc.2008.09.146.

Chure, Griffin, and Jonas Cremer. 2023. "An Optimal Regulation of Fluxes Dictates Microbial Growth in and out of Steady State." *Elife* 12 (March): e84878. https://doi.org/10.7554/eLife.84878.

Coleman, Matthew C., Russell Fish, and David E. Block. 2007. "Temperature-Dependent Kinetic Model for Nitrogen-Limited Wine Fermentations." *Applied and Environmental Microbiology* 73 (18): 5875–84. https://doi.org/10.1128/AEM.00670-07.

Cramer, Amanda C., Sophocles Vlassides, and David E. Block. 2002. "Kinetic Model for Nitrogen-Limited Wine Fermentations." *Biotechnology and Bioengineering* 77 (1): 49–60. https://doi.org/10.1002/bit.10133.

Dalal, Chiraj K, Ignacio A Zuleta, Kaitlin F Mitchell, David R Andes, Hana El-Samad, and Alexander D Johnson. 2016. "Transcriptional Rewiring over Evolutionary Timescales Changes Quantitative and Qualitative Properties of Gene Expression." Edited by Naama Barkai. *Elife* 5 (September): e18981. https://doi.org/10.7554/eLife.18981.

Day, Rachel E., Vincent J. Higgins, Peter J. Rogers, and Ian W. Dawes. 2002. "Characterization of the Putative Maltose Transporters Encoded by YDL247w and YJR160c." *Yeast* 19 (12): 1015–27. https://doi.org/10.1002/yea.894.

Dechant, Reinhard, Shady Saad, Alfredo J. Ibáñez, and Matthias Peter. 2014. "Cytosolic pH Regulates Cell Growth through Distinct Gtpases, Arf1 and Gtr1, to Promote Ras/PKA and TORC1 Activity." *Molecular Cell* 55 (3): 409–21. https://doi.org/10.1016/j.molcel.2014.06.002.

Delgado, Francisco Feijó, Nathan Cermak, Vivian C. Hecht, Sungmin Son, Yingzhong Li, Scott M. Knudsen, Selim Olcum, et al. 2013. "Intracellular Water Exchange for Measuring the Dry Mass, Water Mass and Changes in Chemical Composition of Living Cells." *Plos One* 8 (7): e67590. https://doi.org/10.1371/journal.pone.0067590.

Deng, Xu, Marjorie Petitjean, Marie-Ange Teste, Wafa Kooli, Samuel Tranier, Jean Marie François, and Jean-Luc Parrou. 2014. "Similarities and Differences in the Biochemical and Enzymological Properties of the Four Isomaltases from Saccharomyces Cerevisiae." *Febs Open Bio* 4 (1): 200–212. https://doi.org/10.1016/j.fob.2014.02.004.

Desai, Tasha A., and Christopher V. Rao. 2010. "Regulation of Arabinose and Xylose Metabolism in Escherichia Coli." *Applied and Environmental Microbiology* 76 (5): 1524–32. https://doi.org/10.1128/AEM.01970-09.

Di Tommaso, Paolo, Maria Chatzou, Evan W. Floden, Pablo Prieto Barja, Emilio Palumbo, and Cedric Notredame. 2017. "Nextflow Enables Reproducible Computational Workflows." *Nature Biotechnology* 35 (4): 316–19. https://doi.org/10.1038/nbt.3820.

Dourado, Hugo, and Martin J. Lercher. 2020. "An Analytical Theory of Balanced Cellular Growth." *Nature Communications* 11 (1). https://doi.org/10.1038/s41467-020-14751-w.

Eadie, G. S. 1942. "THE INHIBITION OF CHOLINESTERASE BY PHYSOSTIGMINE AND PROSTIGMINE." *Journal of Biological Chemistry* 146 (1): 85–93. https://doi.org/10.1016/S0021-9258(18)72452-6.

Elliott, David A., and Andrea H. Brand. 2008. "The GAL4 System." In *Drosophila: Methods and Protocols*, edited by Christian Dahmann, 79–95. Methods in Molecular Biology. Totowa, NJ: Humana Press. https://doi.org/10.1007/978-1-59745-583-1_5.

Elsemman, Ibrahim E., Angelica Rodriguez Prado, Pranas Grigaitis, Manuel Garcia Albornoz, Victoria Harman, Stephen W. Holman, Johan van Heerden, et al. 2022. "Whole-Cell Modeling in Yeast Predicts Compartment-Specific Proteome Constraints That Drive Metabolic Strategies." *Nature Communications* 13 (1): 801. https://doi.org/10.1038/s41467-022-28467-6.

Erickson, David W., Severin J. Schink, Vadim Patsalo, James R. Williamson, Ulrich Gerland, and Terence Hwa. 2017. "A Global Resource Allocation Strategy Governs Growth Transition Kinetics of Escherichia Coli." *Nature* 551 (7678): 119–23. https://doi.org/10.1038/nature24299.

Escalante-Chong, Renan, Yonatan Savir, Sean M. Carroll, John B. Ingraham, Jue Wang, Christopher J. Marx, and Michael Springer. 2015. "Galactose Metabolic Genes in Yeast Respond to a Ratio of Galactose and Glucose." *Proceedings of the National Academy of Sciences* 112 (5): 1636–41. https://doi.org/10.1073/pnas.1418058112.

Ewels, Philip, Måns Magnusson, Sverker Lundin, and Max Käller. 2016. "MultiQC: Summarize Analysis Results for Multiple Tools and Samples in a Single Report."

Bioinformatics (Oxford, England) 32 (19): 3047–48. https://doi.org/10.1093/bioinformatics/btw354.

Fernández, Ernestina, Fernando Moreno, and Rosaura Rodicio. 1992. "The ICL1 Gene from Saccharomyces Cerevisiae." *European Journal of Biochemistry* 204 (3): 983–90. https://doi.org/10.1111/j.1432-1033.1992.tb16720.x.

Fishburn, James, Neeman Mohibullah, and Steven Hahn. 2005. "Function of a Eukaryotic Transcription Activator during the Transcription Cycle." *Molecular Cell* 18 (3): 369–78. https://doi.org/10.1016/j.molcel.2005.03.029.

Flick, Karin M., Nathalie Spielewoy, Tatyana I. Kalashnikova, Marisela Guaderrama, Qianzheng Zhu, Hui-Chu Chang, and Curt Wittenberg. 2003. "Grr1-Dependent Inactivation of Mth1 Mediates Glucose-induced Dissociation of Rgt1 from HXT Gene Promoters." *Molecular Biology of the Cell* 14 (8): 3230–41. https://doi.org/10.1091/mbc.e03-03-0135.

Frederick, Debra L., and Kelly Tatchell. 1996. "The REG2 Gene of Saccharomyces Cerevisiae Encodes a Type 1 Protein Phosphatase-Binding Protein That Functions with Reg1p and the Snf1 Protein Kinase to Regulate Growth | Molecular and Cellular Biology." *Molecular and Cellular Biology* 16 (6): 2922–31. https://doi.org/10.1128/MCB.16.6.2922.

Gadura, Nidhi, Lucy C Robinson, and Corinne A Michels. 2006. "Glc7Reg1 Phosphatase Signals to Yck1,2 Casein Kinase 1 to Regulate Transport Activity and Glucose-Induced Inactivation of Saccharomyces Maltose Permease." *Genetics* 172 (3): 1427–39. https://doi.org/10.1534/genetics.105.051698.

Gadura, Nidhi, and Corinne A. Michels. 2006. "Sequences in the N-terminal Cytoplasmic Domain of Saccharomyces Cerevisiae Maltose Permease Are Required for Vacuolar Degradation but Not Glucose-Induced Internalization." *Current Genetics* 50 (2): 101–14. https://doi.org/10.1007/s00294-006-0080-3.

Gancedo, Juana M. 1998. "Yeast Carbon Catabolite Repression." *Microbiology and Molecular Biology Reviews* 62 (2): 334–61.

Gancedo, Juana M., Carmen-Lisset Flores, and Carlos Gancedo. 2015. "The Repressor Rgt1 and the cAMP-dependent Protein Kinases Control the Expression of the SUC2 Gene in Saccharomyces Cerevisiae." *Biochimica et Biophysica Acta (Bba) - General*

Subjects 1850 (7): 1362–67. https://doi.org/10.1016/j.bbagen.2015.03.006.

Gibney, Patrick A., Ariel Schieler, Jonathan C. Chen, Joshua D. Rabinowitz, and David Botstein. 2015. "Characterizing the in Vivo Role of Trehalose in Saccharomyces Cerevisiae Using the AGT1 Transporter." *Proceedings of the National Academy of Sciences* 112 (19): 6116–21. https://doi.org/10.1073/pnas.1506289112.

Gibson, Andrew W., Lori A. Wojciechowicz, Sara E. Danzi, Bin Zhang, Jeong H. Kim, Zhen Hu, and Corinne A. Michels. 1997. "Constitutive Mutations of the Saccharomyces Cerevisiae MAL-Activator Genes MAL23, MAL43, MAL63, and Mal64." *Genetics* 146 (4): 1287–98.

Gietz, R. Daniel, and Robin A. Woods. 2002. "Transformation of Yeast by Lithium Acetate/Single-Stranded Carrier DNA/Polyethylene Glycol Method." *Methods in Enzymology* 350: 87–96. https://doi.org/10.1016/s0076-6879(02)50957-5.

Gill, Grace, and Mark Ptashne. 1988. "Negative Effect of the Transcriptional Activator GAL4." *Nature* 334 (6184): 721–24. https://doi.org/10.1038/334721a0.

Gillespie, Daniel T. 1976. "A General Method for Numerically Simulating the Stochastic Time Evolution of Coupled Chemical Reactions." *Journal of Computational Physics* 22 (4): 403–34. https://doi.org/10.1016/0021-9991(76)90041-3.

Giniger, Edward, Susan M. Varnum, and Mark Ptashne. 1985. "Specific DNA Binding of GAL4, a Positive Regulatory Protein of Yeast." *Cell* 40 (4): 767–74. https://doi.org/10.1016/0092-8674(85)90336-8.

Goddard, M.R., and D. Greig. 2015. "Saccharomyces Cerevisiae: A Nomadic Yeast with No Niche?" *Fems Yeast Research* 15 (3): 1–6. https://doi.org/10.1093/femsyr/fov009.

Goyal, Sidhartha, Jie Yuan, Thomas Chen, Joshua D. Rabinowitz, and Ned S. Wingreen. 2010. "Achieving Optimal Growth through Product Feedback Inhibition in Metabolism." *Plos Computational Biology* 6 (6): 1–12. https://doi.org/10.1371/journal.pcbi.1000802.

Goyal, Sidhartha, and Ned S. Wingreen. 2007. "Growth-Induced Instability in Metabolic Networks." *Physical Review Letters* 98 (13): 138105. https://doi.org/10.1103/PhysRevLett.98.138105.

Greulich, Philip, Matthew Scott, Martin R Evans, and Rosalind J Allen. 2015. "Growth-

Dependent Bacterial Susceptibility to Ribosome-Targeting Antibiotics." *Molecular Systems Biology* 11 (3): 796. https://doi.org/10.15252/msb.20145949.

Groot, Daan H. de, Josephus Hulshof, Bas Teusink, Frank J. Bruggeman, and Robert Planqué. 2020. *Elementary Growth Modes Provide a Molecular Description of Cellular Self-Fabrication. Plos Computational Biology.* Vol. 16. https://doi.org/10.1371/journal.pcbi.1007559.

Guerra, Paolo, Luc-Alban Vuillemenot, Brady Rae, Valeriia Ladyhina, and Andreas Milias-Argeitis. 2022. "Systematic In Vivo Characterization of Fluorescent Protein Maturation in Budding Yeast." *Acs Synthetic Biology*, February. https://doi.org/10.1021/acssynbio.1c00387.

Gunji, Wataru, Takahito Kai, Yoriko Takahashi, Yukihiro Maki, Wataru Kurihara, Takahiko Utsugi, Fumihiro Fujimori, and Yasufumi Murakami. 2004. "Global Analysis of the Regulatory Network Structure of Gene Expression in Saccharomyces Cerevisiae." *Dna Research* 11 (3): 163–77. https://doi.org/10.1093/dnares/11.3.163.

Görke, Boris, and Jörg Stülke. 2008. "Carbon Catabolite Repression in Bacteria: Many Ways to Make the Most out of Nutrients." *Nature Reviews Microbiology* 6 (8): 613–24. https://doi.org/10.1038/nrmicro1932.

Han, Eun-Kyoung, Francis Cotty, Chantal Sottas, Hua Jiang, and Corinne A. Michels. 1995. "Characterization of AGT1 Encoding a General Alpha-Glucoside Transporter from Saccharomyces." *Molecular Microbiology* 17 (6): 1093–1107. https://doi.org/10.1111/j.1365-2958.1995.mmi_17061093.x.

Hatanaka, Haruyo. 2018. "ラガービール酵母のalpha-グルコシドトランスポーターの機能解明と変異型トランスポーター高発現による発酵速度改善." Osaka University.

Hatanaka, Haruyo, Hitoshi Mitsunaga, and Eiichiro Fukusaki. 2018. "Inhibition of Saccharomyces Cerevisiae Growth by Simultaneous Uptake of Glucose and Maltose." *Journal of Bioscience and Bioengineering* 125 (1): 52–58. https://doi.org/10.1016/j.jbiosc.2017.07.013.

Hatanaka, Haruyo, Fumihiko Omura, Yukiko Kodama, and Toshihiko Ashikari. 2009. "Gly-46 and His-50 of Yeast Maltose Transporter Mal21p Are Essential for Its Resistance against Glucose-induced Degradation." *Journal of Biological Chemistry* 284 (23): 15448–57. https://doi.org/10.1074/jbc.M808151200.

Haynes, Samuel, Jamie Auxillos, Weronika Danecka, Abhishek Jain, Clemence Alibert, and Edward Wallace. 2022. "Limitations of Composability of Cis-Regulatory Elements in Messenger RNA." bioRxiv. https://doi.org/10.1101/2021.08.12.455418.

Henderson, Ryan K., Sophie C. de Valk, Bert Poolman, and Robert Mans. 2020. "Energy Coupling of Membrane Transport and Efficiency of Sucrose Dissimilation in Yeast." *Metabolic Engineering*, December. https://doi.org/10.1016/j.ymben.2020.11.014.

Hennaut, C., F. Hilger, and M. Grenson. 1970. "Space Limitation for Permease Insertion in the Cytoplasmic Membrane of Saccharomyces Cerevisiae." *Biochemical and Biophysical Research Communications* 39 (4): 666–71. https://doi.org/10.1016/0006-291X(70)90257-3.

Henriques, David, and Eva Balsa-Canto. 2021. "Monod Law Is Insufficient to Explain Biomass Growth in Nitrogen-Limited Yeast Fermentation." *Biorxiv*, January, 2021.01.05.425518. https://doi.org/10.1101/2021.01.05.425518.

Hentges, Pierre, Benoit Van Driessche, Lionel Tafforeau, Jean Vandenhaute, and Antony M. Carr. 2005. "Three Novel Antibiotic Marker Cassettes for Gene Disruption and Marker Switching in Schizosaccharomyces Pombe." *Yeast (Chichester, England)* 22 (13): 1013–19. https://doi.org/10.1002/yea.1291.

Heredia, Claudio F. 1998. "Impairment by Hexoses of the Utilization of Maltose by Saccharomyces Cerevisiae." *Biochimica et Biophysica Acta - General Subjects* 1425 (1): 151–58. https://doi.org/10.1016/S0304-4165(98)00064-6.

Hermsen, R., H. Okano, C. You, N. Werner, and T. Hwa. 2015. "A Growth-Rate Composition Formula for the Growth of E. Coli on Co-Utilized Carbon Substrates." *Molecular Systems Biology* 11 (4): 801. https://doi.org/te.

Hinrichsen, M., M. Lenz, J. M. Edwards, O. K. Miller, S. G. J. Mochrie, P. S. Swain, U. Schwarz-Linek, and L. Regan. 2017. "A New Method for Post-Translationally Labeling Proteins in Live Cells for Fluorescence Imaging and Tracking." *Protein Engineering, Design & Selection: Peds* 30 (12): 771–80. https://doi.org/10.1093/protein/gzx059.

Hittinger, Chris Todd, and Sean B. Carroll. 2007. "Gene Duplication and the Adaptive Evolution of a Classic Genetic Switch." *Nature* 449 (7163): 677–81. https://doi.

org/10.1038/nature06151.

Hofstee, B. H. J. 1959. "Non-Inverted Versus Inverted Plots in Enzyme Kinetics." *Nature* 184 (4695): 1296–98. https://doi.org/10.1038/1841296b0.

Hohmann, Stefan. 2002. "Osmotic Stress Signaling and Osmoadaptation in Yeasts." *Microbiology and Molecular Biology Reviews: Mmbr* 66 (2): 300–372. https://doi.org/10.1128/MMBR.66.2.300-372.2002.

Horak, J., and D. H. Wolf. 2005. "The Ubiquitin Ligase SCFGrr1 Is Required for Gal2p Degradation in the Yeast Saccharomyces Cerevisiae." *Biochemical and Biophysical Research Communications* 335 (4): 1185–90. https://doi.org/10.1016/j.bbrc.2005.08.008.

Horak, Jaroslav, Jochen Regelmann, and Dieter H. Wolf. 2002. "Two Distinct Proteolytic Systems Responsible for Glucose-induced Degradation of Fructose-1,6-Bisphosphatase and the Gal2p Transporter in the Yeast Saccharomyces Cerevisiae Share the Same Protein Components of the Glucose Signaling Pathway *." *Journal of Biological Chemistry* 277 (10): 8248–54. https://doi.org/10.1074/jbc.M107255200.

Horák, J. 2013. "Regulations of Sugar Transporters: Insights from Yeast." *Current Genetics* 59 (1-2): 1–31. https://doi.org/10.1007/s00294-013-0388-8.

Hu, Xiao-Pan, Hugo Dourado, Peter Schubert, and Martin J. Lercher. 2020. "The Protein Translation Machinery Is Expressed for Maximal Efficiency in Escherichia Coli." *Nature Communications* 11 (1): 5260. https://doi.org/10.1038/s41467-020-18948-x.

Hui, Sheng, Josh M Silverman, Stephen S Chen, David W Erickson, Markus Basan, Jilong Wang, Terence Hwa, and James R Williamson. 2015. "Quantitative Proteomic Analysis Reveals a Simple Strategy of Global Resource Allocation in Bacteria." *Molecular Systems Biology* 11 (2): 784. https://doi.org/10.15252/msb.20145697.

Ideker, Trey, Vesteinn Thorsson, Jeffrey A. Ranish, Rowan Christmas, Jeremy Buhler, Jimmy K. Eng, Roger Bumgarner, David R. Goodlett, Ruedi Aebersold, and Leroy Hood. 2001. "Integrated Genomic and Proteomic Analyses of a Systematically Perturbed Metabolic Network." *Science* 292 (5518): 929–34. https://doi.org/10.1126/science.292.5518.929.

Janke, Carsten, Maria M. Magiera, Nicole Rathfelder, Christof Taxis, Simone Reber, Hiromi Maekawa, Alexandra Moreno-Borchart, et al. 2004. "A Versatile Toolbox for

PCR-based Tagging of Yeast Genes: New Fluorescent Proteins, More Markers and Promoter Substitution Cassettes." *Yeast* 21 (11): 947.

Janssens, Georges E., and Liesbeth M. Veenhoff. 2016. "The Natural Variation in Lifespans of Single Yeast Cells Is Related to Variation in Cell Size, Ribosomal Protein, and Division Time." *Plos One* 11 (12): e0167394. https://doi.org/10.1371/journal.pone.0167394.

Jiang, Fenglei, Benjamin R. Frey, Margery L. Evans, Jordan C. Friel, and James E. Hopper. 2009. "Gene Activation by Dissociation of an Inhibitor from a Transcriptional Activation Domain." *Molecular and Cellular Biology* 29 (20): 5604–10. https://doi.org/10.1128/MCB.00632-09.

Jiang, H, I Medintz, and C A Michels. 1997. "Two Glucose Sensing/Signaling Pathways Stimulate Glucose-Induced Inactivation of Maltose Permease in Saccharomyces." *Molecular Biology of the Cell* 8 (7): 1293–1304. https://doi.org/10.1091/mbc.8.7.1293.

Jiang, H., K. Tatchell, S. Liu, and C. A. Michels. 2000. "Protein Phosphatase Type-1 Regulatory Subunits Reg1p and Reg2p Act as Signal Transducers in the Glucose-Induced Inactivation of Maltose Permease in Saccharomyces Cerevisiae." *Molecular and General Genetics Mgg* 263 (3): 411–22. https://doi.org/10.1007/s004380051185.

Jiang, Hua, Igor Medintz, Bin Zhang, and Corinne A. Michels. 2000. "Metabolic Signals Trigger Glucose-Induced Inactivation of Maltose Permease in Saccharomyces." *Journal of Bacteriology* 182 (3): 647–54. https://doi.org/10.1128/JB.182.3.647-654.2000.

Julou, Thomas, Ludovit Zweifel, Diana Blank, Athos Fiori, and Erik van Nimwegen. 2020. "Subpopulations of Sensorless Bacteria Drive Fitness in Fluctuating Environments." *Plos Biology* 18 (12): e3000952. https://doi.org/10.1371/journal.pbio.3000952.

Kainth, Pinay, Holly Elizabeth Sassi, Lourdes Peña-Castillo, Gordon Chua, Timothy R. Hughes, and Brenda Andrews. 2009. "Comprehensive Genetic Analysis of Transcription Factor Pathways Using a Dual Reporter Gene System in Budding Yeast." *Methods*, Global approaches to study gene regulation, 48 (3): 258–64. https://doi.org/10.1016/j.ymeth.2009.02.015.

Kamrad, Stephan, María Rodríguez-López, Cristina Cotobal, Clara Correia-Melo, Markus Ralser, and Jürg Bähler. 2020. "Pyphe, a Python Toolbox for Assessing Microbial Growth and Cell Viability in High-Throughput Colony Screens." Edited by Kevin J Verstrepen, Aleksandra M Walczak, Kevin J Verstrepen, and Jonas Warringer. *Elife* 9 (June): e55160. https://doi.org/10.7554/eLife.55160.

Kanehisa, M., and S. Goto. 2000. "KEGG: Kyoto Encyclopedia of Genes and Genomes." *Nucleic Acids Research* 28 (1): 27–30. https://doi.org/10.1093/nar/28.1.27.

Kaniak, Aneta, Zhixiong Xue, Daniel Macool, Jeong-Ho Kim, and Mark Johnston. 2004. "Regulatory Network Connecting Two Glucose Signal Transduction Pathways in Saccharomyces Cerevisiae." *Eukaryotic Cell* 3 (1): 221–31. https://doi.org/10.1128/EC.3.1.221-231.2004.

Kar, Rajesh Kumar, and Paike Jayadeva Bhat. 2021. "Cellular Heterogeneity and MTH1 Play Key Roles in Galactose Mediated Signaling of the GAL Switch to Utilize the Disaccharide Melibiose." *Biorxiv*, June, 2021.06.16.448739. https://doi.org/10.1101/2021.06.16.448739.

Karhumaa, Kaisa, Boqian Wu, and Morten C. Kielland-Brandt. 2010. "Conditions with High Intracellular Glucose Inhibit Sensing through Glucose Sensor Snf3 in Saccharomyces Cerevisiae." *Journal of Cellular Biochemistry* 110 (4): 920–25. https://doi.org/10.1002/jcb.22605.

Karr, Jonathan R., Jayodita C. Sanghvi, Derek N. Macklin, Miriam V. Gutschow, Jared M. Jacobs, Benjamin Bolival, Nacyra Assad-Garcia, John I. Glass, and Markus W. Covert. 2012. "A Whole-Cell Computational Model Predicts Phenotype from Genotype." *Cell* 150 (2): 389–401. https://doi.org/10.1016/j.cell.2012.05.044.

Kayikci, Ömur, and Jens Nielsen. 2015. "Glucose Repression in Saccharomyces Cerevisiae." *Fems Yeast Research* 15 (6): fov068. https://doi.org/10.1093/femsyr/fov068.

Kim, Daehwan, Joseph M. Paggi, Chanhee Park, Christopher Bennett, and Steven L. Salzberg. 2019. "Graph-Based Genome Alignment and Genotyping with HISAT2 and HISAT-genotype." *Nature Biotechnology* 37 (8): 907–15. https://doi.org/10.1038/s41587-019-0201-4.

Kirk, P. D. W., A. C. Babtie, and M. P. H. Stumpf. 2015. "Systems Biology (Un)Certainties."

Science 350 (6259): 386–88. https://doi.org/10.1126/science.aac9505.

Koirala, Santosh, Xiaoyi Wang, and Christopher V. Rao. 2016. "Reciprocal Regulation of L-Arabinose and D-Xylose Metabolism in Escherichia Coli." *Journal of Bacteriology* 198 (3): 386–93. https://doi.org/10.1128/JB.00709-15.

Kubitschek, Herbert E. 1987. "Buoyant Density Variation During the Cell Cycle in Microorganisms." *Crc Critical Reviews in Microbiology* 14 (1): 73–97. https://doi.org/10.3109/10408418709104436.

Kuleshov, Maxim V., Matthew R. Jones, Andrew D. Rouillard, Nicolas F. Fernandez, Qiaonan Duan, Zichen Wang, Simon Koplev, et al. 2016. "Enrichr: A Comprehensive Gene Set Enrichment Analysis Web Server 2016 Update." *Nucleic Acids Research* 44 (W1): W90-97. https://doi.org/10.1093/nar/gkw377.

Kumar, P. Rajesh, Yao Yu, Rolf Sternglanz, Stephen Albert Johnston, and Leemor Joshua-Tor. 2008. "NADP Regulates the Yeast GAL Induction System." *Science* 319 (5866): 1090–92. https://doi.org/10.1126/science.1151903.

Lavy, Tali, P. Rajesh Kumar, Hongzhen He, and Leemor Joshua-Tor. 2012. "The Gal3p Transducer of the GAL Regulon Interacts with the Gal80p Repressor in Its Ligand-Induced Closed Conformation." *Genes & Development* 26 (3): 294–303. https://doi.org/10.1101/gad.182691.111.

Lee, A. L., M. M. Ataai, and M. L. Shuler. 1984. "Double-Substrate-Limited Growth of Escherichia Coli." *Biotechnology and Bioengineering* 26 (11): 1398–1401. https://doi.org/10.1002/bit.260261120.

Lee, Michael E., William C. DeLoache, Bernardo Cervantes, and John E. Dueber. 2015. "A Highly Characterized Yeast Toolkit for Modular, Multipart Assembly." *Acs Synthetic Biology* 4 (9): 975–86. https://doi.org/10.1021/sb500366v.

Lemaire, Katleen, Sam Van De Velde, Patrick Van Dijck, and Johan M. Thevelein. 2004. "Glucose and Sucrose Act as Agonist and Mannose as Antagonist Ligands of the G Protein-Coupled Receptor Gpr1 in the Yeast Saccharomyces Cerevisiae." *Molecular Cell* 16 (2): 293–99. https://doi.org/10.1016/j.molcel.2004.10.004.

Levine, Joel, Leanne Tanouye, and Corinne A. Michels. 1992. "The UASMAL Is a Bidirectional Promotor Element Required for the Expression of Both the MAL61 and MAL62 Genes of the Saccharomyces MAL6 Locus." *Current Genetics* 22 (3): 181–89.

https://doi.org/10.1007/BF00351724.

Li, Heng, Bob Handsaker, Alec Wysoker, Tim Fennell, Jue Ruan, Nils Homer, Gabor Marth, Goncalo Abecasis, Richard Durbin, and 1000 Genome Project Data Processing Subgroup. 2009. "The Sequence Alignment/Map Format and SAMtools." *Bioinformatics (Oxford, England)* 25 (16): 2078–79. https://doi.org/10.1093/bioinformatics/btp352.

Li, Q., and S. A. Johnston. 2001. "Are All DNA Binding and Transcription Regulation by an Activator Physiologically Relevant?" *Molecular and Cellular Biology* 21 (7): 2467–74. https://doi.org/10.1128/MCB.21.7.2467-2474.2001.

Li, Yan, Guanjun Chen, and Weifeng Liu. 2010. "Multiple Metabolic Signals Influence GAL Gene Activation by Modulating the Interaction of Gal80p with the Transcriptional Activator Gal4p." *Molecular Microbiology* 78 (2): 414–28. https://doi.org/10.1111/j.1365-2958.2010.07343.x.

Liao, Yang, Gordon K. Smyth, and Wei Shi. 2014. "featureCounts: An Efficient General Purpose Program for Assigning Sequence Reads to Genomic Features." *Bioinformatics (Oxford, England)* 30 (7): 923–30. https://doi.org/10.1093/bioinformatics/btt656.

Lichten, Catherine A., Rachel White, Ivan B.N. Clark, and Peter S. Swain. 2014. "Unmixing of Fluorescence Spectra to Resolve Quantitative Time-Series Measurements of Gene Expression in Plate Readers." *Bmc Biotechnology* 14. https://doi.org/10.1186/1472-6750-14-11.

Liu, Yu. 2007. "Overview of Some Theoretical Approaches for Derivation of the Monod Equation." *Applied Microbiology and Biotechnology* 73 (6): 1241–50. https://doi.org/10.1007/s00253-006-0717-7.

Lodi, T., C. Donnini, and I.YR Ferrero. 1991. "Catabolite Repression by Galactose in Overexpressed GAL4 Strains of Saccharomyces Cerevisiae." *Microbiology* 137 (5): 1039–44. https://doi.org/10.1099/00221287-137-5-1039.

Lohr, D., P. Venkov, and J. Zlatanova. 1995. "Transcriptional Regulation in the Yeast GAL Gene Family: A Complex Genetic Network." *The Faseb Journal* 9 (9): 777–87. https://doi.org/10.1096/fasebj.9.9.7601342.

Longtine, M. S., A. McKenzie, D. J. Demarini, N. G. Shah, A. Wach, A. Brachat, P.

Philippsen, and J. R. Pringle. 1998. "Additional Modules for Versatile and Economical PCR-based Gene Deletion and Modification in Saccharomyces Cerevisiae." *Yeast (Chichester, England)* 14 (10): 953–61. https://doi.org/10.1002/(SICI)1097-0061(199807)14:10<953::AID-YEA293>3.0.CO;2-U.

Love, Michael I, Wolfgang Huber, and Simon Anders. 2014. "Moderated Estimation of Fold Change and Dispersion for RNA-seq Data with DESeq2." *Genome Biology* 15 (12): 550. https://doi.org/10.1186/s13059-014-0550-8.

Lucero, Pilar, and Rosario Lagunas. 1997. "Catabolite Inactivation of the Yeast Maltose Transporter Requires Ubiquitin-Ligase Npi1/Rsp5 and Ubiquitin-Hydrolase Npi2/Doa4." *Fems Microbiology Letters* 147 (2): 273–77. https://doi.org/10.1111/j.1574-6968.1997.tb10253.x.

MacKay, David. 2003. *Information Theory, Inference, and Learning Algorithms*. Cambridge University Press.

Magdolen, Viktor, Ulrich Oechsner, Paul Trommler, and Wolfhard Bandlow. 1990. "Transcriptional Control by Galactose of a Yeast Gene Encoding a Protein Homologous to Mammalian Aldo/Keto Reductases." *Gene* 90 (1): 105–14. https://doi.org/10.1016/0378-1119(90)90445-W.

Malakar, Pushkar, and Kareenhalli V. Venkatesh. 2014. "GAL Regulon of Saccharomyces Cerevisiae Performs Optimally to Maximize Growth on Galactose." *Fems Yeast Research* 14 (2): 346–56. https://doi.org/10.1111/1567-1364.12109.

Mankad, T., and H. R. Bungay. 1988. "Model for Microbial Growth with More than One Limiting Nutrient." *Journal of Biotechnology* 7 (2): 161–66. https://doi.org/10.1016/0168-1656(88)90062-4.

Manzanaro Moreno, Nahuel. 2021. "The Impact of Nutrients and Stress, Including Antifungal Drugs, on Growth and Ribosomal Content in Saccharomyces Cerevisiae." University of Edinburgh.

Marešová, Lydie, and Hana Sychrová. 2007. "Applications of a Microplate Reader in Yeast Physiology Research." *Biotechniques* 43 (5): 667–72. https://doi.org/10.2144/000112620.

Marmorstein, Ronen, Michael Carey, Mark Ptashne, and Stephen C. Harrison. 1992. "DNA Recognition by GAL4: Structure of a Protein-DNA Complex." *Nature* 356

(6368): 408–14. https://doi.org/10.1038/356408a0.

Martin, Marcel. 2011. "Cutadapt Removes Adapter Sequences from High-Throughput Sequencing Reads." *Embnet.Journal* 17 (1): 10–12. https://doi.org/10.14806/ej.17.1.200.

Mayer, Faith V., Richard Heath, Elizabeth Underwood, Matthew J. Sanders, David Carmena, Rhonda R. McCartney, Fiona C. Leiper, et al. 2011. "ADP Regulates SNF1, the Saccharomyces Cerevisiae Homolog of AMP-Activated Protein Kinase." *Cell Metabolism* 14 (5): 707–14. https://doi.org/10.1016/j.cmet.2011.09.009.

Medintz, Igor, Hua Jiang, Eun Kyoung Han, Wen Cui, and Corinne A. Michels. 1996. "Characterization of the Glucose-Induced Inactivation of Maltose Permease in Saccharomyces Cerevisiae." *Journal of Bacteriology* 178 (8): 2245–54. https://doi.org/10.1128/jb.178.8.2245-2254.1996.

Medintz, Igor, Xin Wang, Thomas Hradek, and Corinne A. Michels. 2000. "A PEST-like Sequence in the N-Terminal Cytoplasmic Domain of Saccharomyces Maltose Permease Is Required for Glucose-Induced Proteolysis and Rapid Inactivation of Transport Activity." *Biochemistry* 39 (15): 4518–26. https://doi.org/10.1021/bi992455a.

Megee III, R. D., J. F. Drake, A. G. Fredrickson, and H. M. Tsuchiya. 1972. "Studies in Intermicrobial Symbiosis. Saccharomyces Cerevisiae and Lactobacillus Casei." *Canadian Journal of Microbiology* 18 (11): 1733–42. https://doi.org/10.1139/m72-269.

Metzl-Raz, Eyal, Moshe Kafri, Gilad Yaakov, Ilya Soifer, Yonat Gurvich, and Naama Barkai. 2017. "Principles of Cellular Resource Allocation Revealed by Condition-Dependent Proteome Profiling." *Elife*, 1–21.

Miermont, Agnès, François Waharte, Shiqiong Hu, Megan Nicole McClean, Samuel Bottani, Sébastien Léon, and Pascal Hersen. 2013. "Severe Osmotic Compression Triggers a Slowdown of Intracellular Signaling, Which Can Be Explained by Molecular Crowding." *Proceedings of the National Academy of Sciences* 110 (14): 5725–30. https://doi.org/10.1073/pnas.1215367110.

Molenaar, Douwe, Rogier Van Berlo, Dick De Ridder, Bas Teusink, Rogier Van Berlo, Dick De Ridder, and Bas Teusink. 2009. "Shifts in Growth Strategies Reflect Tradeoffs in Cellular Economics." *Molecular Systems Biology* 5 (323): 1–10. https://doi.org/10.1038/msb.2009.82.

Monod, Jacques. 1942. “Diauxie et Respiration Au Cours de La Croissance Des Cultures de B. Coli.” *Annales de L'institut Pasteur* 68: 548–50.

———. 1947. “THE PHENOMENON OF ENZYMATIC ADAPTATION And Its Bearings on Problems of Genetics and Cellular Differentiation.” *Growth Symposium* XI (12): 223–89. https://doi.org/10.1016/b978-0-12-460482-7.50017-8.

———. 1949. “The Growth of Bacterial Cultures.” *Annu Rev Microbiol.* 3 (Xl): 371–94. https://doi.org/10.1146/annurev.mi.03.100149.002103.

Montaño-Gutierrez, Luis Fernando, Kevin Correia, and Peter S. Swain. 2022. “Multiple Nutrient Transporters Enable Cells to Mitigate a Rate-Affinity Tradeoff.” *Plos Computational Biology* 18 (4): e1010060. https://doi.org/10.1371/journal.pcbi.1010060.

Montaño-Gutierrez, Luis Fernando, Nahuel Manzanaro Moreno, Iseabail L. Farquhar, Yu Huo, Lucia Bandiera, and Peter S. Swain. 2022. “Analysing and Meta-Analysing Time-Series Data of Microbial Growth and Gene Expression from Plate Readers.” *Plos Computational Biology* 18 (5): e1010138. https://doi.org/10.1371/journal.pcbi.1010138.

Moses, Tessa, Johan M. Thevelein, Alain Goossens, and Jacob Pollier. 2014. “Comparative Analysis of CYP93E Proteins for Improved Microbial Synthesis of Plant Triterpenoids.” *Phytochemistry* 108 (December): 47–56. https://doi.org/10.1016/j.phytochem.2014.10.002.

Mosley, Amber L., Jaganathan Lakshmanan, Bishwa K. Aryal, and Sabire Özcan. 2003. “Glucose-Mediated Phosphorylation Converts the Transcription Factor Rgt1 from a Repressor to an Activator *.” *Journal of Biological Chemistry* 278 (12): 10322–27. https://doi.org/10.1074/jbc.M212802200.

Mrwebi, Mandisi. 2004. “Testing Monod : growth rate as a function of glucose concentration in Saccharomyces cerevisiae.” Thesis, Stellenbosch : University of Stellenbosch.

Narang, Atul. 2006. “Comparative Analysis of Some Models of Gene Regulation in Mixed-Substrate Microbial Growth.” *Journal of Theoretical Biology* 242 (2): 489–501. https://doi.org/10.1016/j.jtbi.2006.03.017.

New, Aaron M., Bram Cerulus, Sander K. Govers, Gemma Perez-Samper, Bo Zhu, Sarah Boogmans, Joao B. Xavier, and Kevin J. Verstrepen. 2014. “Different Levels of

Catabolite Repression Optimize Growth in Stable and Variable Environments." *Plos Biology* 12 (1): 17–20. https://doi.org/10.1371/journal.pbio.1001764.

Nissen, Torben L., Ulrik Schulze, Jens Nielsen, and John Villadsen. 1997. "Flux Distributions in Anaerobic, Glucose-Limited Continuous Cultures of Saccharomyces Cerevisiae." *Microbiology* 143 (1): 203–18. https://doi.org/10.1099/00221287-143-1-203.

Okano, Hiroyuki, Rutger Hermsen, Karl Kochanowski, and Terence Hwa. 2020. "Regulation Underlying Hierarchical and Simultaneous Utilization of Carbon Substrates by Flux Sensors in Escherichia Coli." *Nature Microbiology* 5 (1): 206–15. https://doi.org/10.1038/s41564-019-0610-7.

Okano, Hiroyuki, Rutger Hermsen, and Terence Hwa. 2021. "Hierarchical and Simultaneous Utilization of Carbon Substrates: Mechanistic Insights, Physiological Roles, and Ecological Consequences." *Current Opinion in Microbiology* 63 (October): 172–78. https://doi.org/10.1016/j.mib.2021.07.008.

Ostergaard, Simon, Lisbeth Olsson, Mark Johnston, and Jens Nielsen. 2000. "Increasing Galactose Consumption by Saccharomyces Cerevisiae through Metabolic Engineering of the GAL Gene Regulatory Network." *Nature Biotechnology* 18 (12): 1283–86. https://doi.org/10.1038/82400.

Ostergaard, Simon, Kristian O Walløe, Cláudia S. G. Gomes, Lisbeth Olsson, and Jens Nielsen. 2001. "The Impact of GAL6, GAL80, and MIG1 on Glucose Control of the GAL System in Saccharomyces Cerevisiae." *Fems Yeast Research* 1 (1): 47–55. https://doi.org/10.1111/j.1567-1364.2001.tb00012.x.

O'Brien, Edward J, Joshua A Lerman, Roger L Chang, Daniel R Hyduke, and Bernhard Ø Palsson. 2013. "Genome-Scale Models of Metabolism and Gene Expression Extend and Refine Growth Phenotype Prediction." *Molecular Systems Biology* 9 (1): 693. https://doi.org/10.1038/msb.2013.52.

Paiva, Sandra, Neide Vieira, Isabelle Nondier, Rosine Haguenauer-Tsapis, Margarida Casal, and Danièle Urban-Grimal. 2009. "Glucose-Induced Ubiquitylation and Endocytosis of the Yeast Jen1 Transporter." *Journal of Biological Chemistry* 284 (29): 19228–36. https://doi.org/10.1074/jbc.M109.008318.

Pannala, Venkat Reddy, Paike Jayadeva Bhat, Sharad Bhartiya, and K. V. Venkatesh. 2010. "Systems Biology of GAL Regulon in Saccharomyces Cerevisiae." *Wires Systems*

Biology and Medicine 2 (1): 98–106. https://doi.org/10.1002/wsbm.38.

Parker, Steven, Marcin Fraczek, Jian Wu, Sara Shamsah, Alkisti Manousaki, Kobchai Dungrattanalert, Rogerio Almeida, et al. 2017. "A Resource for Functional Profiling of Noncoding RNA in the Yeast Saccharomyces Cerevisiae." *Rna (New York, N.Y.)* 23 (May). https://doi.org/10.1261/rna.061564.117.

Patterson, G. H., S. M. Knobel, W. D. Sharif, S. R. Kain, and D. W. Piston. 1997. "Use of the Green Fluorescent Protein and Its Mutants in Quantitative Fluorescence Microscopy." *Biophysical Journal* 73 (5): 2782–90. https://doi.org/10.1016/S0006-3495(97)78307-3.

Perez-Samper, Gemma, Bram Cerulus, Abbas Jariani, Lieselotte Vermeersch, Nuria Barrajón Simancas, Markus M. M. Bisschops, Joost van den Brink, et al. 2018. "The Crabtree Effect Shapes the Saccharomyces Cerevisiae Lag Phase during the Switch between Different Carbon Sources." *Mbio* 9 (5): e01331-18. https://doi.org/10.1128/mBio.01331-18.

Perkins, Theodore J., and Peter S. Swain. 2009. "Strategies for Cellular Decision-Making." *Molecular Systems Biology* 5 (326): 1–15. https://doi.org/10.1038/msb.2009.83.

Postma, Erik, Cornelis Verduyn, Arthur Kuiper, W. Alexander Scheffers, and Johannes P. Van Dijken. 1990. "Substrate-Accelerated Death of Saccharomyces Cerevisiae CBS 8066 under Maltose Stress." *Yeast* 6 (2): 149–58. https://doi.org/10.1002/yea.320060209.

Pougach, Ksenia, Arnout Voet, Fyodor A. Kondrashov, Karin Voordeckers, Joaquin F. Christiaens, Bianka Baying, Vladimir Benes, et al. 2014. "Duplication of a Promiscuous Transcription Factor Drives the Emergence of a New Regulatory Network." *Nature Communications* 5: 1–11. https://doi.org/10.1038/ncomms5868.

Quinlan, Aaron R., and Ira M. Hall. 2010. "BEDTools: A Flexible Suite of Utilities for Comparing Genomic Features." *Bioinformatics (Oxford, England)* 26 (6): 841–42. https://doi.org/10.1093/bioinformatics/btq033.

Raamsdonk, Léonie M., Jasper A. Diderich, Arthur Kuiper, Monique van Gaalen, Arthur L. Kruckberg, Jan A. Berden, and Karel Van Dam. 2001. "Co-Consumption of Sugars or Ethanol and Glucose in a Saccharomyces Cerevisiae Strain Deleted in the HXK2 Gene." *Yeast* 18 (11): 1023–33. https://doi.org/10.1002/yea.746.

Ramsey, Stephen A., Jennifer J. Smith, David Orrell, Marcello Marelli, Timothy W. Petersen, Pedro De Atauri, Hamid Bolouri, and John D. Aitchison. 2006. "Dual Feedback Loops in the GAL Regulon Suppress Cellular Heterogeneity in Yeast." *Nature Genetics* 38 (9): 1082–87. https://doi.org/10.1038/ng1869.

Randez-Gil, F., and P. Sanz. 1994. "Construction of Industrial Baker's Yeast Strains Able to Assimilate Maltose under Catabolite Repression Conditions." *Applied Microbiology and Biotechnology* 42 (4): 581–86. https://doi.org/10.1007/BF00173924.

Reifenberger, Elke, Eckhard Boles, and Michael Ciriacy. 1997. "Kinetic Characterization of Individual Hexose Transporters of Saccharomyces Cerevisiae and Their Relation to the Triggering Mechanisms of Glucose Repression." *European Journal of Biochemistry* 245 (2): 324–33. https://doi.org/10.1111/j.1432-1033.1997.00324.x.

Ren, Bing, François Robert, John J. Wyrick, Oscar Aparicio, Ezra G. Jennings, Itamar Simon, Julia Zeitlinger, et al. 2000. "Genome-Wide Location and Function of DNA Binding Proteins." *Science* 290 (5500): 2306–9. https://doi.org/10.1126/science.290.5500.2306.

Rhee, Ho Sung, and B. Franklin Pugh. 2011. "Comprehensive Genome-wide Protein-DNA Interactions Detected at Single-Nucleotide Resolution." *Cell* 147 (6): 1408–19. https://doi.org/10.1016/j.cell.2011.11.013.

Ricci-Tam, C., I. Ben-Zion, J. Wang, J. Palme, A. Li, Y. Savir, and M. Springer. 2021. "Decoupling Transcription Factor Expression and Activity Enables Dimmer Switch Gene Regulation." *Science (New York, N.Y.)* 372 (6539): 292–95. https://doi.org/10.1126/science.aba7582.

Rose, Matthias, Werner Albig, and Karl-Dieter Entian. 1991. "Glucose Repression in Saccharomyces Cerevisiae Is Directly Associated with Hexose Phosphorylation by Hexokinases PI and PII." *European Journal of Biochemistry* 199 (3): 511–18. https://doi.org/10.1111/j.1432-1033.1991.tb16149.x.

Rutgers, Michiel, Peter A. Balk, and Karel van Dam. 1990. "Quantification of Multiple-Substrate Controlled Growth-Simultaneous Ammonium and Glucose Limitation in Chemostat Cultures of Klebsiella Pneumoniae." *Archives of Microbiology* 153 (5): 478–84. https://doi.org/10.1007/BF00248430.

Schaechter, M., O. MaalØe, and N. O.YR 1958 Kjeldgaard. 1958. "Dependency on

Medium and Temperature of Cell Size and Chemical Composition during Balanced Growth of Salmonella Typhimurium." *Microbiology* 19 (3): 592–606. https://doi.org/10.1099/00221287-19-3-592.

Scott, Matthew, Carl W. Gunderson, Eduard M. Mateescu, Zhongge Zhang, and Terence Hwa. 2010. "Inter-Dependence of Cell Growth and Gene Expression: Origins and Consequences." *Science* 330 (November): 1099–1102. https://doi.org/10.1126/science.1192588.

Scott, Matthew, Stefan Klumpp, Eduard M Mateescu, and Terence Hwa. 2014. "Emergence of Robust Growth Laws from Optimal Regulation of Ribosome Synthesis." *Molecular Systems Biology* 10 (8): 747. https://doi.org/10.15252/msb.20145379.

Scott, Matthew, and Terence Hwa. 2022. "Shaping Bacterial Gene Expression by Physiological and Proteome Allocation Constraints." *Nature Reviews Microbiology*, November, 1–16. https://doi.org/10.1038/s41579-022-00818-6.

Sellick, Christopher A., Robert N. Campbell, and Richard J. Reece. 2008. "Chapter 3 Galactose Metabolism in Yeast-Structure and Regulation of the Leloir Pathway Enzymes and the Genes Encoding Them." *International Review of Cell and Molecular Biology* 269 (08): 111–50. https://doi.org/10.1016/S1937-6448(08)01003-4.

Shaw, William M., Hitoshi Yamauchi, Jack Mead, Glen-Oliver F. Gowers, David J. Bell, David Öling, Niklas Larsson, Mark Wigglesworth, Graham Ladds, and Tom Ellis. 2019. "Engineering a Model Cell for Rational Tuning of GPCR Signaling." *Cell* 177 (3): 782–96.e27. https://doi.org/10.1016/j.cell.2019.02.023.

Sheff, Mark A., and Kurt S. Thorn. 2004. "Optimized Cassettes for Fluorescent Protein Tagging in Saccharomyces Cerevisiae." *Yeast* 21 (8): 661–70. https://doi.org/10.1002/yea.1130.

Shehata, Talaat E., and Allen G. Marr. 1971. "Effect of Nutrient Concentration on the Growth of Escherichia Coli." *Journal of Bacteriology* 107 (1): 210–16. https://doi.org/10.1128/jb.107.1.210-216.1971.

Simpson-Lavy, Kobi, and Martin Kupiec. 2019. "Carbon Catabolite Repression in Yeast Is Not Limited to Glucose." *Scientific Reports* 9 (1): 1–10. https://doi.org/10.1038/s41598-019-43032-w.

Sirenko, O. I., B. Ni, and R. B. Needleman. 1995. "Purification and Binding Properties of

the Mal63p Activator of Saccharomyces Cerevisiae." *Current Genetics* 27 (6): 509–16. https://doi.org/10.1007/BF00314440.

Song, Carl, Hilary Phenix, Vida Abedi, Matthew Scott, Brian P. Ingalls, Mads Kærn, and Theodore J. Perkins. 2010. "Estimating the Stochastic Bifurcation Structure of Cellular Networks." *Plos Computational Biology* 6 (3). https://doi.org/10.1371/journal.pcbi.1000699.

Spiegelman, S., and Reba Dunn. 1947. "INTERACTIONS BETWEEN ENZYME-FORMING SYSTEMS DURING ADAPTATION." *The Journal of General Physiology* 31 (2): 153–73.

Stambuk, Boris U., and Pedro S. de Araujo. 2001. "Kinetics of Active Alpha-Glucoside Transport in Saccharomyces Cerevisiae." *Fems Yeast Research* 1 (1): 73–78. https://doi.org/10.1111/j.1567-1364.2001.tb00015.x.

Stockwell, Sarah R., Christian R. Landry, and Scott A. Rifkin. 2015. "The Yeast Galactose Network as a Quantitative Model for Cellular Memory." *Molecular Biosystems* 11 (1): 28–37. https://doi.org/10.1039/c4mb00448e.

Sumner-Smith, Martin, Richard P. Bozzato, Nigel Skipper, R. Wayne Davies, and James E. Hopper. 1985. "Analysis of the Inducible MEL1 Gene of Saccharomyces Carlsbergensis and Its Secreted Product, Alpha-Galactosidase (Melibiase)." *Gene* 36 (3): 333–40. https://doi.org/10.1016/0378-1119(85)90188-X.

Sutherland, Catherine M, Simon A Hawley, Rhonda R McCartney, Anna Leech, Michael J R Stark, Martin C Schmidt, and D Grahame Hardie. 2003. "Elm1p Is One of Three Upstream Kinases for the Saccharomyces Cerevisiae SNF1 Complex." *Current Biology* 13 (15): 1299–1305. https://doi.org/10.1016/s0960-9822(03)00459-7.

Swain, Peter S., Keiran Stevenson, Allen Leary, Luis F. Montano-Gutierrez, Ivan B.N. Clark, Jackie Vogel, and Teuta Pilizota. 2016. "Inferring Time Derivatives Including Cell Growth Rates Using Gaussian Processes." *Nature Communications* 7 (May): 1–8. https://doi.org/10.1038/ncomms13766.

Teixeira, Miguel Cacho, Pedro Tiago Monteiro, Joana Fernandes Guerreiro, Joana Pinho Gonçalves, Nuno Pereira Mira, Sandra Costa dos Santos, Tânia Rodrigues Cabrito, et al. 2014. "The YEASTRACT Database: An Upgraded Information System for the Analysis of Gene and Genomic Transcription Regulation in Saccharomyces Cere-

visiae." *Nucleic Acids Research* 42 (D1): D161–66. https://doi.org/10.1093/nar/gkt1015.

Tenaillon, Olivier, David Skurnik, Bertrand Picard, and Erick Denamur. 2010. "The Population Genetics of Commensal Escherichia Coli." *Nature Reviews Microbiology* 8 (3): 207–17. https://doi.org/10.1038/nrmicro2298.

Teste, Marie Ange, Jean Marie François, and Jean Luc Parrou. 2010. "Characterization of a New Multigene Family Encoding Isomaltases in the Yeast Saccharomyces Cerevisiae, the IMA Family." *Journal of Biological Chemistry* 285 (35): 26815–24. https://doi.org/10.1074/jbc.M110.145946.

Thoden, James B., Christopher A. Sellick, Richard J. Reece, and Hazel M. Holden. 2007. "Understanding a Transcriptional Paradigm at the Molecular Level: The Structure of Yeast Gal80p." *Journal of Biological Chemistry* 282 (3): 1534–38. https://doi.org/10.1074/jbc.C600285200.

Torchia, T E, R W Hamilton, C L Cano, and J E Hopper. 1984. "Disruption of Regulatory Gene GAL80 in Saccharomyces Cerevisiae: Effects on Carbon-Controlled Regulation of the Galactose/Melibiose Pathway Genes." *Molecular and Cellular Biology* 4 (8): 1521–27. https://doi.org/10.1128/mcb.4.8.1521-1527.1984.

Travan, Ana, Branka Jelicic, and Mary Sopta. 2006. "Yeast Gal4: A Transcriptional Paradigm Revisited." *Embo Reports* 7 (5): 496–99. https://doi.org/10.1038/sj.embor.7400679.

Tsien, Roger Y. 1998. "The Green Fluorescent Protein." *Annual Review of Biochemistry* 67 (1): 509–44. https://doi.org/10.1146/annurev.biochem.67.1.509.

Ullah, Azmat, Rick Orij, Stanley Brul, and Gertien J. Smits. 2012. "Quantitative Analysis of the Modes of Growth Inhibition by Weak Organic Acids in Saccharomyces Cerevisiae." *Applied and Environmental Microbiology* 78 (23): 8377–87. https://doi.org/10.1128/AEM.02126-12.

Vega, Montserrat, Alberto Riera, Alejandra Fernández-Cid, Pilar Herrero, and Fernando Moreno. 2016. "Hexokinase 2 Is an Intracellular Glucose Sensor of Yeast Cells That Maintains the Structure and Activity of Mig1 Protein Repressor Complex." *Journal of Biological Chemistry* 291 (14): 7267–85. https://doi.org/10.1074/jbc.M115.711408.

Venturelli, O. S., H. El-Samad, and R. M. Murray. 2012. "Synergistic Dual Positive Feedback Loops Established by Molecular Sequestration Generate Robust Bimodal Response." *Proceedings of the National Academy of Sciences* 109 (48): E3324–33. https://doi.org/10.1073/pnas.1211902109.

Venturelli, Ophelia S., Ignacio Zuleta, Richard M. Murray, and Hana El-Samad. 2015. "Population Diversification in a Yeast Metabolic Program Promotes Anticipation of Environmental Shifts." *Plos Biology* 13 (1): 1–24. https://doi.org/10.1371/journal.pbio.1002042.

Verduyn, Cornelis, Erik Postma, W. Alexander Scheffers, and Johannes P.YR 1990 van Dijken. 1990. "Physiology of Saccharomyces Cerevisiae in Anaerobic Glucose-Limited Chemostat Cultures." *Microbiology* 136 (3): 395–403. https://doi.org/10.1099/00221287-136-3-395.

Verduyn, Cornelis, Erik Postma, W. Alexander Scheffers, and Johannes P. Van Dijken. 1992. "Effect of Benzoic Acid on Metabolic Fluxes in Yeasts: A Continuous-Culture Study on the Regulation of Respiration and Alcoholic Fermentation." *Yeast* 8 (7): 501–17. https://doi.org/10.1002/yea.320080703.

Virchow, Rudolf. 1860. *Cellular Pathology as Based upon Physiological and Pathological Histology.* John Churchill.

Voordeckers, Karin, Chris A. Brown, Kevin Vanneste, Elisa van der Zande, Arnout Voet, Steven Maere, and Kevin J. Verstrepen. 2012. "Reconstruction of Ancestral Metabolic Enzymes Reveals Molecular Mechanisms Underlying Evolutionary Innovation through Gene Duplication." *Plos Biology* 10 (12). https://doi.org/10.1371/journal.pbio.1001446.

Wang, Jue, Esha Atolia, Bo Hua, Yonatan Savir, Renan Escalante-Chong, and Michael Springer. 2015. "Natural Variation in Preparation for Nutrient Depletion Reveals a CostBenefit Tradeoff." *Plos Biology* 13 (1): 1–31. https://doi.org/10.1371/journal.pbio.1002041.

Wang, Xin, Mehtap Bali, Igor Medintz, and Corinne A. Michels. 2002. "Intracellular Maltose Is Sufficient to Induce MAL Gene Expression in Saccharomyces Cerevisiae." *Eukaryotic Cell* 1 (5): 696–703. https://doi.org/10.1128/EC.1.5.696-703.2002.

Wang, Xin, Kang Xia, Xiaojing Yang, and Chao Tang. 2019. "Growth Strategy of

Microbes on Mixed Carbon Sources." *Nature Communications* 10 (1): 1279. https://doi.org/10.1038/s41467-019-09261-3.

Warner, Jonathan R. 1999. "The Economics of Ribosome Biosynthesis in Yeast." *Trends in Biochemical Sciences* 0004 (November): 437–40.

Weiße, Andrea Y., Diego A. Oyarzún, Vincent Danos, and Peter S. Swain. 2015. "Mechanistic Links between Cellular Trade-Offs, Gene Expression, and Growth." *Proceedings of the National Academy of Sciences* 112 (9): E1038–47. https://doi.org/10.1073/pnas.1416533112.

Westholm, Jakub Orzechowski, Niklas Nordberg, Eva Murén, Adam Ameur, Jan Komorowski, and Hans Ronne. 2008. "Combinatorial Control of Gene Expression by the Three Yeast Repressors Mig1, Mig2 and Mig3." *Bmc Genomics* 9 (1): 601. https://doi.org/10.1186/1471-2164-9-601.

Wimpenny, Julian W. T. 1979. "The Growth and Form of Bacterial Colonies." *Microbiology* 114 (2): 483–86. https://doi.org/10.1099/00221287-114-2-483.

Winzeler, Elizabeth A., Daniel D. Shoemaker, Anna Astromoff, Hong Liang, Keith Anderson, Bruno Andre, Rhonda Bangham, et al. 1999. "Functional Characterization of the S. Cerevisiae Genome by Gene Deletion and Parallel Analysis." *Science* 285 (5429): 901–6. https://doi.org/10.1126/science.285.5429.901.

Yabo, Agustín G., Jean-Baptiste Caillau, Jean-Luc Gouzé, Hidde de Jong, and Francis Mairet. 2022. "Dynamical Analysis and Optimization of a Generalized Resource Allocation Model of Microbial Growth." *Siam Journal on Applied Dynamical Systems* 21 (1): 137–65. https://doi.org/10.1137/21M141097X.

You, Conghui, Hiroyuki Okano, Sheng Hui, Zhongge Zhang, Minsu Kim, Carl W. Gunderson, Yi Ping Wang, Peter Lenz, Dalai Yan, and Terence Hwa. 2013. "Coordination of Bacterial Proteome with Metabolism by Cyclic AMP Signalling." *Nature* 500 (7462): 301–6. https://doi.org/10.1038/nature12446.

Zhao, Yue, David Granas, and Gary D. Stormo. 2009. "Inferring Binding Energies from Selected Binding Sites." *Plos Computational Biology* 5 (12): e1000590. https://doi.org/10.1371/journal.pcbi.1000590.

Zheng, W., H. E. Xu, and S. A. Johnston. 1997. "The Cysteine-Peptidase Bleomycin Hydrolase Is a Member of the Galactose Regulon in Yeast." *The Journal of Biological*

Chemistry 272 (48): 30350–55. https://doi.org/10.1074/jbc.272.48.30350.

Zimmermann, F. K., and N. R. Eaton. 1974. "Genetics of Induction and Catabolite Repression of Maltase Synthesis in Saccharomyces Cerevisiae." *Molecular and General Genetics Mgg* 134 (3): 261–72. https://doi.org/10.1007/BF00267720.